STUDIES OF THE EFFECTS OF

MOLECULAR ENCOUNTERS

ON N.M.R. SPIN-LATTICE RELAXATION TIMES

Presented for the degree of

DOCTOR OF PHILOSOPHY

by

ENEAS RICARDO VALDIVIESO CEDENO

Department of Chemistry

"The University of Aston in Birmingham"

September 1982.

The University of Aston in Birmingham

Studies of the Effects of Molecular Encounters on N.M.R. Spin-Lattice Relaxation Times.

A Thesis presented for the degree of
Doctor of Philosophy
by
Eneas Ricardo Valdivieso Cedeno
1982

This thesis is concerned with investigations of the effects of molecular encounters on nuclear magnetic resonance spin-lattice relaxation times, with particular reference to mesitylene in mixtures with cyclohexane and TMS. The purpose of the work was to establish the best theoretical description of T_1 and assess whether a recently identified mechanism (buffeting), that influences n.m.r. chemical shifts, governs T_1 also.

A set of experimental conditions are presented that allow reliable measurements of T_1 and the N.O.E. for ^1H and ^{13}C using both C.W. and F.T. n.m.r. spectroscopy.

Literature data for benzene, cyclohexane and chlorobenzene diluted by CCl_4 and CS_2 are used to show that the Hill theory affords the best estimation of their correlation times but appears to be mass dependent. Evaluation of the T_1 of the mesitylene protons indicates that a combined Hill-Bloembergen-Purcell-Pound model gives an accurate estimation of T_1; subsequently this was shown to be due to cancellation of errors in the calculated intra and intermolecular components.

Three experimental methods for the separation of the intra and intermolecular relaxation times are described.

The relaxation times of the ^{13}C proton satellite of neat bezene, 1,4 dioxane and mesitylene were measured. Theoretical analyses of the data allow the calculation of T_1 intra.

Studies of intermolecular NOE's were found to afford a general method of separating observed T_1's into their intra and intermolecular components.

The aryl ^1H and corresponding ^{13}C T_1 values and the NOE for the ring carbon of mesitylene in CCl_4 and C_6H_{12}-TMS have been used in combination to determine T_1intra and T_1inter. The Hill and B.P.P. models are shown to predict similarly inaccurate values for T_1inter. A buffeting contribution to T_1inter is proposed which when applied to the BPP model and to the Gutowsky-Woessner expression for T_1inter gives an inaccuracy of 12% and 6% respectively with respect to the experimentally based T_1inter.

Nuclear magnetic resonance
Spin lattice relaxation
Nuclear Overhauser effects
Steric contributions to relaxation times

ACKNOWLEDGEMENTS

I would like to express my sincere gratitude to my supervisor, Dr. J. Homer, for his invaluable assistance and encouragement throughout the course of this work, as well as many discussions and suggestions, in the fulfilment of this work.

I am grateful to my colleagues: Dr. M.C. Cooke, Dr.C.Percival, Dr. S.Whitburn and Mr. H. Al-Daffaee for helpful advice in the course of this work.

I am very grateful to the university of Carabobo, which, with institutional and financial support, made this work possible.

Finally I would like to thank my wife Mercedes for her assistance in the preparation of this script.

Abbreviations

Within this thesis the following abbreviations have been used in place of their longer equivalents.

NMR	Nuclear Magnetic Resonance
ARPS	Adiabatic Rapid Passage with Sampling
NOE	Nuclear Overhauser Effect
R.F	Radio Frequency
IF	Intermediate Frequency
AF	Audio Frequency
AC	Alternating Current
DC	Direct Current
TMS	Tetra Methyl Silane
Me	Mesitylene
Cy	Cyclohexane
inter	Intermolecular
intra	Intramolecular
BPP	Bloembergen-Purcell-Pound
FID	Free Induction Decay
F.T	Fourier Transform
i.r	Inversion Recovery
P.S	Progressive Saturation

A NOTE ON UNITS

Although it is appreciated that SI units should be used whenever possible, most of the units used in this thesis are c.g.s. s.u units. The reason for this is to facilitate comparison with the past literature dealing with NMR relaxation times.

Some useful equivalences are indicated below.

Physical quantity	**Name (SI)**	**cgs unit**	**Conversion factor**
length	metre	cm, Å	10^{-2}, 10^{-10}
density	Kgm^{-3}	g cm^{-3}	10^{3}
viscosity	Ns. m^{-2}	Poise	10^{-1}
energy	Joule	erg.	10^{-7}
electric field	mKg s^{-3} A^{-1}	emu	10^{6}
magnetic induction	Tesla (T)	gauss	10^{4}

Further information can be found in the following references:

W.J. Duffin "electricity and magnetism", 2nd ed. McGraw Hill (1973)

P. Vigoureux "units and standards of electromagnetism" Wykeham (1971)

M.N. Hughes, A.M. James and N.R. Silvester. "SI units and conversion tables" The machinery publishing Co. (1970)

LIST OF CONTENTS

Chapter One. An Introduction of Nuclear Magnetic Resonance Spectroscopy.

LIST OF CONTENTS

LIST OF CONTENTS

Chapter Three. Relaxation Processes.

LIST OF CONTENTS

LIST OF CONTENTS

LIST OF CONTENTS

LIST OF CONTENTS

LIST OF CONTENTS

LIST OF ILLUSTRATIONS

LIST OF TABLES

CHAPTER I

An Introduction to Nuclear Magnetic Resonance Spectroscopy

1.1 Introduction

In 1924 W. Pauli (1) ascribed to nuclei a magnetic dipole moment and associated angular momentum in order to account for the hyperfine structure of atomic spectra. Stern and Gerlach (2) then demonstrated that the measurable values of the magnetic moment are discrete in nature and, when an atom is placed in a magnetic field, this corresponds to a space quantization of the atom. In their experiment, an atom with magnetic moment μ moves along a direction OX in an inhomogeneous field B_o which, as well as its gradient $\partial B_o/\partial z$, is perpendicular to OX. The atom experiences a force $\mu_z (\partial B_o/\partial z)$ that deflects it through an amount proportional to μ_z. For a spin $1/2$, μ_z may have two values $\pm \mu$, and the atoms after crossing the inhomogeneous field produce two symmetrical spots where they impinge on a screen perpendicular to OX. From the distance between the spots, μ can be obtained if the field gradient and the time spent by the atoms in the inhomogeneous field are known. In a "resonant" version of this experiment (3) the atoms cross two regions A and

B of inhomogeneous fields with rigorously opposite gradients $\partial B_o / \partial z$ separated by a region C of homogeneous field. The construction of the apparatus is such that atoms or molecules emerging from a point source O, converge after crossing the three regions A, B, C to an image D, where a particle detector can be placed. Although the trajectories of particles with different orientations of their magnetic moments are different inside the beam, they all converge onto D if no reorientation of these moments occur on the way. A small r.f. field placed in the region C of homogeneous field B_o, will, if it has the correct frequency, induce transitions between the different magnetic states of the particle, causing it to change its trajectory in the second inhomogeneous region B and to miss the detector. A measurable change in the flux of particles striking the detector determines the frequency at which the resonance occurs. The resonant exchange of energy is not restricted to molecular beams and it is detectable in all forms of matter. Gorter (4)(5) suggested that it might be possible to detect the passage through resonance by observing a rise in the temperature of the sample, following a sudden increase at resonance in the absorption of electromagnetic energy by the nuclear spins. This method failed mainly because of the unfavourable materials employed.

In 1945 two groups of physicists working independently, Purcell, Torrey and Pound (6) at Harvard University and Bloch, Hansen and Packard (7) at Stanford University first succeeded in observing the phenomenon of nuclear magnetic resonance in solids and liquids. At the beginning of the 1950's, the phenomenon was called upon for the first time in the solution of a chemical problem (8). Since that time its importance has steadily increased and almost countless papers concerning nuclear magnetic resonance or its applications in all branches of chemistry have been published.

It is convenient when discussing the theory of nuclear magnetic resonance spectroscopy to first consider an isolated nucleus in a magnetic field in order to deduce equations for the resonant condition, and then to consider the properties of bulk samples to elucidate such important aspects as the nuclear energy level distribution, relaxation, saturation and finally the chemical shift and spin-spin coupling.

1.2 Magnetic Properties of Nuclei

All nuclei with odd mass number possess the property of spin; the angular momentum vector $\vec{I}\,\hbar$, where $\hbar$ is Plank's constant divided by 2π . The value of the spin, I is a multiple of $^1/_2$. Nuclei with even isotope number may be either, without spin if the nuclear charge is even, or possess an integral spin I with value 1,2,3, etc

The chemist is mostly concerned with the simplest nuclei having spin $^1/_2$, and of these, the nuclei of Hydrogen and Carbon - 13 are very important.

The possession of both, spin and charge confers on the nucleus a magnetic moment μ which is proportional to the magnitude of the spin, that is,

$$\mu = \gamma \hbar I \qquad (1.1)$$

γ is called the magnetogyric ratio and is measured in radians. sec $^{-1}$. Tesla $^{-1}$.

Quantum theory demands that the allowable nuclear spins states are quantized; the component m_I is called the nuclear spin quantum number. For the proton with $I = ^1/_2$, m_I may only take the values $+ ^1/_2$ or $- ^1/_2$. This means that the magnetic moment only can have two orientations with respect to some selected direction.

1.3 Nuclei in a Magnetic Field

If we apply a steady magnetic field B_o to the proton, there is an interaction between the field and the magnetic moment $\vec{\mu}$, which may be represented in terms of the Hamiltonian

$$\mathcal{H} = - \vec{\mu} \cdot \vec{B}_o \qquad (1.2)$$

The precise meaning of this equation, when the magnetic field is in the z direction, is

$$\mathcal{H} = -\gamma \hbar B_o Iz \qquad (1.3)$$

Where Iz, the allowed component of the nuclear spin in the z direction, has the value + 1/2 or - 1/2. These possibilities are summarized in terms of the energy level diagram shown in Fig. (1.1). The lower level with $m_I = +1/2$ corresponds to the situation in which the magnetic field B and the nuclear moment are parallel; in the upper level they are antiparallel. We shall denote the state for which $m_I = +1/2$ by the symbol $|\alpha\rangle$ and that with $m_I = -1/2$ by $|\beta\rangle$

In order to induce transitions between the two nuclear spin levels, an oscillating electromagnetic field is now applied to the system. The frequency ν of the radiation associated with absorption must be calculated from $E=h\nu$ and thus a given nucleus has only one characteristic resonant frequency in a given magnetic field (9)

$$\nu = \gamma B_o / 2\pi \qquad (1.4)$$

1.4 Conditions for Nuclear Magnetic Resonance

1.4A The Classical Description of Nuclear Resonance

When a magnetic field $\vec{B}$ is applied to a spin system, $\vec{B}$ will produce a torque on the magnetic moment $\vec{\mu}$ of

amount $\vec{\mu} \times \vec{B}$. Because of its angular momentum $\vec{J}$, the spin will follow a motion according with Newton's law.

$$\text{i.e.} \quad \frac{d\vec{J}}{dt} = \vec{\mu} \times \vec{B} \qquad (1.5)$$

Since $\vec{\mu} = \gamma \vec{J}$, we may eliminate $\vec{J}$, getting

$$\frac{d\vec{\mu}}{dt} = \vec{\mu} \times (\gamma \vec{B}) \qquad (1.6)$$

This equation, which holds regardless of whether or not $\vec{B}$ is time dependent, tells us that at any instant the changes in $\vec{\mu}$ are perpendicular to both $\vec{\mu}$ and $\vec{B}$. In Fig. (1.2) the angle θ between $\vec{\mu}$ and $\vec{B}$ does not change. If $\vec{B}$ is independent of time, the vector follows the surface of a cone.

In order to understand the pulse technique, and some theoretical analysis we introduce a rotating coordinate system (9). Thus, we can rewrite equation (1.6) in terms of a coordinate system rotating with an as yet arbitrary angular velocity $\vec{\Omega}$ about B

$$\frac{\delta \vec{\mu}}{\delta t} + \vec{\Omega} \times \vec{\mu} = \vec{\mu} \times \gamma \vec{B} \qquad (1.7)$$

In the equation (1.7), $\frac{\delta \mu}{\delta t}$ represents the time derivative of μ in the rotating coordinate system and $\vec{\Omega} \times \vec{\mu}$ is an additional term, to take into account the rotation of the system with respect to the laboratory

system. Rearranging equation (1.7), we have

$$\frac{\delta \vec{\mu}}{\delta t} = \vec{\mu} \times (\gamma \vec{B} + \vec{\Omega}) \qquad (1.8)$$

This equation tells us that the motion of $\vec{\mu}$ in the rotating coordinate system obeys the same equation as in the laboratory system, provided we replace the actual magnetic field $\vec{B}$ by an effective field $\vec{B}_{eff}$

$$\vec{B}_{eff} = \vec{B} + \frac{\vec{\Omega}}{\gamma} \qquad (1.9)$$

If $\vec{B}$ is a static field, $\vec{B}=\vec{k}\ B_o$, it is possible to make Beff=0 if $\vec{\Omega} = -\gamma\ B_o\ \vec{k}$. Since in this reference frame $\frac{\delta \mu}{\delta t} = 0$, μ remains fixed with respect to the rotating frame. In other words, rotates at an angular velocity $\vec{\Omega} = -\gamma\ B_o\ \vec{k}$ with respect to the laboratory. The angular frequency $\gamma\ B_o$ is called the "Larmor frequency".

When a small magnetic field $B_x\ (t) = B_{xo} \cos \omega\ t$ is applied at right angles to the main field B_o, the effect will be a change in the angle θ between $\vec{\mu}$ and $\vec{B}$. It can be understood by resolving $B_x\ (t)$ into two rotating components, each of amplitude B_1, one rotating clockwise in a plane perpendicular to $\vec{B}$ and the other counterclockwise (see Fig (3)), thus their frequencies are $\pm\omega$. If ωz is used to represent both frequencies the rotating magnetic fields B_R, B_L can be written

$$\vec{B}_1 = B_1 \quad [\vec{i}\cos \omega zt + \vec{j} \sin \omega zt] \qquad (1.10)$$

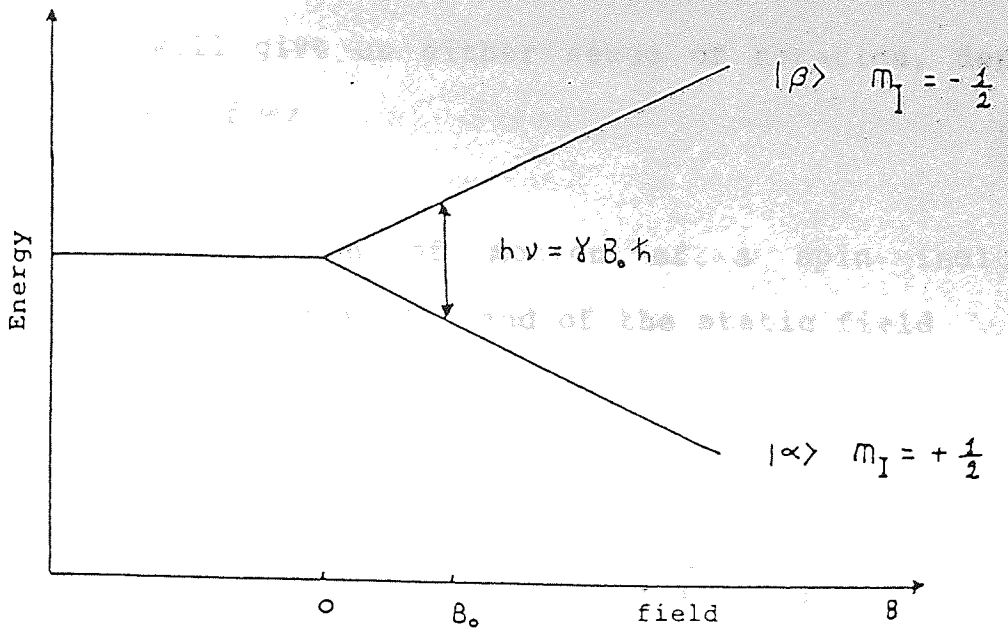

Figure 1.1 Proton spin levels in a magnetic field

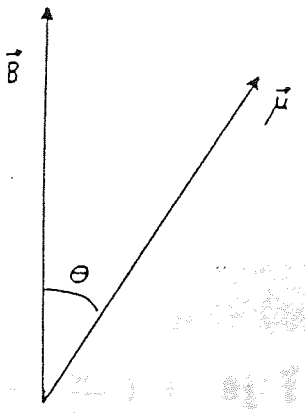

Figure 1.2 Relation of $\vec{\mu}$ to $\vec{B}$

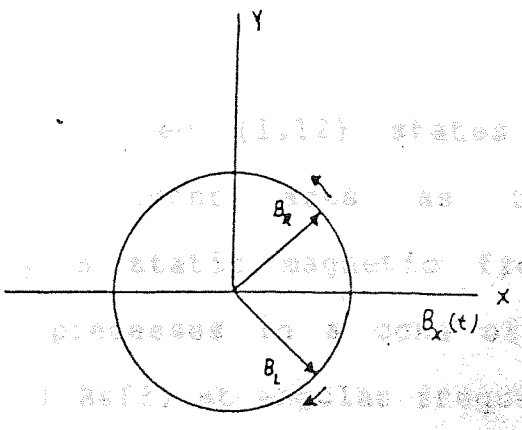

Figure 1.3 Decomposition of a linear oscillating field into two rotating elements

which will give us either sense of rotation, depending on the sign of ω_z

The equation of motion of a spin including the effects both of B_1 (t) and of the static field $\vec{B}_o = \vec{K}\ B_o$ is

$$\frac{\delta \vec{\mu}}{\delta t} = \vec{\mu} \times [\vec{k} (\omega_z + \gamma B_o) + \vec{i}\ \gamma B_1] \qquad (1.11)$$

We can write eq (1.11) as

$$\frac{\delta \vec{\mu}}{\delta t} = \vec{\mu} \times \gamma \vec{B}_{eff} \qquad (1.12)$$

where

$$\vec{B}_{eff} = \vec{K} (B_o - \frac{\omega}{\gamma}) + B_1 \vec{i} \qquad (1.13)$$

when

$$\omega_z = -\omega$$

Physically, eq (1.12) states that in the rotating frame, the moment acts as though it experienced effectively a static magnetic field Beff. The moment, therefore, precesses in a cone of fixed angle about the direction of Beff, at angular frequency γ Beff.

In standard continuous wave NMR experiments, there is a coil which produces the B_x (t) field at the Larmor

frequency; it means according to eq (1.13) that the effective field at "resonance" is $\vec{B}_{eff}=B_1\vec{i}$. As a result, the magnetic moment $\vec{\mu}$, will rotate around $\vec{B}_1$ by $\theta = \gamma B_1 \Delta t$, where Δt is the time in which B_x is on. This change can be detected by using another coil in the y axis. In pulse experiments, it is sometimes convenient to use a 90° pulse or 180° pulse, which means that B_x (t) is applied for a time $\Delta t = \frac{\pi}{2} (\gamma B_1)^{-1}$ or $\pi (\gamma B_1)^{-1}$. As a result, $\vec{\mu}$ will lie on the xy plane or in the -z direction, respectively. But for $t > \Delta t$, the orientation of $\vec{\mu}(t)$ will tend to the equilibrium value.

1.4 B Quantum Mechanical Description of Nuclear Magnetic Resonance.

When a nucleus of total spin I is placed in a magnetic field B_o acting along the z direction, the stationary - state wave functions may be labelled by m, the component of I in the z direction. If, in addition, we have an oscillating magnetic field in the x direction with amplitude $B_{xo} = 2 B_1$ and frequency $\omega = 2\pi\nu$, there will be an extra term in the Hamiltonian

$$\mathcal{H}' = 2 \mu_x B_1 \cos 2\pi \nu t \qquad (1.14)$$

Using the relation between the nuclear magnetic moment μ and its spin I, this may also be written

$$\mathcal{H}' = 2 \gamma \hbar B_1 I_x \cos 2\pi \nu t \qquad (1.15)$$

By the usual transition probability theory (10), this may give rise to a transition between two states m and m' corresponding to absorption or emission of radiation. The probability for such a transition is

$$P_{mm'} = \gamma^2 B_1^2 \, | (m' | I_x | m) |^2 \, \delta(\nu_{mm'} - \nu) \quad (1.16)$$

where δ is the Dirac function, $(m' | I_x | m)$ is the quantum-mechanical matrix element of Ix between states m and m', and $\nu_{mm'}$ is the frequency corresponding to the energy gap between these states

$$\text{i.e.} \quad h\nu_{mm'} = \frac{|m - m'|}{I} \mu B_o \quad (1.17)$$

It is well known (8) that the matrix element $(m'|Ix|m)$ vanishes unless $m'=m\pm1$, so that we immediately derive the selection rule that only transitions in which the quantum number m is changed by $\pm$ 1 can occur i.e. $h\nu_{mm'}=\pm\hbar\gamma B_o$. It is noted that equation (1.16) predicts absorption only if the frequency ν exactly coincides with the natural frequency $\nu_{mm'}$.

The complete quantum - mechanical theory of the motion of a magnetic moment in a variable magnetic field was considered by Schwinger(11) and Rabi(12), using the time dependent Schrodinger equation. When a small rf magnetic field is applied to the spin system(13), it can be seen

that the expectation value $\langle \mu_z (t) \rangle$ behaves as in the classic case

$$\langle \mu_z (t) \rangle = \langle \mu_z (o) \rangle \cos \gamma B_1 t \qquad (1.18)$$

1.5 The Population of Spin States

The absorption coefficients obtained in optical spectroscopy are independent of the intensity of the radiation source. Normally, a rapid return is made from the excited to the ground state, the liberated energy being dissipated as heat.

In nuclear magnetic resonance spectroscopy the intensity of irradiation (B_1) may weaken the absorption signals or cause them to disappear entirely. The situation is a consequence of the non-equilibrium of a nucleus with its surrounding lattice. In the case of a liquid, the nucleus may remain in a state of non-equilibrium for periods of a few seconds.

Whilst for most of the electromagnetic spectra the probability of stimulated emission induced by irradiation is negligible, for nuclear magnetic resonance it is large (14) and in comparison the probability of spontaneous emission is negligible (15). Because of this, irradiation with an intense radiofrequency field would rapidly equalise the population of the energy levels.

Nevertheless, there is a very good reason why resonance experiments are always carried out at as high a value of B_1 as possible. When radiation of frequency ν falls on a specimen containing hydrogen atoms it is not only possible for the radiation to be absorbed and excite a proton from the lower energy level to the higher one but it can also stimulate a proton which is already in the higher level to fall down to the lower level and, in so doing, to emit an additional quantum of the same frequency.

Einstein showed quite early in radiation theory that the coefficients for absorption and stimulated emission were, in fact equal and if there were equal numbers of protons in the lower and upper levels there would be just as many moving up, under the influence of the incoming radiation, as there were coming down, and hence there would be no net effect whatsoever.

The only reason why there is any net absorption of radiation during resonance is that, at equilibrium, there are more protons in the ground state than in the excited level and hence, there will be a slightly greater number being excited up from the lower level, than are being stimulated to fall down from the higher level. So, the intensity of the absorption signal will depend crucially on the difference in population between the two energy levels, and for most normal systems in equilibrium at absolute temperature T, there is a Boltzmann distribution

between the number of participants N_β in the higher and N_α in the lower of two energy states. The relative population is

$$\frac{N_\beta}{N_\alpha} = \exp\left(-\frac{\Delta E}{KT}\right) \qquad (1.19)$$

where $\Delta E = 2\mu B$, then

$$\frac{N_\beta}{N_\alpha} \approx 1 - \frac{2\mu B}{KT} \qquad (1.20)$$

Thus, hydrogen nuclei in a field of one Tesla have an excess population in the lower state of $N_\beta / N_\alpha \approx 7.10^{-6}$.

The observation of nuclear magnetic resonance depends upon the net absorption of energy by this small excess population. Under certain circumstances NMR signals may disappear as the excess number of nuclei in the lower state tends to zero, this phenomenon being known as saturation. It is apparent that in order to maintain an excess of nuclei in the lower energy state, some mechanism must exist whereby nuclei can return from the higher to the lower energy after resonance.

1.6 Magnetic Relaxation

If we perturb a physical system from its equilibrium condition and then remove the perturbing influence, the system will return to its original equilibrium condition. It does not return instantaneously, however, but takes a finite time to readjust to the changed

conditions. The system is said to undergo relaxation and this usually occurs exponentially. In the case of a spin system, we have already mentioned the relaxation times T_1, T_2, where T_1 is the spin lattice relaxation time and represents the exchange of energy between the spin system and the lattice. T_2 is the spin-spin relaxation time which is related to the lifetime of an excited state. These two processes will now be outlined briefly.

1.6 A Spin Lattice Relaxation

This process is based upon an interaction between spins and their surroundings, commonly referred to as the lattice. If transitions are induced by application of a radiofrequency field at resonance, the equilibrium populations are perturbed in that a net number of spins are promoted to the higher energy level. In other words, the net energy of the spin system has increased. In order to return to thermal equilibrium the excess energy has to be dissipated. This is brought about by an energy exchange between the spin system and the lattice. The excited ("hot") spins are cooled by the thermal bath they are immersed in i.e., the lattice. Since the spins are isolated from the lattice, the mutual interaction is small and consequently the time constant for the process leading to a restoration of equilibrium is long.

Another way of looking at this process involves the macroscopic spin magnetization, i.e., the vector sum of

oriented spins. In the absence of an external field there is no net magnetization because the spins are randomly oriented. Only if placed in a static field will spins eventually line up, some parallel to the field, some antiparallel, with a slight predominance of the former. The vector sum of individual magnetic moments is the magnetization which consequently points along the field axis. However, this polarization does not take place instantaneously when the sample is placed in the field but with a certain time constant. In most cases the magnetization builds up exponentially with a time constant equal to the longitudinal relaxation time T_1, as illustrated in Fig. (1.4a). Likewise, if the spin system has been subjected to a strong saturating r.f. field, the return towards thermal equilibrium takes place with a time constant T_1.

1.6.B. Spin-Spin Relaxation

This form of relaxation results from interactions among the spins themselves. In the absence of r.f. field, the spins precess about the external field axis with their phases at random. There is, consequently, no net magnetization perpendicular to the main field (transverse magnetization). Let us suppose a r.f. field is applied at resonance with the precessing spins . If the time of application of the field is long enough, the individual magnetic moments are polarized along the axis of this rotation field and a net transverse magnetization

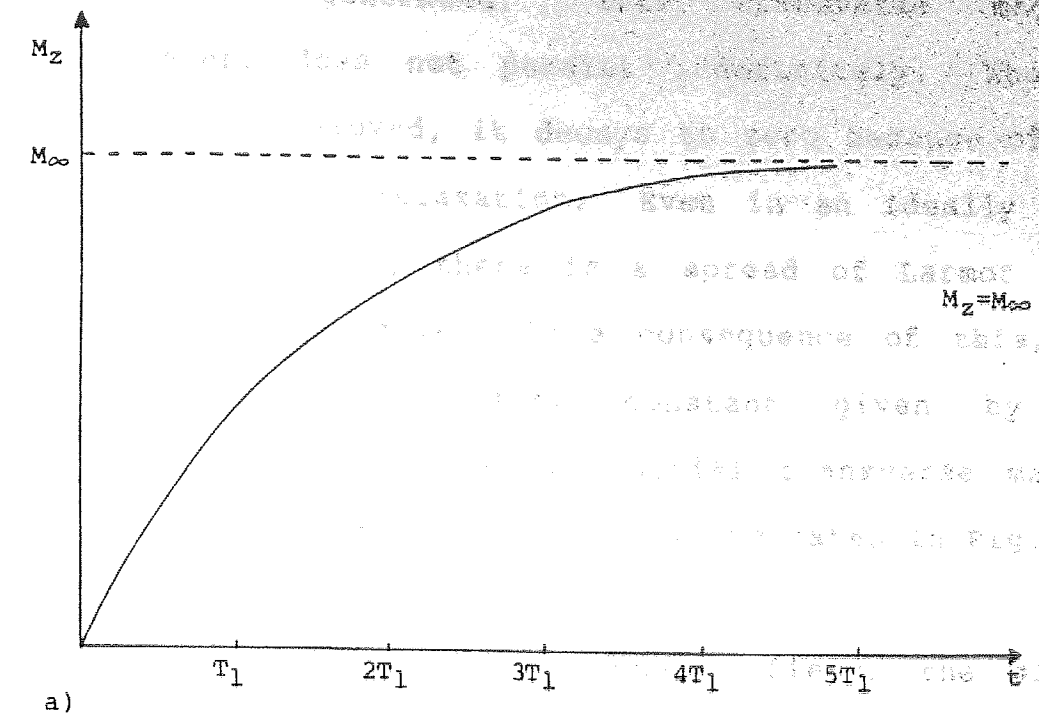

a)

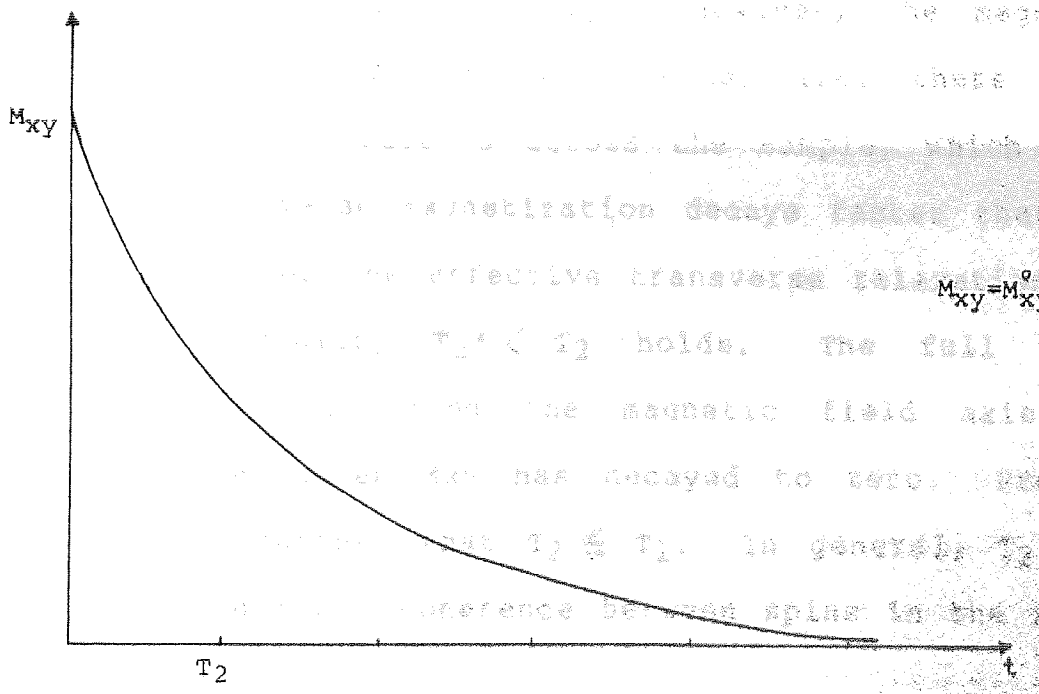

b)

Figure 1.4
a) Recovery of the longitudinal magnetization M_z towards its thermal equilibrium value M_∞
b) Decay of an initial transverse magnetization towards its equilibrium value zero

Mxy is generated. This transverse magnetization, however, does not persist indefinitely. When the r.f. field is removed, it decays to zero because of transverse or spin-spin relaxation. Even in an ideally homogeneous magnetic field, there is a spread of Larmor frequencies across the sample. As a consequence of this, the spins dephase with a time constant given by T_2. The exponential decay of an initial transverse magnetization $\mathring{M}xy$ as a function of time is illustrated in Fig. (1.4b).

In a perfectly homogeneous field, the slow passage width of a resonance line is inversely proportional to T_2; i.e. $\Delta \nu\, {}^1/_2 = {}^1/(\pi\ T_2)$. However, the magnetic field is never perfectly homogeneous, i.e. there are always transverse gradients across the sample, which means that the transverse magnetization decays faster than predicted by T_2. For the effective transverse relaxation time T_2^*, the inequality $T_2^* < T_2$ holds. The full equilibrium magnetization along the magnetic field axis can only build up after Mxy has decayed to zero. From this it follows further that $T_2 \leq T_1$. In general, T_2 is a time in which phase coherence between spins in the xy plane is lost.

1.7 Saturation and Relaxation Effects

The interaction between the nuclear system and the lattice is responsible for maintaining an absorption signal. If no such interaction occurred, the number of

nuclei in the upper level would rapidly become equal to that in the lower level as absorption of the incoming radiation raised their energy. If such equality were produced no further absorption would take place. Also, if the power of the incoming radiation is high, it may drive nuclei up to the higher level at a faster rate than the spin lattice relaxation interaction can restore thermal equilibrium, and again in this case the absorption will gradually decrease and the line will become broadened.

Fig. (1.5) shows the case of protons in an applied magnetic field and with two energy levels $|\alpha\rangle$, $|\beta\rangle$. If n is the difference in population, when the radiofrequency resonance radiation is applied we can write the rate of change of n as

$$dn/dt = (dn/dt)_{rf} + (dn/dt)_{SL} \qquad (1.21)$$

where $(dn/dt)_{rf}$ represents the rate of change due to a r.f. perturbation. If P is the stimulated transition probability $P = P_{\alpha\beta} = P_{\beta\alpha}$, then the rate of change of population of the $|\alpha\rangle$ state due to the radiation is

$$\frac{dN_\alpha}{dt} = N_\beta P_{\beta\alpha} - N_\alpha P_{\alpha\beta} \qquad (1.22)$$

therefore

$$\frac{dN_\alpha}{dt} = P(N_\beta - N_\alpha) \qquad (1.23)$$

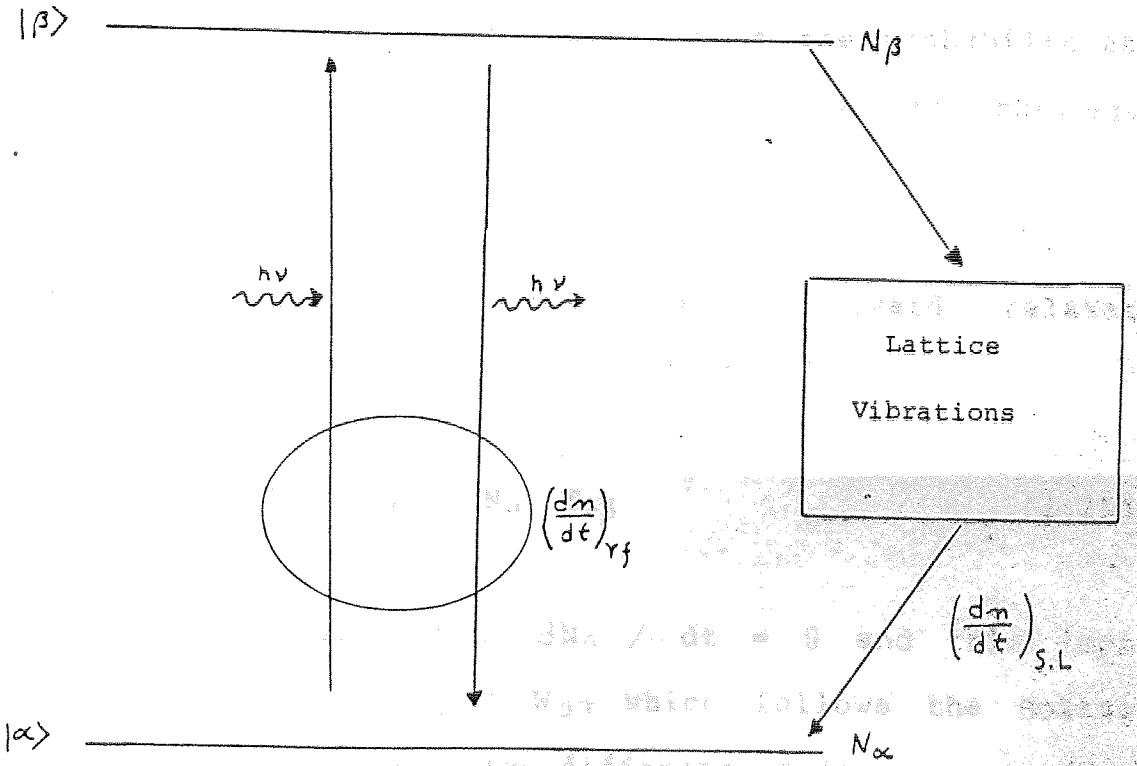

Figure 1.5 Saturation of resonance condition. The effects of the electromagnetic radiation and the spin lattice interaction are indicated schematically in the diagram.

then

$$\left(\frac{dn}{dt}\right)_{rf} = -2Pn \qquad (1.24)$$

where

$$n = N_\alpha - N_\beta$$

The term $(dn/dt)_{SL}$ in eq (1.21) originates in the lattice. The fundamental point is that the lattice is at thermal equilibrium, this means that the probabilities of spontaneous spin transitions up and down are not equal, as they were for r.f. induced transitions.

We denote the upward and downward relaxation probabilities by $W_{\alpha\beta}$ and $W_{\beta\alpha}$, then (16)

$$\frac{dN_\alpha}{dt} = N_\beta W_{\beta\alpha} - N_\alpha W_{\alpha\beta} \qquad (1.25)$$

At thermal equilibrium $dN_\alpha / dt = 0$ and this implies that $N_\beta^\circ / N_\alpha^\circ = W_{\alpha\beta} / W_{\beta\alpha}$ which follows the Boltzmann law. Then, the population difference n is

$$\frac{dn}{dt} = -\frac{(n - no)}{T_1} \qquad (1.26)$$

with

$$T_1^{-1} = W_{\alpha\beta} + W_{\beta\alpha} \qquad (1.27)$$

T_1 is the "spin lattice relaxation time". It is a measure of the time it takes for energy to be transferred to other degrees of freedom. The equation (1.21) can be rewritten as

$$\frac{dn}{dt} = -2\,pn - \frac{(n - no)}{T_1} \qquad (1.28)$$

and at equilibrium eq (1.28) becomes

$$n = \frac{no}{1 + 2\,PT_1} \qquad (1.29)$$

For protons, the probability P is[8]

$$P = \frac{1}{4}\,\nu^2\,B_1^2\,g\,(\nu) \qquad (1.30)$$

where $g(\nu)$ is the line shape function

A second relaxation time T_2, is defined as

$$T_2 = {}^1/_2\,g\,(\nu)\,\max \qquad (1.31)$$

The ratio n/no is known as saturation factor Z. When $g(\nu)$ is a maximum Z is minimum, i.e.,

$$Zo = [1 + \nu^2\,B_1^2\,T_1\,T_2]^{-1} \qquad (1.32)$$

The saturation effects produced by large values of T_1 and B_1, will not only reduce the actual power absorption, but also alter the line shape, showing its effect in the centre before the wings, and thus increasing the apparent width. This explains why it is so important to apply a low r.f. field B_1 in order to avoid saturation as much as possible.

1.8 The Bloch Equations

In 1946 Felix Bloch (17) proposed for the description of the magnetic properties of ensembles of nuclei in external magnetic fields a set of very simple equations derived from phenomenological arguments, that have proved for liquid samples at least, to be a correct quantitative description.

If $N\alpha$ spins and $N\beta$ spins are in the states α and β after the application of a magnetic field B_o, the z component of the bulk magnetic moment M is

$$Mz = \gamma \hbar \ (N\alpha - N\beta) \qquad (1.33)$$

or

$$Mz = \gamma \hbar \ n \qquad (1.34)$$

at equilibrium Mz will be

$$Mo = \gamma \hbar \ n_o = \chi_o B_o \qquad (1.35)$$

where χ_o is the magnetic susceptibility

$$\chi_o = \frac{N \gamma^2 \hbar^2 I (I+1)}{3 KT} \qquad (1.36)$$

According to eq (1.26) the relaxation of Mz now obeys the equation

$$\frac{dMz}{dt} = - \frac{(M_z - M_o)}{T_1} \qquad (1.37)$$

The transversal magnetization Mx, My will decay exponentially to zero after some period of time measured in terms of T_2, such that

$$\frac{d\,Mx}{dt} = - \frac{Mx}{T_2} \qquad (1.38)$$

$$\frac{d\,My}{dt} = - \frac{My}{T_2} \qquad (1.39)$$

In addition to the decay parameters, we have to consider the motion of the spins around the homogeneous field B_o; thus, according to the clasical equation of motion, eq. (1.6) we have,

$$\frac{d\vec{M}}{dt} = \gamma\,(\vec{M}x\,\vec{B}_o) \qquad (1.40)$$

which can be written as,

$$\frac{dMx}{dt} = \omega o\ My$$

$$\frac{d\,My}{dt} = -\omega o\ Mx$$

$$\frac{d\,Mz}{dt} = 0 \qquad (1.41)$$

Then, we must combine the effects of relaxation and Larmor precession into a new set of equations for $\vec{M}$. These are called the Bloch equations:

$$\frac{dMx}{dt} = \omega_o My - \frac{Mx}{T_2}$$

$$\frac{dMy}{dt} = -\omega_o Mx - \frac{My}{T_2} \qquad (1.42)$$

$$\frac{dMz}{dt} = -\frac{(Mz - Mo)}{T_1}$$

The spins perform a damped precession in which the rotating transverse components of M decay to zero with a characteristic time T_2, while Mz relaxes towards its equilibrium value M_o with a decay time T_1.

When an r.f. field is applied, the total field is $\vec{B}=B_o\ \vec{K}+\vec{B}_x(t)$, where $\vec{B}x$ can be expressed in the rotating frame x', y', z' as in the eq. (1.10). If we take only the circularly polarized r.f. field B_1, which rotates within the xy plane in the same sense as the Larmor precession

$$B_1 = B_1\ (\vec{i}\cos\omega t - \vec{j}\sin\omega t) \qquad (1.43)$$

The Bloch equations now become

$$\frac{d\vec{M}}{dt} = \gamma\ (\vec{M}X\vec{B}_o) + \gamma\ (\vec{M}\ X\ \vec{B}_1) - \frac{\vec{i}\ Mx + \vec{j}\ My}{T_2} - \frac{\vec{K}(Mz-Mo)}{T_1} \qquad (1.44)$$

where i, j, k, are the unit vectors in the laboratory frame. If we analysed the motion in a new coordinate system, rotating with the field B_1, at the frequency ω, we have, as Fig. (1.6) shows,

$$\vec{M}' = \vec{i}'u + \vec{j}'v + \vec{k}' Mz$$

$$\vec{B}_1' = \vec{i}' B_1 \qquad (1.45)$$

$$\vec{\omega}' = - \omega \vec{k}'$$

where $\vec{i}'$, $\vec{j}'$, $\vec{k}'$ are the unit vectors in the rotating frame.

To change M into M' in the Bloch equation we need

$$\frac{d\vec{M}}{dt} = \frac{\delta \vec{M}'}{\delta t} + \vec{\omega}' \times \vec{M}' \qquad (1.46)$$

The Bloch equation in the rotating frame is now given by

$$\frac{\delta \vec{M}'}{\delta t} = \gamma \vec{M}' \times (\vec{B}_o' + \vec{\omega}'/\gamma) + \gamma (\vec{M}' \times \vec{B}_1') - \frac{(\vec{i}'u + \vec{j}'v)}{T_2} - \frac{\vec{k}'(Mz - M_o)}{T_1} \qquad (1.47)$$

After separation of the three components of M' we obtain

$$\frac{du}{dt} = (\omega_o - \omega) v - \frac{u}{T_2}$$

$$\frac{dv}{dt} = - (\omega_o - \omega) u + \gamma B_1 Mz - \frac{v}{T_2} \qquad (1.48)$$

$$\frac{d\,Mz}{dt} = - \gamma B_1 v - \frac{(Mz - Mo)}{T_1}$$

In the steady state the stationary solutions of eq. (1.48) are

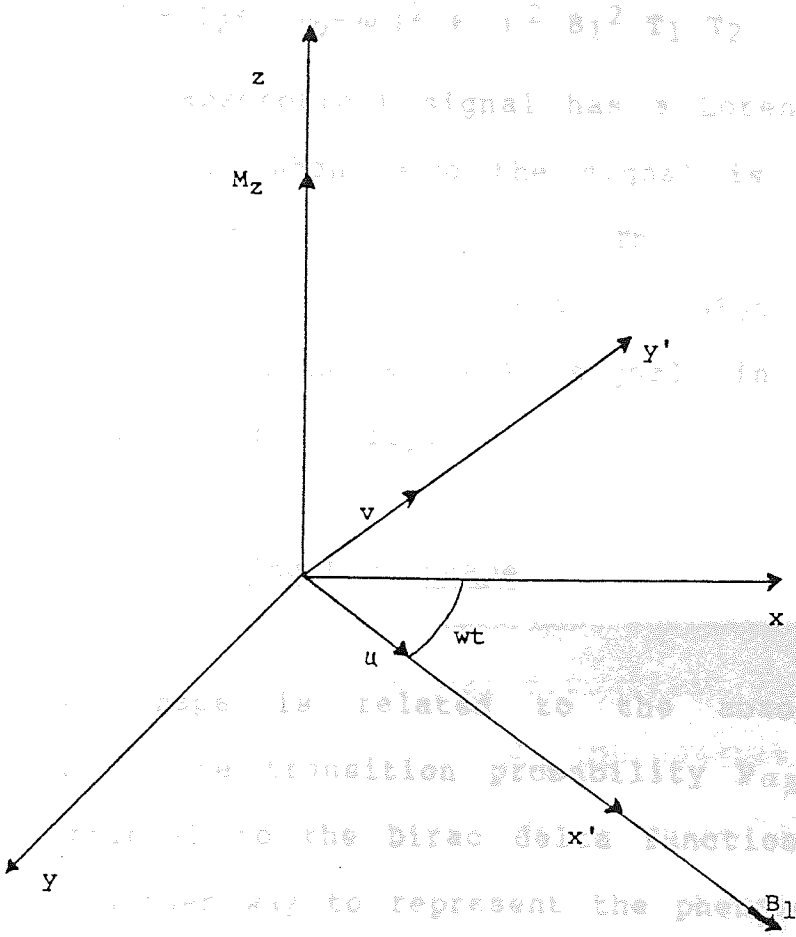

Figure 1.6 The rotating coordinate system

$$u = Mo \frac{\gamma B_1 T_2^2 (\omega_o - \omega)}{1 + T_2^2 (\omega_o - \omega)^2 + \gamma^2 B_1^2 T_1 T_2}$$

$$v = Mo \frac{\gamma B_1 T_2}{1 + T_2^2 (\omega_o - \omega)^2 + \gamma^2 B_1^2 T_1 T_2} \quad (1.49)$$

$$Mz = Mo \frac{1 + T_2^2 (\omega o - \omega)^2}{1 + T_2^2 (\omega_o - \omega)^2 + \gamma^2 B_1^2 T_1 T_2}$$

The v mode (absorption) signal has a Lorentzian line shape (17)(18)(19). When $\omega = \omega o$ the signal is at maximum and proportional to $\gamma B_1 T_2$. The u mode (dispersion) signal is mainly used, in high resolution spectroscopy to provide a lock signal in order to maximise the field homogeneity.

1.9 Factors Affecting Line Shape

The line shape is related to the absorption of energy, i.e. to the transition probability $P_{\alpha\beta}$. Since it is proportional to the Dirac delta function, we have to think in another way to represent the phenomenon. For that reason (8) a shape function $g(\nu)$ is introduced, which can be Lorentzian (liquids) or Gaussian (solids). The line width in a Lorentz line is $2/T_2$ where T_2 is the spin relaxation time which is included in the absorption function v obtained from the Bloch equations. In addition, a number of physical phenomena may contribute to the width of the resonance line. The parameter T_2 itself has many sources of interactions but can be expressed by

$$\frac{1}{T_2} = \frac{1}{T_2'} + \frac{1}{2T_1} \qquad (1.50)$$

where T_2' comes from energy fluctuations. Consequently, any mechanism affecting T_1 will affect T_2 and of course $T_2 < T_2'$ and $T_2 < 2T_1$. Because an inhomogeneous magnetic field can also affect the line width, the effective T_2 is expressed as(20).

$$\frac{1}{T_{2eff}} = \frac{1}{T_2} + \frac{1}{T_2^*} \qquad (1.51)$$

where

$$T_2^* = \frac{1}{\gamma \delta B_o}$$

and δB_o is the field inhomogeneity. In standard NMR experiments it is important therefore, to have very good field homogeneity and to keep the r.f. field low to avoid broadening effects. Spinning of the sample is very helpful in obtaining good resolutions.

There are also other contributions to line width, which will now be discussed.

1.9.A Dipolar-Dipolar Interactions

The magnetic field at a distance r from a dipole whose magnetic moment is μ depends on μ/r^3 Consequently, the total field acting on one dipole at a distance r from another, is

$$B = B_o \pm \frac{\mu}{r^3}\left[{}^1/_2 \left(3 \cos^2 \theta - 1 \right)\right] \qquad (1.52)$$

where θ is the angle between the r direction and Bo. Equation (1.52) will result in two lines, so the overall line shape has two maximums (21). This effect extended to a crystal can be expressed as a sum of terms like equation (1.52) in order to analyse the line shape through the use of second moments (22). In liquids, because of the random motion of the molecules the trigonometric term in equation (1.52) is averaged to zero.

1.9.B Spin-Spin and Spin-Lattice Relaxation

Because of the processes of spin-lattice relaxation which govern the decay of Mz, nuclear spin states have a finite lifetime. For a line whose width at half height is $\Delta\nu\,{}^1/_2$; it follows, because a nucleus remains in a given energy level no longer than T_1 on the average, from the Heinsenberg uncertainty principle that

$$\left(h\,\Delta\nu\,{}^1/_2 \right) T_1 \geq \hbar \qquad (1.53)$$

T_2 is related to the exchange between two nuclear dipoles, in which one dipole loses magnetic energy to another, which gains energy. Because this process places an uncertainty on the lifetime of a nucleus in a particular state, a similar equation to eq. (1.53) can be applied.

1.9.C The Effect of Paramagnetic Impurities

The presence of oxygen or other paramagnetic impurities, which produce strong local magnetic fields, will reduce the value of T_1. This results in a large broadening of the absorption line which may, in some cases, cause the peak to remain undetected. This implies that it is important to seal the NMR tubes under vacuum to avoid broadening of the lines due to oxygen, in particular, when high resolution spectra are required.

1.9.D Quadrupole Effects

Some muclei with $I > 1/2$ have an electric quadrupole moment eQ which occurs because the distribution of electric charge density $\rho(r)$ inside the nucleus is ellipsoidal rather than spherical. Such a quadrupole moment can interact with environmental electric field gradients to create a very efficient mechanism for spin-lattice relaxation. For reasons given earlier this gives rise to significant line broadening.

1.10 Chemical Shifts

Because of the rapid molecular motions, in liquid and gases, dipole-dipole interactions are usually averaged to zero and sharp NMR lines are observed. It is found that the exact frequency of the absorption line of a

particular nucleus depends on the nature of the molecule containing the nucleus. The frequency differences are referred to as chemical shifts. They arise because the magnetic field B actually experienced by the nucleus is not equal to the applied field B_o, but that modified by the fields produced by the field induced motion of the surrounding electrons in the molecule. In order to account for this effect, it is usual to write

$$B = B_o \ (1 - \sigma) \qquad (1.54)$$

where σ is the "magnetic shielding" factor or screening constant. The chemical shift between two nuclei i and j is strictly defined as

$$\delta_{ij} = \sigma_i - \sigma_j \qquad (1.55a)$$

however, because it is impractical to measure directly, chemical shifts are generally measured in terms of differences between the resonant fields or frequencies of the relevant absorptions. Usually, some compound with suitable properties is chosen as an arbitrary reference. Tetramethylsilane is often chosen as reference for both ^1H and ^{13}C spectra but dioxane, carbon disulfide are also used in the case of ^{13}C spectra, in practice, any compound suited to the problem in hand can be used as reference material. Chemical shifts are dimensionless p.p.m. units

$$\delta = 10^6 \times \frac{(\nu_{sample} - \nu_{standard})}{\nu_{standard}} \qquad (1.55b)$$

where $\nu_{standard}$ is the frequency at which the reference nuclei undergo resonance.

The chemical shift range of ^{13}C (250 ppm) is very much greater than that of protons (10 ppm) and ^{13}C resonances for a given molecule may be well resolved with the corresponding proton resonance overlap. The greater the number of resolved resonances, of course, the greater is the amount of information that can be extracted from the spectrum. Because the chemical shifts originate in molecular environment it is evident that they are an extremely powerful tool for the elucidation of molecular structure. The use of the chemical shift for this purpose probably still dominates the applications of nmr in chemistry, although the use of relaxation times, with which this thesis is concerned, is finding increased popularity.

1.10.A The Origins and Contributions to the Chemical Shift

According to the general theory of Buckingham and Pople (24), any suitably chosen equilibrium property of a

gas may be written as an inverse power series in the molar volume Vm. Thus for the magnetic screening constant σ, we have

$$\sigma = \sigma_o + \frac{\sigma_1}{Vm} + \frac{\sigma_2}{Vm^2} + \ldots\ldots \quad (1.56)$$

where σ_o is the screening constant of the isolated molecule and σ_1, σ_2, are parameters which depend on temperature but which are density independent. They refer to the screenings caused by binary, tertiary and higher order molecular interactions. Although it has been found that the terms higher than σ_1/Vm can usually be neglected the chemical shift respect to some reference is nevertheless composed of discrete intramolecular and intermolecular contributions. For a nucleus A, the total screening is:

$$\sigma^A = \sigma^A_{intra} + \sigma^A_{inter} \quad (1.57)$$

The two contributions can be subdivided [25][26]

$$\sigma^A_{intra} = \sigma^A_o = \sigma^{AA}_{dia} + \sigma^{AA}_{para} + \sum_{A \neq B} \sigma^{AB} + \sigma^A_{deloc} \quad (1.58)$$

$$\sigma^A_{inter} = \sigma_b + \sigma_a + \sigma_w + \sigma_E + \sigma_s \quad (1.59)$$

These terms will now be discussed in a general form.

1.10.B Intramolecular Contributions

1.10B$_1$ $\overset{AA}{\sigma}_{dia}$ The diamagnetic screening constant

When there is spherically symmetric circulation of electrons around the nucleus this leads to diamagnetic shielding, which reduces the field at the nucleus (25). Consequently, more field must be applied to satisfy the resonance condition, and signals move to higher applied field or to the right, on conventionally produced spectra. An increase in the electron density in the hydrogen 1s orbital causes an increased shielding.

1.10B$_2$ $\overset{AA}{\sigma}_{para}$ The paramagnetic screening constant

The paramagnetic contribution depends on the excited electronic states of the atom containing the resonant nucleus. The static field, B_o, tends to induce the mixing between the ground and excited electronic states which gives rise to electronic circulations that produce secondary paramagnetic fields, i.e., opposite to those responsible for $\overset{AA}{\sigma}_{dia}$. The nuclei are thus deshielded. The value of $\overset{AA}{\sigma}_{para}$ is difficult to evaluate accurately, requiring a knowledge of both the energy and wave function of the ground and excited electronic states of the molecule (13)

1.10 B_3 $\sum_{A \neq B} \sigma^{AB}$ Interatomic Shielding

The diamagnetic shielding of a proton by its 1s electron density is relatively small compared with the shielding of nuclei of heavier atoms that have filled inner shells. Therefore, additional effects such as the influence of magnetic dipoles at neighbouring atoms or groups, that can alter the local magnetic field responsible for the resonance frequency are much more significant in determining the shift of the proton resonance than that of heavier nuclei.

In the case of a diatomic molecule AB through the external field B_o a magnetic moment μ_A is induced at A, which is proportional to the magnetic susceptibility, χ_A, of A, if A is magnetically anisotropic, i.e., to an extent it can, according to its orientation cause a paramagnetic or a diamagnetic shift of the resonance frequency of the nucleus B. By means of the relation

$$\Delta \chi = \chi_{\parallel} - \chi_{\perp} \qquad (1.60)$$

the anisotropy of a group with an axis of symmetry is defined as the difference between the susceptibilities parallel and perpendicular to the axis of symmetry. The magnetic contribution to the chemical shift of individual protons can then be determined by the Mc Connell equation (27).

$$\sigma_{AB} = \Delta\chi (1 - 3 \cos^2 \theta) / 3R^3 \qquad (1.61)$$

where θ is the angle between the direction of μ_A and the A-B bond axis and R the distance between the centre of A and the nucleus of B.

1.10 B_4 $\hat{\sigma}_{deloc}$-The Delocalised Electron Screening Constant

The π electrons in the benzene ring represent the best example of long range shielding arising from current circulating within a molecule. Due to the dependence of the current upon the orientation of the molecule to the field, these effects do not average out with random tumbling but make the aromatic ring appear to be surrounded by a magnetic field. The field opposes the applied field within the ring and reinforces it in the plane of the ring outside the ring, as it is indicated in Figure (1.7)

1.10 C Intermolecular Effects

The screening term $\hat{\sigma}_{inter}$ arises from various effects due to the presence of a solvent surrounding the solute: here the terms solute and solvent are not used in a strict thermodynamic sense but solute refers to the material containing the resonant nuclei and solvent refers to all other material present.

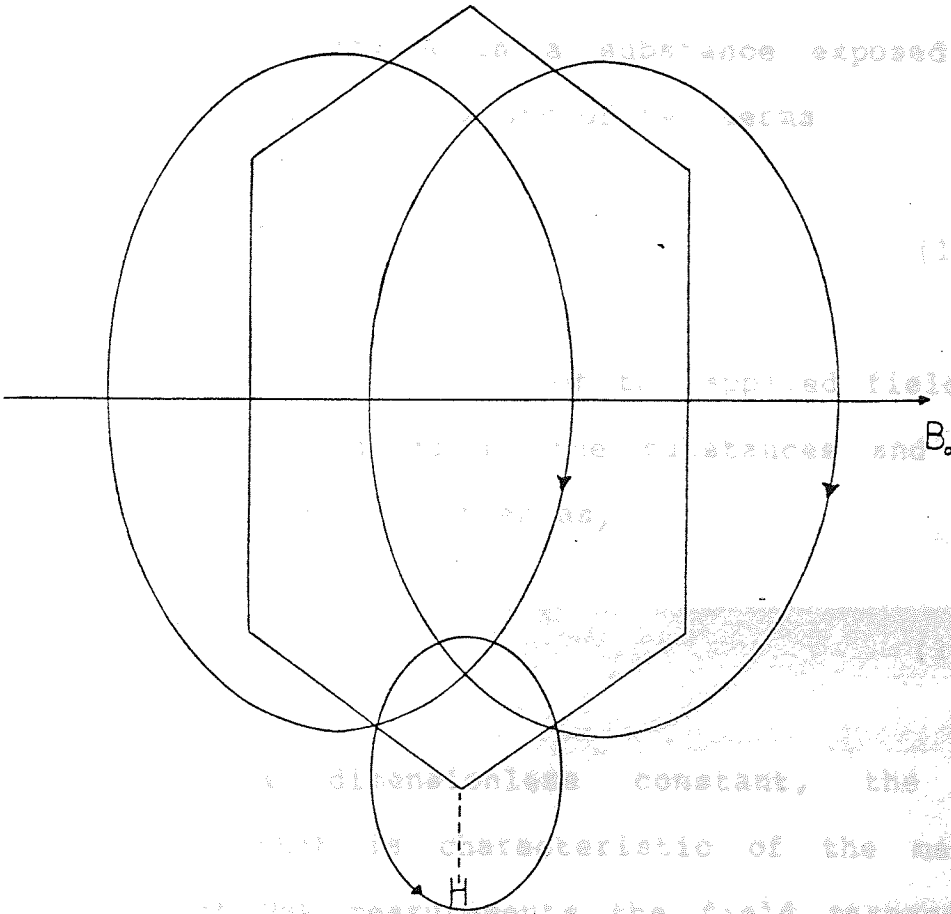

Figure 1.7 Free electrons ring currents in benzene

In a sense the term solute essentially refers to just the one molecule containing the resonant nucleus.

1.10 C1 The Bulk Susceptibility Screening Term

Following the classical electromagnetic equations the magnetic flux density B in a substance exposed to an external magnetic field consists of two terms

$$\vec{B} = \mu_o (\vec{H} + \vec{M}) \qquad (1.61)$$

where $\vec{H}$ is the field strength of the applied field, $\vec{M}$ is the magnetization induced in the substances and μ_o the permeability. $\vec{M}$ can be written as,

$$\vec{M} = \chi_v \vec{H} \qquad (1.62)$$

where χ_v is a dimensionless constant, the volume susceptibility, that is characteristic of the material. In the case of NMR measurements the field strength that exists within the nmr tube is influenced by the magnetic susceptibility of the solvent. For this reason an internal standard is employed. That is, the reference substance and the sample are contained in the same solution so that both are exposed to the same magnetic environment and correction of the experimental results is not necessary. On the other hand, with an external standard, when the reference substance is contained, usually, in a coaxial capillary separated from the volume

that contains the sample, the field strengths that exist in the capillary and the sample solution are different, because of the different volume susceptibilities and geometric configurations. The chemical shifts recorded must then be corrected (28). For an external reference contained in a sphere vessel the value of σ_b is $\sigma_b = 0$, but for a cylinder $\sigma_b = 2/3\,\pi\,\chi_v$. The correction for a cylindrical n.m.r. tube and cylindrical reference capillary, both of them with their axes perpendicular to the magnetic field is

$$\delta^{corr}_{S-R} = \delta^{exp}_{S-R} + \frac{2\pi}{3}\left(\chi_{VR} - \chi_{VS}\right) \qquad (1.63)$$

where the subscripts S and R refer to sample and reference, respectively.

1.10 C2 σ_A Anisotropy in the molecular susceptibility of the solvent

Aromatic solvents tend to cause high field shift to solute resonances (29)(30)(31). This has been interpreted by Bothner - By and Glick (30) in terms of the "disk" shape of these molecules combined with their large diamagnetic anisotropies. Benzene rings have large induced magnetic moments only when the ring is at right angles to the field; also their disk-like shape enables them to lie closer to the solute when its plane faces the solute molecule than when the edge faces the solute. Since the secondary magnetic field due to this induced

magnetic moment is proportional to the inverse third power of the separation, the first effect may be expected to dominate, leading to a mean distribution of the external field at the solute nucleus and a resulting shift to high field. Similarly, it is to be expected that rod-shaped solvent molecules, like carbon disulfide or acetylene, whose largest diamagnetic susceptibility is along the axis of the rod, would lead to low field shifts. The solvent cage model have been used by Homer and Redhead (32) to calculate the magnetic anisotropy screening constants of non-polar solutes in benzene and in carbon disulphide with good agreement with experimental values.

1.10 C3 σ_E The Electric Field Screening Constant

An electric field E acting along the axis of a bond to a resonant nucleus, for example, an X-H bond, tends to draw electrons away from the nucleus, thus causing a shift to low field (33). An approximate calculation shows that the screening arising from such electric fields is given by:

$$\sigma_E = -2 \times 10^{-12} E_Z - 10^{-18} E^2 \qquad (1.64)$$

where E_Z is the component of the total field E along the X-H bond. Buckingham (33) has developed a theory of polar solvent effects using the Onsager model. A

dissolved polar molecule polarizes the surrounding medium giving rise to an electric field, the reaction field E, at the solute.

In equation (1.64) E is, then

$$E = \frac{2\,(\epsilon_2 - 1)\,(n_1^2 - 1)}{3\,(2\,\epsilon_2 + n_1^2)} \cdot \frac{\mu_1}{\alpha_1} \cos\theta \qquad (1.65)$$

Where ϵ_2 is the dielectric constant of the medium, n_1 the refractive index of the solute as a liquid, μ_1 the dipole moment of the solute in gas phase, α_1 the polarizability of the solute and θ is the angle between the directions of the solute electric moment and the X-H bond. For this theory of the reaction field, the solute molecule is represented as a polarizable dipole at the centre of a spherical cavity in the solvent. More complex models for the reaction field calculation have been developed by Scholte [34] and Dekker [35]. P Diehl and R Freeman [36] have concluded that the shape of the molecule is an important factor in determining the magnitude of the reaction field and the consequent chemical shift.

1.10 C4 σ_s The Specific Screening Constant

The term "specific molecular interactions" is related to several effects [37][38], e.g. hydrogen-bonded, charge transfer, dipole-dipole, dipole-induced dipole interactions, etc. In some mixtures, e.g., $CHCl_3$ in $(CH_3)CO/C_6H_{12}$ there is evidence for the formation of collision

complexes that explains the observed shifts (39). In general, solvent effects on polar solutes have to be considered from the point of view of continuum theories and collision complex effects (40)(41). It is probably worth noticing that σ_s is usually used to accommodate any contribution to σ^{A}_{inter} that is not properly explained by theories appropriate to the other screening contributions to equation (1.59)

1.10 C5 σ_w. The Van der Waals Screening Constant

Interactions occur between molecules of any type which perturb their electronic structures, with the result that the distortion leads to a solvent-dependent nuclear screening constant. For non-polar isotropic solvents the only contribution to observed shifts, after correction for σ_b(42), are σ^{A}_{intra} and σ_w. By measuring gas-to-liquid shifts σ_{intra} can be eliminated and σ_w obtained explicitly.

In general, intermolecular forces are attributed to long range interactions between permanent dipoles, between permanent and induced dipoles and interactions arising from the mutual polarization of the electron clouds of neighbouring atoms or molecules (dispersion effect). In the absence of permanent dipoles the last is the sole contributor to the total attractive force. Stephen (43), and also Marshall and Pople (44), have shown that the shift due to the dispersion effect should

be proportional to the mean square field, i.e.,

$$\sigma = - B E^2 \qquad (1.66)$$

In their analysis of gas to solution shift Howard et al [45] have found in common with other workers that after making bulk susceptibility correction, the plot of δ vs E^2 does not pass through the origin, as expected; this criterion has been used to test several models used to characterize σ_w. Rummens [46] argues that one of the reasons for the failure of the continuum model used by Howard et al [45], and other workers, is that they considered that the first solvent shell has identical properties as the bulk solvent. Subsequently, De Montgolfier [47][48] modified the continuum approach, by assuming that the reaction field is not homogeneous over the solute and proposed that

$$\sigma = - K B \langle R^2 \rangle \qquad (1.67)$$

where R is the reaction field and K is a site constant.

Most molecular interaction theories and models use the centre of mass of the molecule to calculate the interaction potential governing the observed property. In NMR the measurements are made on the peripheral nuclei (^1H, ^{19}F) and this fact has to be taken into account. Accordingly, Rummens [49][50] considered it necessary to introduce a site factor to account for the off-centre

position of the resonant nucleus in the solute molecule and obtained good fit of experimental data to his theorem. It should be noticed,however, that a site factor has no place in normal continuum theory for which the solute is considered a point dipole at the centre of an Onsager cavity.

Homer and Percival (51) have developed a modification of conventional reaction field theory and argue that the solute molecule feels two reaction fields, one originated in the solute itself and the other generated by the solvent molecules (considered in the first solvation shell). This extra perturbation is a good help in explaining the gas to solution chemical shifts. However, the test mentioned above respecting equation (1.66) was still not found to be fulfiled. Consequently, they recognized that the use of the Onsager cavity (52) as a spherical exclusion zone for the solvent molecules has to be reconsidered. Consequently, they considered that the local environment of the solute nuclei should influence the nature of the solute-solvent collisions and have shown that, when these encounters are forced by steric constraints to be anisotropic, an additional square field generated by the solvent at the solute nucleus occurs. The Van der Waals screening constant is then represented by

$$\sigma_w = -B \left(\langle R_1^2 \rangle + \langle R_2^2 \rangle \right) - B \langle E^2 \rangle \qquad (1.68)$$

where R_1 and R_2 are the reaction fields generated by the solute molecule and the solvent molecules (on the first shell) and $\langle E^2 \rangle$ is the average electric field due to the pairwise close encounter of solute-solvent molecules. This term is called the "buffeting" term which we will detail at the end of this chapter. The theoretical model which leads to equation (1.68) predicts σ_w values well within the required order of magnitude and provides a consistent method of analysing experimental gas-to-solution chemical shifts.

1.11 Spin - Spin - Coupling

It has been found (53)(54) that chemically shifted peaks may themselves be composed of several fine structure lines. Gutowsky and Mc Call (54) have shown that fine structure may arise in any molecule containing two or more nuclei which resonate at different field strengths.

In addition to the magnetic fields that cause chemical shifts a nucleus i may also experience the fields associated with the presence of neighbouring spins. Theoretically, two mechanisms of interaction between the nuclear magnetic dipoles can operate, viz a direct through space interaction depending on the internuclear distances, and an indirectly transmitted one through the bonding electrons.

The direct coupling arises from the local magnetic field, generated by a nucleus j with magnetic moment μj, and spin $1/2$, on the nucleus i situated at a distance r from j. If θ is the angle between $\vec{r}$ and $\vec{B}_o$, and the $\pm$ sign refers to the spin state of j, the local field is given by (55)

$$B_{loc} = \pm \frac{\mu o \ \mu j}{4 \pi r^3} \ (3 \cos^2 \theta - 1) \qquad (1.69)$$

The numerous dipolar couplings which exist in a solid explain the very broad band observed. However, in the liquid state the molecular motions are fast, and θ fluctuates isotropically, so that the average value of B_{Loc} tends to zero. The fine structure observed in the spectra of liquids actually results from through-bond or indirect coupling, which cannot be averaged out to zero by molecular motion. Such coupling involves several types of electron-nucleus interactions and is a somewhat complicated function of electronic distribution in the intermediate bonds. These interactions lead to the spectral fine structure which is characterized by the spin-spin coupling constant J. Two basic types of spectra may be observed, namely, first order spectra and second order spectra that arise when the respective conditions δ_{AX} (Hz) $\gg$ J_{AX}(Hz) and δ_{AB}(Hz) $\approx$ J_{AB} (Hz) are obeyed. When the former condition holds the nuclei are identified by letters at the extreme of the alphabet, e.g., AX but when the latter condition holds letters similarly placed in the alphabet are used, e.g., AB.

Consequently, some important characteristics of the spin-spin coupling are:

(a) coupling is not observed between groups of magnetically equivalent nuclei. Nuclei are magnetically equivalent if in addition to being chemically equivalent they individually couple identically to each other nucleus in a molecule.

(b) The coupling constant is independent of the strength of the applied magnetic field (56).

(c) The magnitude of the coupling constant between two nuclei generally increases with the atomic number of both nuclei. In hydrogen resonance, typical values of the coupling constants ($J_{HH'}$) are of the order of 10 Hz. For ^{13}C spectra, however, J ^{13}C-H can be about 200 Hz. In general, for isotopic substitution the two coupling constants are related through the magnetogyric ratios

$$\frac{J_{NK}}{J_{NL}} = \frac{\gamma k}{\gamma_L} \qquad (1.70)$$

(d) The magnitude of the coupling constant J_{AX} normally decreases as the number of bonds separating A and X increases.

(e) The coupling constant is independent of temperature.

Consistent with these characteristics it has been suggested(58) that the coupling mechanism is mainly related to the bonding electrons. The spin of a nucleus A interacts with the electrons in several ways, one of

the most important being the contact coupling a.I.S, which tends to align the spins of the electrons of A antiparallel to the nuclear spin. As the directions of the electron spins in different parts of the molecule are coupled via the chemical bonds, the electron spin polarization at A is accompanied by a slight excess of α or β electrons near the other nucleus B which orients its spin antiparallel or parallel to that of A.

The simple coupling mechanism is described by the coupling Hamiltonian

$$\mathcal{H} = J.I_1.I_2 \qquad (1.71)$$

where J is the coupling constant, and I_1, I_2 the spins involved in the coupling. When the coupling is between equivalent spins as in CH_3-CHO, where O takes no part in the coupling, the quantum mechanic analysis of the system[16] shows that there are only two lines for the methyl protons at frequencies

$$\nu = \nu_o \ (1- \sigma_{CH3}) \mp {}^1/_2 \ J \qquad (1.72)$$

which reflect the orientations of the aldehyde proton. The aldehyde proton makes transitions at the frequency

$$\nu = \nu_o \ (1- \sigma_H \ ) + J \ M_{CH3} \qquad (1.73)$$

where $M_{CH3} = m_1 + m_2 + m_3$ and m_1, m_2, m_3 are quantum numbers. There are four possible lines caused by the arrangement of the methyl proton spins, as it is shown below,

$$\begin{array}{ll} \alpha\ \alpha\ \alpha & M_{CH_3} = \frac{3}{2} \\ \alpha\beta\alpha,\ \alpha\alpha\beta\ ,\ \beta\alpha\alpha & M_{CH_3} = \frac{1}{2} \\ \beta\beta\alpha\ ,\ \alpha\beta\beta\ ,\ \beta\alpha\beta & M_{CH_3} = -\frac{1}{2} \\ \beta\ \beta\ \beta & M_{CH_3} = -\frac{3}{2} \end{array} \qquad (1.74)$$

In general, for first order spectra (second order spectra being beyond the scope of this thesis) arising from n_A nuclei with spin I_A and n_X nuclei of spin I_X the A resonance has $2n_X(I_X + 1)$ lines while the X resonance has $2n_A(I_A + 1)$ lines. The relative intensities of lines in each band, say A, depend on the number of times each value of m occurs for the other nucleus. Thus for spin $I = 1/2$ nuclei, n_X equivalent nuclei will cause $n_X + 1$ lines to be seen in the A resonance and these will have the relative intensity distribution.

$$1,\ n,\ \frac{n(n-1)}{2!},\ \frac{n(n-1)(n-2)}{3!},\ \ldots\ldots$$

Evidently, these rules coupled with the fact that the magnitude of J is governed by intramolecular electron

distribution results in spin-spin coupling providing a wealth of information about molecular structures.

The analysis of spectra by means of the simple rules given above applies only to systems which have a chemical shift large compared with the coupling constant ($\delta \gg J$). When two groups of nuclei are separated by a chemical shift which is of same order of magnitude as the coupling constant ($\delta \approx J$), then the spectrum does not obey the rules for multiplicity and relative intensity given above. A more complex, second order pattern is obtained which requires a more detailed, quantum mechanical analysis and perhaps the use of a suitable computer programe.

1.12 The Buffeting Interaction Term

In section 1.10 C5 attention was directed to a recently proposed contribution to Van der Waals forces between molecules, and its effect on chemical shifts. The present section attempts to present the theoretical background to this so-called buffeting effect. The reason for devoting particular attention to this is to lay the foundation for studies subsequently described in this thesis which attempt to establish if the buffeting interaction influences spin-lattice relaxation times as well as chemical shifts. In equation (1.68) the buffeting term was generated by an average electric field which arises from the electronic oscillations

constituting the solvent dipole[59][60]. When a solvent molecule collides with a solute molecule, the collision can occur in several directions respect to the bond containing the resonant nucleus in the solute molecule. If the bond is equally symetrical as for C-H it is convenient when calculating the effective square field E^2 required for equation (1.75)

$$\sigma_{BI} = - B \langle E^2 \rangle \qquad (1.75)$$

to consider [51] an octant of space centred at the solute resonant hydrogen nucleus. On a time average the moment $\bar{m}$ on an incoming peripheral atom of the solvent, can be considered to be along an axis at an angle of 54° 44' to each of the three coordinate axes of any chosen cartesian system.

The electric field $\vec{E}$, produced at the solute atom is given by

$$\vec{E} = 3 \frac{(\vec{m}. \vec{r})\, \vec{r}}{r^5} - \frac{\vec{m}}{r^3} \qquad (1.76)$$

where r is the distance from the spontaneous dipole $\vec{m}$ to the solute hydrogen nucleus.

If it is assumed [51] that:

a) The average position of the solvent atom may be considered to reside successively for equal times on each solute axis.

b) Each of the moments $\vec{m}_x'$, $\vec{m}_y'$, $\vec{m}_z'$, from the solvent are effective at the same time on each solute axis for $1/3$ of time in one octant.

c) In an anisotropic situation, when the solute atom is approached along directions parallel or perpendicular to the C-H bond, the corresponding electric fields generated by the solvent atom are modulated by factors β and α respectively ($0 \leq \beta \leq 1$ and $0 \leq \alpha \leq 1$). Then, by using equation (1.76) on each axis x,y,z, of figure (1.8), it follows that

$$\vec{E}_x = \alpha\ (2\ \vec{m}_x' - \vec{m}_y' - \vec{m}_z')\ r^{-3}$$

$$\vec{E}_y = \alpha\ (2\ \vec{m}_y' - \vec{m}_x' - \vec{m}_z')\ r^{-3} \qquad (1.77)$$

$$\vec{E}_z = \beta\ (2\ \vec{m}_z' - \vec{m}_x' - \vec{m}_y')\ r^{-3}$$

where $\vec{E}_z$ is the field generated on H when the dipole $\vec{m}$ is approaching H from the z direction. The average electric field in one octant over all time is

$$\vec{E}_{av} = \frac{(2\beta - 2\alpha)}{6r^3}\ (2\ \vec{m}_z' - \vec{m}_x' - \vec{m}_y') \qquad (1.78)$$

Finally, the total field can be written [51] as

$$\vec{E}^2_{TOT} = \frac{k}{r^6}\ (2\beta - \zeta)^2 \qquad (1.79)$$

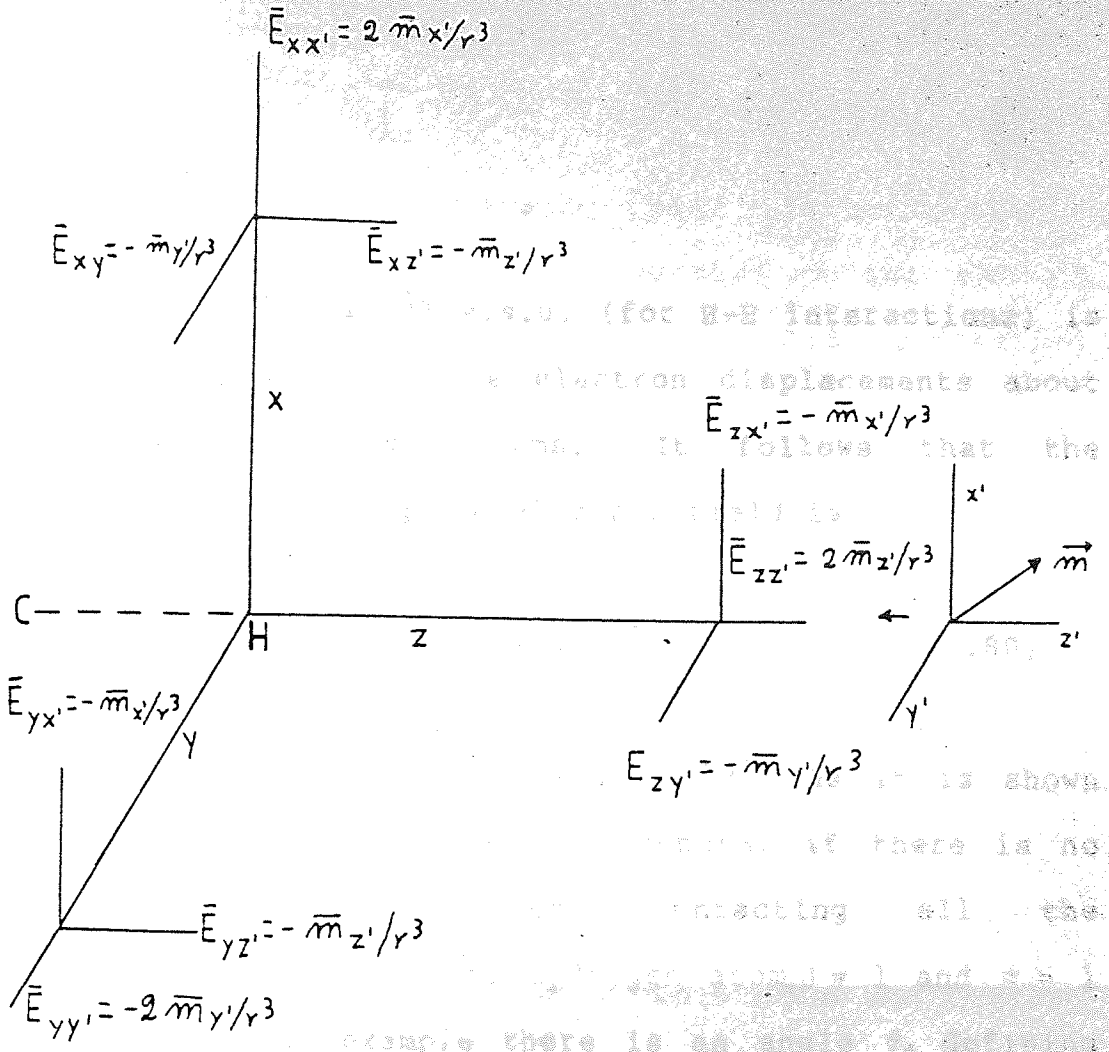

Figure 1.8 Time average electric field with respect to encounters parallel and perpendicular to the axis of the C-H bond.

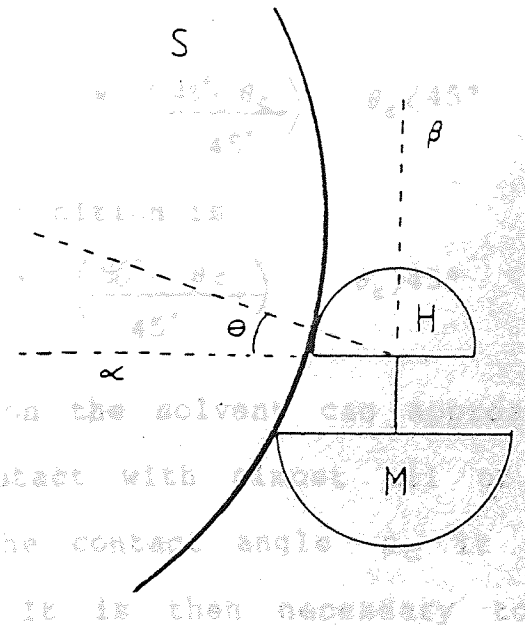

Figure 1.9 Two dimensional representation of a methane molecule encountered by an isotropic molecule S

with

$$\xi = 2\alpha$$

where $K = 1.377 \times 10^{-34}$ e.s.u. (for H-H interactions) is a constant depending on the electron displacements about the peripheral solvent atoms. It follows that the screening due to this square electric field is

$$\sigma_{BI} = - \frac{B.K}{r^6} (2\beta - \xi)^2 \qquad (1.80)$$

The parameters β , α are defined (51) as it is shown in Figure (1.9) for methane. In general if there is no restriction on the solvent contacting all the hemispherical surface of the hydrogen atom, $\beta = 1$ and $\alpha = 1$ but in the present example there is an angle θ_c defining a region of no contact and implicitly indicates some anisotropy in the collisional process. In this case

$$\beta_c = 1 \quad \text{and} \quad \alpha_c = \left(\frac{45^\circ - \theta_c}{45^\circ}\right) \qquad \theta_c < 45^\circ \qquad (1.81)$$

for $\theta_c > 45^\circ$ the definition is

$$\alpha_c = 0 \qquad \beta_c = \left(\frac{90^\circ - \theta_c}{45^\circ}\right) \qquad \theta_c > 45^\circ \qquad (1.82)$$

During collision the solvent can approach the solute atom and make contact with almost all of the hydrogen surface, but at the contact angle θ_c it starts to get out of contact. It is then necessary to consider an average distance modulation defined as

$$R_{AV}^{-6} = \frac{\int_{r_c}^{r'} r^{-6}\, dr}{\int_{r_c}^{r'} dr} \qquad (1.83)$$

where r_c is the contact distance and r' is the distance over which the influence of $\vec{m}$ operates during the no contact portions of α or β. The total modulation parameters are

$$\beta_T = \beta_c + (1- \beta_c)\ R_{AV}^{-6} / r^{-6} \qquad (1.84)$$

$$\xi_T = \xi_c + (2- \xi c)\ R_{AV}^{-6} / r^{-6}$$

where

$$\xi_T = 2\ \alpha_T$$

These are the parameters to enter in equation (1.80) in order to evaluate the screening effect. The calculation of β and ξ is conveniently effected using models of the molecules involved.

The buffeting interaction has proved to be an invaluable contribution to the understanding of the Van der Waals screening term and it has been suggested (51) that it may well be applicable to other problems in Chemistry.

1.13 Investigation To Be Performed In This Thesis

Although a common opinion may be that the contemporary level of understanding of spin-lattice relaxation times is adequate, it has to be acknowledged

that inadequacies in existing theories do exist. The intention in this thesis is to evaluate existing theories for relaxation times and identify any areas of weakness with a view to strengthening them. Consequently, having now introduced most of the basic principles of N.M.R., some of the experimental and theoretical tools necessary to the work described later will be detailed in the immediately following chapters in order to help us understand the relaxation processes at the centre of these studies, sample preparation and the evaluation of experimental data will be the subject of special attention since they are fundamental to the reliability of tests applied to the existing theories for NMR relaxation times. The intermolecular and intramolecular contributions to relaxation times will be analysed with particular attention being paid to experimental methods of separating these contributions. The buffeting interaction, which has been identified as an important mechanism in the analysis of the gas-to-solution chemical shifts (51) will be considered in the analysis of relaxation times in solutions, in order to see whether or not it can improve existing representations of molecular interactions and their effects on spin-lattice relaxation times.

Chapter Two.

NMR INSTRUMENTATION: C.W. and F.T SPECTROMETERS.

2.1 Introduction.

Spectrometers are used to detect and measure the characteristics of electromagnetic radiation associated with transitions between stationary energy states of matter. In N.M.R. these energy levels are created within the spectrometer by means of a permanent intense magnetic field B_o. This is derived from a suitable magnet which together with associated electronic circuitry contained in a console comprise the essential components of one spectrometer.

Two main electronic circuits are necessary to detect the resonant signal: an r.f. transmitter and a coresponding receiver; both are tuned to the Larmor frequency of the nuclei under investigation. The transmitter which delivers an r.f. oscillating magnetic field at the sample consists of an r.f. oscillator, an amplifier and a terminal coil whose axis y lies perpendicular to the direction of B_o.

The receiver contains the circuitry necessary to process the weak signal arising from the rotating transverse nuclear magnetization Mxy. This magnetization induces a small e.m.f. in a receiving coil which is also

positioned co-axially with a transverse axis x. The weak induced potential is then amplified and phase detected in order to extract a d.c. absorption signal, which is finally displayed or collected in a recording device. This signal is proportional to the out of phase component v of nuclear magnetization.

The transmitter and the receiver coils are placed around the sample tube within a compact device called the probe. This is a detachable unit which may be positioned between the magnetic poles and connected to the appropriate plugs of the console.

Two types of spectrometers are used for N.M.R. experiments viz continuous wave (c.w) and Fourier transform (F.T) spectrometers. Although basically similar, they differ in the power and time depedence of the r.f. wave and in the mode of signal acquisition.

2.2 Basic components of C.W. spectrometers

For continuous wave spectroscopy either the frequency can be maintained constant and the magnetic field varied continuously or viceversa. For simplicity the former mode of operation will be referred to.

2.2A The Magnet

The magnetic field B_o produced by the magnet must be intense, time independent and homogeneous. A continuously and linearly variable magnetic field is also superimposed on B_o in order to create a field sweep ΔB_o and thus stimulate sequentially the whole set of resonances for a given nucleus observed in the c.w mode at constant frequency ν_o. It is important to use high magnetic fields in order to improve signal discrimination through the dependence of chemical shift on B_o and also to increase the signal to noise ratio because theoretically the signal intensity is proportional to B_o^2. The permanent or electromagnets commonly used in NMR studies, produce field strengths between 1.0 and 2.5 tesla. For studies at higher fields superconducting solenoids are used.

Electromagnets generally consist of a highly stable one piece yoke terminated by two pole pieces. The pole cap material must be metallurgically uniform and almost optically flat. The magnetic field arises from a high intensity electrical current running through two main field coils wound near the pole pieces. A significant quantity of heat is consequently dissipated, which is dispersed through a heat exchanger. The operation of such magnets is therefore, accompanied by expensive consumption of electrical power.

Permanent magnets are basically stabilized by maintaining them at constant temperature in a thermostatted enclosure; it is advantageous also for the operating room to be thermostatically controlled and the samples to be preheated before introduction to the magnet. Permanent magnets can achieve a degree of field stability far beyond the reach of unlocked electromagnets at much lower running costs. Consequently, they are often used in preference to electromagnets for routine work based on the lower field instruments.

For either type of magnet, the probe should fit tightly between the pole faces, which are often only 3 cm apart and have a diameter about ten times larger than the air gap in order to produce an uniform magnetic field over a volume of the sample in the range 0.5 - 1.0 cm^3.

Because of the stringent requirements of high resolution n.m.r. spectroscopy, the magnetic field must be both stable and homogeneous. The maximum amplitude of the variation of magnetic field intensity within the sample is reduced from an intensity value of about 10^{-6} to 10^{-8} by means of pairs of "shim" coils situated on either side of the probe. These rectangular or circular coils produce weak additional magnetic fields of carefully controlled strength and geometry to compensate for the inhomogeneities of the main field. The line broadening arising from the residual inhomogeneities is decreased by a rapid rotation of the sample about its

vertical axis y. Field gradients along the x,z axis and the second order correction xy and yz are therefore averaged out by spinning the sample about the y axis. The same is not true for the field gradient along the y axis. For this reason, the y gradient correction is particularly critical. The often observed loss of resolution with time arises mainly from a progressive degradation of the y homogeneity control.

Field stabilization usually depends on a flux stabilizer designed to compensate for rapid fluctuations in the magnetic flux. Over the long term, field variations are compensated by a correction signal derived from an n.m.r. resonance lock circuit by monitoring changes in the dispersion mode resonance conditions of a suitable signal. Thus, any accidental fluctuation ΔB_o brings the lock circuit out of resonance. An output voltage proportional to ΔB_o is then produced, amplified and fed back to an appropriate coil which delivers in turn an opposed magnetic field - ΔB_o.

2.2.B The magnet field sweep

In order to observe the n.m.r. spectrum of a given sample, the magnetic field or the frequency used has to be scanned. In the first case the frequency is fixed and the magnetic field is swept at a constant rate. This can be done by using a saw tooth generator which feeds two small Helmholtz coils mounted on the probe and having

their axes in the same direction of the main magnetic field. The purpose of the recurrent sweep is to allow oscillographic presentation of the signal. The region to be scanned can be selected by adjusting the magnetic field or by changing the intensity of the sweep field. In order to produce a permanent record of a spectrum the sweep of the magnetic field (or frequency) is often controlled by a potentiometer linked directly to the drive of a chart recorder.

Care has to be taken over selecting the correct sweep rate because when this greatly exceeds the relaxation time of the nucleus under examination, the absorption line shows a ringing after the signal whereas a very slow sweep rate produces saturation (61).

2.2C The R.F. Transmitter

Any spectrometer should ideally be provided with at least three r.f. channels: one for measuring spectra, one for lock and one for decoupling. These channels are fed by high precision quartz oscillator frequency sources. These are mounted in a thermostatically regulated high stability oven so as to obtain a short term stability of about 10^{-10} per second and a long term stability of about 10^{-8} per day. Their output is amplified to the desired power level which is controlled finally by means of an attenuator, generally calibrated in steps of 1db. The r.f. frequencies are derived from a master oscillator by division and multiplication procedures.

2.2D The probe and detection system

The probe consists of a large number of individual parts which have to be contained between the pole faces. These are:

a) A vertical cylindrical cavity which receives the sample tube. This is usually created by a cylindrical glass former that often carries the various irradiation/receiver coils. This former is often mounted in a double walled glass Dewar container to permit variable temperature studies; the whole is called the insert.

b) Two inlets and outlets for compressed gas, One of which provides a means for the rotation of the sample while the other is used for temperature control.

c) A system for centering and fixing the probe in the magnet.

d) Coils for the r.f. transmitter and receiver, for modulation, field sweep and decoupling.

e) Shim coils, which can also be mounted in the magnet.

f) An r.f. preamplifier.

g) Regulatory devices for the paddles in crossed coil models.

The n.m.r. signal at the terminal of the receiver coil is estimated typically at a few tens of m.volts for a sample of water [62]. There are nevertheless many factors which contribute to the difficulty of satisfactorily detecting the signal, one of them being

the supression of the induction signal coming from the transmitter coil. In order to overcome this problem, the detection system has to be carefully designed with as its basis either the single or double coil system.

The cross coil probe was first employed by Bloch, Hansen and Packard (63). For this, the reduction of leakage between the transmitter and receiver coils is achieved by placing the receiver coil orthogonal to the transmitter coil. In this way the induced voltage can be reduced by a factor of 10^4. However, some leakage is usually desirable in order to select the absorption or dispersion signal coming from nuclear resonance. The control of the leakage flux is made by adjustment of a semicircular sheet of metal or "paddle" placed at the end of the transmitter coil.

With the single coil probe (6) a bridge circuit is used to balance out the transmitter signal and allow the small absorption or dispersion n.m.r. signal, to appear as an out of balance electromotive force across the bridge. In high resolution work, a twin T-bridge is often used, which has the advantage of good stability and the facility to discriminate between u and v mode signals. The absorption mode is selected by introducing a leakage of the transmitter signal out of phase with the dispersion signal.

A schematic diagram of a c.w n.m.r spectrometer is presented in fig (2.1). The general purpose is to detect the n.m.r signal which is composed of two components u, v with phases differing 90°. Each component may be obtained independently of the other by means of an r.f. phase - sensitive detector. After detection, the d.c. signal can be written as

$$V_r \text{ (d.c.)} \propto v \sin\varphi + u \cos\varphi \qquad (2.1)$$

where φ is the phase angle of the r.f. detector. Therefore, by adjusting the angle φ it is possible to obtain the absorption signal or the dispersion signal. Because the n.m.r. signal is very small, a r.f. preamplifier is used, before the n.m.r. signal V_r and the transmitter induced signal V_t are balanced. At this stage, the n.m.r. signal is still very small and any fluctuation of V_t will mask it. A classical means of eliminating this problem is to audio-modulate the main magnetic field. This audiofrequency modulation ω_m only affects the resonant nuclei, and not the transmitter output. Therefore the r.f. phase sensitive detector yields a d.c. component for the V_t fluctuation and an oscillating A.F. component for V_r at a frequency ω_m. The d.c component is rejected and the oscillating component is retained using a second A.F. phase sensitive detector referenced to ω_m. A d.c potential proportional to the nuclear resonance is finally obtained, and provides a representative plot of the absorption signal v as a

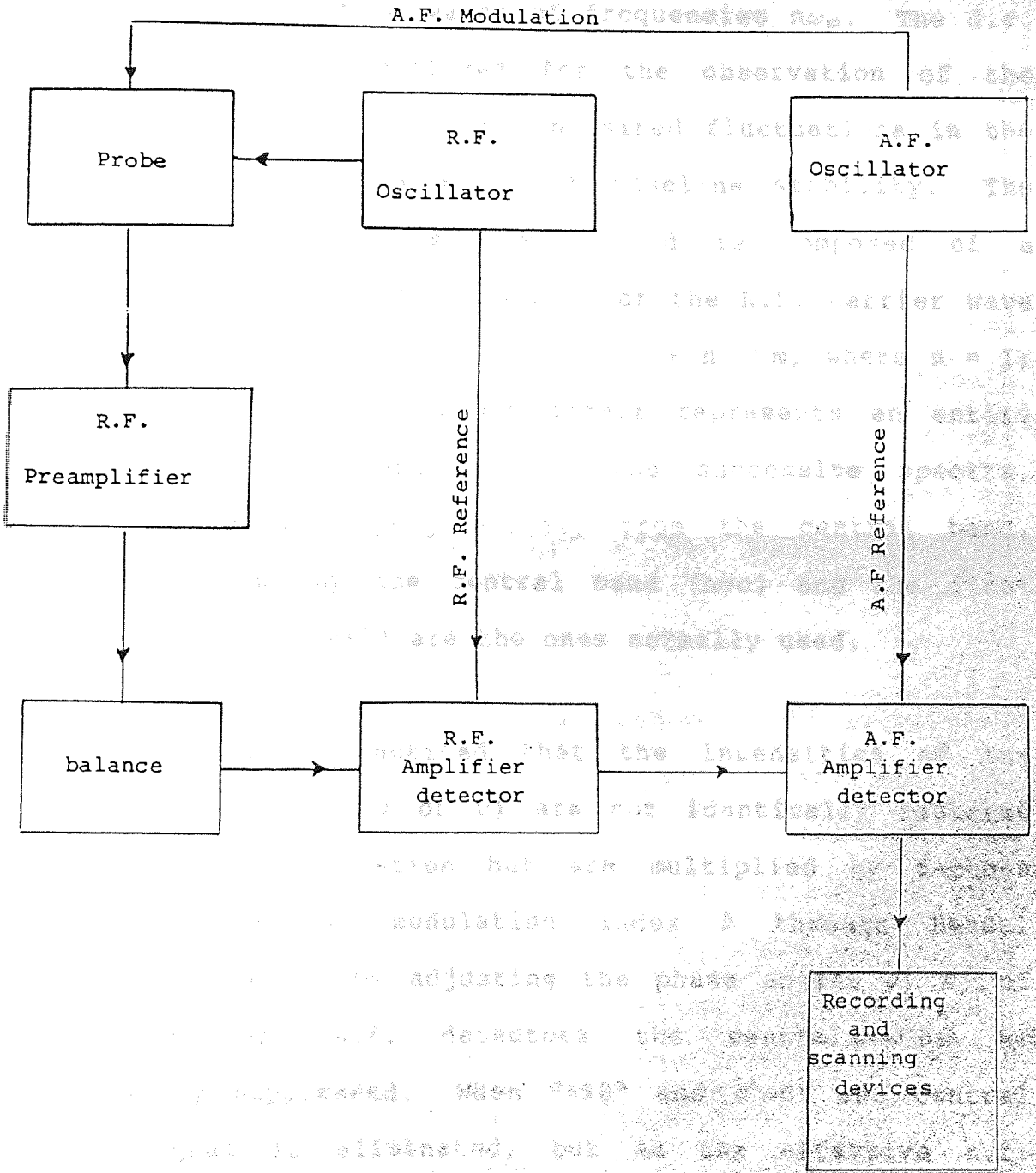

Figure 2.1 Schematic diagram of a C.W. NMR Spectrometer

function of the frequency through a scanning and recording device.

In the presence of A.F. modulation, r.f detection of the signal yields not only a d.c component, but also a series of oscillating waves of frequencies $n\omega_m$. The d.c. component is not utilized for the observation of the signal since it carries the undesired fluctuations in the r.f. carrier wave which affect baseline stability. The signal of interest is complex and is composed of a central band at the frequency ν_o of the R.F. carrier wave and of side bands at frequencies $\nu_o + n\ \nu_m$, where n = 1, 2,... Each of these bands itself represents an entire spectrum. The intensities of the successive spectra, however, decrease progressively from the central band. This explains why the central band (n=o) and the first upper side band (n=1) are the ones normally used.

It should be noticed that the intensities of the resulting signals (v or u) are not identically restored through A.F. modulation but are multiplied by factors depending on the modulation index β through Bessel functions. Also, by adjusting the phase angles φ, φ' of the R.F. and A.F. detectors the central band can be completely suppressed. When φ=90° and φ'=0° the central band signal is eliminated, but as the effective r.f. field is a function of the modulation index, it is necessary to increase the r.f. power to obtain a usable sideband signal.

In this work we used the sideband mode to measure the relaxation times with the A.R.P.S. technique and the centreband mode when measuring T_1 by the progressive saturation technique.

2.3 The Varian HA100D Spectrometer

This instrument is based on an electromagnet that provides optimum field homogeneity at 2.349 Tesla (64) and allows hydrogen resonance spectra to be obtained at 100 MHz. It has two modes of operation viz the unlocked HR mode or the field/frequency locked HA mode. Although nominally operating at 100 MHz, audiofrequency 2.5 and 2.5-3.5 KHz variable modulations of this are used to facilitate spectral stabilization by phase detection techniques.

The magnet has a closed yoke design which provides a good magnetic circuit and good mechanical stability. The main low impedance coils are cooled with thermostatted water, resulting in a steady temperature within the pole pieces; this is usually established at about 33°c. The whole magnet assembly is contained in an insulated jacket to minimise the effects of ambient temperature changes on the field intensity and sample temperature. The magnet current can be finely adjusted to obtain the best resonance conditions. Any variation of line current within $\pm$ 10% is compensated by a regulator.

The probe contains coils for sweeping the polarizing magnetic field B_o, a transmitter coil for producing the B_1 rotating field, a receiver coil for detecting the small n.m.r. signal and two sets of paddles for adjusting the leakage between the transmitter and receiver coils. The detection system is of the cross coil type.

In the probe design, materials have been carefully chosen to reduce background n.m.r. signals arising from nuclei resonating in the probe itself. The probe body is fabricated from aluminium. Also a Faraday shield, located between the two coils, reduces the electrostatic coupling to a minimum.

Leakage from the transmitter coil to the receiver coil is adjusted by orientating the receiver coil orthogonal to the transmitter coil. Even with the coils so positioned a small amount of coupling between the transmitter and receiver coil still exists.

This leakage can effectively be cancelled by the paddles, which are equivalent to inductors, coupled to both the transmitter and the receiver. A controlled leakage introduced in phase with the absorption signal effectively suppresses the dispersion mode.

Field sweep coils are located in annular slots on the sides of the probe, at a small distance from the transmitter and receiver coils, with their magnetic axes parallel to the transverse axis of the probe.

The linear sweep unit of the HA100D spectrometer provides the linear sweep signal which is applied to the d.c. sweep coils in the probe. A phantastron oscillator generates a sawtooth voltage which is applied to one of the push-pull amplifiers to modulate the 50 KHz signal applied separately from a 50 KHz oscillator. The 50 KHz component in the output of the push-pull amplifier is 180° out of phase with the reference signal and when these two outputs are mixed a stable sweep waveform is produced. This signal is applied to the modulation coils on the probe in order to sweep the magnetic field B_o and allow oscillographic presentation of the n.m.r. signal by feeding the output of the sweep amplifier to the x-plates of the oscilloscope.

As mentioned earlier, the Varian HA100D spectrometer can be used in two modes: the HA mode, which uses the field/frequency lock system, and the HR mode, which only has a field sweep facility. Some of the relaxation times determination in this thesis have utilized the HR mode of operation.

2.4 The HR Mode

In the HR mode the field/frequency lock system is not used, and the system is simplified to the r.f. unit and detector, an integrator/decoupler unit and presentation facilities. The system is based on phase sensitive detection circuits and field modulation which enable the

stability of the spectrum base line to be improved. The detailed operation of the HR mode is shown in schematic form in figure(2.2).

The r.f. unit consists of a stable, crystal driven oscillator which supplies a fixed frequency transmitter and a high gain superheterodyne receiver; the latter being isolated from subsequent circuitry by a buffer amplifier which prevents frequency variation with impendance changes. The r.f. power is stabilized by an automatic gain control circuit to 0.5 watt and is attenuated by means of a comprehensive array of push button switches. A 2.5 KHz signal of variable phase and amplitude derived from the integrator decoupler unit is applied to the a.c modulation coils in the probe to modulate the 100 MHz signal. Resonance is therefore detected as an amplitude modulated signal at 99.9975 on 100.0025 MHz with components being observed at 100MHz also.

The field sweep is nominally applied from a slow sweep unit which drives the flux stabilizer, but in practise may be supplied just as easily from the linear sweep unit which drives the d.c coils in the probe, although fine adjustment of the sweep rate is not possible by this method. The n.m.r. signal detected at the receiver is returned via the detector preamplifier in the probe to the r.f. unit, where it is amplified in two stages, the gain adjustment being provided by bias

variation rather than direct impedance loading via a potentiometer. The r.f. signal is reduced to a nominal 5MHz $\pm$ 2.5 KHz intermediate frequency by mixing with a local oscillator output of 95 MHz and, after further amplification, is mixed with a 5MHz signal derived from the control I.F. amplifier of the unit. The subsequent n.m.r. signal appears as an audiofrequency signal at 2.5KHz. This is subsequently detected in an A.F. detector. The resulting d.c voltage corresponding to the n.m.r. signal is applied to the y axis of an oscilloscope or recorder, or may be integrated before final presentation. High frequency noise components in the signal may be filtered out by a switchable RC circuit before being displayed.

The effect of the modulation technique employed in the HR mode is to discriminate against changes in the r.f. levels due to variation in probe balance, and r.f. leakage since all variations are effectively cancelled and not detected.

Because the HA mode of operation was not employed in the studies reported herein no discussion of this will be presented.

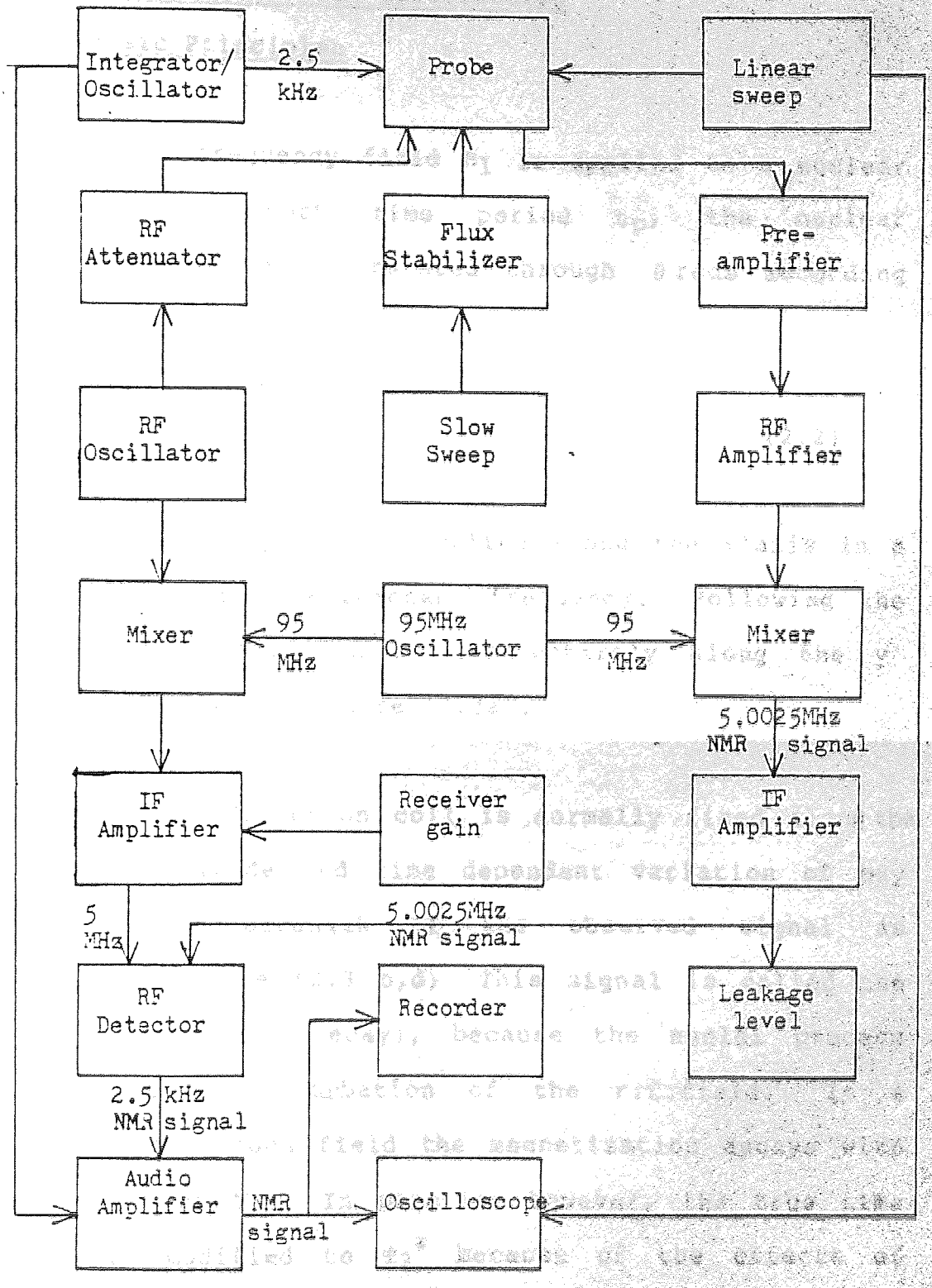

Figure 2.2 A schematic representation of the Varian HA100D NMR Spectrometer operating in the HR mode.

2.5 Fourier Transform Spectroscopy

2.5A Basic Principles

If a radiofrequency field B_1 is applied to a nuclear system for a short time period t_p, the nuclear magnetization vector is rotated through θ rads according to

$$\theta = \gamma B_1 t_p \qquad (2.2).$$

Suppose a 90° pulse is applied along the x'axis in a rotating frame at the resonant frequency. Following the pulse, the magnetization $\vec{M}$ lies entirely along the y' axis, as indicated in figure (2.3a).

Because the detection coil is normally fixed along the yaxis, the magnitude and time dependent variation of Mxy determines the strength of the observed signal as indicated in Figure (2.3 b,d) This signal is called the FID (free induction decay), because the nuclei precess "freely" without perturbation of the r.f.field. In a perfectly homogeneous field the magnetization decays with a time constant T_2. In practise however, the true time constant is modified to T_2^* because of the effects of field inhomogeneity. Figure (2.3d) shows the exponential decay (FID) that results from a r.f. pulse applied exactly at the resonance frequency of a single type of nucleus. The detector has a reference in phase with the r.f signal and if the r.f. is slightly different from

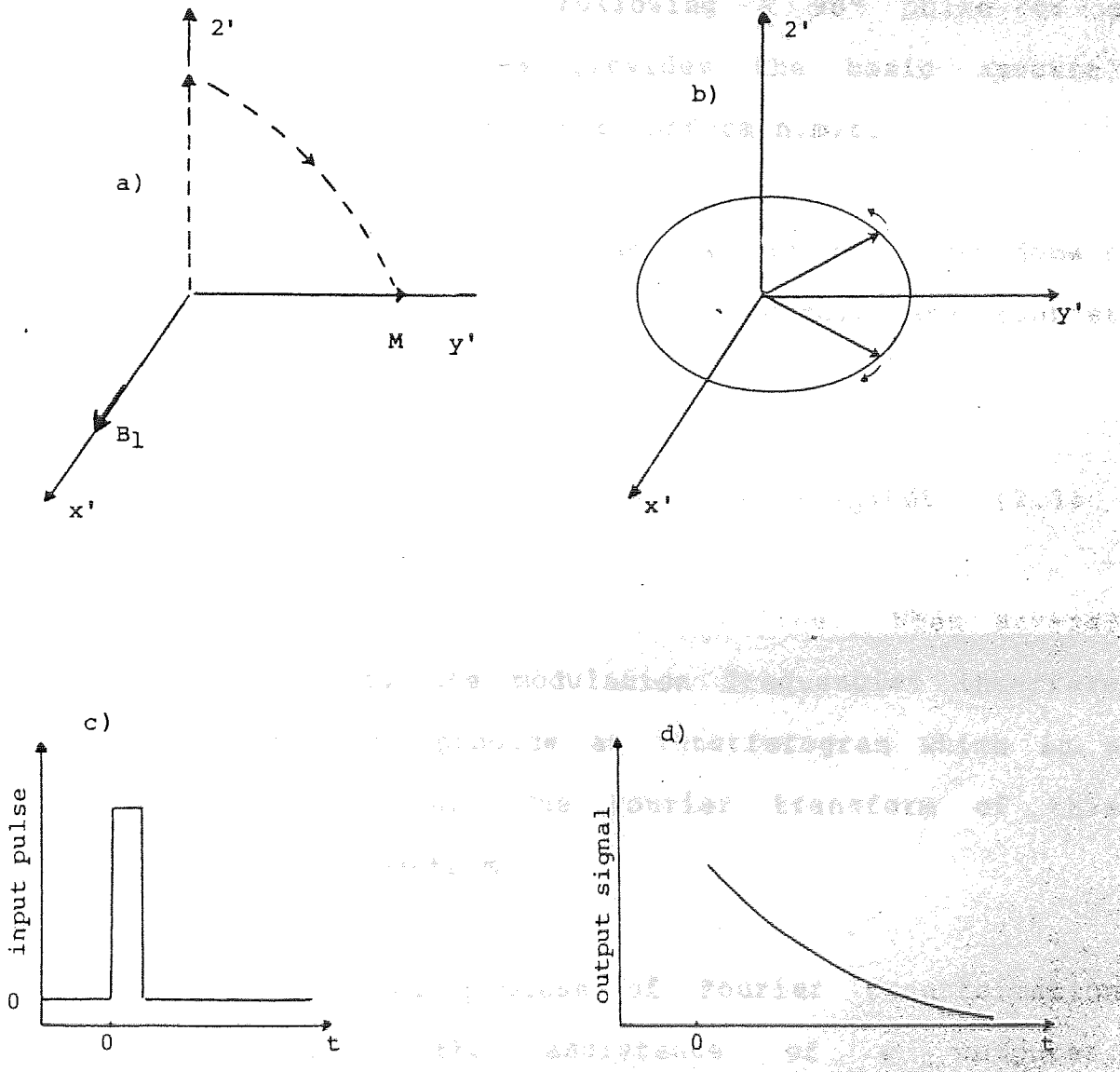

Figure 2.3 A representation of the F.I.D.
a) 90° pulse along X' rotates M to the y' axis
b) M_{xy} decreases
c) input r.f. pulse
d) free induction decay signal F.I.D. corresponding to b)

the Larmor frequency of the nuclei, there will be interference between the Mxy signal and the reference. Measurement of the FID is the basic way in which the magnitude and other characteristics of the magnetization are determined. The FID following a 90° pulse or a sequence of $n\theta$ pulses provides the basic spectral information needed in Fourier transform n.m.r.

It is known that an exponential in the time domain and a Lorentzian in the frequency domain are Fourier transforms of each other i.e.

$$\frac{T_2}{1+T_2^2(\omega - \omega_o)^2} = \int_o^\infty \exp(-t/T_2)\cos(\omega - \omega_o)t\,dt \qquad (2.3)$$

which refers to a single absorption line. When several lines are present, the modulation frequencies interfere with each other to produce an interferogram which is a regular beat pattern. The Fourier transform of this gives the n.m.r. spectrum.

The mathematical process of Fourier transformation usually requires the assistance of a computer. Consequently, prior to transformation the F.I.D. must be stored on the computer and digitization of the analogue signal is thus necessary. This is achieved by means of analogue - digital converter (ADC). The F.I.D. is sampled at regular time intervals and as many data points as there are available computer words, N, maybe retained. The N samples of the time domain fk are then

transformed into N points of the frequency domain Fj. The acquisition rate of data is determined by the sampling theorem i.e. in order to be well defined, a given sine wave has to be characterized by at least two points within a single period (2F points per second, where F is the frequency). As a consequence of the sampling theorem, acquisition of a frequency spectrum $\Delta \nu_o$ Hz in width requires a minimum sampling rate of $2 \Delta \nu_o$ points per second. If the selected computer memory size is N, the free induction decay has to be acquired in a time A_t which fulfils the condition

$$2 \Delta \nu_o A_t = N \qquad (2.4)$$

the longer the acquisition time the better defined the spectrum and the higher the resolution, which is defined by

$$R\ (Hz) = \frac{1}{A_t} \qquad (2.5)$$

An increase in computer size N or a decrease in the frequency range $\Delta \nu_o$ enhances the resolution.

2.5B Basic Components of F.T. Spectrometers

Superficially, C.W. and F.T. n.m.r. spectrometers are quite similar; however, the requirements are not the same. The reason for this is the unique characteristic of the F.T. spectrometers to acquire spectral information

in such a short time. In order to do this the F.T. spectrometer transmitter must generate higher power, to produce a B_1 in the range of 10-400 Gauss at the sample and stimulate the whole resonance spectra and flip the corresponding magnetization before any transversal decay occurs. The pulsed n.m.r. receiver must consequently be able to handle larger voltages and recover very quickly to detect the nuclear signal without interferences.

When a strong pulse is applied to the spin system for a short period t_p many nuclei with Larmor frequency ν_i within a certain range $\Delta\nu$ can be excited simultaneously. The reason for this is that the rf pulse envelope can be described as a square wave and it can be represented for many Fourier components covering the approximate range $\nu \pm 1/t_p$ where ν is the applied radio frequency. Thus a short rf pulse is equivalent to simultaneous application of a wide range of radio frequencies to the spin system, which is equivalent to having a multichannel spectrometer with numerous transmitters distributed over the spectral range of interest.

Despite the requirements referred to above, Fourier transform spectrometers have esentially similar basic units to those on C.W. spectrometers, but with the main difference that the transmitter and receiver circuits are adapted for pulsed operation. In addition, there are two suplementary units: a pulse programmer and a system for acquiring and processing the data. Figure (2.4) shows

the basic scheme of the F.T. spectrometers.

2.5.B1 The pulse programmer

The pulse programmer controls when, for how long and for which channel the gate will be open. The output of the r.f transmitter is interrupted by a sequence of pulses. If it is a periodic single pulse of width tp, it can be compared to the sweep field in order to detect the absorption signal in C.W. n.m.r. operations. More complex sequences of two or more pulses are used to measure relaxation times (20) (65).

2.5.B2 The RF Gate Unit

In order to produce pulse sequences, the r.f. output channel is equipped with a gate which can be switched on or off by means of a pulse generator whose timing is determined by digital programming. The r.f gate is used to drive the transmitter which contains a very stable (Quartz Crystal) r.f oscillator and an r.f switch which is "on" in the presence of a d.c. pulse signal form the pulse programmer and off otherwise (66).

2.5.B3 The R.F. Power Amplifier

The power required for pulse spectroscopy is higher than needed for C.W. n.m.r., typically 100 watts compared with 1 watt for a c.w. instrument. After the pulse, less

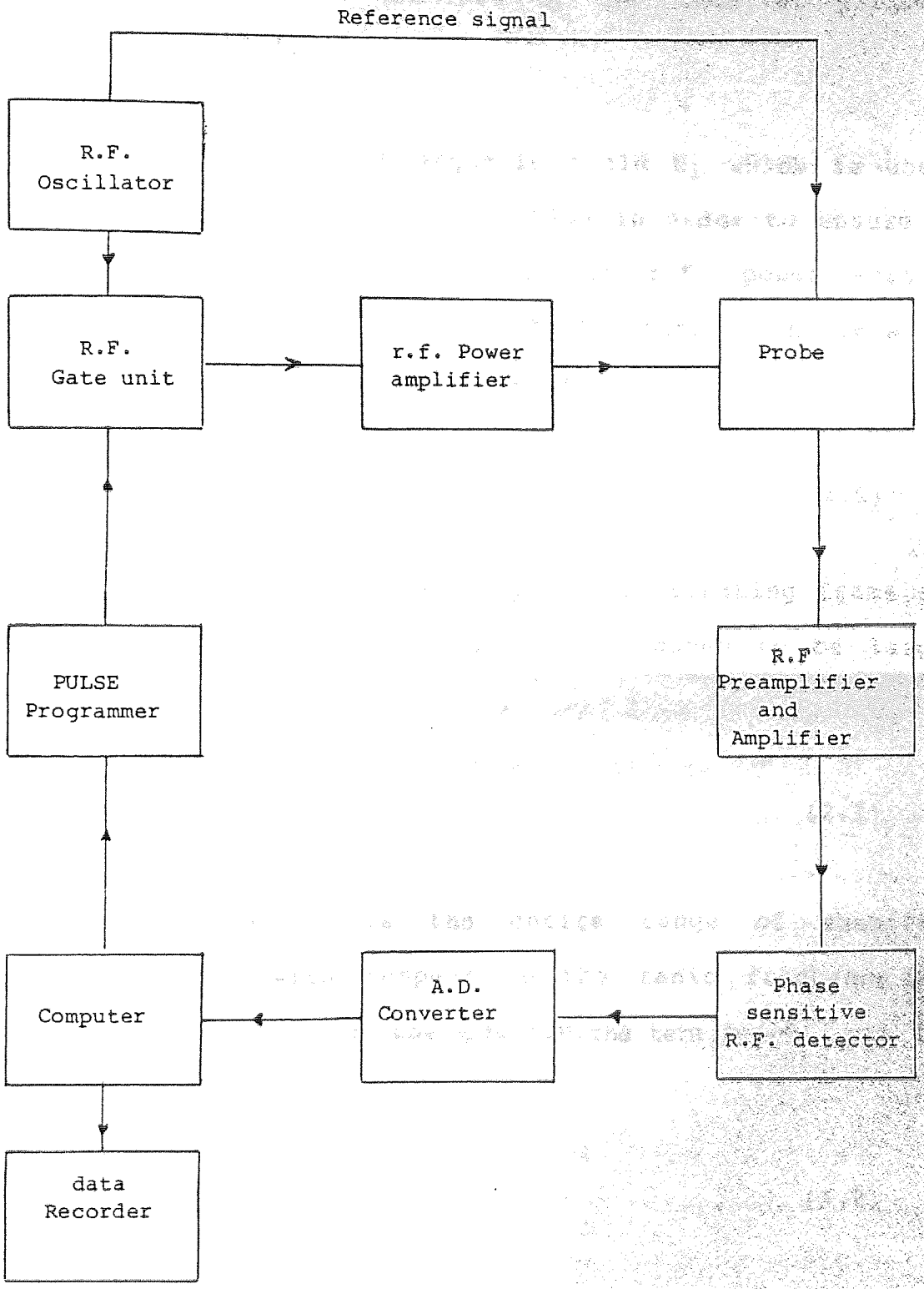

Figure 2.4 Basic diagram of a F.T. NMR Spectrometer

than 10^{-9} of the output power is radiated, so that the interferogram can be obtained by the receiver without perturbations (67).

The value of the rf magnetic field B_1 which is used in F.T. spectrometers has to be high in order to ensure a sufficiently uniform distribution of r.f. power across the spectrum. The effective field that a nucleus i experiences in the rotating frame is

$$B_{eff} = \frac{1}{\gamma} [(\gamma B_1)^2 + (\omega_i - \omega)^2]^{1/2} \qquad (2.6)$$

where ω is the angular frequency of the rotating frame as was shown in chapter one. If B_1 is chosen to be large enough for

$$\gamma B_1 \gg 2\pi\Delta \qquad (2.7)$$

where Δ (in Hertz) is the entire range of chemical shifts measured with respect to the radio frequency ω, then for any ω_i within the spectrum, the term $\frac{1}{\gamma}(\omega_i - \omega)$ can be neglected and

$$B_{eff} \approx B_1. \qquad (2.8)$$

That is, the magnetization precesses about B_1, which is along the x' axis, for all nuclei with Larmor frequencies in the range Δ. For a 90° pulse we know that

$$\gamma B_1 t_p = \pi/2 \qquad (2.9)$$

Then, from equation (2.7) we obtain

$$t_p \ll {}^1/_4 \Delta \qquad (2.10)$$

and we therefore need a short, intense pulse for F.T. N.M.R.. These considerations are very important when the relaxation times for several lines in a spectrum are to be measured. In this case, the R.F. carrier has to be placed in the middle of the spectrum.

2.5.B4 The Receiver

During the free precession period following a pulse, the signal enters the receiver (r.f. detector) as a band of radio frequencies near the basic transmitter frequency. Passing through the phase detector results in a series of audiofrequencies which are filtered by being fed through a low pass filter with a band width usually just equal to the chosen spectral width. Since single phase detection does not allow distinction between positive and negative frequencies, the r.f. carrier has to be placed so that the audiofrequencies $\nu i - \nu o$ all have the same sign. If the rf carrier is placed at the end of the spectrum and the set spectral width is bigger than the chemical shift range Δ, the frequencies can be digitized unambiguosly. But if the spectral width is set to a value smaller than Δ, some of the frequencies corresponding to lines at the other end of the spectrum can be folded. This effect is avoided by using an

experimental technique called quadrature detection (68), which differentiates between high and low field frequencies by means of two phase sensitive detectors.

2.5.B5 The Probe

The requirements of the sample probe are rather stringent. In general it must be able to handle the large r.f. voltages present while the pulse is on; it must recover rapidly from such a powerful pulse and quickly receive and process the weak nuclear signals following the pulse.

In addition there are usually the decoupling system, spinning system, temperature detector and several tuning controls. The coil system can be of the single or crosscoil type (69). Single coil probes are characterised by generating larger rf fields. Cross coil type, on the other hand benefit from the superior homogeneity of the rf field which is important in multiple pulse experiments. (70)

2.5.B6 The Analogue to Digital Converter (A.D.C.)

This device samples the free induction decay at regular time intervals and converts each voltage measured to a binary number that can be stored in the corresponding memory location of the computer. The rate at which a spectrum of width ΔF must be collected by the

A.D.C. is twice the spectral width 2 Δ F, consistent with the sampling theorem. Ideally, in order to avoid line shape distortions, the F.I.D. should be sampled until its amplitude has fallen off to zero. If the signal is sampled over a period of T seconds, this defines a total of 2 Δ FT sampling points. Since each point is stored, a memory of N words is needed i.e. N=2 Δ FT. The time T is called the acquisition time and is related to the digital resolution of the instrument e.g. when 4K data points are available for the spectral range of 5KHz, the resolution is $R=T^{-1}=1.22$ Hz for the frequency spectrum, no matter how good the actual resolution due to magnet homogeneity may be.

The dynamic range of the signals that are to be digitized is a critical parameter when weak signals have to be detected in the presence of strong signals, as for example in the case of ^{13}C satellites in proton spectra. For an A.D.C. of 12 bytes, the voltage is normally measured in steps of $\frac{10.000}{2^{12}-1}=2.44mV$, if the voltage range is $\pm$ 10 volts. This means that all signals which correspond to a potential lower than 2.44mV will not be read by the converter. When the interferogram is displayed on the screen of the oscilloscope, the minicomputer represents the maximum peak to peak amplitude by a number close to 2^{12}. Then, if the largest signal detected has the intensity H_S, the smallest signal which can be recorded will have an intensity H_W such that (71)(72)

$$\frac{H_S}{H_W} = 2^{12} \qquad (2.11)$$

This ratio is called the dynamic range of the spectrum.

2.5.B7 The Computer

A computer basically consists of input and output units, control, storage and arithmetic units. To use it a program is read into the storage unit. It controls the transmitter and the receiver, stores and processes the F.I.D data and transfers the results to display units such as the oscilloscope or the recorder. The minicomputer is characterized by two important parameters that define its storage capacity, the number of memory location and the word length. Memory locations are counted in multiples of K, which stands for $2^{10}=1024$.

In general, computers with a memory of 12K can be regarded as the minimum requirement for an F.T spectrometer. The word length determines the amount of data or their magnitude that can be stored in each memory location. The information is stored in binary form. In general, for n bytes the largest possible decimal number that can be represented is 2^n-1, so it is very important to have large values of n e.g. n=12, in order to detect small signals, as indicated in equation (2.11).

In a typical ^{13}C F.T NM.R experiment, 1000 pulses are normally required in order to give reasonable signal to

noise ratio. This means that each scan has to be with the same characteristics. Any change in field homogeneity will cause observed peak shapes to change on different passes, damaging the final spectrum. This problem can be overcome by the computer. In one approach, the height of an absorption peak of a reference compound (Lock signal) is monitored. With field homogeneity optimized, the peaks show a maximum height. Any change from the optimal condition is detected. The error signal is then used to control the shim current and return the field to the optimum value.

2.6 The Jeol FX90Q F.T N.M.R Spectrometer

The Jeol FX90Q is a F.T. NMR spectrometer system which has a proton resonance frequency of 89.60 MHz and a carbon-13 resonance of 22.55 MHz. The system, which can be supplied to a variety of specifications, includes new facilities such as: digital quadrature detection (D.Q.D), light pen control system (L.P.C.S) and autostacking software.

The version of the spectrometer used for the present studies features a probe system, which is able to detect many nuclei in five different ranges of frequencies (73). The computer memory is 24 K words where 8 K words are used for the program and 16 K words for the data.

2.6 A The magnet System

A voltage and current regulated power supply system supplies a stable excitation current to the electromagnet which produces a magnetic field of 2.11 Tesla. The magnet is housed in a compact console in order to avoid sudden changes in temperature.

The magnetic field homogeneity can be improved by using several controls on the spectrometer table which adjust the current in the shim coils placed on the probe between the pole faces. The specification for the resolution of the ^{13}C line is less than 0.3Hz. However, as the magnetic field stability is 0.1 Hz/hr, some broadening of the signals could appear in long term experiments. The latter can be overcome by using the autoshim unit which corrects for small drift of the magnetic field homogeneity.

2.6.b Transmitter, Receiver and Data Systems

These basic systems of the spectrometer are presented in a block diagram in figure (2.5), where only some of the units have been considered in order to emphasize the detection method of the FX90Q spectrometer.

The transmitter system has three channels: observation, irradiation and lock oscillators units which have a reference frequency of 44 MHz provided by a master

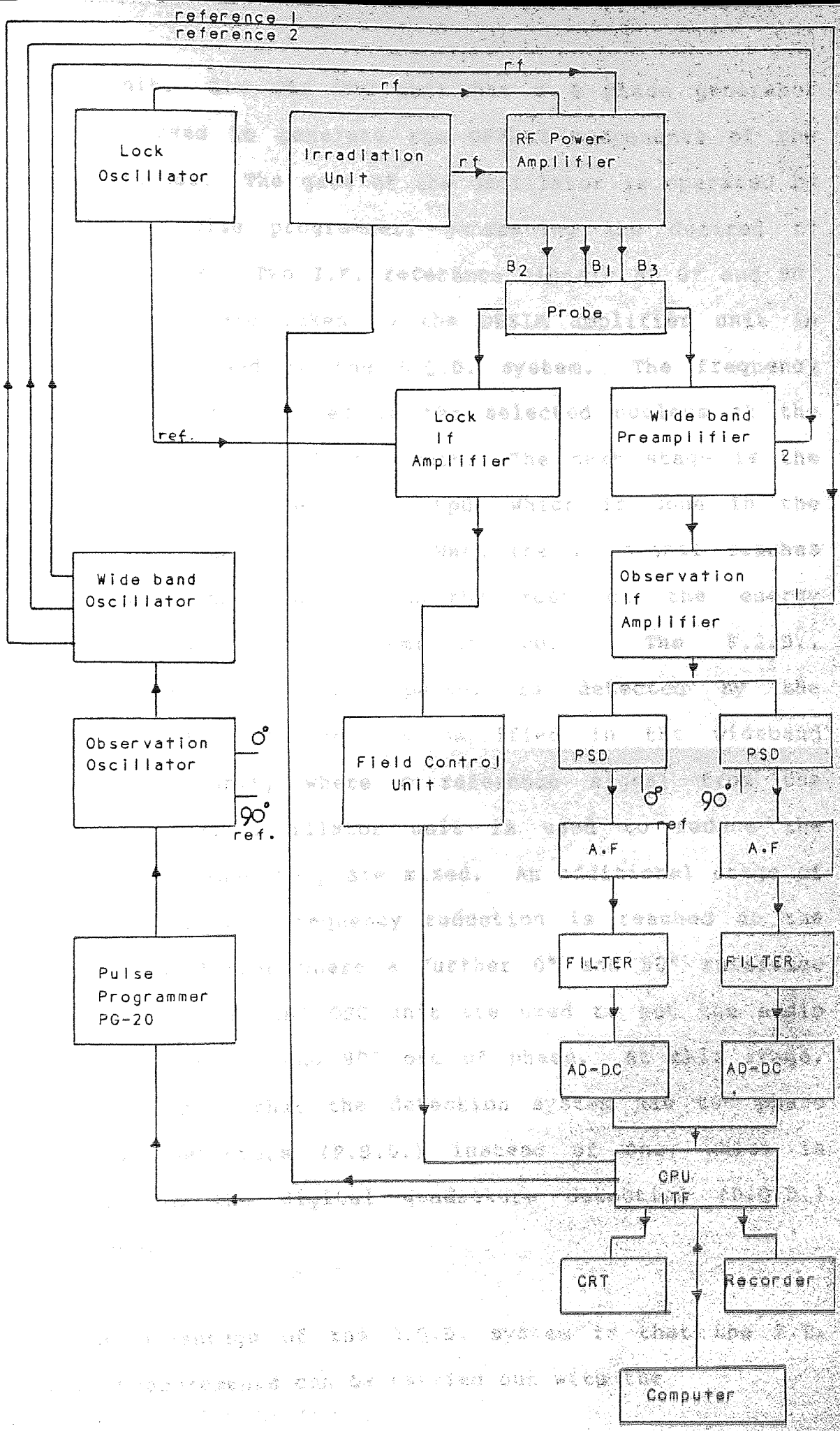

Figure 2.5 Basic units in the FX90Q Spectrometer

clock unit. The OBS OSC unit has a 4 phase generator which is used to generate the OFFSET components of the OBS RF output. The gate of the oscillator is operated by the PG20 pulse programmer, generating the desired rf pulse sequence. Two I.F. reference signals at 0° and 90° out of phase are taken to the OBS.I.F. amplifier unit in order to be used in the D.Q.D. system. The frequency signal is then adjusted to the selected nucleus at the wide band local oscillator unit. The next stage is the amplification of the r.f. output which is done in the R.F. power amplifier unit. When the rf signal reaches the probe, the sample absorbs most of the energy generated at the transmitter coil. The F.I.D., generated after the r.f. pulse, is detected by the receiver coil and then is amplified in the wideband preamplifier unit, where a reference signal from the wideband local oscillator unit is used to reduce the signal level when they are mixed. An additional stage of amplification and frequency reduction is reached at the OBS I.F. amplifier where a further 0° and 90° reference signals from the OBS OSC unit are used to get the audio frequencies at 0° and 90° out of phase. At this stage, it can be seen that the detection system has two phase sensitive detectors (P.S.D.) instead of one; which is required in the digital quadrature detection (D.Q.D.) technique.

The advantage of the D.Q.D. system is that the F.T. N.M.R. measurements can be carried out with the

excitation pulse placed in the center of the observation width. This allows the observation band width to be reduced to only half that required for single phase detection (S.P.D.) resulting in a $\sqrt{2}$ fold improvement of the signal to noise ratio. Since the R.F. pulse is given at the centre of the spectrum, the efficiency of the R.F. power is enhanced 4 times when compared with S.P.D. It also helps to obtain more accurate relaxation times when several signals are considered.

The AD-DA unit receives filtered signals which are converted to digital form. Then they are transferred via C.P.U. (controller) to the computer where the information is stored. When it is required, the F.I.D. transformed to get the spectrum signal in digital form. The D.A. unit changes the information to analogue signals which can be recorded or displayed in the oscilloscope screen.

In the FX90Q spectrometer, the conversation between the operator and the computer is done by using the light pen unit. After pointing to a particular function or command on the screen, this order is transferred to the C.P.U. unit which establishes a link between the computer and the spectrometer units controlling its operations. In this way, the pulse mode, irradiation mode, frequencies, etc., can be selected.

In the FX90Q spectrometer the lock signal is obtained as in any continuous wave spectrometer. The lock osc.

unit produces the r.f. signal at the appropriate resonance frequency and this is amplified in the R.F. power amplifier. The Field control unit produces a sawtooth signal which modulates the magnetic field and allows the observation of the resonance signal which is phase sensitive detected at the LOCK I.F. amplifier unit; which receives a reference signal from the LOCK osc unit. In addition to being used for lock the signal can also be used for rapid monitoring of the adjustments to the resolution of the magnet. The rf oscillator for the lock signal can be used with two nuclei $^{2}D/^{7}Li$, normally we used ^{2}D in the present experiments.

The R.F. irradiation oscillator units can be selected according to the experiment: noise irradiation and single R.F. output. In both cases the irradiation power has to be amplified, but at different levels that are controlled by the irradiation selector unit which is linked to the R.F. power amplifier. The noise irradiation modulation width can be selected to be 0.5KHz, 1, 2.5 and 5 KHz. Normally we used 1KHz to irradiate protons when detecting ^{13}C. In this case the R.F. power is preset on the instrument but in the cases of selective proton irradiation or homonuclear irradiation (^{1}H) the r.f. power can be adjusted to the required level and the OFFSET of the R.F. irradiation field can be adjusted in a fine range of $\pm$ 5Hz.

Several modes of irradiation are available, some of them are gated in order to permit selected experiments. It is also possible to combine them by using the extension facilities which identify the mode of operation with a binary code. The most common irradiation modes are: COM (complete decoupling or noise), SEL (hetero selective decoupling used in $^{13}C-\{^{1}H\}$ systems). HOM (Homo decoupling used in protons and is characterized for a time share between the irradiation system and receiver system). In chapter four some of the characteristics of these irradiation modes will be detailed.

2.6.C The Probe

The probe is placed between the poles of the magnet and has several modules:

a) the permabody which is fixed. It houses replaceable modules (OBS, Irr and insert), which are housed in a double walled dewar for variable temperature work. On it, irradiation coils and a thermocouple are mounted. The spinner mechanism with a photosensor for detecting the sample spinning rate is placed on the top. On both sides of the permabody, current shim boards are attached. Air and water are used respectively, to spin the sample tube and to keep the temperature of the permabody constant.

b) The r.f. tunable module, which allows for easy selection of nuclei, has five ranges of frequencies with five independent impedance matching channels and fine tuning which maintains optimum sensitivity.

c) the irradiation module which enables the tuning of the irradiation circuit so that most of the energy is used in the irradiation coil to produce a maximum field. This is indicated by a minimum S.W.R. meter deflection

d) the sample insert. This is exchangeable for different sample tube sizes and holds the sample coil and LOCK coil wound around the glass tube. At the bottom of the insert there is a plug that permits electrical connection of the coils to the spectrometer.

2.6.D AUTOSTACKING Program

The computer JEC - 980B has a memory of 24K words. The program is stored in the initial 8K word memory; the remaining memory 16K words are used as the entire data memory. The different operations that can be carried out by the computer are contained in the autostacking program.

The autostacking program consists of the following three programs: a) Normal program b) Stacking program and c) Analysis program.

a) Normal Program.

This program is used for routine measurements, it has several command patterns which can be called by using the light pen. The basic operations require the setting of pulse width, pulse mode, pulse repetition, frequency range, observation frequency, irradiation mode, irradiation frequency and the OBSET which has to be placed in the middle of the spectrum. The number of scans is selected according to the nuclei and sample concentration.

When the accumulation ends the FID is adjusted with mathematical parameters which modify the final spectra in terms of $^{S}/_{N}$, resolution, line shape, etc. Also, several measurements can be done on the screen via the light pen e.g. line width, chemical shift, etc. Finally, the data can be printed and recorded on a conventional chart.

b) Stacking Program

This permits automatic measurements according to pre-set orders and stores the resulting data in a cassette tape or similar unit (I.C. memory - Recorder).

Because the program can be used to set the spectrometer conditions, it provides for continuous measurements under different decoupling conditions. Consequently, relaxation times can be measured using an appropriate pulse sequence.

The stacking program contains three "run" parameter tables. Each table can have a completely different set of acquisition parameters, decoupling modes and data storage modes. With this facility we can perform different experiments which will be carried out automatically by the spectrometer. For example we can feed instructions to the computer in run # 1 to measure the nuclear Overhauser enhancement for ^{13}C nuclei by setting the parameter IRR MODE (1 or 4) which correspond to C.O.M. or NNE respectively. Then for run # 2 the spectrometer conditions can be changed to measure the relaxation time in the same sample, eg using progressive saturation method with the parameter PR***. Finally for run #3 it is possible to make another experiment, e.g. to measure the relaxation time in the same sample by the inversion recovery method with the parameter P_I***. At the end of the three runs, all the data sets are stored on the cassette tape and at the appropriate time the information can be processed. In the case of relaxation times this has to be done using the analysis program.

C) Analysis Program

With this program, NMR data that were continuosly measured by means of the stacking program are processed continuously under the set conditions and the calculation of the T_1 value is executed. The value of the relaxation time is calculated using the method of least squares. This program enables the user to indicate the calculated value of T_1 for each line of the spectrum and to plot the

observation points, which define a straight line. The measured T_1 and the error (variance) are also indicated on the oscilloscope screen. In the course of this work all these programs have been used, in particular the stacking program and analysis program, in the calculation of nuclear Overhauser enhancements and relaxation times. The "Menu" experiment represented by the three runs has been used mainly overnight and over weekend. Some other details relevant to the present work using the Jeol FX90Q spectrometer can be found in chapter four.

Chapter Three

Relaxation Processes

3.1 Introduction

Most of the investigations reported in this thesis depend on spin lattice relaxation times which are related to the motion of molecules and their interaction. Consequently, in order to assist in the interpretation of experimental relaxation times, theories relevant to these will be reviewed.

First, a general treatment for single or equivalent spins where all the spins should have the same relaxation time will be considered. Second, the case of two non-equivalent spins I, S will be dealt with and then the nuclear Overhauser effect will be introduced through the Solomon's equations. As we will see, NOE enhancements depend on the geometry of the spins system and also on which nucleus has been saturated by an r.f. field. Finally, a general review of the application of NMR in the analysis of molecular motion is presented.

3.1.A The Origin of Magnetic Relaxation

The Bloch equations have taught us that the two relaxation times play quite distinct roles. The spin-lattice relaxation time T_1 determines the degree of

saturation and T_2 determines the unsaturated line width. Both kinds of relaxation are caused by time dependent magnetic, or electric fields, at the nucleus, and these fields in turn come from random thermal motions. A nuclear spin of $^1/_2$, for example, may experience local magnetic fields from the spins of other nuclei moving past it, from unpaired electrons, or from spin rotational interactions in which the molecular rotation itself generates magnetic fields at the nucleus. There may also be changes in the chemical shielding of the nucleus as a molecule rotates, and these modulate the total effective field which acts on the spin. Nuclei with electric quadrupole moments are further affected by changes in the local electrostatic field gradient when the molecule rotates or vibrates.

In general, two conditions are necessary for a successful relaxation mechanism. Firstly, there must be some interaction which acts directly on the spins; secondly, it must be time dependent. Thus, any interaction which causes transitions between the α and β spin states and fluctuates strongly at the resonance frequency, produces powerful spin-lattice relaxation and line broadening; for liquids, most of the effects arise from random Brownian motion of the molecules as they rotate and diffuse through the fluid.

3.1.B Frequency Distribution of Molecular Motions

The frequencies of the motions of the molecules in a liquid sample cover a wide range. If we assume that a molecule on average remains in one state of motion for about 10^{-12} sec, then, after this time undergoes a collision which changes its state of motion, this can be compared to a sine wave pulse oscillator which is turned on for a short time, τ sec; we obtain not only a frequency component at the frequency of the oscillator f_c, but also components at frequencies over the range $(f_c \pm \tau^{-1})H_z$. As the molecules move about in space they carry the nuclear spins with them and the motions of the nuclear magnetic moments generate fluctuating magnetic fields, which we can denote by $\vec{b}$, and behave like the field generated by an NMR transmitter.

The interaction of the fluctuating field $\vec{b}$ with a macroscopic magnetization $\vec{M}$, which is precessing in the laboratory frame at the frequency $\omega_o = \gamma B_o$ about the two axes, is a mechanism for T_1 relaxation if $\vec{b}$ has components perpendicular to the stationary magnetic field B_o, and can produce a torque on M_o. As in the case of transmitter B_1 rf field the components $b_\perp$ have to rotate at the frequency ω_o, to be effective. Whilst high frequency processes can affect T_1, there are contributions to T_1 from motional frequencies at twice the resonance frequency, i.e., $2\omega_o$ (74).

In order to discuss in a more quantitative way how the relaxation time T_1 is related to molecular motion, we need to introduce some new parameters. Let us denote by τ_c the "average" time between molecular collisions for a molecule in some state of motion. If the value of τ_c is such that we have large Fourier components of the molecular motion at the resonance frequency, ω_o, then we expect relaxation to be most efficient; consequently, we would expect the relaxation times to be minimized. If however, τ_c is too long or too short, we expect much smaller Fourier components at ω_o and much longer values for T_1. These deductions were made by Bloembergen et al (74), whose results are shown in Figure (3.1). For a sample of glycerine they plotted the dependence of $T_1(^1H)$ on the molecular correlation time $\tau_c \propto \eta/T$, where η is the viscosity of the sample and T the temperature in °K, at two different resonance frequencies. In the high temperature region, to the left of the T_1 minima, T_1 is found to be frequency independent and it decreases with decreasing temperature. This behaviour is typical of any molecule which is characterized by small τ_c values where $\omega_o \tau_c \ll 1$, as for small molecules in the liquid state. At the resonance frequency where $\omega_o \tau_c \sim 1$, T_1 goes through a minimum and for $\omega_o \tau_c \gg 1$, T_1 is frequency dependent.

For a quantitative analysis of T_1, it will be necessary to introduce two more parameters which are closely related to one another, namely a correlation

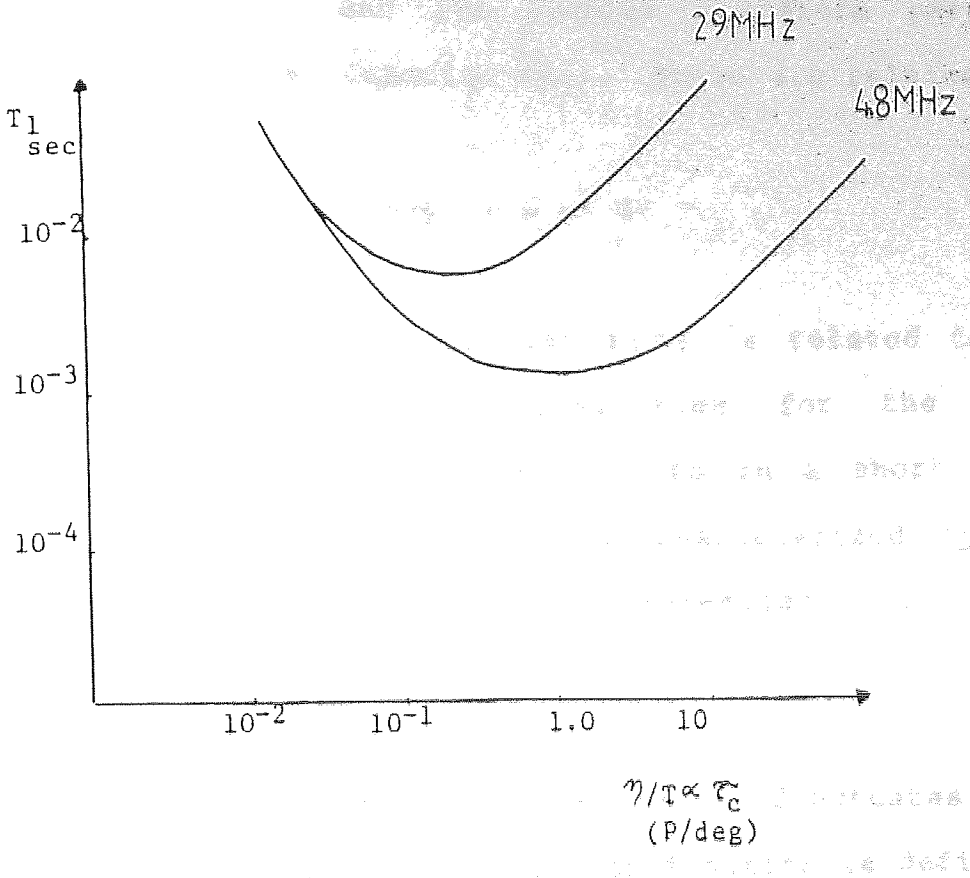

Figure 3.1 Variation of T_1 with the correlation time at 29 MHz and 4.8 MHz for a sample of glycerine (74)

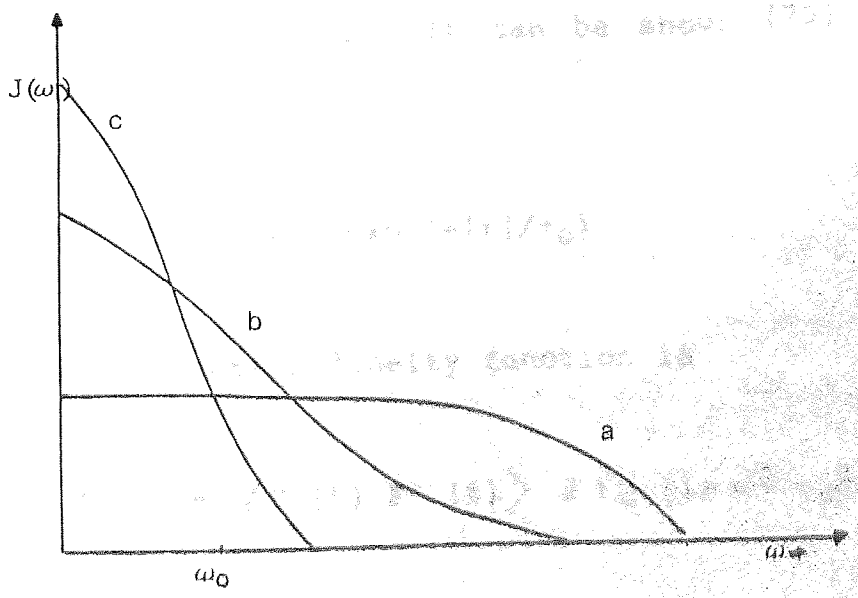

Figure 3.2 Plot of the spectral density $J(\omega)$ versus the frequency ω

function $K(\tau)$ and its Fourier transform partner, the spectral density function $J(\omega)$. These are related by

$$J(\omega) = \int_{-\infty}^{\infty} K(\tau) \exp(i \omega \tau) d\tau \qquad (3.1)$$

The correlation function $K(\tau)$ is related to a phase memory time or correlation time for the molecular motions. If $K(\tau)$ decays to zero in a short time this tells us that our sample is characterized by a short correlation time and that the molecular motions are very fast.

If F(t) is the function which fluctuates with the molecular motion the correlation function is defined as

$$K(\tau) = \langle F(t) F^*(t+\tau) \rangle \qquad (3.2)$$

where the symbol $\langle\ \rangle$ indicates an average over the ensemble of nuclei. It can be shown [75] that $K(\tau)$ can be represented by

$$K(\tau) = K(o) \exp(-|\tau|/\tau_c) \qquad (3.3)$$

and the spectral density function is

$$J(\omega) = \langle F(t) F^*(t) \rangle\ 2\tau_c (1+\omega^2 \tau_c^2)^{-1} \qquad (3.4)$$

Figure (3.2) indicates how the function $J(\omega)$ varies with frequency for several values of τ_c, i.e., $(\omega_o \tau_c \ll 1)$ case a,

($\omega_o \tau_c \sim 1$) case b and ($\omega_o \tau_c \gg 1$) case c. In the case of liquids τ_c is short ($\omega_o \tau_c \ll 1$) and the molecular motions are distributed over a very wide frequency range and all motional frequencies in the range (o - τ_c^{-1} Hz) have a small but equal probability of being found for any given molecule.

3.2 Spin-Lattice Interactions

T_1 depends not only on the value of $J(\omega_o)$ but also on the strength of the coupling between the spin system and the lattice. A number of different physical interactions have been found to be important in coupling the nuclei to the lattice and hence providing a link through which energy between these two systems can be exchanged.

These interactions are:

1. magnetic dipole-dipole
2. spin rotation
3. electric quadrupole
4. chemical shift anisotropy
5. scalar-coupling

In general, any mechanism which gives rise to fluctuating magnetic fields at a nucleus is a possible relaxation mechanism. Consequently, we can write

$$T_1^{-1} = \sum_i R_i = E_{ci}^2 f_i(\tau_c) \qquad (3.5)$$

where E_{ci} represents the strength of the particular

relaxation interaction and τ_c is the molecular correlation time.

The interactions mentioned above will now be discussed with particular emphasis being placed on those important to the work described herein.

3.2.A Dipole-Dipole Relaxation

The classical interaction energy E between two magnetic moments $\vec{\mu}_1$ and $\vec{\mu}_2$ is

$$E = \frac{\vec{\mu}_1 \cdot \vec{\mu}_2}{r^3} - 3 \frac{(\vec{\mu}_1 \cdot \vec{r})(\vec{\mu}_2 \cdot \vec{r})}{r^5} \qquad (3.6)$$

where $\vec{r}$ is the radius vector from $\vec{\mu}_1$ to $\vec{\mu}_2$. For the quantum mechanical Hamiltonian, $\vec{\mu}_1$ and $\vec{\mu}_2$ are treated as operators. If we express I_{1x} and I_{1y} in terms of the raising and lowering operators I_1^+ and I_1^- respectively and express the rectangular coordinates x, y, z, in terms of spherical coordinates r, θ, φ (Figure 3.3), the Hamiltonian can be written from equation (3.6) as (13)

$$\mathcal{H}_d = \frac{\gamma_1 \gamma_2 \hbar^2}{r^3} (A + B + C + D + E + F) \qquad (3.7a)$$

where

$A = \bar{A} F_0$, $B = \bar{B} F_0$, $C = \bar{C} F_1$, $D = \bar{D} F_1$, $E = \bar{E} F_2$, $F = \bar{F} F_2$

are operators related to the raising and lowering operators I^+, I^-.

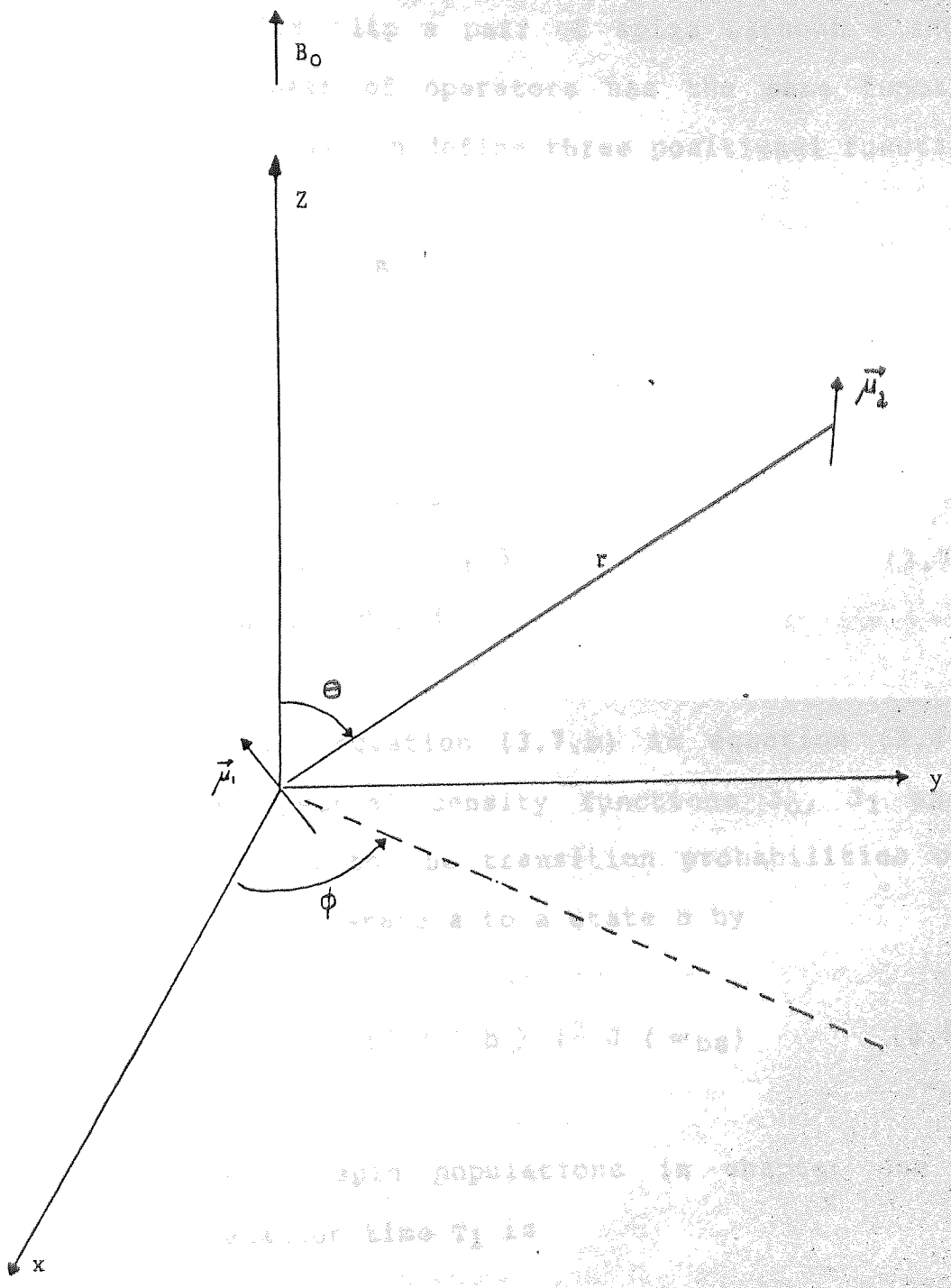

Figure 3.3 Axes system and polar coordinates for the dipolar coupling of two spins

This Hamiltonian $\mathcal{H}_d$ can be treated as a small perturbation, where the terms C, D join states of energy which differ by $\hbar\omega_o$. E and F connect states that differ by $2\hbar\omega_o$ and A,B flip a pair of spins without change in energy. Each pair of operators has the same functional form, from which we can define three positional functions:

F_o related to A, B

F_1 related to C, D

F_2 related to E, F

where

$$F_o = (1-3\cos^2\theta)\, r^{-3}$$

$$F_{\pm 1} = \sin\theta\cos\theta\, e^{\pm i\varphi}\, r^{-3} \qquad (3.7.b)$$

$$F_{\pm 2} = \sin^2\theta\, e^{\pm 2i\varphi}\, r^{-3}$$

If we substitute equation (3.7.b) in equation (3.4), we obtain three spectral density functions J_o, J_1 and J_2, which are related to the transition probabilities of the spin system from a state a to a state b by

$$W_{ab} = \frac{1}{\hbar^2} \left| \langle a \left| \mathcal{H}_d \right| b \rangle \right|^2 J(\omega_{ba}) \qquad (3.8)$$

The analysis of spin populations in chapter one shows that the relaxation time T_1 is

$$T_1^{-1} = 2W \qquad (3.9)$$

where W represents the total transition probability which involves changes in energy $\hbar\omega_o$ and $2\hbar\omega_o$, as required for

the operators C,D and E,F in the dipolar dipolar Hamiltonian $\mathcal{H}_d$. Thus, by using equation (3.8) and equation (3.9) it has been found (74) that

$$T_1^{-1} = \frac{3}{2} \gamma^4 \hbar^2 I (I+1) [J_1(\nu_o) + \frac{1}{2} J_2(2\nu_o)] \quad (3.10)$$

This equation can be written as well using the fact that J_1, J_2 govern the intensity of the local field (16). The result is

$$T_1^{-1} = \gamma^2 [\overline{bx^2} + \overline{by^2}] \frac{\tau_c}{1 + \omega_o \tau_c^2} \quad (3.11)$$

where b_x, b_y are the components of the local field, in the rotating frame at the frequency $\omega_o = \gamma B_o$.

3.2.A.1 Intramolecular and Intermolecular dipolar contributions to relaxation processes

The term intramolecular interaction, refers to those coming from magnetic fields generated by nuclei in the same molecule and intermolecular those from different molecules.

In the case of intramolecular contributions, the molecule is considered approximately rigid, so the internuclear distance r is a constant (r=b) and the "F" function from equation (3.7) has only to be averaged over orientations (θ, φ).

The original calculations for T_{intra} by Bloembergen et al (74) were corrected slightly by Kubo and Tomita (76). The result is

$$T_1^{-1}intra = \frac{\hbar^2 \gamma_1^2 \gamma_2^2}{b^6} \tau_c \qquad (3.12)$$

for non-identical spins and

$$T_1^{-1}intra = \frac{3}{2} \frac{\hbar^2 \gamma^4}{b^6} \tau_c \qquad (3.13)$$

for identical spins. This result was also obtained by Solomon (77), who also gave a more complete derivation for non identical nuclei which we will consider later.

The correlation time τ_c, is considered (74) through an extension of the Debye theory (78) of dielectric dispersion, i.e., $\tau_{c\ NMR} = \frac{1}{3} \tau_D$. This is based on a model of a sphere turning in a viscous fluid and gives

$$\tau_c = \frac{4 \pi \eta a^3}{3KT} \qquad (3.14)$$

where η is the viscosity and a the radius of the sphere.

Intermolecular contributions to T_1, were calculated by Bloembergen et al (74) for water, considering nuclei whose distances from the central molecule lie between r and r + dr. By using equation (3.13) it is possible to evaluate the contribution to T_1 from each pair of nuclei after averaging over all directions; τ_c is estimated as the time that a molecule takes to diffuse across a

relative distance r. This is $r^2/12D$ where D is the diffusion coefficient. The total contributions is then obtained by multiplying by the number of nuclei per unit of volume $2N_o$ (in water) and integrating over all the space outside the sphere r=2a, corresponding to two spheres in contact. This gives

$$T_{1inter}^{-1} = 2N_o \int_{2a}^{\infty} \frac{3/2\ \hbar^2 \gamma^4}{r^6} \frac{r^2}{12D} 4\pi r^2\, dr \qquad (3.15)$$

$$= \frac{\pi N_o \hbar^2 \gamma^4}{2Da}$$

The diffusion coefficient D may be related to the viscosity by the Stokes - Einstein relation $D=KT/6\pi\eta a$, giving the final result

$$T_{1inter}^{-1} = \frac{3\pi^2 \gamma^4 \hbar^2 \eta N_o}{KT} \qquad (3.16)$$

When applied to the case of water in the Bloembergen (74) experiment equation (3.16) gave $T_{1intra}^{-1} = 0.26$ sec $^{-1}$ and $T_{1inter}^{-1} = 0.4$ sec^{-1} or $T_1 = 2.5$ sec, in good agreement with the experimental value of $T_1 = 2.3 \pm 0.5$ sec.

These basic approaches for the intra and intermolecular contributions to T_1 were extended by Gutowsky and Woessner (79). They showed that the relaxation time for the ith nucleus may be written:

$$(T_{1_i}{}^{-1})_{intra} = \hbar^2 \gamma_i{}^2 \left(\frac{3}{2} \gamma_i{}^2 \Sigma_j r_{ij}{}^{-6} + \gamma_f{}^2 \Sigma_f r_{if}{}^{-6}\right) \tau_c$$

$$(T_{1_i}{}^{-1})_{inter} = \pi^2 \hbar^2 \gamma_i{}^2 \eta N a/KT \left[3\gamma_i{}^2 \Sigma_j (1/r_{ij}^2) + 2 \gamma_f^2 \Sigma_f (1/r_{if}^{\circ})\right] \qquad (3.17)$$

in which the symbol f refers to non-identical nuclei and r° is the distance of closest approach of nuclei in different molecules which can be approximated to $r^\circ = 2a$ where a is calculated from the molar volume.

Hubbard (80) made the point that Gutowsky and Woessner have assumed that identical nuclei within a molecule are distinguishable and that they have neglected interference effects. Consequently, he included interference terms, to calculate the term dependence of the z component of magnetization for systems of three and four equidistant identical spin $1/2$ particles approaching equilibrium in a field B_o. For three spins it is found that

$$M_z(t) - M_o = [M_z(o) - M_o] (ae^{-\alpha t/T_1} + b\, e^{-\beta t/T_1}) \qquad (3.18)$$

Abragam (62) has concluded that making $a=o$, $b = \beta = 1$ in equation (3.18) is an excellent approximation to the exact formula. The same conclusions have been reached by

Mitchell and Eisner (81) who calculated the intramolecular relaxation for three and four spins, using Hubbard's model, as $T_{1intra} = T_o/3.016$ and $T_{1intra} = T_o/4.458$ where $T_o = r^6/\gamma^4 \hbar^2 \tau_c$. They then applied the formula of Gutowsky and Woessner to these two systems and found $T_{1intra} = T_o/3$ and $T_{1intra} = T_o/4.5$ respectively. Moreover, Kattawar and Eisner (82) used the Redfield equation to calculate numerically the relaxation time for a three-spin asymmetric molecule in a liquid. They have found that the plot of ln $(M_z - M_o)$ vs t can be approximated by a single straight line for $t \leq 1.5\ T_1$. Also, the term constant for this straight line differs less than 1% from the average relaxation time calculated from the formulae of Gutowsky and Woessner.

J. Powles et al (83) have used a similar equation to that of Gutowsky - Woessner for n identical nuclei in the same molecule. Their equation is

$$T_{1intra}^{-1} = \frac{3}{2} \hbar^2 \gamma^4 \frac{2}{n} \left(\sum_{i>j} d_{ij}^{-6} \right) \tau_c \qquad (3.19)$$

Intermolecular contributions to T_1, have been also studied by several workers (62)(84)(85) and one potentially interesting result, is that obtained by Hubbard (86). He has considered that the time dependence of the relative position of two nuclei in different molecules depends on the translational motion of the molecules if the nuclei are not at the centre of the molecules when the closest distance between the

interacting muclei is not longer $r^\circ \approx 2a$. His result for T_{1inter} is

$$T_{1inter}^{-1} = \frac{n\pi\gamma^4\hbar^2}{5\,aD}\left\{1 + 0.233\left(\frac{b}{a}\right)^2 + 0.15\left(\frac{b}{a}\right)^4 + \ldots\right\} \quad (3.20)$$

where b is the distance of each nucleus from the centre of the molecule in which it is contained, n is the number of spins per unit volume and a is the molecular radius. In equation (3.20) for the typical case $(b/a) \approx \frac{1}{2}$, the second and third terms are 6.8% of the first term.

Most workers recognise (87) that there are crude approximations in the equations for intermolecular contribution to T_1, particularly in the value of effective distance of closest approach r°. Inlow et al (88) in their studies on mixtures of CH_3OH in several solvents, have concluded that the "hard sphere" model is deficient in several respects; it does not distinguish between the intermolecular interactions of two methyl groups and the markedly different type of interaction between hydroxyl groups in a hydrogen bonding system. So, they adjust the r° value to $r^\circ=2a$ for methylmethyl interaction $r^\circ=1.2a$ for hydroxyl-hydroxyl interaction and $r^\circ=4a$ for hydroxyl-methyl interaction.

Intramolecular relaxation as well has some difficulties in its analysis. If the molecule is not spherical, there are generally three rotational diffusion coefficients about the three molecular axes (89), and

three time constants describing the reorientation of the molecules about the three axes. As a result, the experimental correlation time τ_c is only an average of the ones which represent the rotation of the molecule. There is also another complication which is of interest, namely when the spin-spin vector performs an internal rotation in addition to the molecular rotation as it happens in CH_3 groups. This problem was considered by Woessner (90), who showed that the effect of the internal motion is to reduce the effective correlation time.

In addition to these problems, the Debye equation used by Bloembergen et al (74) in the evaluation of T_1 has been questioned (81)(91)(92). Therefore, it is important to select a suitable model to explain experimental results. According to the B.P.P. theory (74) $(\eta T_1)^{-1}$ should be a linear function of the concentration of solute in a mixture of liquids. This has been confirmed by Giulotto, Lanzi and Tosca (93) by plotting $(\eta / \eta_o T_1)^{-1}$ vs mole fraction of C_6H_5Cl in CCl_4. They have also found an abnormal behaviour of C_6H_5OH in CCl_4 and have concluded that it was because of the presence of molecular associations. Homer and Coupland (94) have found that for benzene and cyclohexane $(\eta T_1)^{-1}$ is a linear function of N, the number of protons per c.c. over most of the range when the compound is diluted with CCl_4. Mitchell-Eisner (81) have reported good linearity for $(\eta T_1)^{-1}$ vs V, where V is the volume fraction of the same compounds in CCl_4, but for CS_2 as a solvent there is

no linearity . This was identified as a real failure of the B.P.P. theory, and they advocated the use of the Hill (95) model for describing correlation times and self-diffusion coefficient; with this basis better agreement between experiment and theory was obtained.

Another consequence of the B.P.P. theory is that the plot of $\eta T_1/T$ vs temperature should not depend on temperature. However, Powles and Neale (96) have found from their experiments with several organic liquids that $\eta T_1/T$ is not constant and concluded that for non-spherical molecules their motions are complex and the dependence of T_1 on viscosity has to be reconsidered.

3.2.B Other Nuclear Relaxation Mechanisms

3.2.B.1 The Spin-Rotation Interaction

Relaxation can also arise from the local fields produced by the spin-rotation (S.R.) interaction. A molecular system possessing angular velocity constitutes a rotating charge system and thus can give rise to a magnetic field at the resonant nucleus. Fluctuations in this field result from modulation of both, the magnitude and direction of the angular momentum vector associated with the rotating molecule. Let us consider one particular electron and a given nucleus. As the molecule rotates, the electron will change its movement accordingly. The molecular rotational frequency is

$$\nu_{rot} = hL/2\pi I \qquad (3.21)$$

where the molecule is in the Lth rotational state and I is the moment of inertia of the molecule. Therefore, the electric current generated is $i = e/c\ \nu_{rot}$ and the magnetic moment associated with this circulating current is

$$\mu_L = i\pi R^2 \approx \mu_N L \qquad (3.22)$$

where μ_N is the nuclear magneton and R the distance between the electron and the nucleus. This magnetic moment generated by the motion of the electron produces a local magnetic field at the resonant nucleus of the order of $\mu_N L/R^3$. For the hydrogen molecule this field is (97) 27 gauss and for HCl it is 9.7 gauss. Since this effect is proportional to the rotational velocity and inversely proportional to the moment of inertia of the molecule, we can predict that, in general, the smaller the molecule the more important the spin-rotation interaction will be. For a spherical molecule the spin-rotation contribution to T_1 is given by (98)

$$\frac{1}{T_{1\ S.R.}} = \frac{2}{3}\ \frac{I_o KT}{\hbar^2}\ (2\ C_\perp^2 + C_\parallel^2)\ \tau_{SR} \qquad (3.23)$$

where I_o is the moment of inertia, $C_\perp$ and $C_\parallel$ are the diagonal components of the spin rotation interaction tensor C and τ_{SR} is the spin rotation correlation time.

3.2.B.2 Quadrupole Relaxation

For nuclei with spin $I > \frac{1}{2}$ as deuterium, ^{35}Cl, ^{37}Cl, ^{14}N, there are quadrupolar moments, because the charge distribution in the nucleus can be imagined to be cigar-shaped. In the case of hydrogen or ^{13}C, with spin $1/2$, there are no quadrupolar moments. In most molecules the charges of the surrounding valence electrons at other nuclei produce a large non-uniform electric field gradient at each nucleus (99) and this can interact with a quadrupolar moment.

Classically, the interaction energy E of a charge distribution of density ρ with a potential V due to external sources is

$$E = \int \rho(r)\, V(r)\, d\tau \qquad (3.24)$$

the potential V(r) can be expanded in a Taylor's series about the mass centre of the nucleus. The third term after the expansion of V(r) in equation (3.24) is called electric quadrupole term

$$E^* = \frac{1}{6} \Sigma_{\alpha\beta} V_{\alpha\beta} \; Q_{\alpha\beta} \qquad (3.25)$$

where

$$Q_{\alpha\beta} = \int (3\, X_\alpha\, X_\beta - \delta_{\alpha\beta})\, \rho\, d\tau \qquad (3.26)$$

and

$$V_{\alpha\beta} = \left(\frac{\partial^2 V}{\partial X_\alpha \; \partial X_\beta} \right)_{r=0} \qquad (3.27)$$

It is convenient to rewrite equation (3.24) to obtain a different expression for the Hamiltonian, by using the commuters for the operators of the total angular momentum

$$(Ix, Y_k) = i\, Z_k, \text{ etc}$$

After long mathematical work (13) $\mathcal{H}_Q$ has been found to be given by

$$\mathcal{H}_Q = \frac{eQ}{4I(2I-1)} [Vzz(3I_z^2-I^2) + (Vxx-Vyy)(Ix^2-Iy^2)] \qquad (3.28)$$

It is useful to define the terms eq and η as follows

$$eq = Vzz$$

$$\eta = \frac{Vxx-Vyy}{Vzz}$$

These parameters are called the field gradient and the asymmetry parameter.

Abragam (62) has considered the interaction between the nuclear quadrupole moment and the local electric field gradient as

$$\mathcal{H}_Q = I.\ Q\ (t).\ I \qquad (3.29)$$

where Q(t) is a certain tensor with elements proportional to the quadrupole moment Q and the field gradients Vzz, Vyy, Vxx, etc. As the molecule reorients, the components of the quadrupole coupling tensor become random functions of time and provide a relaxation mechanism for

quadrupolar nuclei. Then, the quadrupolar contribution of T_1 is [62] for $\omega_o \tau_c \ll 1$

$$T_1^{-1} = \frac{3}{40} \frac{2I+3}{I^2(2I-1)} \left(1+\frac{\eta^2}{3}\right)\left(\frac{e^2 Qq}{\hbar}\right)^2 \tau_c \qquad (3.30)$$

The term $(e^2Qq/\hbar)$ is the quadrupole coupling constant.

For nuclei with $I > 1/2$ the quadrupolar interaction is usually the dominant relaxation mechanism, but this interaction may be weak if the molecule is symmetric (100) because there is then no electric field gradient. For ^{11}B in symmetric molecules, such as $^{11}BH_4^-$, where $e^2Qq/\hbar = 0$, T_1 (^{11}B) = 10 sec, but in three-coordinate Boron compounds, where $(e^2Qq/\hbar) \approx 3$ MHz, T_1 (^{11}B) values are typically about 10 msec.

Indirect quadrupole effects can be evident in ^1H or ^{13}C spectra when these nuclei are spin-spin coupled with say ^{14}N. For example, the proton resonance of $^{14}N\,H_3$ is broadened because of the averaging of the coupling with ^{14}N which is being relaxed rapidly by quadrupolar effects, i.e., the ^1H line is broadened by averaging between the fully coupled and decoupled interactions with ^{14}N to an extent governed by the efficiency with which the quadrupole relaxation decouples the ^{14}N.

3.2.B.3 Chemical Shift Anisotropy

The local field B_{loc} which is acting on a nucleus after applying a magnetic field B_o is given by

$$B_{loc} = B_o - \sigma B_o = B_o (1 - \sigma) \qquad (3.31)$$

where σ is called the shielding constant. This interaction is represented by the Hamiltonian $\mathcal{H}_{cs} = - \gamma h \, B.\sigma.I.$, where σ is the chemical shift tensor; thus the magnitude of the shielding at a nucleus is dependent upon the orientation of the molecule in the magnetic field. Rapid molecular motions in the liquid state average the σ value to

$$\sigma = \frac{1}{3} (\sigma xx + \sigma yy + \sigma zz) \qquad (3.32)$$

Although the nucleus on the average sees a chemical shift value represented by σ, on a short time scale i sees fluctuations in B_{loc} because σxx, σyy, σzz are not equal. This random effect creates a relaxation mechanism. It may be shown (62) that in liquids

$$T_{1CSA}^{-1} = \frac{2}{15} \gamma^2 B_o^2 (\sigma_{\parallel} - \sigma_{\perp})^2 \tau_c \qquad (3.33)$$

where $\sigma_{\parallel}$ and $\sigma_{\perp}$ refer to the shielding along and perpendicular to the symmetric axis in the molecule. In the case of the absence of axial symmetry the equation becomes more complicated (62).

For protons $\Delta\sigma = \sigma_{\parallel} - \sigma_{\perp}$ is typically less than 10ppm for covalently bound hydrogens (101) and this relaxation mechanism is negligible for protons even when the high fields of superconducting magnets are used, i.e., despite

the dependance of the effect on B_o^2. For toluene, the contribution to ^{13}C T_1 by using $\Delta\sigma$ = 180 ppm was found (102) $T_{1CSA} \approx$ 3000 sec at 25 MHz. In benzene and cyclohexane (103), the value of ^{13}C T_1 was constant at 15.1 MHz, 25.1 MHz and 62.5 MHz.

3.2.B.4 Scalar Relaxation

The multiplet structure observed in high-resolution n.m.r. is a second order effect originated in coupling of nuclei through electrons. This spin-spin coupling is observed for magnetically non-equivalent nuclei existing in the same molecule provided (62) that,

a) there exists no rapid time-dependent processes that average the spin coupling constant ($A=2\pi J$) to zero or,
b) the inverse of A is much less than the T_1 value of either coupled nucleus. Rapid chemical exchange would lead to a violation of condition a) if the frequency of exchange is much greater than the frequency of the induced coupling. The exchange process thus gives rise to a fluctuating local field at the site of the non-exchanging nucleus. Such a relaxation mechanism is denoted by Abragam (62) as "scalar-relaxation of the first kind". Violation of criterion b) may arise if nucleus j is relaxed by a fast quadrupolar process that collapses the spin coupling with nucleus i. If the local magnetic field thus produced at i is fluctuating (due to flipping of spin j) at a frequency comparable to the

Larmor frequency of i, relaxation can be induced. Such a process is termed scalar relaxation of the second kind (62).

The perturbing Hamiltonian $\mathcal{H}_{sc}$ is given by (62)

$$\mathcal{H}_{sc} = \hbar A \vec{I} \vec{S} \qquad (3.34)$$

In scalar relaxation of the first kind the coupling constant A (= $2\pi J$) carries the time dependence, while for scalar relaxation of the second kind the time dependence originates with the coupled spin S. The formula for T_1^{sc} is the same in both cases. The result is (62)

$$\frac{1}{T_1^{sc}} = 2 \frac{A^2}{3} S(S+1) \frac{\tau_{sc}}{1+(\omega_I-\omega_S)^2 \tau^2_{sc}} \qquad (3.35)$$

where the correlation time for scalar coupling τ_{sc} is the chemical exchange time τ_e in one case ($\tau_{sc} = \tau_e$) and the quadrupolar relaxation time for the second case ($\tau_{sc} = T_1^Q$).

As an example of scalar relaxation of the first kind, we can mention the case of pure methanol at 31°, where have been estimated (88) $[T_1(CH_3)]^{-1}_{sc} = 0.004$ sec^{-1} and $[T_1(OH)]^{-1}_{sc} = 0.012$ sec^{-1}. This contribution is about 8% of the total experimental relaxation rate for the hydroxyl proton and 3% of the experimental relaxation rate for the methyl protons. As methanol is diluted, the

correlation time for proton exchange increases, and the scalar mechanism becomes less important.

Quadrupole nuclei having $I \geq 1$, i.e., nuclei whose charge distribution is not spherically symmetrical, relax so fast, for instance, that they accelerate the relaxation of neighbouring nuclei. The contribution of the S.C. mechanism, which can be recognized from a frequency and temperature dependence of T_1 is particularly large when the coupling nuclei precess with similar Larmor frequencies. This applies to ^{13}C and the quadrupole ^{79}Br. As a consequence ^{13}C nuclei bound to Br relax relatively fast (104).

3.2.C Separation of Relaxation Contributions

In general, the interactions that determine the spin-lattice relaxation time T_1, may be divided into two types. a) interactions within the same molecule like dipole-dipole, quadrupolar, spin rotation or chemical shift anisotropy, the most important being the dipolar-dipolar and the spin rotation interactions, when the spins are $^1/_2$ and the magnetic field corresponds to a ^1H resonance frequency between 60 MHz and 100 MHz. b) interactions between different molecules.

In the case of a) the intramolecular interactions are sensitive to the reorientational motion of the molecule while in b) the intermolecular interaction is affected by

both translational and reorientational motion of the molecules. It is, therefore, reasonable that the two sets of interactions contribute independently to the total transition probability. Consequently, T_1 may be given by

$$\frac{1}{T_1} = \frac{1}{T_{1intra}} + \frac{1}{T_{1inter}} \qquad (3,36)$$

Since T_1 inter and T_{1intra} depend differently on the two types of motion, an important experimental aim is the separation of the two contributions to T_1. This is not so straightforward as may appear at first sight. For example in the case of protons the intramolecular contribution to T_1^{-1} can be measured by extrapolating the relaxation times of the protons, in the compound being investigated, to infinite dilution in a suitable solvent. The dilution is carried out either, in the deuterated analogue of the compound under study or in a solvent such as CS_2 or CCl_4. The former procedure is clearly the best, since it will yield an essentially true value for the intramolecular contribution to T_1; however, the intermolecular D-H dipole-dipole coupling at infinite dilution must still be calculated and substracted from the extrapolated T_1^{-1} to yield the true T_1^{-1} (intra). Extrapolations in CCl_4 or CS_2 assume that these compounds have intermolecular interactions similar to those of the deuterated compound being investigated. This assumption is often reasonable but need not be true and obviously dilution with this type of solvent need not yield the true value of T_{1intra}.

Assuming that a value for T_{1intra} may be obtained, the intramolecular T_1 is then calculated from

$$T_{1\ inter}^{-1} = T_{1\ (neat)}^{-1} - T_{1\ intra}^{-1} \qquad (3.37)$$

To illustrate the point made above some typical proton relaxation times are listed in tables (3.1) and (3.2) for a number of small molecules; in some of the examples the solvent is the deuterated analogue of the solute.

The relaxation times are often not corrected for the residual D-H intermolecular relaxation in experiments where extrapolations are carried out in deuterated solvents. Powles et al [109] corrected the relaxation time for a fraction X of protonated benzene molecule using equation (3.38)

$$T_{1x}^{-1} = T_{1intra}^{-1} + x\,T_{1inter\ C_6H_6}^{-1} + (1-x)\,T_{1inter\ C_6D_6}^{-1} \qquad (3.38)$$

where $T_{1inter\ C_6D_6}$ is the proton T_1 corresponding to the interaction of one C_6H_6 molecule entirely surrounded by C_6D_6 molecule and

$$\frac{T_{1inter\ C_6H_6}^{-1}}{T_{1inter\ C_6D_6}^{-1}} = \frac{3}{2}\left(\frac{\gamma_H}{\gamma_D}\right)^2 \frac{[I_H(I_H+1)]}{[I_D(I_D+1)]} = 24 \qquad (3.39)$$

Hence

$$T_{1x}^{-1} = T_{1intra}^{-1} + \frac{1}{24}(1+23X)\,T_{1inter\ C_6H_6}^{-1} \qquad (3.40)$$

Table (3.1) Relaxation Times of Aromatic Protons in Selected Molecules.

Molecule	T_1neat	T_1intra	T_1inter	Solvent	Reference
benzene	22	100	29	CS_2	(62)
benzene	19	110	23	deut	(105)(106)
pyridine	12	100	14	deut	(105)(106)
toluene(ring)	16	56	23	CS_2	(62)
p-xylene(ring)	14	45	21	CS_2	(105)(106)
o-xylene(ring)	12	56	16	CS_2	(105)(106)
chlorobenzene	18	80	23	CS_2	(81)
bromobenzene	14	67	18	CS_2	(81)
mesitylene	10	40	13	CS_2	(105)(106)

Table (3.2) Relaxation times of Methyl Protons in Selected Molecules.

Molecule	T_1neat	T_1intra	T_1inter	Solvent	Reference
CH_3 Br	5	5	-	CS_2	(108)
CH_3 I	14	20	45	CS_2	(108)
acetone	16	29	34	deut	(105)
toluene	10	15	-	CS_2	(62)
p-xilene	7.4	10.5	30	CS_2	(62)
o-xilene	6.7	12	-	CS_2	(62)
$(CH_3)_2SO$(DMSO)	2.9	5.6	6.1	deut	(105)

They found that T_{1X}^{-1} vs X was linear in the extrapolation to X = 0. They deduced in this way that T_{1intra}=103 sec and T_{1inter} = 26 sec at 25°C, which means T_{1neat}=207 sec

If the solvent is CCl_4, the result of equation (3.39) is 30 assuming $\gamma(^{35}Cl) \approx \gamma(^{37}Cl)$.

The spin-rotation interaction increases with the temperature as it was shown by Powles (97) in experiments performed on toluene and fluorobenzene. In the toluene case, the ring proton shows an increase in T_1 with temperature but T_1 for methyl reaches a maximum at about 120°C. In fluorobenzene the T_1 of the ring proton increases steadily with temperature while the fluorine T_1 reaches a maximum at about 20°C. This behaviour of the CH_3 protons and the fluorine is explained in terms of the existence of a spin rotation interaction. In some conditions, this can control the intramolecular interaction despite a dipolar contribution.

$$T_{1\ intra}^{-1} = T_{1\ intra\ dipolar}^{-1} + T_{1\ S.Rot}^{-1} \qquad (3.41)$$

For a spherical molecule the spin rotation contribution to T_1 is given by equation (3.23). It can be shown that for spherical molecules τ_d and τ_{SR} are related (98) by

$$\tau_d\ \tau_{SR} = I_o/6\ KT \qquad (3.42)$$

By using equations (3.23) in equations (3.41) and (3.42) we have

$$T_{1\,SR}^{-1} \times T_{1\,intra\ dip}^{-1} = \frac{1}{6}\hbar^2\gamma^4 I_o^2\left(\Sigma r_{ij}^{-6}\right)\left(2C_\perp^2+C_\parallel^2\right)=C \qquad (3.43)$$

where C is a constant independent of temperature for a given molecule.

Equations (3.41) and (3.43) enable us to separate the two contributions $T_{1intra\,d}$ and T_{1SR} from T_{1intra}. In particular, at the maximum of T_{1intra} we have $T_{1SR}=T_{1intra^d}= 2T_{1intra}$ from which C is obtained. In the case of benzene, Powles (106) found the maximum at 170°C, but at room temperature $T_{1\,SR}^{-1} \ll T_{1\,intra\ d}^{-1}$. Parker and Jonas (110) have isolated the intramolecular contribution for toluene and they have reported that at 25°C $T_{1\,SR}$ is comparable to T_1 intra-dipolar. They found $T_{1\,DD}=25.5$ sec and $T_{1\,SR}=35$ sec at 25°C.

Evidently, it is difficult to interpret T_1 for methyl groups when obtained at a single temperature because both dipolar and spin-rotation interaction contribute simultaneously to relaxation.

3.3 Relaxation In A Two-Spin System

In the case of a system of two loosely coupled spins, $I=\frac{1}{2}$ and $S=\frac{1}{2}$, there are four eigenstates of the spins. The energy levels for this system are indicated in figure

(3.4), where α refers to a spin with nuclear moment parallel to the magnetic field B_o and β indicates the opposite spin direction. The transition probabilities per unit of time W_1^I and W_1^S refer to the transition of the spin I and S respectively, while W_2 and W_o denote the transition probabilities for a double and zero quantum jump respectively.

In chapter one, we have mentioned that the changes in spin population depend on the transition probabilities. We will now extend this to the case of two spins, by using the same technique. Thus if $N_{\alpha\alpha}$, $N_{\beta\beta}$, $N_{\alpha\beta}$ and $N_{\beta\alpha}$ refer to the population of the energy levels, their variation with time is:

$$dN_{\alpha\alpha}/dt = -(W_1^I+W_1^S+W_2)N_{\alpha\alpha}+W_1^I N_{\beta\alpha}+W_1^S N_{\alpha\beta}+W_2 N_{\beta\beta}+\text{constant}$$

$$dN_{\alpha\beta}/dt = W_1^S N_{\alpha\alpha}+W_o N_{\beta\alpha}-(W_o+W_1^I+W_1^S)N_{\alpha\beta}+W_1^I N_{\beta\beta}+\text{constant} \qquad (3.44)$$

$$dN_{\beta\alpha}/dt = W_1^I N_{\alpha\alpha}-(W_1^S+W_1^I+W_o)N_{\beta\alpha}+W_o N_{\alpha\beta}+W_1^S N_{\beta\beta}+\text{constant}$$

$$dN_{\beta\beta}/dt = W_2 N_{\alpha\alpha}+W_1^S N_{\beta\alpha}+W_1^I N_{\alpha\beta}-(W_1^S+W_1^I+W_2)N_{\beta\beta}+\text{constant}$$

The constants are obtained by considering the system at temperature equilibrium by inserting the proper Boltzmann's factor, and are unimportant in the computation of the relaxation times (77).

The experimentally observable quantities are the macroscopic magnetic moment $\langle I_z \rangle$ and $\langle S_z \rangle$ distinguishable by their different Larmor frequencies and proportional to the difference between lower and upper spin populations

$$(N_{\alpha\alpha}+N_{\alpha\beta}) - (N_{\beta\alpha}+N_{\beta\beta}) = K \langle I_z \rangle$$

$$(N_{\alpha\alpha}+N_{\beta\alpha}) - (N_{\alpha\beta}+N_{\beta\beta}) = K \langle S_z \rangle \qquad (3.45)$$

Taking the derivative of $\langle I_z \rangle$ in equation (3.45), it results,

$$K \frac{d\langle I_z \rangle}{dt} = \frac{dN_{\alpha\alpha}}{dt} + \frac{dN_{\alpha\beta}}{dt} - \frac{dN_{\beta\alpha}}{dt} - \frac{dN_{\beta\beta}}{dt} \qquad (3.46)$$

Then, by substituting equations (3.44) in equation (3.46) we obtain,

$$K \frac{d\langle I_z \rangle}{dt} = -(2W_1^I+2W_2)N_{\alpha\alpha}+(2W_1^I+2W_0)N_{\beta\alpha}-(2W_1^I+2W_0)N_{\alpha\beta} \qquad (3.47)$$
$$+(2W_2+2W_1^I)N_{\beta\beta} + \text{constant}$$

equation (3.47) can be expressed as

$$K \frac{d\langle I_z \rangle}{dt} = aK\langle I_z \rangle + bK\langle S_z \rangle + \text{constant} \qquad (3.48)$$

Then, by comparison of equation (3.47) with equation (3.48) we get

$$a = -(W_0 + 2W_1^I + W_2)$$

$$b = -(W_2 - W_0)$$

Therefore, we can write equation (3.47) as

$$\frac{d\langle I_z \rangle}{dt} = -(W_0+2W_1^I+W_2)\langle I_z \rangle-(W_2-W_0)\langle S_z \rangle+\text{constant} \qquad (3.49)$$

and similarly

$$\frac{d\langle S_z\rangle}{dt} = -(W_2-W_o)\langle I_z\rangle-(W_o+2W_1^s+W_2)\langle S_z\rangle+\text{constant} \quad (3.50)$$

in equilibrium, $\frac{d\langle Iz\rangle}{dt}=0$ and $\frac{d\langle Sz\rangle}{dt}=0$. Therefore,

equations (3.49) and (3.50) can be written as

$$\frac{d\langle I_z\rangle}{dt} = -\rho_I(\langle I_z\rangle-I_o)-\sigma_{IS}(\langle S_z\rangle-S_o) \quad (3.51)$$

and

$$\frac{d\langle S_z\rangle}{dt} = -\rho_s(\langle S_z\rangle-S_o)-\sigma_{SI}(\langle I_z\rangle-I_o) \quad (3.52)$$

where

$$\rho_I = 2W_1^I + W_o + W_2 \quad (3.53)$$

$$\rho_S = 2W_1^s + W_o + W_2 \quad (3.54)$$

$$\sigma_{IS} = W_2 - W_o = \sigma_{SI} \quad (3.55)$$

In equations (3.51) and (3.52) the rotation used is that of Solomon [77]. Abragam [62] has found the same equation by using a different procedure and different notation, i.e.

$$\rho_I = 1/T_1{}^{II} \qquad \sigma_{IS} = 1/T_1{}^{IS}$$

$$\rho_S = 1/T_1{}^{ss} \qquad \sigma_{SI} = 1/T_1{}^{SI}$$

The σ terms are often referred to as the cross-relaxation terms. In order for this term to be

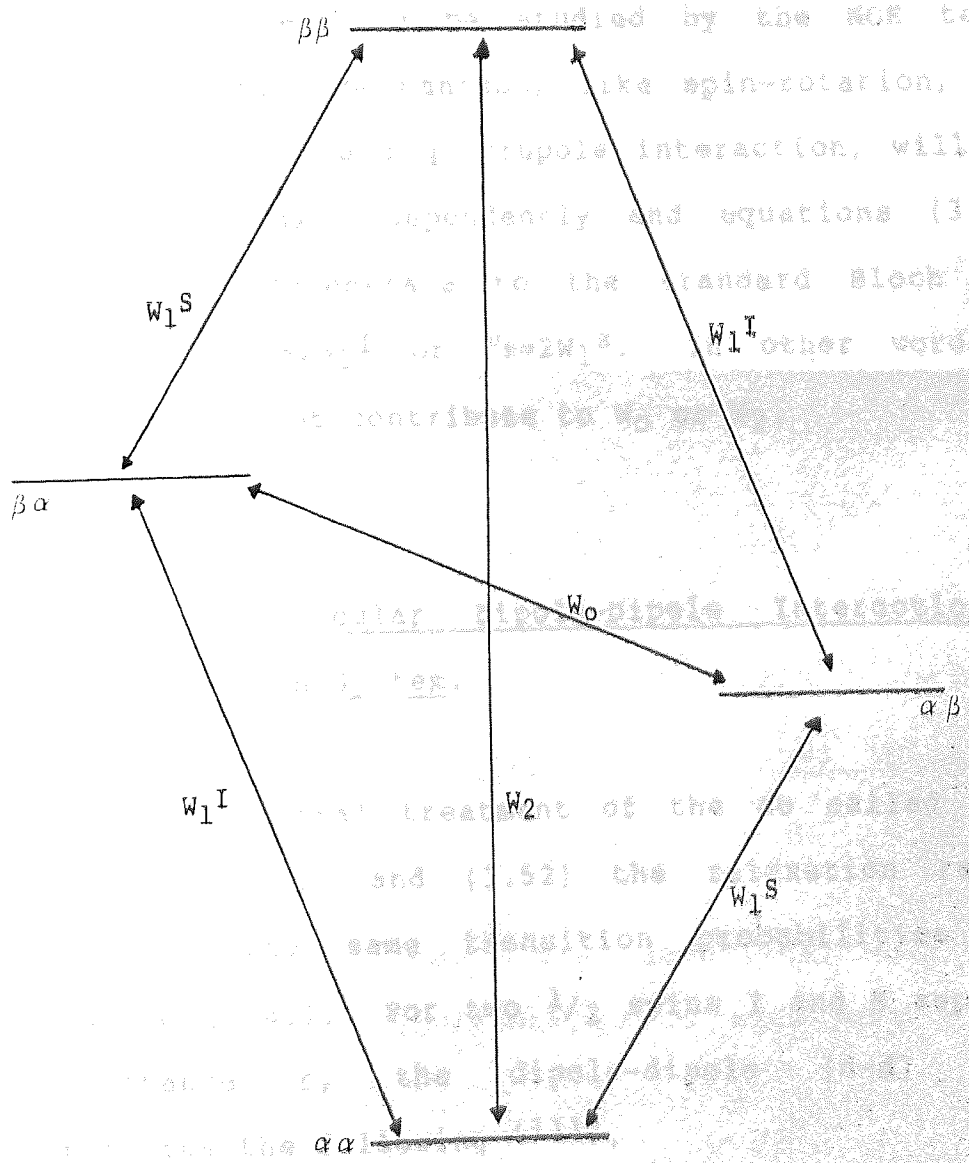

Figure 3.4 The energy level diagram for the interaction of two spins $\frac{1}{2}$

nonzero, a relaxation mechanism which couples I and S must be present; there are three such mechanisms,

a) dipole-dipole relaxation between I and S

b) I to S scalar (J) coupling modulated by chemical exchange or internal motion (J is time dependent)

c) I to S scalar (J) coupling modulated by rapid relaxation of S.

Only (a) and (b) will be significant for systems which are likely to be studied by the NOE technique. Other relaxation mechanisms, like spin-rotation, chemical shift anisotropy and quadrupole interaction, will cause I and S to relax independently and equations (3.51) and (3.52) will degenerate to the standard Bloch equation with $1/T_1{}^I = \rho_I = 2W_1{}^I$ or $\rho_S = 2W_1{}^S$. In other words, these mechanisms do not contribute to W_0 or W_2.

3.3.A Intramolecular Dipole-Dipole Interaction in a Two-Spin System.

In the general treatment of the so called Solomon's equations (3.51) and (3.52) the relaxation rate terms ρ and σ use the same transition probabilities function (equation (3.8)). For two $1/2$ spins I and S separated by a distance r, the dipole-dipole (d-d) mechanism contributes the following (111).

$$W_1(dd) = \frac{3}{20} \frac{\gamma_I^2 \gamma_S^2 \hbar^2}{r^6} \frac{\tau_c}{1+\omega_I^2 \tau_c^2} \qquad (3.56)$$

$$W_o(dd) = \frac{1}{10} \frac{\gamma_I^2 \gamma_S^2 \hbar^2}{r^6} \frac{\tau_c}{1+(\omega_I-\omega_S)^2 \tau_c^2} \qquad (3.57)$$

$$W2(dd) = \frac{3}{5} \frac{\gamma_I^2 \gamma_S^2 \hbar^2}{r^6} \frac{\tau_c}{1+(\omega_I+\omega_S)^2 \tau_c^2} \qquad (3.58)$$

In most cases, extreme narrowing prevails and the frequency terms in the denominator can be neglected. In this limit the relaxation rate parameters in the Solomons's equations (3.51) and (3.52) are:

$$\sigma(dd) = \frac{1}{2} \gamma_I^2 \gamma_S^2 \hbar^2 \tau_c/r^6 \qquad (3.59)$$

$$\rho(dd) = \gamma_I^2 \gamma_S^2 \hbar^2 \tau_c/r^6 \qquad (3.60)$$

therefore,

$$\sigma = \frac{1}{2} \rho \qquad (3.61)$$

3.3.B Relaxation Time For Two Identical spins; the 3/2 effect.

If the spins I and S are identical, only $\langle I_z \rangle + \langle S_z \rangle$ can be observed. Therefore, from equations (3.51) and (3.52) we obtain.

$$\frac{d}{dt} (\langle I_z \rangle + \langle S_z \rangle) = -(\rho+\sigma)[(\langle I_z \rangle + \langle S_z \rangle) - (I_o+S_o)] \qquad (3.62)$$

where the relaxation time of the observed signal is

$$1/T_1 = \rho + \sigma \qquad (3.63)$$

Since, for dipole-dipole relaxation between I and S, $\sigma = \frac{1}{2}\rho$ we see that for dipole-dipole coupling of identical spins T_1 is

$$1/T_1 = \frac{3}{2}\rho \qquad (3.64)$$

while for non-identical spins (111) $1/T_1 \approx \rho$. This is the origin of the so-called "$^3/_2$ effect", which we will use in chapter eight.

3.4 The Nuclear Overhauser Effect

3.4.A Introduction

The term "Overhauser effect" referred originally to the dynamic polarization of nuclei in metals (112) when the spin resonance of the electrons was saturated. The first application of this effect in systems containing only nuclear spins was made by Solomon and Bloembergen (113) in their study of chemical exchange in hydrogen fluoride. The nuclear Overhauser effect (NOE) next found application in the assignment of complex NMR spectra (114) in the study of chemical exchange (115), nuclear relaxation (116) and in signal to noise improvement in NMR spectra (117). The potential of the NOE for providing information on the conformation and

configuration of molecules in solution was first demonstrated by Anet and Bourn (118) and since that time applications in this area have grown rapidly. Bell and Saunders (119) have reported direct correlation between NOE enhancements and internuclear distances and Schirmer et al (120) have demonstrated that relative internuclear distances can be determined quantitatively from NOE measurements on systems containing three or more spins.

3.4.B FRACTIONAL ENHANCEMENTS (NOE)

The nuclear Overhauser effect (NOE) is a change in the integrated nuclear magnetic resonance (NMR) absorption intensity of a nuclear spin, when the NMR absorption signal of another spin is saturated. The spins involved may be either heteronuclear or chemically shifted homonuclear spins.

NOE experiments essentially require that:

a) a strong r.f. field is applied at the Larmor frequency of spins S, so that $\langle Sz \rangle = 0$.

b) $\langle I_z \rangle$ is measured by a weak r.f. field with a frequency near the Larmor frequency of spin I. The fractional enhancement of the integrated intensity of $I(\langle I_z \rangle)$ when S is saturated, compared to the equilibrium intensity of $I(I_o)$ is defined as

$$f_I(S) = \frac{(\langle I_z \rangle - I_o)}{I_o} \qquad (3.65)$$

When a steady state is reached, $\frac{d}{dt}\langle I_z\rangle = 0$ and equation (3.51) gives.

$$\langle I_z\rangle = I_o + \sigma_{IS}\ \frac{S_o}{\rho_I} \tag{3.66}$$

or

$$f_I(S) = \frac{\sigma_{IS}}{\rho_I}\ \frac{S_o}{I_o} \tag{3.67}$$

but

$$I_o \propto I(I+1)\,\gamma_I; \qquad S_o \propto S(S+1)\,\gamma_s$$

giving

$$f_I(S) = \frac{\gamma_S\ \sigma_{IS}\ S(S+1)}{\gamma_I\ \rho_I\ I(I+1)} \tag{3.68}$$

If spin I relaxes only by dipole-dipole coupling with S then (62)

$$\frac{\sigma_{IS}}{\rho_I} = \frac{I(I+1)}{2S(S+1)} \tag{3.69}$$

and then, by using equation (3.68) in equation (3.69) we have

$$f_I\ (S) = \frac{\gamma_S}{2\ \gamma_I} \tag{3.70}$$

which represents the "maximum" NOE observable in any case.

When $I = S = \frac{1}{2}$ equation (3.68) becomes

$$f_I\ (S) = \frac{W_2 - W_o}{2W_1^I + W_o + W_2} \tag{3.71}$$

If relaxation processes in addition to dipole-dipole are present, they will contribute to W_1^I, which becomes,

$$W_1^I \text{ total} = W_1^I + W_1^\circ \qquad (3.72)$$

and therefore,

$$f_I(S) < f_I(S) \max = \eta_o \qquad (3.73)$$

By referring to this condition, it is possible to know how effective the "other" relaxation processes are.

3.4.C Relaxation in Multispin Systems

The Solomon's equations (3.51) and (3.52) can be generalized by considering a multispin system as a sum of pairwise interactions and summing the relaxation effects of each pair of spins. For a spin i coupled to a group of spins j, we have

$$\frac{d}{dt}\langle I_{zi}\rangle = -R_i(\langle I_{zi}\rangle - I_{oi}) - \sum_{j\neq i}\sigma_{ij}(\langle I_{zj}\rangle - I_{oj}) \qquad (3.74)$$

where

$$R_i = \sum_{j\neq i}\rho_{ij} + \rho_i^*$$

where the symbols have the usual meaning and ρ^* is the direct relaxation of spin i due to "other" relaxation paths, i.e. spin rotation relaxation, anisotropic chemical shift, paramagnetic relaxation and so on.

ρ_{ij} is the direct dipole-dipole relaxation between ij

$$\rho_{ij} = \gamma_i^2 \gamma_j^2 \hbar^2 \tau_{c(ij)}/r_{ij}^6 \qquad (3.75)$$

and

$$\rho_{ij} = 2 \sigma_{ij} \qquad (3.76)$$

3.4.C.1 The NOE In Multi-Spin Systems

The fractional enhancement of the total integrated intensity of the resonance of the detected spin I_d when spins I_s are saturated is defined as

$$f_d(s) = [\langle I_{zd}\rangle - I_{od}]/I_{od} \qquad (3.77)$$

Equation (3.74) can be solved for $f_d(s)$ by setting $\langle I_{zs}\rangle = 0$ for all of the saturated spins and using the steady-state assumption for spin d

$$\frac{d}{dt}\langle I_{zd}\rangle = 0$$

This gives

$$f_d(s) = \sum_s \sigma_{ds} I_{os}/R_d I_{od} - R_d^{-1} \sum_n \sigma_{dn} \frac{I_{on}}{I_{od}} \frac{(\langle I_{zn}\rangle - I_{on})}{I_{on}} \qquad (3.78)$$

where n labels the spins not saturated not including d. But $(\langle I_{zn}\rangle - I_{on})/I_{on}$ is $f_n(s)$, the enhancement of spin n when s is saturated. Likewise

$$I_{oi} = I_i (I_i + 1) \gamma_i \qquad (3.79)$$

and, for dipole-dipole relaxation

$$\sigma_{ij} \propto (\rho_{ij}/2)\ I_i\ (I_i + 1)/I_j(I_j + 1)$$

This gives (111)

$$f_d(s) = \sum_s \gamma_s\ \rho_{ds}/2\gamma_d\ R_d - \sum_n \gamma_n \rho_{dn}\ f_n^{(s)}/2\gamma_d\ R_d \quad (3.80)$$

The sum over s includes all saturated spins; the sum over n includes all spins except d and s. By implication d is a single spin; if d is one of a group of equivalent spins the enhancement of each member of the group is the same. Some examples are (111).

a) Case $a_2\ X_3$

In this case by using equation(3.78) we have

$$f_a(x) = 3\ \rho_{ax}(\gamma_x/2\gamma_a)/(^3/_2\ \rho_{aa} + 3\ \rho_{ax} + \rho_a^*) \quad (3.81)$$

$$f_x(a) = 2\ \rho_{xa}(\gamma_a/2\gamma_x)/(3\rho_{xx} + 2\rho_{xa} + \rho_x^*) \quad (3.82)$$

b) Three spins a,b,c, linear

$$f_a(b) = \rho_{ab}/2Ra - \rho_{ac}\ f_c^{(b)}/2\ Ra \quad (3.83)$$

or

$f_a(b) \approx \rho_{ab}/2Ra$ neglecting the second term; if the end spin is observed while the other end spin saturated, we have

$$f_c(a) \approx -f_c(b) f_b(a) \qquad (3.84)$$

In the case of multiple saturation we have

$$f_b(a+c) \approx f_b(a) + f_b(c) \qquad (3.85)$$

The effect of multiple resonance NOE is approximately the sum of the enhancements when one spin is saturated at a time.

Many more examples can be found in reference (111) where the measurements of NOE enhancements are used in determining relative internuclear distances in spin systems with more than three spins.

Numerous applications of NOE measurements in structural organic chemistry have been described (121)(122)(118). In particular the work of Bell and Saunders (123) on ochotensimine have shown positive and negative enhancements when selected protons were irradiated and those were correlated with the molecular structure. They have found (119) a linear relationship between the intramolecular nuclear Overhauser enhancements (NOE) and the sixth power of the intermolecular distance for protons in compact organic molecules in deuterochloroform solution. This happens because the intramolecular relaxation is competing with an essentially constant intermolecular contribution from the solvent. The enhancement is

$$f_d(S)^{-1} = 2 + Ar^6_{ds} \qquad (3.86)$$

where the constant A depends on the ratio between intermolecular and intramolecular contribution. For a non-rigid molecule (dimethil formamide) they have found[124] that irradiation of the high field CH_3 signal caused 3% enhancement of the formyl proton signal at 31°C whereas it caused 24% enhancement at 70°C, i.e., more rapid exchange at higher temperature transfers saturation from the methyl group site cis to the formyl proton.

3.4.C.2 Intermolecular NOE

In addition to the intramolecular NOE there can be an intermolecular contribution, that is effective when high concentrations of nuclei (e.g. ^1H or ^{19}F) are present. It is very inconvenient as far as NOE structural studies are concerned since the intramolecular NOE enhancements tend to decrease because of it. Kaiser (125), who observed an intermolecular NOE between the protons of cyclohexane and chloroform, suggested that such experiments should be of interest in the study of liquids and intermolecular forces.

According to Hertz (87) the relaxation rate of spin I due to intermolecular dipole-dipole (xd) interactions with a spin S is approximately

$$\rho_{IS}^{xd} = \frac{8\pi}{45} \frac{N_S \gamma_I^2 \gamma_S^2 \hbar^2 S(S+1)}{D_{IS}\, a} \qquad (3.87)$$

where N_S is the concentration of spins S, a is the distance of closest approach between spins I and S, and D_{IS} is the mutual (translational) self-diffusion constant of the molecules containing I and S and is given by

$$D_{IS} = \frac{1}{2} (D_I + D_S) \qquad (3.88)$$

where D_I and D_S are the self-diffusion constant of I and S respectively. The value of ρ_{IS}^{xd} can be expressed as well by using the results of other authors (79)(86) but it is always difficult to test the outcome due to the poorly defined quantity a and the evaluation of the self-diffusion constant.

It has been shown (125) that the saturation of protons in solvent molecules can enhance the signals of protons in solute molecules. Mackor and Maclean (126) have used a collision complex A-B model to analyse the intermolecular interactions, where the transition probabilities are defined analogously to those in the intramolecular case. The analysis of Bell and Saunders (119) for getting the relationship between enhancement and internuclear distances, uses the model of dipole-dipole interaction between the protons in the molecule under study and other protons in the first shell around this molecule. Other workers (127)(128) have used the Solomon's equation to obtain information about

intermolecular interactions and the relative success of this kind of approach suggests that the standard equation (3.80) which is applied to intramolecular interactions can be extended to the case of intermolecular interactions in order to correlate the enhancement obtained after saturation of the solvent with the characteristic intramolecular and intermolecular relaxation times.

3.5 ^{13}C Relaxation Processes

Relaxation data relate closely to overall and local molecular geometry, bonded and non-bonded interactions, and other factors controlling molecular motions.

The ^{13}C nucleus is particularly suited for relaxation studies for several reasons:

1) Since carbon is usually not found at the periphery of molecules, the interpretation of its relaxation behaviour is generally not complicated by intermolecular relaxation processes, unlike the situation for ^{1}H and ^{19}F nuclei.
2) ^{13}C spectra are primarily observed under proton decoupled conditions, where each carbon in the molecule is generally represented by a single spectral line whose spin-lattice (T_1) and spin-spin (T_2) relaxation times are governed by single exponential time constants (129).

3) The rather large chemical shift range of the ^{13}C nucleus makes it possible to resolve most individual carbons, even in complex molecules. Thus several sites are often available at which to probe a molecule's motional features.

Carbon-13 spin-lattice relaxation studies can, therefore, give the chemist an additional set of parameters that may be used to characterize organic molecules.

3.5.A Spin-Lattice Relaxation Mechanisms

The four relaxation mechanisms that are generally considered to facilitate energy transfer between nuclear spins and the lattice arise as explained earlier from dipole-dipole interactions, spin-rotation interactions, chemical shift anisotropy and scalar interactions. All of these mechanisms can be operative to various extents for individual carbons in different molecules. However, only the first two are commonly observed.

The general treatment of relaxation mechanisms has been covered in section 3.2. Conceptual descriptions of ^{13}C relaxation mechanisms are provided elsewhere (130)(131)(102).

3.5.A.1 Chemical Shift Anisotropy (CSA) Relaxation

Significant anisotropy in the shielding of a nucleus can give rise to fluctuating magnetic fields when molecules tumble in fluids (relative to the fixed laboratory magnetic field). The C.S.A. can be large for carbon e.g., for carbon nuclei such as those involved in double bonds, in carbonyl groups and aromatic systems, when the anisotropy of the chemical shift, $\Delta\sigma$, is typically of the order of 150-200 p.p.m.(132)(133). Nevertheless, C.S.A. relaxation is almost never significant for ^{13}C nuclei at normal spectrometer fields of, say, less than 2 Tesla. However, because the efficiency of C.S.A. relaxation follows the square of the magnetic field, this mechanism may play a more important role in experiments performed at very high fields. Even so, at 5.9 Tesla (63 MH_Z), C.S.A. relaxation does not dominate relaxation for the non-protonated carbon in toluene (131). The first example where the C.S.A. relaxation mechanism could be demonstrated in liquids was for ^{13}C relaxation in CS_2 (134). The importance of the C.S.A. relaxation contribution in relation to the dipolar contribution (135) is influenced by the value of γ for adjacent nuclei. For this reason the C.S.A. contribution for the carbonyl carbon of deuterated acetone is bigger than the dipolar contribution.

3.5.A.2 Relaxation By Scalar Coupling

A ^{13}C nucleus that is spin-spin (scalar) coupled to a quadrupolar nucleus X that is undergoing rapid spin-lattice relaxation may, in principle, be relaxed by the rapid modulation of the spin-spin coupling constant J_{C-X}. However, scalar ^{13}C spin-lattice relaxation is very rare and has been observed thus far, only for carbons attached to bromine atoms because of their similar values of $\gamma(131)$. As a consequence, ^{13}C nuclei bound to Br relax relatively quickly e.g. ($CHCl_3$: T_1=32 sec),($CHBr_3$: T_1=1.65 sec)

3.5.A.3 Spin-Rotation (S R) Relaxation

Small molecules and freely rotating CH_3 groups can be effectively relaxed by a mechanism involving local magnetic fields produced by the rotational motion of the molecule or group itself. In these cases SR relaxation often competes with D.D. relaxation for protonated carbons, while the SR interaction dominates the relaxation of non-protonated carbons. At high temperatures and low viscosities T_1^{SR} becomes shorter as a result of increased molecular motion. Observed SR relaxation times in small molecules are typically 15-50 sec (130)(131)

3.5.A.4 Dipole-Dipole Interaction and NOE

Each nuclear spin generates a local magnetic field. If two magnetic nuclei such as ^{13}C and ^{1}H are linked by a bond, then each of the nuclei will "feel" not only the external field B_o, but also the local fields of the other nuclear spins (intramolecular dipole-dipole interaction). In liquids molecular motion is very rapid and the spatial rotation of C-H bonds are correspondingly fast in dissolved organic molecules. Consequently, the orientation of 1H and 13C relative to B_o will be constantly changing. As a result, the magnetic reorientations of the two nuclear spins generate fluctuating local fields which contribute to the relaxation of the nuclei. Most of the ^{13}C nuclei in organic molecules, especially those linked to hydrogen (CH, CH_2, CH_3) are relaxed predominatly by intramolecular dipole-dipole interaction.

Intermolecular contributions are usually small and for example, the intermolecular contribution to the carbon-13 relaxation of formic acid is negligible (136). Kuhlmann and Grant (137) have concluded that in mesitylene and O-Xylene the intermolecular contribution is approximately 4% and 7% of the intramolecular contribution, which is really quite small. However, for carbons without nearby protons the intermolecular effect can be significant. A similar conclusion have been reported for benzene and cyclohexane (103). Evidence for

an intermolecular nuclear Overhauser effect for enriched CCl_4 and CS_2 in alkanes [138] has been found. The effect varies between 8% and 50% of the maximum depending on the solvent characteristics.

The Solomon's equation (3.51) for ^{13}C-H is

$$\frac{dI_z}{dt}(^{13}C) = -\rho_c(\langle I_z(^{13}C)\rangle - I_o(^{13}C)) - \sigma(\langle I_z(^{1}H)\rangle - I_o(^{1}H)) \qquad (3.89)$$

where

$$\rho_c = W_o + 2W_{1c} + W_2 = \frac{1}{T_{1c}} \qquad (3.90)$$

$$\sigma = W_2 - W_o = \frac{1}{T_{1CH}} \qquad (3.91)$$

Because of the coupling C-H the recovery of $I_z(^{13}C)$ will be non-exponential and requires analysis of data in terms of two relaxation times $\frac{1}{\rho_c}$ and $\frac{1}{\sigma}$ [139]. Fortunately, T_1 values of ^{13}C can usually be measured with proton noise decoupling and then $\langle I_z(^{1}H)\rangle = 0$ in equation (3.89). The effect of this is to simplify matters so that

$$\frac{\langle I_z(^{13}C)\rangle}{I_o(^{13}C)} = 1 + \frac{\sigma}{\rho_c}\frac{I_o(^{1}H)}{I_o(^{13}C)} = 1 + \frac{\sigma}{\rho_c}\frac{\gamma_H}{\gamma_C} \qquad (3.92)$$

The nuclear Overhauser enhancement (NOE) factor η is defined by

$$\eta = \frac{\langle I_z(^{13}C)\rangle - I_o(^{13}C)}{I_o(^{13}C)} = \frac{\sigma}{\rho_c}\frac{\gamma_H}{\gamma_C} \qquad (3.93)$$

which has a maximum value when the only interaction is dipolar-dipolar, of

$$\eta = \frac{1}{2}\,\frac{\gamma_H}{\gamma_C} = 1.988 \qquad (3.94)$$

In the extreme narrowing limit, the value of $\rho_C = T_{1C}^{-1}$ is:

$$\frac{1}{T_{1C}} = \frac{\hbar^2 \gamma_H^2 \gamma_C^2}{r^6}\,\tau_C \qquad (3.95)$$

which applies to the relaxation of a carbon nucleus bonded to a single proton. Equation (3.95) can be modified to take into account interaction from other protons directly attached to the carbon or attached to other atoms in the molecule. For this case the ^{13}C relaxation time due to the C-H dipolar interaction, $T_1^{DD} = T_{1C}$, is given by

$$\frac{1}{T_1^{DD}} = \sum_{i=1}^{N} \frac{\gamma_H^2\,\gamma_C^2\,\hbar^2}{r_{CH_i}^6}\,\tau_C^{eff} \qquad (3.96)$$

where τ_C^{eff} is the effective isotropic correlation time. In most instances of a carbon directly bonded to hydrogen the relaxation interactions from non-bonded protons can be ignored, due to the shortness of the C-H bond relative to non-bonded C-H distances. The expression for $T_1^{-1}{}^{DD}$ then reduces to (140)

$$\frac{1}{T_{1DD}} = \frac{n_H\,\gamma_H^2\,\gamma_C^2\,\hbar^2}{r_{CH}^6}\,\tau_C^{eff} \qquad (3.97)$$

where n_H is the number of protons directly attached to the carbon of interest.

3.5.B Relationship of T_{1DD} to the Nuclear Overhauser Enhancement Factor η

It is important to notice that even if several mechanisms compete in the ^{13}C spin-lattice process, the recovery of M_Z from a perturbation is exponential provided that T_1 is determined under proton-decoupled conditions. This result is apparent from the fact that only the C-H dipolar mechanism gives rise to W_2 and W_o transitions, because all the other mechanisms affect only W_{1C} (129). Consequently, if $\overset{\circ}{W}_{1C}$ represents a non-dipolar relaxation mechanism, T_{1C} is given by

$$\frac{1}{T_{1c}} = W_o + 2\overset{DD}{W}_{1C} + 2\overset{\circ}{W}_{1C} + W_2 \qquad (3.98)$$

$$\frac{1}{T_{1C}} = \frac{1}{T_1^{DD}} + \frac{1}{T_1^{\circ}} \qquad (3.99)$$

where T_1° represents other, or non-dipolar interactions. By using equation (3.68) the NOE factor η is

$$\eta = \frac{\gamma_H}{\gamma_C} \quad \frac{\sigma}{\rho_C} = \frac{\gamma_H}{\gamma_C} \quad \frac{W_2 - W_o}{Wo + 2\overset{DD}{W}_{1C} + 2W_1^{\circ} + W_2} \qquad (3.100)$$

$$\eta = \frac{\gamma_H}{\gamma_C} \quad \frac{W_2 - W_o}{(T_1^{DD})^{-1} + (T_1^{\circ})^{-1}} \qquad (3.101)$$

but in the motionally narrowed region $W_2 - W_o = \frac{1}{2} T_{1DD}^{-1}$

$$T_{1DD} = T_{1C} \quad \frac{1.988}{\eta} \qquad (3.102)$$

where T_{1C} is the experimental relaxation time determined under noise decoupling condition.

Equation (3.102) has an intermolecular analogue. For the case of CS_2 and CCl_4 in alkanes (138) the extension of equation (3.102) is

$$T_1 \text{inter} = T_{1C} \frac{1.988}{\eta_{\text{inter}}} \qquad (3.103)$$

where T_{inter} and η_{inter} represent the intermolecular relaxation time and intermolecular NOE factor respectively.

3.5.C Separation of Relaxation Contributions

A combination of variable field and variable temperature T_1, and NOE experiments can distinguish DD, SR and CSA relaxation processes. Since T_1^{-1} is given by

$$\frac{1}{T_1} = \frac{1}{T_{1DD}} + \frac{1}{T_{1SR}} + \frac{1}{T_{1CSA}} + \frac{1}{T_{1sc}} \qquad (3.104)$$

a typical approach to the separation of the mechanisms is to determine T_1 and the $^{13}C\ \{^1H\}$ NOE. Use of equation (3.104) then enables T_1^{DD} and $T_1°$ to be readily separated. Often it is assumed that CSA and SC contribute negligibly, so that $T_1° \approx T_1^{SR}$. If chemical shift anisotropy is operative, then constant temperature variable field experiments enable T_1^{CSA} to be extracted from $T_1°$ via the square field dependence of T_1^{CSA} (135).

Tables (3.3) and (3.4) give an idea of the magnitudes of several individual contributions to ^{13}C relaxation.

Table 3.3 Individual contributions to ^{13}C Relaxation times for serveral compounds.

Compound	Carbon	T_1	NOE(η)	T_{1DD}	T_{1SR}	T_{1O_2}	T_{1CSA}
benzene(102)							
degassed	all	29.3	1.6	37	146		
undegassed	all	23.0	1.3	35		107	
Toluene(102)							
degassed	1	89	0.59	297	130		≥3.000
	2,3,4	22	1.68	26	147		≥3.000
undegassed	1	58	0.43	270		155	
	2,3,4	19.5	1.45	27		135	
cyclohexane(103)		17.5	2	18	100		
mesitylene(137)	ring	41	0.96	85	78		
	CH	7	2	7	80		
	CH_3	11	1.04	23	25		

Table (3.4) Carbon-13 spin-lattice relaxation times and NOE for several compounds.

Molecule		C_1	C_2	C_3	Solvent	T(°K)	Ref
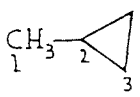	T_1	12.2	15.2	13.5	$CDCl_3$	303	141
	η	0.8	0.5	0.6			
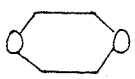	T_1		10.7		neat	303	142
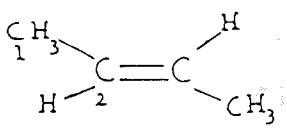	T_1	27	14.5		neat	313	143
	η	1	0.2				

3.6 Molecular Dynamics

Introduction

The nuclear spin relaxation rates in nuclear magnetic resonance for two like nuclei of spin $^1/_2$ having a constant separation distance are proportional to Jh(w), the Fourier intensities of the correlation functions $\langle Fh(t)Fh^*(t+\tau)\rangle$, which relate the orientation of the vector joining the two nuclei. Bloembergen (74) has calculated the relaxation times attending the tumbling of the internuclear vector by assuming it is attached to a sphere undergoing isotropic rotational diffusion in a continuous medium just as in the Debye (78) theory of dielectric relaxation.

If a molecule acts like an ellispsoid rather than a sphere undergoing anisotropic rotational diffusion in a continuous dielectric medium, the rotational motions about the different axes of the ellipsoid occur at different rates. Perrin (144)(145) has calculated the dielectric relaxation for this model by extending the Debye theory for spheres to ellipsoids with the correlation times related to molecular axes a,b,c. Woessner (89) has calculated the nuclear spin relaxation time T_1, T_2 for two identical nuclei of spin $I=^1/_2$ fixed in an ellipsoid undergoing rotational Brownian motion. He found five nuclear correlation times; for non-viscous liquids $T_1=T_2$; when the rotation probabilities about two

axes are equal, the number of correlation times is reduced to three. In the case of isotropic motion, only one correlation time was obtained.

Relaxation measurements on protons have provided insight into the dynamic behaviour of many relatively simple molecules (87), but in this case contributions from inter and intramolecular dipole-dipole interactions must be separated through appropriate dilution studies.

3.6.A Investigation Of Molecular Motion By ^{13}C Spin Relaxation

The study of molecular motion by using ^{13}C relaxation seems a desirable alternative to ^{1}H studies because the ^{13}C-H intramolecular dipole-dipole interaction is the dominant mechanism for the spin-lattice relaxation of ^{13}C in all except the very smallest molecules (146). The intermolecular ^{13}C-^{1}H dipole-dipole interaction does not contribute significantly to ^{13}C relaxation in most organic molecules. For example, for toluene (102) the intermolecular dipole-dipole relaxation for the protonated and non-protonated carbons corresponds to $T_1^{DD}inter \geq 1.500$ sec which is a very small contribution to T_1. Because the ^{13}C relaxation rate arises mainly from intramolecular coupling and $T_1^{DD}intra$ can be extracted using the NOE factor, it is evident that this facilitates a detailed study of molecular reorientation.

The effect of anisotropic overall or internal motion on T_1's for the different carbons in a molecule depends on the angular relationships between each carbon and the proton relaxing it relative to the preferred mode of rotation. For example (102), in monosubstituted benzene, rotation around the C_2 molecule symmetry axis (coincident with the substituent ring-bond) is favoured. If the substitute is large and heavy or highly polar, then rotation around the C_2 axis may be 5-20 times faster than rotation around the remaining perpendicular axis; rotation around the C_2 symmetry axis does not lead to any modulation of the T_1^{DD} of the para ^{13}C and its directly attached protons. However, such a rotation for the ortho and meta carbons because the C-H bonds in these instances make angles (θ) of 60° and 120° with the C_2 axis and move relative to this axis.

Differing T_1 values for CH_3, CH_2 and CH carbon nuclei within a molecule can arise not only by methyl rotation or anisotropic molecular motion but also from the segmental mobility of partial structures. For example, in decane (147) the molecular periphery is found to be more flexible that the centre.

Campbell et al (148) have used pyridine as a motional anisotropy probe, assuming that the formation of a complex between two species slows down the tumbling rate about axes perpendicular to the direction of the newly formed bond. This change in the rotational diffusion

tensor can be followed by measuring ^{13}C spin lattice relaxation times.

Kuhlmann and Grant (137) have studied the ^{13}C relaxation times for O-xylene and mesitylene. They have concluded that in mesitylene the internal methyl rotation is very rapid with respect to overall molecular diffusion while in O-xylene it is not as rapid as in the case of mesitylene.

3.6.B Other Methods For Analysis of Molecular Motion

In addition to the use of ^{1}H T_1 and ^{13}C T_1 for the study of molecular motion, investigations of this have also been based on ^{2}H quadrupolar relaxation times, the chemical shift anisotropy interaction and light scattering experiments, in order to provide additional information about the molecular movement.

3.6.B.1 Quadrupolar Relaxation Times

For covalently bonded quadrupolar nuclei, the electric field gradient at the nucleus is often quite large, and the quadrupolar interactions can become two or three orders of magnitude larger than that of any other interaction, which can then be ignored. This means that the only source of relaxation is of intramolecular origin. Therefore, the relaxation time for nuclei such as ^{2}H, ^{35}Cl, etc, provides the rotational correlation time directly.

Huntress (149) has related τ_{rot} to the components of the rotational diffusion tensor for anisotropic rotational diffusion. For symmetric top molecules such as Deutero - chloroform, τ_{rot} is a function of the rotational diffusion constants $D_{\parallel}$ and $D_{\perp}$. He deduced the deuteron relaxation time (150) to be:

$$T_{1D}^{-1} = \frac{(e^2 Q q)^2 D}{16 D_{\perp}} \qquad (3.105)$$

because there is no field gradient fluctuation when the molecule rotates about the symmetry axis along C-D. Since the chlorines are at $\theta = 110°$ to the symmetry axis along the C-D bond, the expression for T_{1Cl} is a complicated function of $D_{\parallel}$, $D_{\perp}$ and θ. If the quadrupole coupling constants for ^{2}H and ^{35}Cl in deuterochloroform are known, it will be possible to calculate $D_{\perp}$ and then $D_{\parallel}$ which determine the motion of the molecule.

Gillen et al (151) explored the relaxation of several nuclei in methyl iodide and found agreement between rotational parameters obtained from spin-lattice relaxation measurements on ^{13}C, ^{1}H and ^{2}D but they did not use the nuclear Overhauser enhancement to measure the dipolar contribution to the relaxation of ^{13}C.

Shoup et al (152) have measured the ^{13}C relaxation rates for $^{13}CHCl_3$ which is given by

$$R_{1DD} = \gamma_C^2 \gamma_H^2 \hbar^2 \tau_{c_\perp} (r_{CH})^{-6} \qquad (3.106)$$

After correcting R_1 by using the (NOE) factor η the correlation time is $\tau_{c_\perp} = 6(D_\perp)^{-1}$ which agreed with the values obtained by Huntress (150). Spiess et al (153) have found that in toluene, the effective correlation times for ^{13}C and ^{2}D reflect the same average over the anisotropic motion of the molecule. A similar result is reported by Jacobsen (154). The above examples serve to illustrate the importance of studies of quadrupolar nuclei.

3.6.B.2 Light Scattering

Pecora and co-workers (155)(156) have made extensive measurements probing the reorientation of anisotropic molecules. They combined ^{13}C spin-lattice relaxation times with those obtained from depolarized Raleigh spectra.

The simplest molecules studied by these authors were benzene and mesitylene (156). Both of these molecules are symmetric tops and hence have only two relaxation times for reorientation. One of these reorientations is about the symmetry axis perpendicular to the plane of the ring (called $\tau_{\|}$). There is no change in optical anisotropy associated with the reorientation about this axis and hence it does not affect the light scattering spectrum. Reorientation about an axis in the plane of

the ring (perpendicular to the symmetry axis) does, however, affect the light scattering spectrum. The single molecule reorientational correlation function that contributes to the depolarized light scattering spectrum, in the rotational diffusion approximation, has a relaxation time

$$\frac{1}{\tau_\perp} = 6\theta_\perp \qquad (3.107)$$

The carbon-13 spin-lattice relaxation time measurements are related to the reorientation time of a C-H bond axis. For mesitylene the C-H bond axis observed was that for the ring carbons. For symmetric top molecules such as benzene and mesitylene the τ_{NMR} is related to both $\tau_\parallel$ and $\tau_\perp$ by [149]

$$\tau_{NMR} = \frac{1}{4}\tau_\perp + \frac{9}{4}\frac{\tau_\perp \tau_\parallel}{\tau + 2\tau} \qquad (3.108)$$

Consequently, a measurement of $\tau_\perp = \tau_{LS}$ from light scattering, and τ_{NMR} can be used to determine $\tau_\parallel$.

Pecora et al [156] have performed depolarized Raleigh scattering and ^{13}C spin-lattice relaxation time measurements on solutions of benzene and mesitylene as a function of solvent viscosity. The solvents used were isopentane, cyclooctane, cyclohexanol, carbon tetrachloride and mixtures of these compounds. These authors found that the light-scattering reorientation times varied linearly with solvent viscosity (Figure 3.5)

The resultant $\tau_{\parallel}$, $\tau_{\perp}$ vary linearly with η. The experimental slopes and intercepts are given in table (3.5). Whilst $\tau_{\parallel}$ for benzene has essentially zero slope, $\tau_{\parallel}$ for mesitylene does have a slope but only slightly greater than zero. The other reorientation time $\tau_{\perp}$ is strongly viscosity dependent in both cases. For a molecule of spherical shape, we can expect that the particle does not have to displace or to push any fluid out of its path in order to rotate. There will, therefore, not be any viscosity dependence for $\tau_{\parallel}$ in benzene but as the molecule becomes less spherical (as in mesitylene) there should be a dependence of $\tau_{\parallel}$ on the solution viscosity. From similar considerations, the reorientation described by $\tau_{\perp}$ should be more strongly viscosity dependent, as illustrated in Figure (3.5)

Pecora and co-workers [156] have suggested that the rotational reorientation time about a given molecular axis is

$$\tau = C\,\eta + \tau_o \qquad (3.109)$$

where τ_o is a constant whose value correlates well with the classical "free rotor reorientation" time.

$$\tau_{FR} = \frac{2\pi}{9}\left(\frac{I}{KT}\right)^{1/2} \qquad (3.110)$$

in which I is the moment of inertia about the axis under consideration.

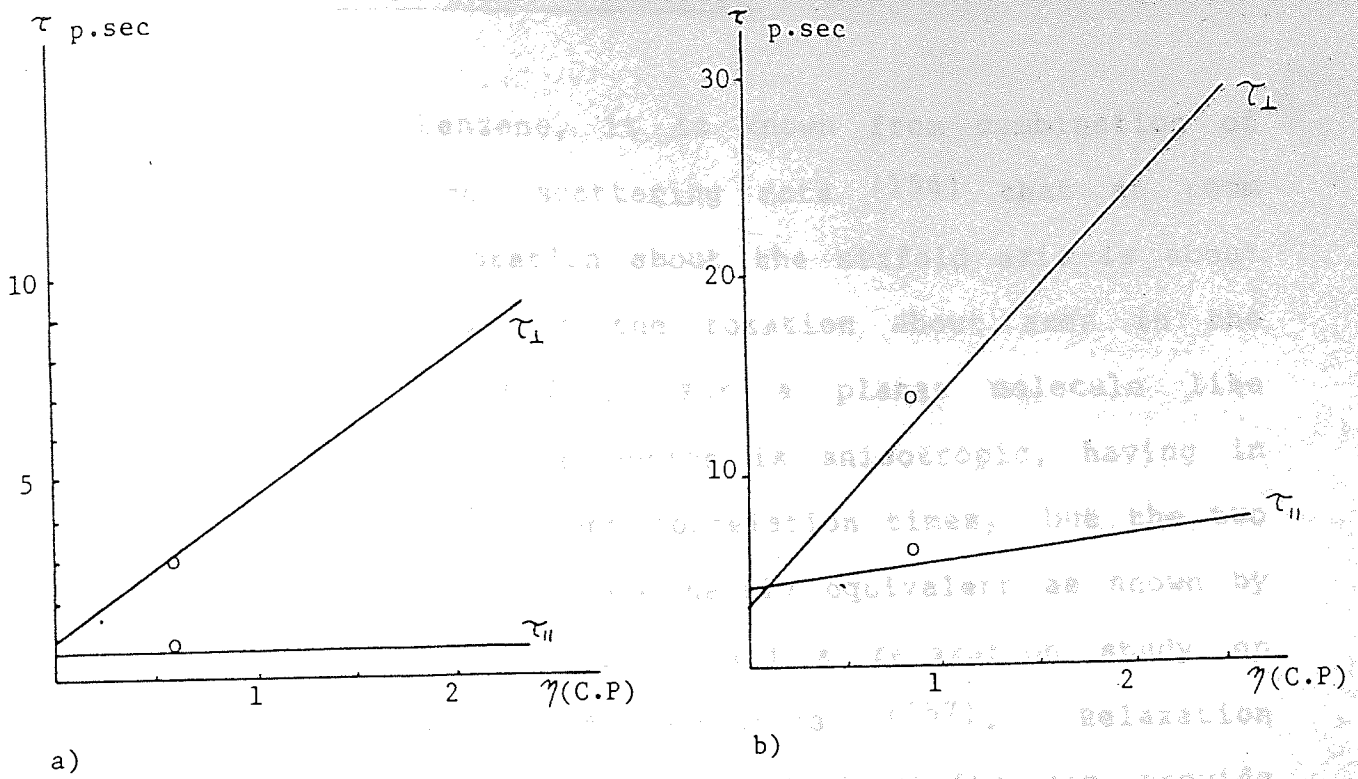

Figure 3.5 Correlation time Vs solution viscosity for
a) benzene solutions
b) mesitylene solutions
the dot (o) refers to neat compounds

Table (3.5) Viscosity dependence of $\tau_{\perp}$ and $\tau_{\parallel}$ for benzene and mesitylene (156).

	$\tau_{\perp}$	$\tau_{\parallel}$
benzene		
slope C Psec/c.p.	3.5 ± 0.1	0.0 ± 0.1
τ_o (P.sec)	0.8 ± 0.5	0.7 ± 0.1
$\tau_{f\cdot r}$ (P.sec)	0.45	0.64
mesitylene		
slope C P.sec/c.p	10.6 ± 0.8	1.0 ± 0.5
τ_o (P.sec)	3.2 ± 1.0	4.4 ± 1.0
$\tau_{f\cdot r}$ (P.sec)	0.8	1.2

3.6.B.3 Chemical Shift Anisotropy

In liquid benzene, it is known from combination of ^{13}C nmr and light scattering data (156) that at room temperature the rotation about the sixfold axis is about 3.5 times as fast as the rotation about axes in the plane; thus $\tau_\perp = 3.5\ \tau_\parallel$. For a planar molecule like pyridine the molecular motion is anisotropic, having in principle three different correlation times, but the two in-plane rotation axes are nearly equivalent as shown by high-resolution ^{13}C studies and a relaxation study on selectively deuterated pyridines (157). Relaxation through the anisotropy in chemical shifts can provide information about $\tau_\parallel$, $\tau_\perp$. To analyse this, we have to know the tensor of the chemical shift for ^{15}N in pyridine; this is obtained from the ^{15}N powder spectrum of solid pyridine (158). The correlation for relaxation is $\tau_{CS} = \tau_\perp$. In order to determine whether or not the motion is anisotropic, it is necessary to determine $\tau_\parallel$ and therefore ^{15}N data and ^{13}C relaxation rates must be combined. The relaxation rate for pyridine is (158) $\tau_\perp / \tau_\parallel = 1.4$. A similar experiment has been done for deuterated toluene (153), there, $\tau_\perp / \tau_\parallel = 3.5$. The use of the anisotropic chemical shift in combination with ^{13}C relaxation time yields valuable information for studying anisotropic motions of molecules in liquids.

3.6.C Quantitative Analysis of Molecular Motions

The basic theory for the evaluation of the anisotropy in molecular motion by measuring spin-lattice relaxation times has been given by Woessner (89). For protons, the relaxation is a complicated process, influenced by both intra and intermolecular motions. As was mentioned before, the relaxation of ^{13}C and ^{2}H in liquid molecules is usually a relatively simple process, the dynamic of which is controlled by the rotational motion of fixed molecular vectors. For ^{13}C, because T_1^{DD} can be obtained easily by using T_1 observed and the NOE factor (129), the reorientational correlation time is of great utility. Evaluation of τ_{eff} from T_1^{DD} data via equation (3.97) provides a measure of the time required for a given C-H vector to reorient by approximately 1rad. τ_c^{eff} can be considered as quantitative only in the case of isotropic reorientation of a molecule with $\tau_c^{eff}=1/6\ D$ where D is the diffusion constant. The simplest case of an anisotropic system is that of a symmetric top molecule. Woessner and Snowden (159) and Huntress (160) have developed expressions for T_1^{DD} where τ_c^{eff} is expressed in terms of $D_{\parallel}$ and $D_{\perp}$. The Woessner expression (modified for ^{13}C relaxation) is given by (161)

$$\frac{1}{T_1^{DD}} = \frac{n_H \hbar^2 \gamma_H^2 \gamma_C^2}{r_{CH}^6} \left[\frac{A}{6D_{\perp}} + \frac{B}{5D_{\perp}+D_{\parallel}} + \frac{C}{2D_{\perp}+4D_{\parallel}} \right] \qquad (3.111$$

where A,B,C are geometrical constants and are functions of the direction cosines of the angle between the C-H

vectors and the symmetry axis. Thus

$$\tau^{c}_{eff} = D^{-1}\left(\frac{A}{6} + \frac{B}{5+\sigma} + \frac{C}{2+4\sigma}\right) \qquad (3.112)$$

where $\sigma = D_{\parallel}/D_{\perp}$. In order to evaluate both diffusion constants, an independent source of information must be available for one of the parameters, e.g. dipolar relaxation times, L-scattering, quadrupolar, CSA, etc. For asymmetric top molecules, all three principal values of the rotational diffusion tensor are required to characterize the molecular dynamics. There, three different T_1^{DD} values of non-equivalent geometrical configuration are required to solve the three independent simultaneous equations necessary to evaluate the diffusion constants. Again, Woessner [89] has given an expression for T_1^{DD}, which is for ^{13}C nuclei (141)

$$\frac{1}{T_1^{DD}} = \frac{n_H \hbar^2 \gamma_H^2 \gamma_c^2}{r_{CH}^6}\left[\frac{c_+ b_+}{b_+^2 + w^2} + \frac{c_- b_-}{b_-^2 + w^2} + \frac{c_1 b_1}{b_1^2 + w^2} + \frac{c_2 b_2}{b_2^2 + w^2} + \frac{c_3 b_3}{b_3^2 + w^2}\right] \qquad (3.113)$$

The five b variables are linear combinations of the rotational diffusion constants

$$b_1 = 4R_1 + R_2 + R_3 \qquad (3.114)$$

$$b_2 = R_1 + 4R_2 + R_3 \qquad (3.115)$$

$$b_3 = R_1 + R_2 + 4R_3 \qquad (3.116)$$

$$b_{\pm} = 6R \pm 6\sqrt{R^2 - L^2} \qquad (3.117)$$

with

$$R = \frac{1}{3}(R_1 + R_2 + R_3) \qquad (3.118)$$

$$L^2 = \frac{1}{3}(R_1R_2 + R_2R_3 + R_3R_1) \qquad (3.119)$$

According to Woessner, the C_1, C_2 and C_3 coefficients are a function only of the directional cosines, while the C_+ and C_- terms depend on both directional cosines and the Ri variables.

The first application of the theory of anisotropic motion to ^{13}C relaxation times was given by Grant and coworkers (162), when they studied molecules containing three T_1's with three rotational diffusion constants. A computer program has been written to calculate the rotation diffusion tensor for anisotropic motion from ^{13}C relaxation data (141)(163).

The treatment of internal rotation impossed on an isotropic overall motion has been undertaken for a methyl group (164) for which T_1^{DD} is given by

$$\frac{1}{T_1^{DD}} = \frac{n_H \gamma_H^2 \gamma_C^2 \hbar^2}{r^6_{CH}} \left(\frac{A}{6D} + \frac{B}{6D} + \frac{C}{6D+4R_{int}} \right) \qquad (3.120)$$

In the case of a methyl group undergoing free rotation ($R_{int} \gg D$), $1/T_1^{DD}$ reduces to $1/9$ of the value for a rigidly attached CH_3 (i.e. for methyl group geometry A=0.111 in equation (3.120), so that $1/T_1^{DD} \simeq 0.111/6D$

for fast motion but $^{1}/_{T_1}{}^{DD} \propto {}^{1}/_{6}D$ for no internal motion (A+B+C=1). For mesitylene, it has been found (137) that $T_1{}^{DD}$ for the methyl group is 23 sec while the ring carbon values are 7.8 sec. While, the effectiveness (relative to the ring) of each C-H interaction is reduced by a factor of 9, there are 3 times as many interactions for the methyl carbon vs the methine, thus $^{1}/_{T_1}{}^{DD}$ for the methyl is $^{1}/_{3}$ that of the methine carbon.

Calculation of dipolar nuclear magnetic relaxation times in molecules with multiple internal rotations has been carried out for isotropic motion (165), also for anisotropic motion (166). More recently, there have appeared several applications of ^{13}C T_1 calculation that enable the analyses of internal motion in molecules (167)(168).

CHAPTER FOUR

EXPERIMENTAL PROCEDURES

4.1 Introduction

This chapter refers to the preparation of samples and the techniques used in this work for the determination of spin-lattice relaxation times, T_1 and the N.O.E. factor.

The measurements of T_1's for mesitylene protons that are reported in chapter six were carried out using a Varian HA100D spectrometer. The measurements of ^{13}C T_1's were performed using the Jeol FX90Q spectrometer. Each instrument has different characteristics, which implies a special approach to the measurement of the relaxation times. Therefore, in order to understand the methods of analysis, the techniques used in each case, have to be explained in detail.

4.2 Sample Preparation

The value of the nuclear spin lattice relaxation time, T_1, is very dependent on sample purity. It is important therefore to use uncontaminated compounds and to prepare solutions in clean containers. The presence of dust for example, can spoil the homogeneity of the magnetic field. Consequently, it is important to ensure that sample preparation is performed under optimal experimental conditions.

When preparing samples of liquid mixtures the first step was to weigh each of the components, in their desired proportions, into a flask fitted with a "subaseal" to avoid evaporation when using volatile liquids. It was noticed that the "subaseal" absorbed some of the vapor in the flask. The samples were not therefore kept for a long time in that condition and changes in the composition avoided. A syringe was used to transfer the compound from its initial container to the solution flask. In the case of TMS, which has a boiling point of 27°C, it was necessary to cool the syringe to facilitate the procedure.

The presence of dissolved oxygen or other paramagnetic impurities in the sample can significantly affect the value of relaxation times T_1. This is particularly true for protons, which are located at the periphery of the molecules, and experience dipolar-dipolar interactions with the paramagnetic sources, that become the most important relaxation mechanism , e.g. in the case of neat benzene the relaxation time is T_1=4.8sec, in normal air saturated samples, but after degassing by chemical procedures (169) it was measured as T_1=24.8sec at 309°K.

Until recently two methods have normally been used to remove oxygen from the samples: the freeze-pump thaw and the inert gas bubbling procedure. In the first method, the sample is placed in a suitable container, on a vacuum

line. After freezing the sample, the sample-container is evacuated. The sample is then isolated from the vacuum system and warmed to melt it. As the sample melts the oxygen is released. The sample is then re-frozen and the container re-evacuated. This process is repeated 4 or 5 times. The second method involves allowing a chemically inert and diamagnetic gas to diffuse through the liquid sample and flush out the oxygen. Nitrogen, helium and argon have all been used in this procedure. It is considered that the bubbling method is less efficient than the freeze-pump-thaw method (169). Recently a third method (chemical degassing) has been demostrated to be far better than the bubbling or freeze-pump-thaw methods (169). For this reason, this chemical method was employed for the deoxygenation of samples prepared in this work.

The main chemical degassing compound is $Co(biPy)_3 (ClO_4)_2$ which is used in the presence of $NaBH_4$. The cobalt compound is golden brown in colour when solid. When it is dissolved with sodium borohydride in a suitable solvent it removes oxygen in a reversible, colour indicating reaction and when all dissolved oxygen has been removed the solution turns deep blue.

A special piece of glassware has been designed,(169) (see Figure (4.1), in order to permit the most versatile use of the degassing compound viz either dissolved in the solution to be degassed or, if they are insoluble in

this, dissolved in an intermediate solvent that is stirred heterogeneously with the main sample in order to effect degassing. The latter approach was used here. After weighing the solvent and the solute components, the deoxygenating compounds were dissolved in water. All the parts of the apparatus were evacuated, except the flask containing the intermediate solvent (water) which was frozen with liquid nitrogen. The sample material was then added to the flask and thus frozen as well. The volumes of solvent and samples were selected to be such that the capillary tube by which the transfer of the sample was made had its end well away from the unwanted layer in order to prevent the introduction of superfluous material. The flask was evacuated until a vacuum of 10^{-3} torr was reached, and then isolated from the rest of the system and allowed to warm up. Once the contents of the flask had melted they were stirred for 10 minutes using a magnetic follower. This gave adequate time for the deoxygenating complex to work. The procedure was repeated. The liquid was allowed to settle into two layers and part of the sample layer was transferred to a reservoir close to the n.m.r. tube by cooling the end of the capillary tube, near the rotaflow tap. Finally, the three way tap was set to all isolated position and very slowly, the pertinent rotaflow tap was opened to allow sample liquid to pass into the n.m.r. tube; this was assumed to be free of absorbed oxygen molecules on its wall because it was heated using a pencil flame at an early stage of the experiment. Once the sample had been

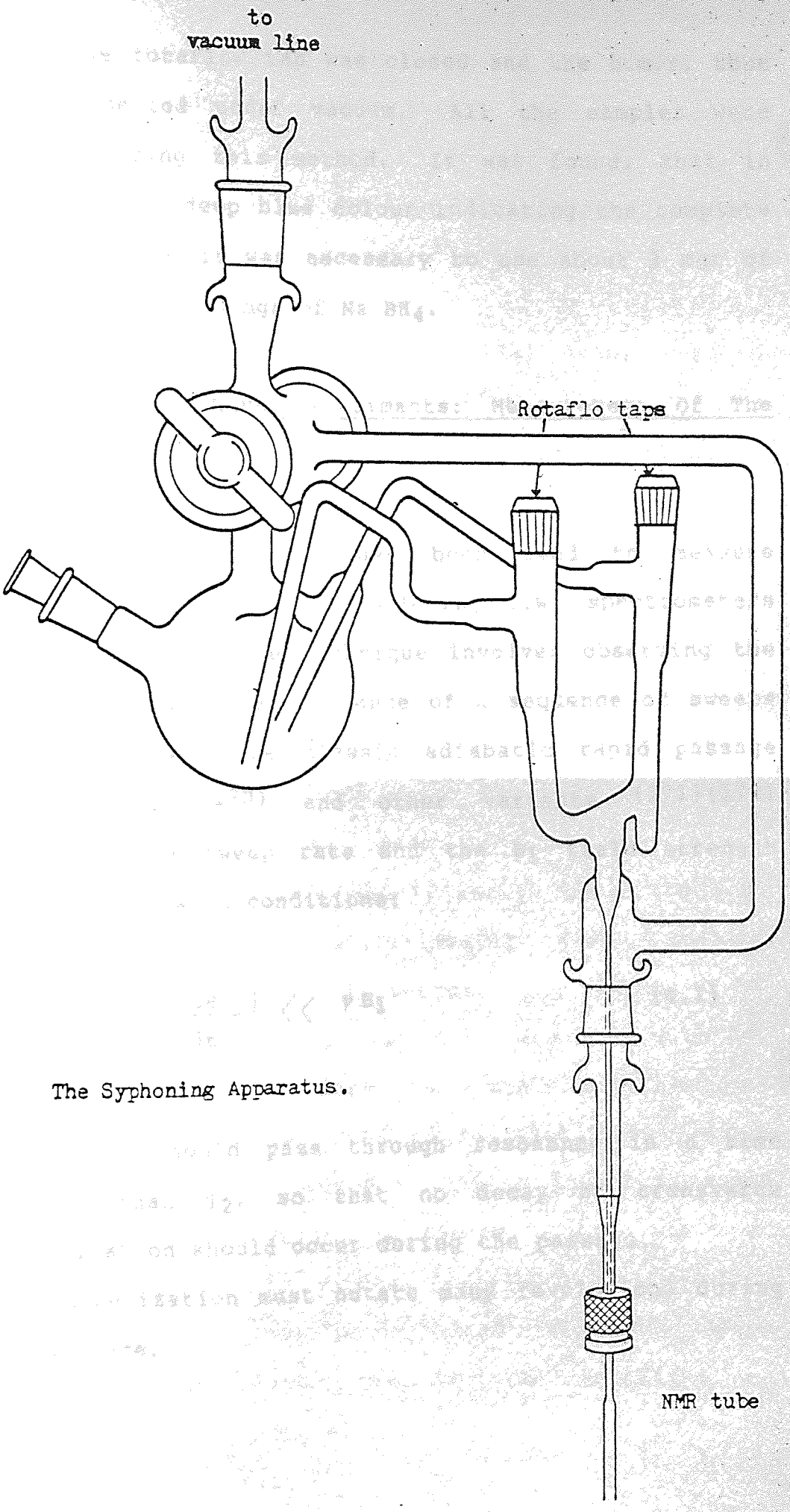

Figure 4.1 The Syphoning Apparatus.

collected the rotaflow tap was closed and the n.m.r. tube cooled and sealed under vacuum. All the samples were prepared by using this method. It was found, that in order to get the deep blue colour indicating the complete removal of oxygen it was necessary to use about 3 mgr of cobalt complex and 30 mgr of Na BH_4.

4.3 Continuous Wave Experiments: Measurement Of The Relaxation Time T_1

A number of methods have been used to measure relaxation times (65)(74). Employing c.w. spectrometers an experimentally simple technique involves observing the magnetization under the influence of a sequence of sweeps through resonance. The classic adiabatic rapid passage (ARP) technique (170) and other variants (171)(172) require that the sweep rate and the B_1 field strength satisfy the following conditions:

$$\frac{1}{T_2} \ll \frac{1}{B_1}\left|\frac{dB_o}{dt}\right| \ll \gamma B_1 \qquad (4.1)$$

which means,

a) the sweep should pass through resonance in a time shorter than T_2, so that no decay of transverse magnetization should occur during the passage.

b) the magnetization must nutate many revolutions during the passage.

These conditions may always be obtained by making the sweep rate and B_1 sufficiently large.

4.3.A The Adiabatic Rapid Passage With Sampling (ARPS) Technique.

In the ARPS method (173) an initial sweep through resonance is made under ARP condition, inverting the nuclear magnetization. On subsequent sweeps the B_1 field is reduced to a level low enough to monitor the signal recovery without significant subsequent perturbation of the system. The initial sweep is ideally arranged to provide a 180° inversion of the equilibrium magnetization. In order to achieve the ARPS condition with the varian HA100D, the signal of interest is monitored in the sideband mode where the R.F. level is a function of the modulation index and has low power. Then, by switching from sideband to centre band, the R.F. power is increased by approximately 40db, causing inversion of the magnetization vector. The return of M_Z to equilibrium is observed in the side band mode with low B_1 field. In the present work the signals were recorded using a S.E. Laboratories 3006 ultraviolet Galvanometer recorder. This recorder proved to have a linear response to increasing signal output. A typical chart-output of M_Z vs time is shown in Figure (4.2); Δt is the time between signals, and can be selected using the sweep frequency control consistent with the ARP conditions and other experimental parameters.

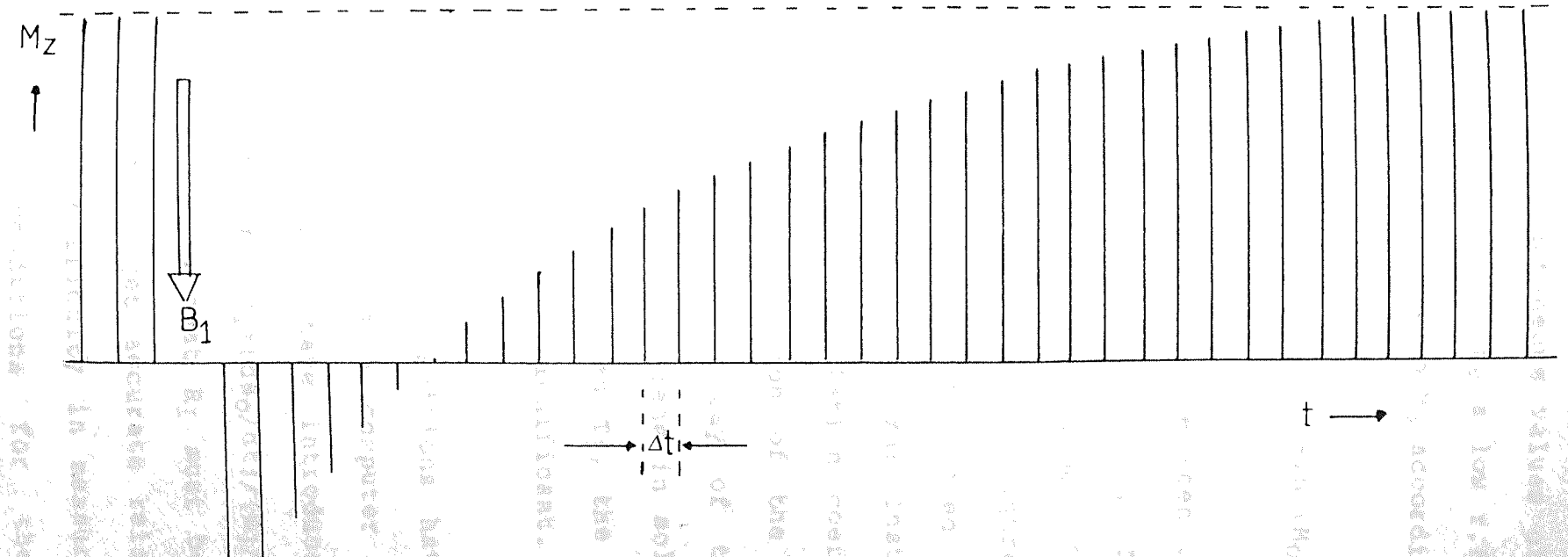

Figure 4.2 A schematic example of an ARPS experiment

After the application of a strong r.f. field, the magnetization $M_z=M_o$ is changed by a factor $a\approx-1$ at $t=0$. The instantaneous values of $M_z(t)$ which are subsequently detected by using a low r.f. field, follow an exponential decay from aM_o to M_o according to equation (4.2)

$$\ln (M_o-M_z)= -t/T_1+\ln (M_o-aM_o) \qquad (4.2)$$

from this it can be seen that a need not actually be -1 or indeed known at all. The value of T_1 is obtained by calculating the slope of the semilog plot of this equation as shown in figure (4.3). Most of the reported T_1 values were calculated by using the linear regression program of the Texas Instrument T.I programmable 58/59 where the correlation coefficient r gives an indication of the dispersion of the data. In figure (4.3) which represents the decay of the magnetization of the ring proton of mesitylene in solution, it can be seen that for times longer than T_1, the dispersion of the experimental points is most significant.

The ARP conditions have been studied by Parker and Jonas[172] using a computer to plot the values of M_z vs time. They have introduced in the Bloch equations the parameters $R_1=(dB_o/dt)/(B_1/T_1)$ and $R_2=\gamma B_1^2/(dB_o/dt)$ and have found that R_1 must be larger than 100 and $R_2>15$ in order to get accurate relaxation times. In practice, we found difficulty in measuring the r.f. field B_1 and the best conditions for the experiment on the HA100D instrument were fixed by empirical methods.

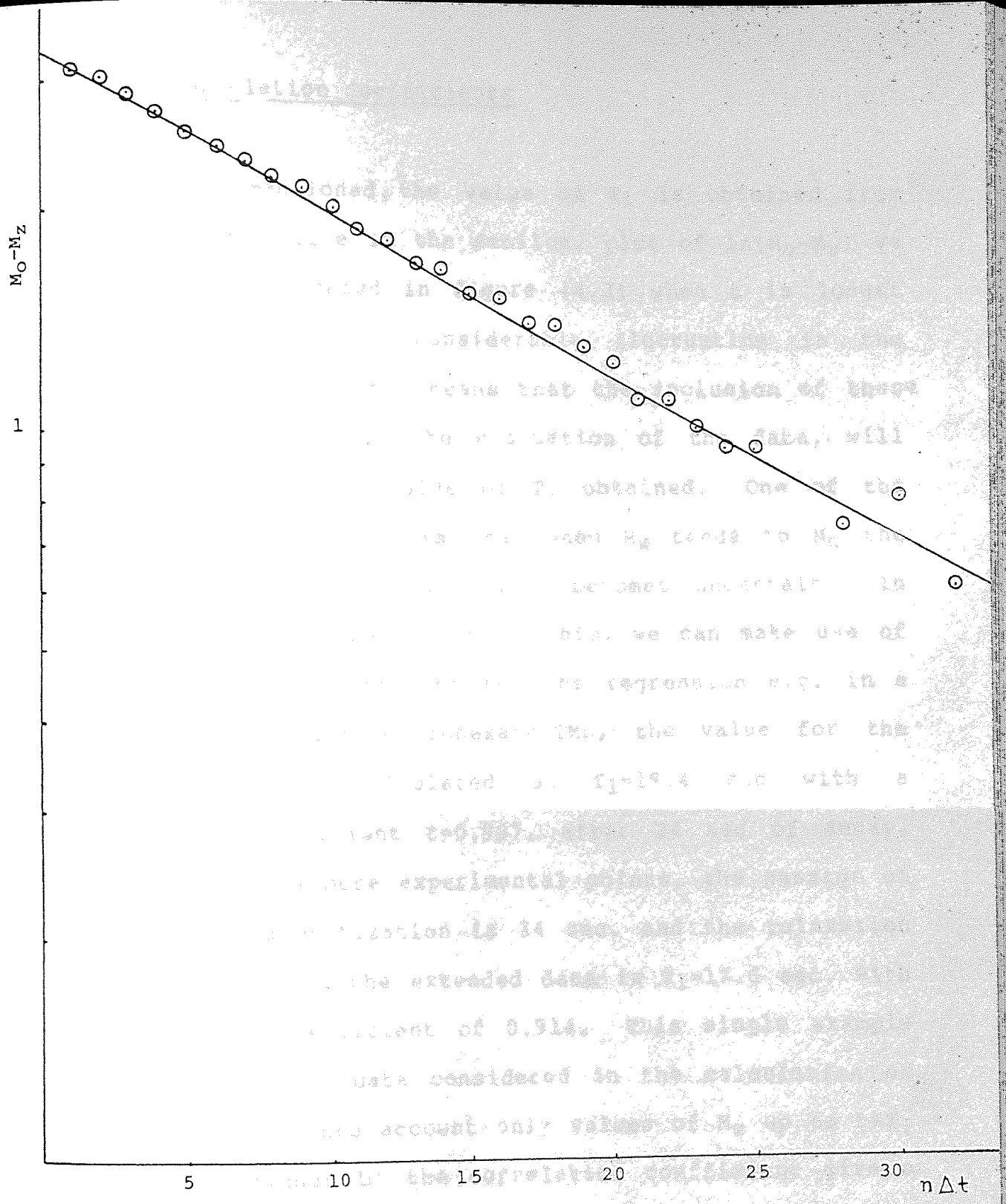

Figure 4.3 The variation of the magnetization M_z for the ring proton of mesitylene in CCl_4 (X_{Me}=0.45) using the ARPS method (T_1=16.5 sec). Δt=0.84 sec.

4.3.A.1 Correlation Coefficients

As just mentioned, the value of T_1 is obtained from the slope of a line in the semilog. plot of $\ln(M_o-M_z)$ vs time and as indicated in figure (4.3) when t is longer than T_1 there is a considerable fluctuation in the experimental data. This means that the inclusion of these experimental points in the evaluation of the data, will adversely affect the value of T_1 obtained. One of the reasons for this effect is that when M_z tends to M_o the value of $\ln(M_o-M_z)$ i.e. $\sim \ln(o)$ becomes uncertain. In order to estimate the effect of this, we can make use of the correlation coefficient for the regression e.g. in a sample of mesitylene-cyclohexane-TMS, the value for the ring proton was calculated as T_1=19.4 sec with a correlation coefficient r=0.997, after 24 sec of decay. If we include 10 more experimental points, the passage of time for the magnetization is 34 sec. and the relaxation time obtained from the extended data is T_1=17.6 sec. with a correlation coefficient of 0.914. This single example shows that a) the data considered in the calculation of T_1 have to take into account only values of M_z up to $t \leq T_1$ or slightly higher b) the correlation coefficient gives a good indication as to the quality of the data provided we always use the same conditions; it is possible to use this coefficient as a criterion to select the best values of T_1.

4.3.A.2 Instrumental Conditions

The choice of the optimum instrumental parameters, that yield reliable relaxation times, had to be done in the earliest stage of the research. According to Coupland [174] the signal height which is taken as a measure of M_Z, is influenced by several parameters, viz depth of sweep field, sweep field scan speed, position of the peak on the sweep, the direction of the sweep, the r.f. attenuation, the phase (line shape) and field homogeneity. He concluded that the percentage of nutation i.e. $(h/H)x100$, where h is the maximum in the fluctuation of the peak height and H is the minimum peak height is minimised by adopting the following conditions:

R.F. field strength corresponding to 10db of attenuation, sweep field depth $1x2\frac{1}{2}$, sweep duration 3x2 (1.05sec), field homogeneity (non-spinning), peak position at the right hand side of the oscilloscope.

In view of the fact that these experiments were carried out on steady state signals, it was considered that a review of the analysis of the variation of T_1 with respect to the above parameters could help identify the best conditions for the experiments.

It is expected that the optimum conditions will give the maximum relaxation time with the highest correlation coefficient for the relevant regression.

For the preliminary investigations a sample with a mole fraction of 0.07 of mesitylene dissolved in cyclohexane and TMS was used, the ring proton relaxation time being studied.

The variation of relaxation time of the ring proton of mesitylene with R.F. power can be seen in table (4.1); when the attenuation is zero, the r.f. transmitter power is maximum. This condition produces partial saturation of the spins with the result that the relaxation time is reduced. The relaxation time reaches a maximum at 18db of attenuation and this was considered the optimum value. Above 24db, the r.f. field can not completely invert the magnetization on the initial sweep and the signal to noise ratio of the subsequent spectra is poor. The latter fact, is reflected in the lower correlation coefficient.

Table (4.2) shows the variation of T_1 with other parameters and it is clear that the conditions with 18db of attenuation, sweep frequency 3x1 and sweep field 1x2.5 produce the best T_1 value. In addition to these experiments the probe tuning was misadjusted from the optimum position and it was found that, T_1 was reduced by two seconds from the optimum value 22.7 sec. the homogeneity was also altered, resulting in a 50% reduction of the equilibrium magnetization signal height. This caused a decrease of T_1 by 1.4 sec. from the optimum value. The reproducibility of the relaxation

Table (4.1)

The Variation of the Relaxation Time of the ring proton of mesitylene with the r.f. attenuation in a Me-Cy-TMS sample with $X_{TMS}=0.62$, $X_{ME}=0.07$

r.f. attenuation (db)	T_1 (sec)	corr. coeff.
0	7.5	0.996
6	11.5	0.995
13	17.6	0.993
14	19.8	0.998
15	21.04	0.995
16	20.05	0.997
18	22.7	0.994
20	19.4	0.997
24	21.3	0.987
26	18.2	0.949
28	27.2	0.582

Table (4.2)

The Variation of the Relaxation Time when the instrumental conditions are changed. The same sample as table (4.1) was used.

condition	sweep frequency	T_1(sec)	corr. coeff.
18 db	2 x 6	20.6	0.9959
1x2.5 sweep field	3 x 1	22.7	0.9947
	3 x 2	21.4	0.9957
	3 x 3	20.2	0.985
	3 x 4	21.4	0.989
18 db	sweep field		
3 x 1 sweep fr	0.1 x 10	21.06	0.9969
	1 x 2.5	22.7	0.9947
	1 x 3	22.5	0.9969
double irradiation at	1 x 3	21.37	0.998
18 db, 3x1 sweep fr.	1 x 2	22.1	0.998

times obtained with the optimum conditions over four measurements was very good, with a deviation from the average of $\pm$ 0.1 sec. Double irradiation experiments were performed, to see whether or not the cross relaxation between the methyl and the ring proton is important. According to the results on table (4.2) it seems that they are negligible or perhaps masked by some saturation of the observed signal.

One possible application of relaxation time studies in the HA100D spectrometer is to check the r.f. power after the probe has been changed from the proton frequency to fluorine frequency and viceversa. This procedure involves tuning of the r.f. transmitter and receiver according to the drive crystal frequency. Table (4.3) shows the results of the analysis of T_1 for the standard sample before and after changing the tuning of the r.f. transmitter.

Table (4.3) variation of relaxation time after and before the r.f. transmitter is retuned.

	T_1(sec)	M_o(cm)	r.f. attenuation(db)
before	22.7	5.5	18
after	18.5	4.5	18
after	22.9	5.1	16

From the results on table (4.3) it can be concluded that the procedure of retuning the r.f. transmitter has produced a decrease in the B_1 r.f. field due to mismatching in the unit. So, in order to return to the

previous experimental condition an attenuation of 16db should be used instead of 18db or alternatively the r.f. transmitter should be retuned.

4.3.B The Progressive Saturation Method

The ARPS technique is best suited to the measurement of relaxation times for resonances with good signal to noise ratios. However, for weak signals or signals corresponding to long relaxation times, the signal to noise ratio may render the ARPS method unsatisfactory, because of the necessity in this of maintaining a low non perturbing B_1 field level which yields a weak signal. The effect of using higher r.f. fields B_1 is to shorten the effective relaxation time. This effect can be put to good use in the case of the progressive saturation method (175), where a saturating r.f. field is applied. Figure (4.4) shows the effect of the saturating field on repeated spectral scanning. At t=0, the magnetization at equilibrium is ($M_Z=M_O$). Each subsequent passage through resonance changes the magnitude and orientation of the nuclear magnetization vector to an extent determined by the sweep rate and the B_1 field strength. If M_Z^- and M_Z^+ are the longitudinal components of M_Z before and after resonance, the effect of any sweep is

$$M_Z^+ = a\, M_Z^- \qquad -1 \leq a \leq 1 \qquad (4.3)$$

if a is close to +1, the sweep effectively samples M_Z, if

a=0, then saturation occurs, if a=-1, we have an ARP sweep (175).

The magnetization just before the nth resonance is :

$$M_Z^-(n)=M_Z^+ (n-1)\exp(-\tau/T_1)+M_Z^\circ(1-\exp(-\tau/T_1)) \qquad (4.4)$$

By using the recurrence relationship

$$M_Z^- (n)=ax\ M_Z^- (n-1)+M_Z^\circ(1-x) \qquad (4.5)$$

we find in the limit of large n that $M\bar{z}(n)$ reaches a constant equilibrium value

$$M_Z^- (\infty) = \frac{M_Z^\circ(1-x)}{1-ax} \qquad (4.6)$$

where $x=e^{-\tau/T_1}$

By repeated use of equation (4.5) and with the help of equation (4.6) it is found that

$$M_Z^- (n)-M_Z^-(\infty)=(ax)^{n-1}\left\{M_Z^-(1)-\frac{M_Z^\circ(1-x)}{1-ax}\right\} \qquad (4.7)$$

Whence

$$\frac{d}{dn}\left\{\ln\ |\ M_Z^-(n)-M_Z^-(\infty)|\right\} = \ln\ (|a|x) = \frac{\tau}{T_1^*} \qquad (4.8)$$

and

$$\frac{1}{T_1^*} = \frac{1}{T_1} - \ln\left(\frac{|a|}{\tau}\right)$$

is the effective relaxation time.

From the semilog. plot of $M_Z^-(n)-M_Z^-(\infty)$ we can find $\ln(|a|x)$; then by using equation 4.6 we get

$$x=(ax-1)\frac{M_Z^-(\infty)}{M_Z^-(0)}+1 \qquad (4.9)$$

Finally $T_1=(\ln x)^{-1}(-\tau)$, where τ is the sweep time.

The change of $M_Z^-(n)-M_Z^-(\infty)$ with time, for the ring protons of mesitylene in CCl_4 is shown in Figure (4.5). It can be seen that when the time of decay is $n\tau \approx T_1$, the fluctuation of $M_Z^-M_Z^-(\infty)$ is highest. This suggests that we have to take into account only smaller values of n. Heatley has recommended [175] for maximum accuracy in determining T_1, the choice of a and τ such that there is a significant decrease in signal intensity with n, in order that the difference $M_Z^-(n)-M_Z^-(\infty)$ be accurately measurable, with sufficient number of peaks recorded during the decay process.

A simple method of measuring relaxation times by using the progressive saturation technique is to set the sweep field to very low intensity and away from the resonant signal under study (ring proton) as shown in Figure(4.6). After the magnetization reaches equilibrium, the intensity of the sweep field is increased, so the signal of the ring proton will appear on the scope and will follow a decay pattern as shown in Figure 4.4.

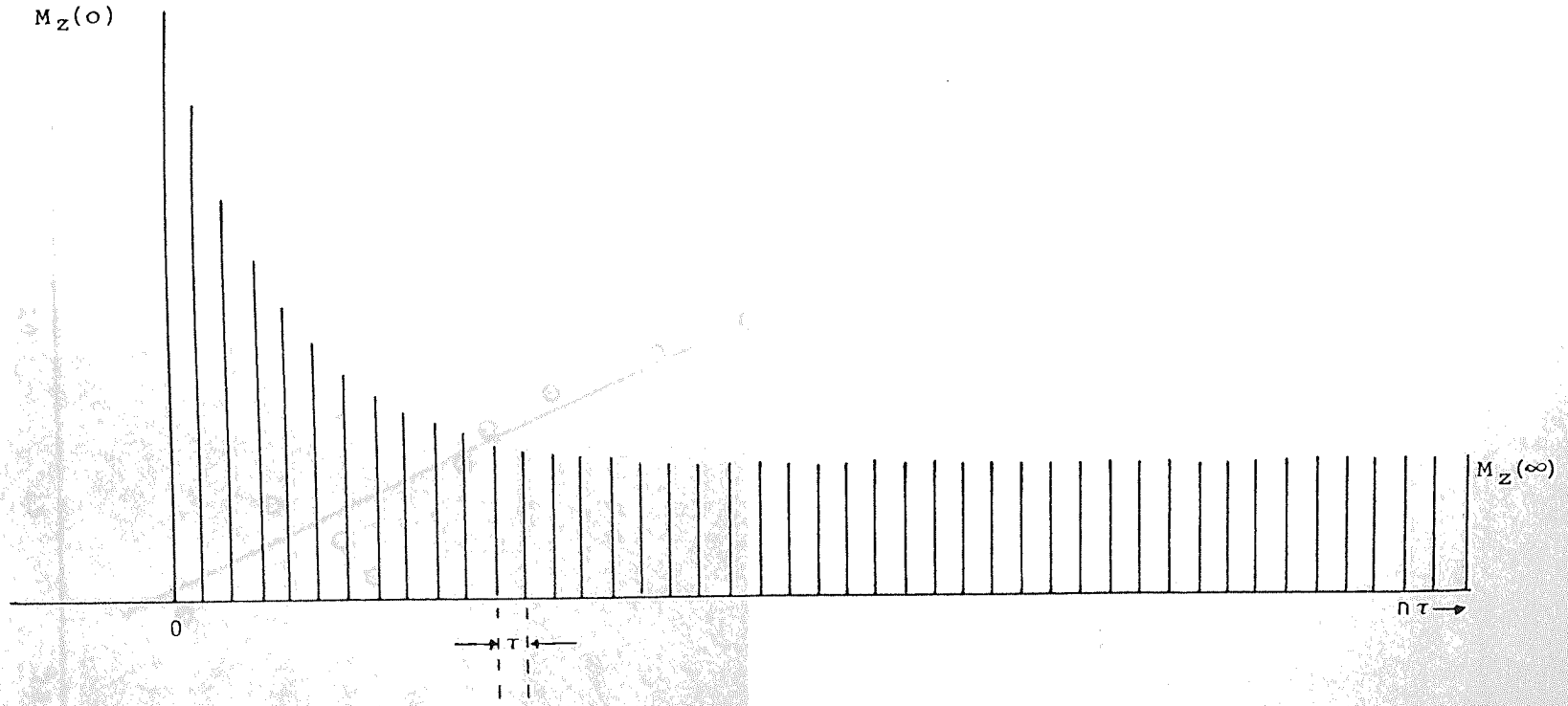

Figure (4.4) Progressive saturation experiment on the ring proton of mesitylene in TMS/C_6H_{12} where X_{Me}=0.07, X_{TMS}=0.62. τ=1.2 sec and T_1=22.5 sec.

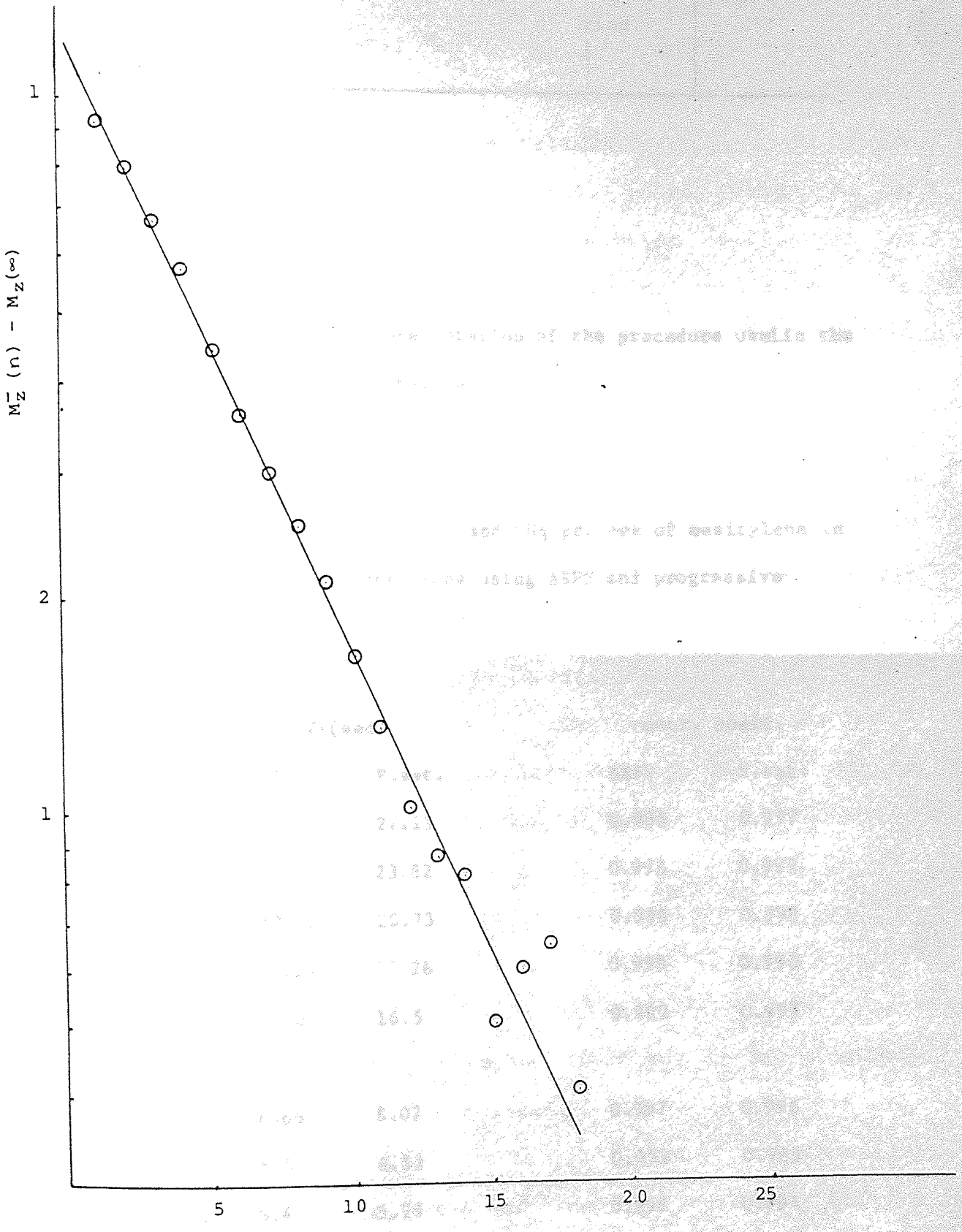

Figure 4.5 The variation of the magnetization M_Z for the ring proton of mesitylene in CCl_4 (X_{Me}=0.199) using the progressive saturation method.
T_1=20.2 sec, τ=1.2 sec

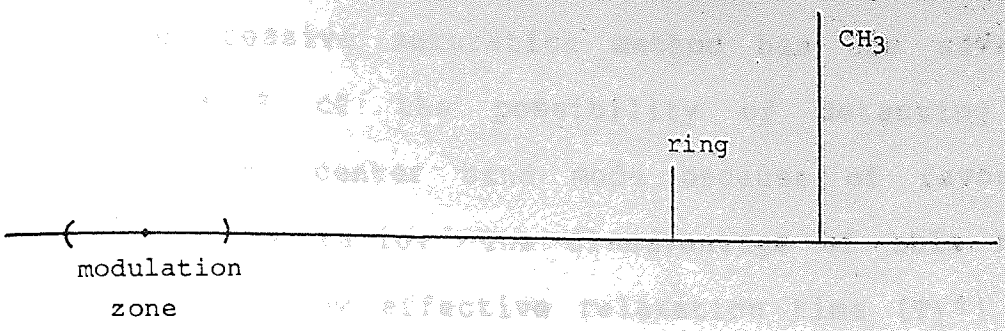

Figure (4.6) Schematic representation of the procedure used in the progressive saturation technique

Table 4.4

Comparison of T_1 values of ring and CH_3 protons of mesitylene in CCl_4 at different concentrations using ARPS and progressive saturation techniques.

Sample		T_1(sec)		corr. coeff.	
		ARPS	P.sat.	ARPS	P.sat.
	a	26.33	27.15	0.995	0.997
	b	23.7	23.82	0.998	0.999
ring	c	20.37	20.23	0.998	0.999
protons	d	15.19	15.26	0.999	0.990
	e	15.04	16.5	0.999	0.999
	a	6.66	8.07	0.997	0.998
	b	6.5	6.53	0.999	0.985
CH_3	c	6.4	5.98	0.999	0.994
protons	d	5.63	6.33	0.999	0.998
	e	5.99	6.19	0.999	0.998

The progressive saturation method has the advantage over the ARPS of the possibility of detecting weak signals in the center band mode because of favourable signal to noise ratio. The disadvantage of this method however is the low effective relaxation time (T_1*) which reduces the number of experimental points that can be obtained. As a result, the correlation coefficient is very sensitive to the number of points considered. In the case of methyl protons with short T_1, it is recommended that data with a correlation coefficient of no less than 0.999 are accepted. Table (4.4) shows a comparison of the T_1 values obtained by using ARPS and progressive saturation techniques on the same samples. It shows that the results from both methods are similar and, that the progressive saturation results are reliable, provided that the correlation coefficient for the appropriate regression of the data are close to 1 i.e. 0.998. A further comparison of both methods can be seen in the data presented in chapter six.

4.3.C Effects of Sample Length and Resolution Spoiling on T_1

In order to get optimum values of T_1, it is necessary to ensure that all the sample is well inside the transmitter coil (109). This avoids any complications due to nuclei, which have not been subjected to A.F.P., diffusing, or in any way moving into the receiver coil. Another important factor is the spoiling of the resolution,

which according to Van Geet Hume [176] is necessary, to avoid transverse relaxation effects. The method used here to fulfil this condition was the same used by Coupland [174] i.e. the non spinning of the sample.

The receiver coil in the varian HA100D is about 1cm in length and the transmitter coil is about 1.5cm long. According to this, the sample length should be between 1cm to 1.5cm. In practice it was found difficult to make all the samples of the same length and those samples of length between 1cm and 1.5cm showed bad signal to noise ratio which made it difficult to measure the relaxation times for low concentrated samples.

Table (4.5) The effect of sample length on T_1's for mesitylene ring protons and cyclohexane at 303°K

A. Mesitylene in C_6H_{12}-TMS ($X_{Me}=0.07$, $X_{Cy}=0.72$, $X_{TMS}=0.21$)

length(cm)	2.2	2.5	4.6
T_1(sec)	16.27	16.99	15.63
correlation coefficient	0.986	0.994	0.996

B. Cyclohexane

length	1	1.7	2	4
T_1(sec) C_6H_{12} neat	6.6	6.4	6.3	5.9
T_1(sec) 10% $^{v}/_{v}$ C_6H_{12} in CCl_4	14.1	-	14.2	13.5

The effects of sample length on T_1's were analysed in three different sets of samples. Table (4.5.A) shows the T_1's for the ring proton of mesitylene in C_6H_{12}-TMS solutions, degassed by chemical methods. The mole fraction of mesitylene is $X_{Me}=0.07$, $X_{C_6H_{12}}=0.72$ and $X_{TMS}=0.21$. The second and third sets studied were: neat cyclohexane and 10% $^{v}/_{v}$ cyclohexane dissolved in CCl_4. In this case the samples were degassed by three freeze-pump-thaw cycles.

From the results in Table (4.5.A) it can be seen that the relaxation time decreases about 1.5 sec. when the length is increased from 2.5cm to 4.6cm in measurements with about the same correlation coefficient and about 1 sec. from the datum with lower correlation coefficient, which means that at least a 5% in variation of T_1 is due to the length effect. Table (4.5.B) shows a 10% variation of T_1 in neat cyclohexane when the sample length varies from 1cm to 4cm and 6% of T_1 variation when the sample length varies from 2cm to 4cm. In the case of 10% cylohexane in CCl_4, the variation of T_1 is 4% when the sample length varies from 1 to 4cm. From these results, it can be concluded that there is a diffusion effect present and that this effect is more important when the compound is neat.

4.4 FOURIER TRANSFORM EXPERIMENTS

4.4A Introduction

Fourier transform spectroscopy is a very powerful technique that is capable of producing the frequency spectra of many nuclei (^{1}H, ^{13}C, F etc). When a compound is very dilute in a solvent or the sensitivity of the nuclei under observation is low, it is possible to accumulate many FID in order to improve the signal to noise (S/N) ratio of the spectrum. The S/N after n pulses increases with respect to the S/N for one pulse according to (177) equation (4.10).

$$(S/N)_n = (S/N)_1 \sqrt{n} \qquad (4.10)$$

This relation establishes the importance of using high n values.

Superficially, it might appear that only an increase in the number of scans will produce the required spectrum. The fact, however, is that several parameters have to be taken into account and optimized e.g. pulse width (PW) and repetition time (PR), because of their dependence on nuclear relaxation times. Ernst and Anderson (178) have found the optimum value of the flip angle θopt. in order to maximise the S/N after several scans i.e.

$$\cos \theta \text{ opt} = e^{-PR/T_1} \qquad (4.11)$$

where

$$\theta \text{ opt} = \gamma B_1 \text{ PW}$$

According to this equation, when $PR=T_1$, θ opt=70°, if $PR= 0.1\ T_1$, θ opt=20°. The general situation is that researchers initially do not know the relaxation times for the compound under study, so practical values for PW and PR have to be selected on the basis of experience. One common choice is θ=10° and $PR \approx 1$ sec. Without any doubt, it is important to assess suitable values for these using a rough idea of the relaxation times expected for the compound studied.

Other parameters that have to be selected when determining the spectrometer condition and which affect the characteristics of the spectra obtained are: r.f. carrier, spectral width (179) and number of data points (180). These have to be selected according to the particular sample and objectives of the experiments. Finally, the FID can be modified mathematically before the Fourier transformation (179)(180) by multiplying it by an exponential function with the objective of improving the spectral resolution; the exponential factor is selected in such a way that the broadening of the lines is very small. In the case of T_1 measurements, the instrumental conditions have to be chosen very carefully.

4.4.B Relaxation time determination

There are several pulse techniques to determine spin lattice relaxation times T_1, but, only three of them will be considered here; these permit saturation recovery (s.r.), inversion recovery (i.r.) and progressive saturation (p.s.) measurements of T_1. Each technique has its advantages and disadvantages (70). For example, the progressive saturation technique requires a precise 90° pulse and any mis-setting of this can cause false values of T_1 to be determined . Nevertheless in practical terms it is the fastest technique available for obtaining T_1's with the FX90Q configuration used. Edwin Becker et al (181) have found that the i.r. technique is always quicker than saturation recovery in obtaining a fixed precision in the estimate of T_1. In the present work it was found that the i.r. technique required very long instrumental times which were not always available. Nevertheless all three approaches will now be outlined.

4.4.B1 Inversion Recovery method

This method is illustrated in Figure (4.7). First a 180° pulse inverts the magnetization along the z' axis in the rotating frame (182). Longitudinal relaxation now occurs, causing $M_{z'}$ to start returning form the value $-M_o$ through zero to its equilibrium value M_o. If at a time τ after the 180° pulse a 90° pulse is applied (see figure 4.7b) along the x' axis, Mz' is rotated to the y'axis.

A free induction signal results, proportional to the value of M_z' at the time τ . If the system is now allowed to return to equilibrium by waiting a time $t \geq 5T_1$, and the 180°, τ , 90° sequence repeated for a different value of τ , the decay rate of M_z can be established, as indicated in Figure (4.7d). The decay of M_z follows equation (4.12) which is obtained from the Bloch equations with the initial condition M_z-M_o at t=o i.e

$$Mz(t) = M_o\ (1-2\ \exp-t/T1) \qquad (4.12)$$

In most cases it is necessary to apply several pulse sequences to get reasonable signal to noise ratio for each experimental point in Figure (4.7d), so the complete sequence is

$$(\pi - \tau - \frac{\pi}{2} - A_t - D)_n \text{ with } A_t + D \geq 5T_1$$

as shown in Figure (4.7c) where A_t is the acquisition time or sampling time and D is the delay. The use of homospoil pulse is recommended to avoid phase distortion in the signal (70).

In the Jeol FX90Q spectrometer the parameter τ is PI*** and A_t+D=PR. The basic settings include the estimation of the 90° pulse by setting it at approximately half the pulse width corresponding to 180° estimated from the appearance of the FID that must be a minimum for 180° pulse.

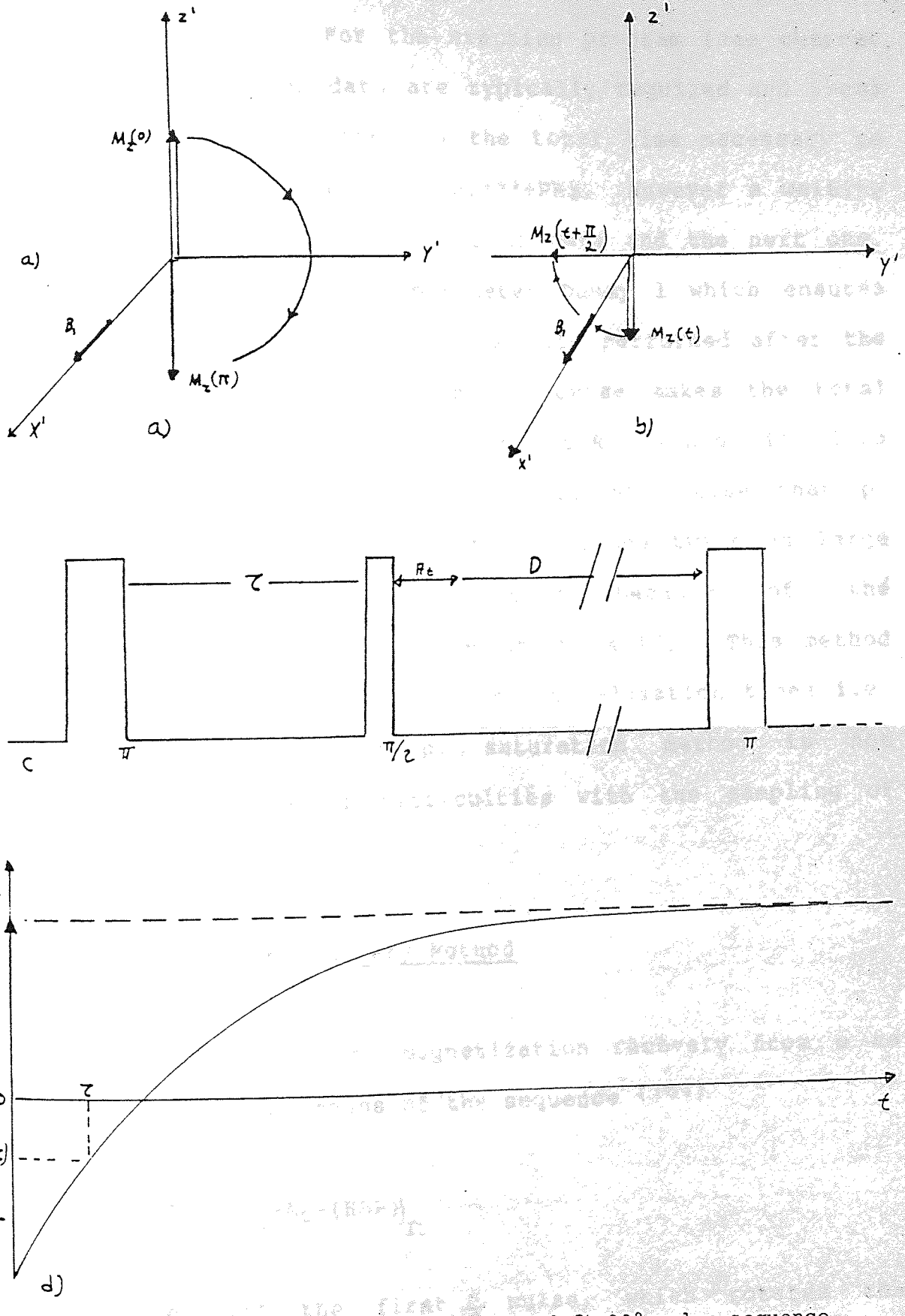

Figure 4.7 Determination of T_1 by the 180°-τ-90° pulse sequence
a) M_z is inverted by 180° pulse at t=0
b) after a time τ M_z is rotated π/2
c) the 180°-τ-90° sequence
d) variation of M_z with τ after a 180° pulse

The parameter τ or PI*** has to be chosen at least up to 1.5 T_1, (70)(183). For the stacking program (see chapter Two), seven sets of data are typically required and these include n scans per set, so the total time necessary to acquire each data set is n(PI***+PR). However a waiting time is needed between one set of data and the next one. This is provided by the parameter Dummy 1 which ensures that the sampling of the FID is only performed after the second pulse sequence. This of course makes the total experimental time longer. The I.R method is less dependent on the mis-setting of the 90° pulse than p. saturation (70), and has a dynamic range twice as large as the p. saturation method because of the proportionality with $2M_o$ in equation (4.12). This method is recommended in the case of short relaxation times i.e. $T_1 \leq 3$ sec. when the p. saturation method is not applicable because of difficulties with the sampling of the FID.

4.4B2 Saturation Recovery Method

In this method the magnetization recovery from o to $+M_o$ is followed by means of the sequence (184)

$$\left\{\frac{\pi}{2} - (HSP) - \tau - \frac{\pi}{2} - A_t - (HSP)\right\}_n$$

at the end of the first $\frac{\pi}{2}$ pulse, which rotates the magnetization vector into the xy plane as shown in Figure (4.8a), the longitudinal magnetization is reduced to zero.

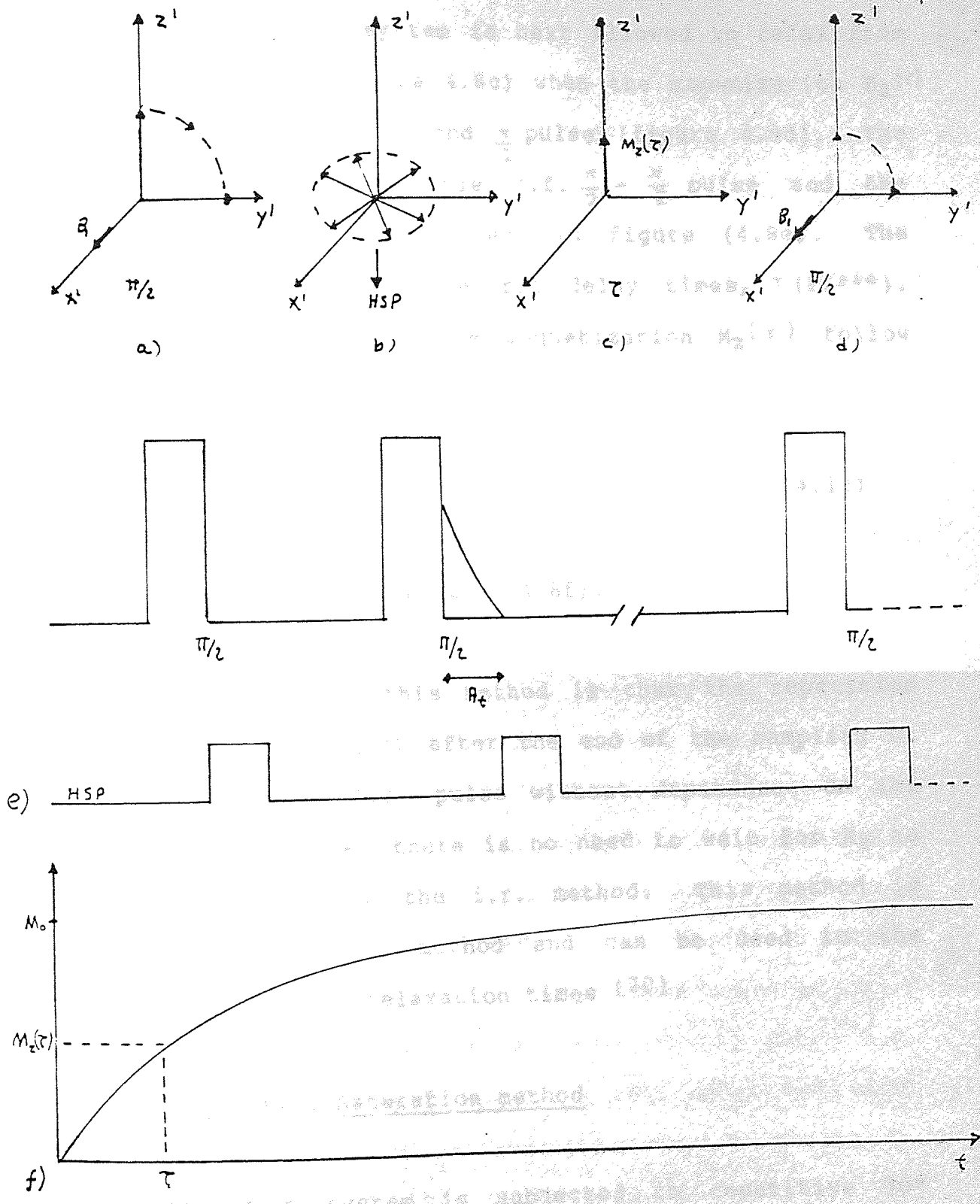

Figure 4.8 Variation of the magnetization in a saturation recovery experiment a, d magnetization behaviour
e) pulse sequence and Homospoil pulse (HSP)
f) variation of the magnetization with τ, after a 90° pulse in the sat. rec. sequence.

By applying a field spoiling (homospoil) pulse in the z axis (figure 4.8b) the transverse magnetization is then destroyed. The spin system is next allowed to relax from zero for a time τ (figure 4.8c) when the magnetization $M_z(\tau)$ is sampled after a second $\frac{\pi}{2}$ pulse (figure 4.8d). The relation between the double r.f. $\frac{\pi}{2} - \frac{\pi}{2}$ pulse and the homospoiling pulse can be seen in figure (4.8e). The process is repeated for several delay times, τ (PI***). The resulting values of the magnetization $M_z(\tau)$ follow the equation (4.13).

$$M_z(t) = M_o(1-\exp-t/T_1) \qquad (4.13)$$

which is illustrated in figure (4.8f).

The advantage of this method is that the repetition time PR can be set just after the end of the sampling of the FID and the H.S.P. pulse without dependence on the relaxation times i.e. there is no need to wait for M_z to recover to M_o as in the i.r. method. This method is faster than the I.R. method and can be used in the measurement of short relaxation times (70).

4.4B3 Progressive Saturation method

If the spin system is subjected to repetitive 90° pulses, a dynamic equilibrium will eventually be established in which the effect of saturation caused by

the r.f. pulses and that of relaxation, balance each other. Freeman and Hill (185) have calculated that the steady state condition is nearly reached after three or four 90° pulses. The sequence can be written in the following way

$$(\frac{\pi}{2}-A_t-D)-(\frac{\pi}{2}-A_t-D)_n$$

not sampled

Figure (4.9a) illustrates the effect of the three 90° pulse applied to the spin system. In this case a homospoiling pulse (186) (figure 4.9b), is introduced after each pulse, to avoid any constructive $M_{x,y}$ formation or "echo" (186)(187). This ensures that $M_{x,y}=0$ before the 90° pulse is repeated. The sampling 90° pulse is repeated n times in order to increase the S/N ratio. If several values of τ (PR***) are selected, the plot of the signal versus time will follow the exponential equation (4.13). The value of A_t+D is expressed in the stacking program as τ=PR***. The so-called dummy parameter is used in the Jeol FX90Q spectrometer to start the sampling after a particular conditioning pulse e.g. if dummy is set to zero this means that after the first pulse, the FID will be sampled; if dummy is set to 3, this means that after the fourth pulse the FID will be sampled; this last condition was employed in the present work.

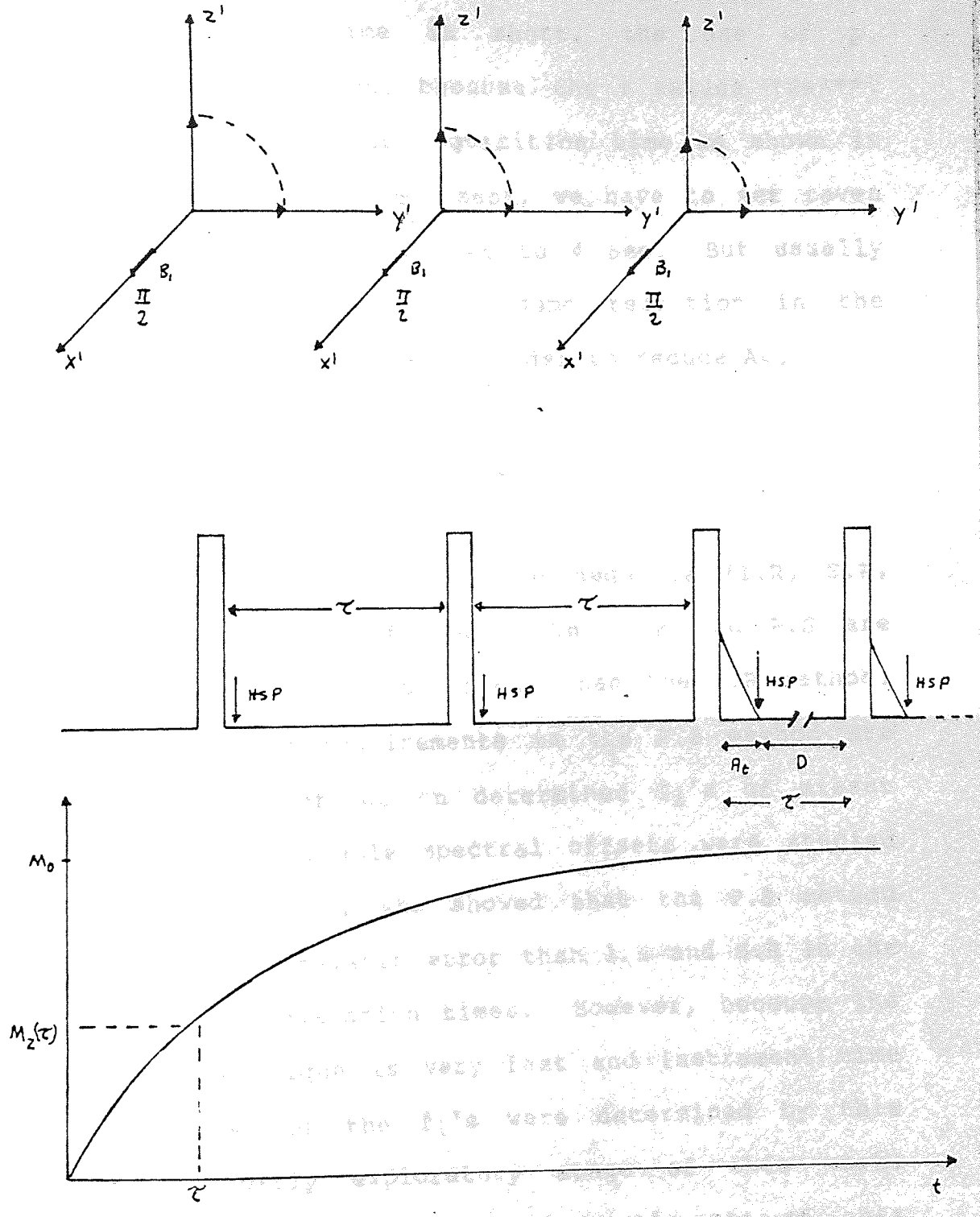

Figure 4.9 Determination of T_1 by using the progressive saturation method a,b,c magnetization behaviour
d) p.sat. sequence with homospoil pulse
e) variation of M_z with τ after the 90° pulse

The advantage of the p. saturation method is that long relaxation times can be measured in a short time. When the relaxation time is short, the use of p. saturation becomes limited, because the τ values (PR***) cannot be shorter than the acquisition time as shown in Figure (4.9d). e.g. If $T_1 \approx 3$ secs, we have to set seven values of PR*** from say 0.2 sec to 4 sec. But usually $A_t \approx 1$ sec, which implies that some reduction in the sample points have to be done, in order to reduce A_t.

4.4B4 Selection of Pulse Sequences

The choice of a specific pulse sequence (I.R, S.R, P.S) depends on several factors. The S.R and P.S are faster and somewhat more convenient than the I.R method. However, the pulsing requirements in the P.S method are more exigent. The effect on determined T_1's of misset pulse lengths and variable spectral offsets were studied by Levy and Peat (70), who showed that the P.S method gives 5-10% more systematic error than I.R and S.R in the determination of relaxation times. However, because the p. saturation technique is very fast and instrument time was limited, most of the T_1's were determined by this method in the early exploratory stage of this work. Therefore, it was decided to continue the use of this technique in order to get results by a consistent approach.

4.4C Selection of Optimum Parameters for T_1's Measurements.

Once a pulse sequence has been selected for the measurement of relaxation times, a number of practical problems remain to be solved regardless of the nature of the sequence. These problems can arise from the following factors (70):

a) quantity of sample,

b) sample state (solvent, paramagnetic impurities, etc),

c) temperature control problems,

d) instrument resolution and sensitivity stability,

e) effective pulse flip angles,

f) computer limitation,

g) data processing,

h) non-exponential relaxation behaviour. Some of these problems have been assessed in this work.

The size of the sample can affect the value of the T_1 (142)(179) because the B_1 field is not homogeneous inside the transmitter coil; this fact is more notorious in the case of single coil probes. If the sample occupies a larger volume than the coil the value of B_1 at a point away from the centre of the coil can be very different from that at the centre. This means that these remote nuclei can affect the value of the true relaxation time if they diffuse into the central region of the coil. It was established (70) that for ^{13}C T_1's $\leq$50 sec and for

samples $\leq$ 30mm in length the effect of diffusion is negligible. The same sort of consideration must be given to volatile solutions because the T_1's obtained for those molecules may appear anomalously short because of liquid vapour molecular interchange and rapid spin rotation relaxation in the gas phase (188). The solution of the implicit problems seems to be the use of a microcell (or samples with the size of the coil) or specially constructed tubes for volatile samples.

Good temperature control is very important to the accurate measurement of T_1. The identification of temperature problems is relatively easy because all of the observed T_1's either increase or decrease according to the change in temperature and the type of relaxation mechanism of the nuclei under study. However, we know that there are samples that when they are noise irradiated (e.g. in ^{13}C experiments) become hotter because of dissipation of the decoupling signal power. With the Jeol FX90Q this effect is difficult to detect because the reference stabilization thermocouple is not actually in contact with the sample but someway below the sample. Simon and Vold (189) have reported an increase in temperature of 6°C in some compunds when noise decoupled. The effect has been mentioned additionally by several authors of whom Led and Peterson (190) have analysed extensively the heating effects on aqueous solutions caused by proton noise decoupling.

Other important points to be borne in mind are the systematic errors resulting from off-resonance effects and maladjustment of pulse angles. The effective field at a nucleus is $B_{eff}=(\Delta B^2+B_1^2)^{1/2}$, in the rotating frame, where B_1 is the r.f. field in gauss and the magnetization component is offset ΔB gauss from resonance. The parameter $\Delta B/\Delta B_1$ has been used to assess the accuracy of sequences used for determining T_1. Freeman et al (191) have found that if $\Delta B/B_1$ is smaller than $1/3$ and the error in the flip angle is 5%, the error in T_1, obtained by using the progressive saturation method is not significant. It is possible to say, therefore, that for the study of a single line the carrier frequency should be set such that $\Delta B \approx 0$ in order to give reasonable confidence in the progressive saturation method, provided the 90° pulse is determined with reasonable accuracy.

The handling of acquired data is an important factor in determining the accuracy of measured T_1's. If for example the spectral resolution changes slightly during the course of an experiment the analysis of T_1 using peak heights alone is dubious and only signal areas should be used. However, it is possible to imposse a small exponential weighing factor to the FID which broadens the signals and masks resolution instabilities, so that heights can be used to represent M_Z with some confidence.

4.4C1 Determination of the 90° pulse width

An approximate idea of the condition for a 90° pulse can be obtained indirectly by looking for the minimum F.I.D. by varying the pulsewidth (PW_1**). This can be done rapidly by using the LINE facilities in the normal program. This enables the repetitive acquisition and displaying of the F.I.D. The resultant pulse width corresponds to a 180° pulse. From an analysis of this type it was established that for ^{1}H the 90° pulse is about 45 μsec and for ^{13}C it is about 22 μsec.

The use of the LINE command produces the FID for the pulse selected with the light pen every PR seconds, where PR is the repetition time of the pulse, which usually is 21 sec. The FID that results from this procedure corresponds to the stationary magnetization in the xy plane (M_{xy}) after several pulses, but it should be pointed out that this does not necessarily represent the 180° pulse, because PR$\approx$21 sec is a very short waiting time for samples with T_1 in the order of 20 sec.

There are other methods which can be used to determine the 90° pulse, e.g. a pulse of about 270° can be applied which should produce a negative signal with good shape (no shoulders) and when this has been optimized, the pulse width obtained is simply divided by 3 to get the 90° pulse. In the present work, however, it was considered preferable to observe the variation of

the peak height when a pulse width PW_1^{**} is applied, which will produce a maximum signal when PW_1^{**} corresponds to a 90° pulse and smaller signals for other PW_1^{**} values. In this procedure it is necessary to wait a time $t \geq 5T_1$ between measurements to guarantee that the sample is at equilibrium ($M_Z=M_O$). This method consists in changing PW_1^{**} in steps of 1 μsec for several values around the suspected 90° value. This process can be done automatically by using the stacking program with PW_1^{**} as variable parameter. The data are transferred to the analysis program where after data reduction on data No1, the following signals will have the same phase and normalized gain. For example, a sample of neat cyclohexane was selected to analyse the ^{13}C 90° pulse. Two different sets of PW_1^{**} were selected, one in the region of the 90° pulse and the other close to the 180° pulse. In order to ensure that the signals correspond to the equilibrium magnetization M_O a double pulse sequence was used, i.e. $\{1\ \mu\text{sec-PI-PW}_1^{**}\}$, where the 1 μsec pulse just perturbs the spin system; $PI \approx 5T_1$ guarantees that each set of data is sampled when the spin system is at equilibrium and PW_1^{**} is varied in steps of 1 μsec. Figure (4.10) shows the signal for six values of PW_1^{**} close to the 180° pulse from which it was estimated that the 90° pulse is 21.5 μsec for a sample of neat cylohexane. Figure (4.11) shows the results for PW_1^{**} close to the 90° pulse in the same sample, from which it was deduced that 22μsec is the 90° pulse. This procedure can give an error of $\pm$ 1 μsec, i.e. 5%. Different 90°

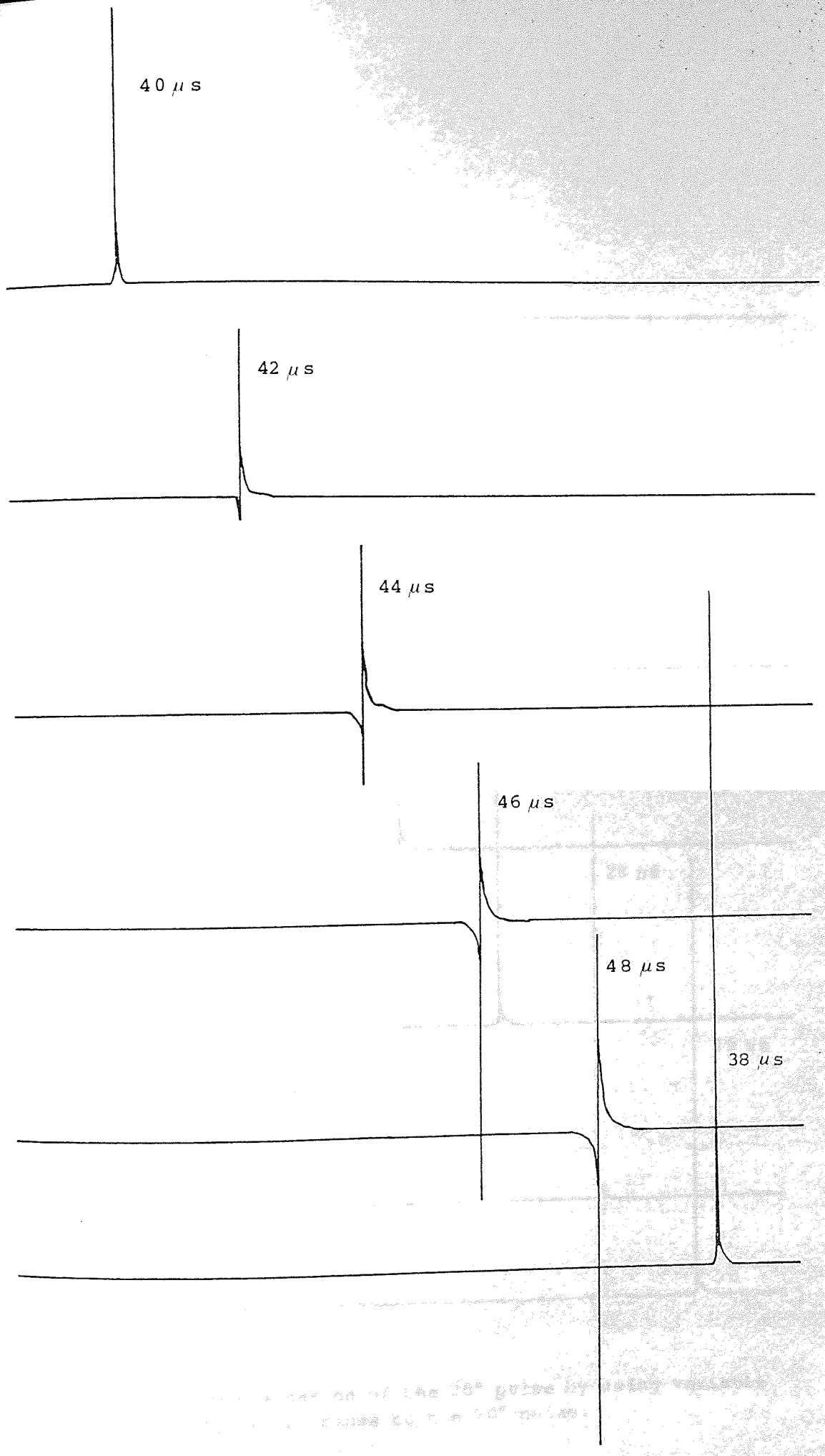

Figure 4.10 Determination of the 90° pulse by using variable pulse width (PW_1 ** μs) close to the 180° pulse.

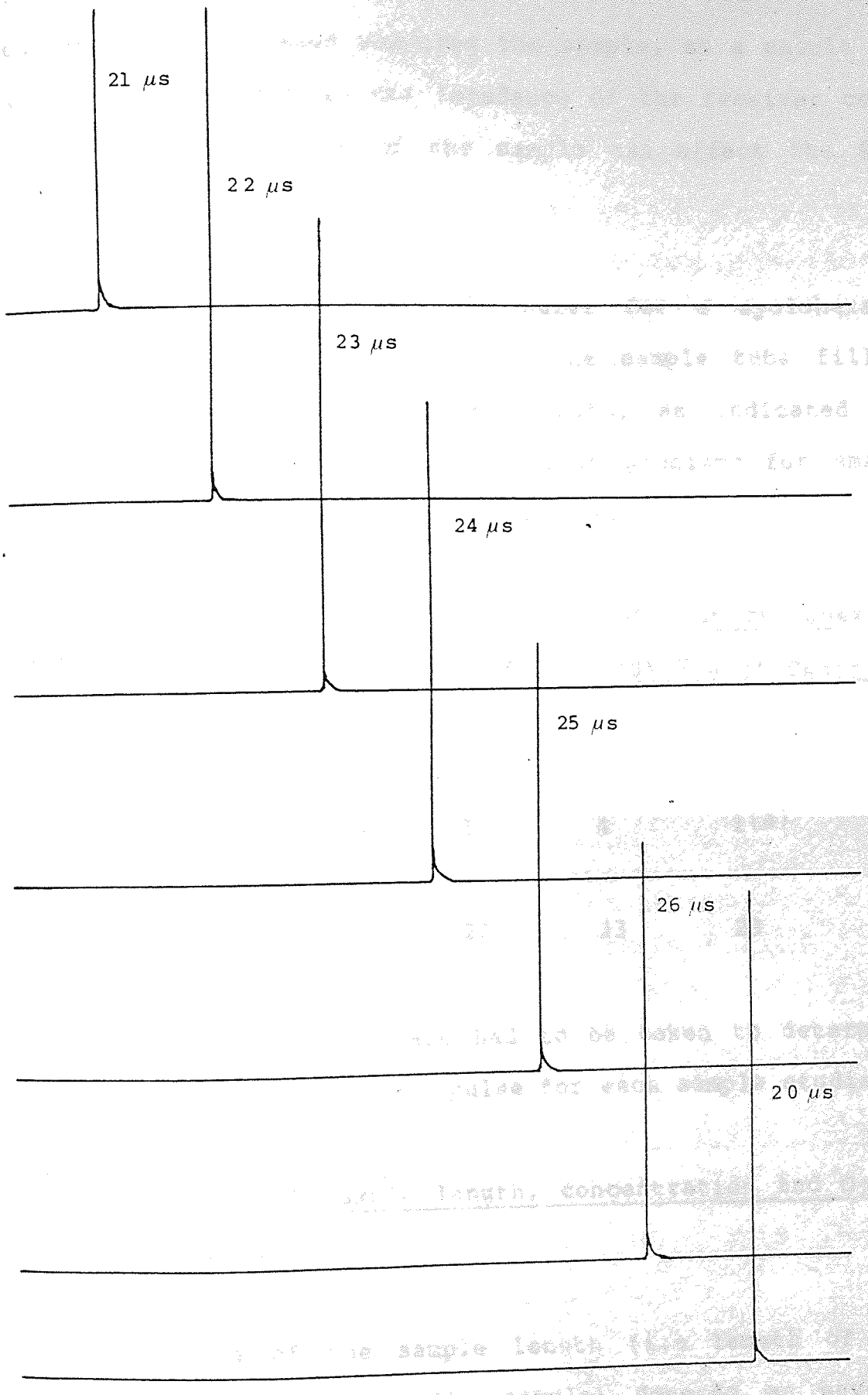

Figure 4.11 Determination of the 90° pulse by using variable pulse width (PW_1 ** μs) close to the 90° pulse.

pulses can arise when changing the sample, as a result of slight modification in the impedance of the receiver coil (192). Also the size of the sample can affect the 90° pulse value.

The analysis of the 90° pulse for a cyclohexane sample with different lengths of the sample tube filled showed an increment with the length, as indicated in table (4.6.). However the resolution problems for small samples could explain some of this behavior.

Table (4.6) 90° pulses in samples of neat cyclohexane with different lengths—sample (a) has 10% $^{v}/_{v}$ of C_6H_{12} in CCl_4.

Size (cm)	0.4	1	4	1(a)
90° pulse (μsec)	21	22	23	23

It is evident that care had to be taken to determine the conditions giving a 90° pulse for each sample studied.

4.4C2 Effects of sample length, concentration and O_2 on ^{13}C T_1's

The choice of the sample length (i.e length of nmr sample tube occupied by the sample) depends on several factors which as mentioned before, are the rf field B_1 inhomogeneity and the diffusion of molecules into the coil

excitation volume (142). It would appear, therefore, convenient to use small samples. Levy and Peat (70) recommend the identification of a sample size beyond which the sample size becomes a source of error. In our case it was found that the spectral resolution of the instrument is affected by samples shorter than 3cm and from table (4.6), that the 90° pulse width appears to vary with the sample size. In order to study these effects on T_1, several samples of cyclohexane were analysed at 30°C using the progressive saturation method. The average values of the measurements are shown in table (4.7). In general, it can be seen that T_1 tends to decrease when the sample length is increased, but this effect is less important in dilute samples. The presence of O_2 and the concentration of cyclohexane have little effect on the ^{13}C T_1 values.

Table (4.7) ^{13}C T_1's values of cyclohexane at 303°K

(a) in 5 mm O.D n.m.r. tubes

(b) obtained at 309°K

Condition	Length (a) (cm) 0.4	1	2	4	----
neat non-degassed	21.77	19.9	19	17.2	---
neat degassed	---	20.6	20.2	17.9	---
10% in CCl_4, degassed	---	19.6	19.9	19	---
neat degassed (146)	---	---	---	---	19.6(b)

It does appear that for neat samples it is important to have similar sample lengths in order to avoid errors in the determination of the relaxation time, but for dilute samples this is less important.

4.4.C.3 Effects of Resolution Instabilities on ^{13}C T_1's

The progressive saturation method requires the use of a homospoil pulse applied on the z axis after each 90° pulse. This sudden change in homogeneity can interrupt the lock signal and cause the loss of homogeneity (193). As a result, errors as great as 30% in the experimental values of T_1 can be found. The use of an "auto shim" unit (193)can improve the situation as is shown in Figure (4.12).

In the course of our experiments, the Jeol FX90Q spectrometer had a sudden period of resolution instability. It was noticed that the line-width became broader in few minutes in a totally irreproducible way. As a result, the meter indicating the lock level would reduce its value corresponding to loss of resolution and broader signals. As the progressive saturation method in the analysis program uses the heights rather than intensities of the peaks to find the T_1 from equation (4.13), the resulting T_1 will be far from the true value. For example, in one of the experiments, where loss of resolution occurred, a T_1 of 33.8 sec was obtained in comparison with the expected true value for T_1 of 11.3

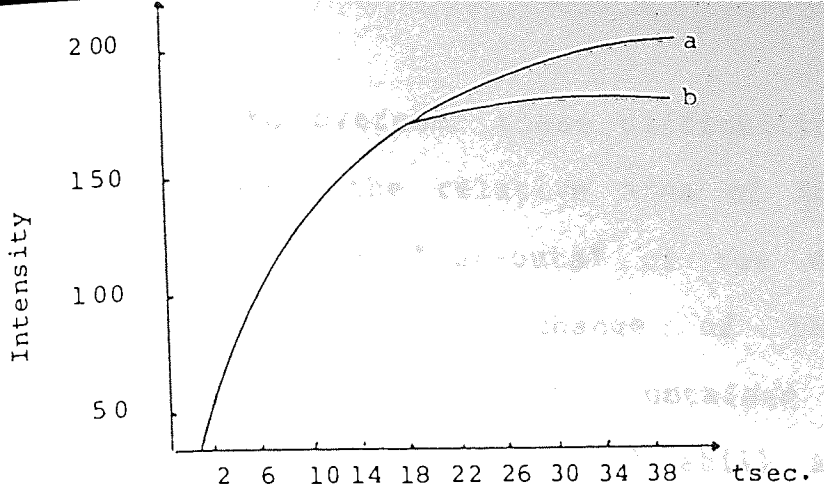

Figure 4.12 Effect of the autoshim on observed intensities (193)
a) autoshim ON
b) without autoshim

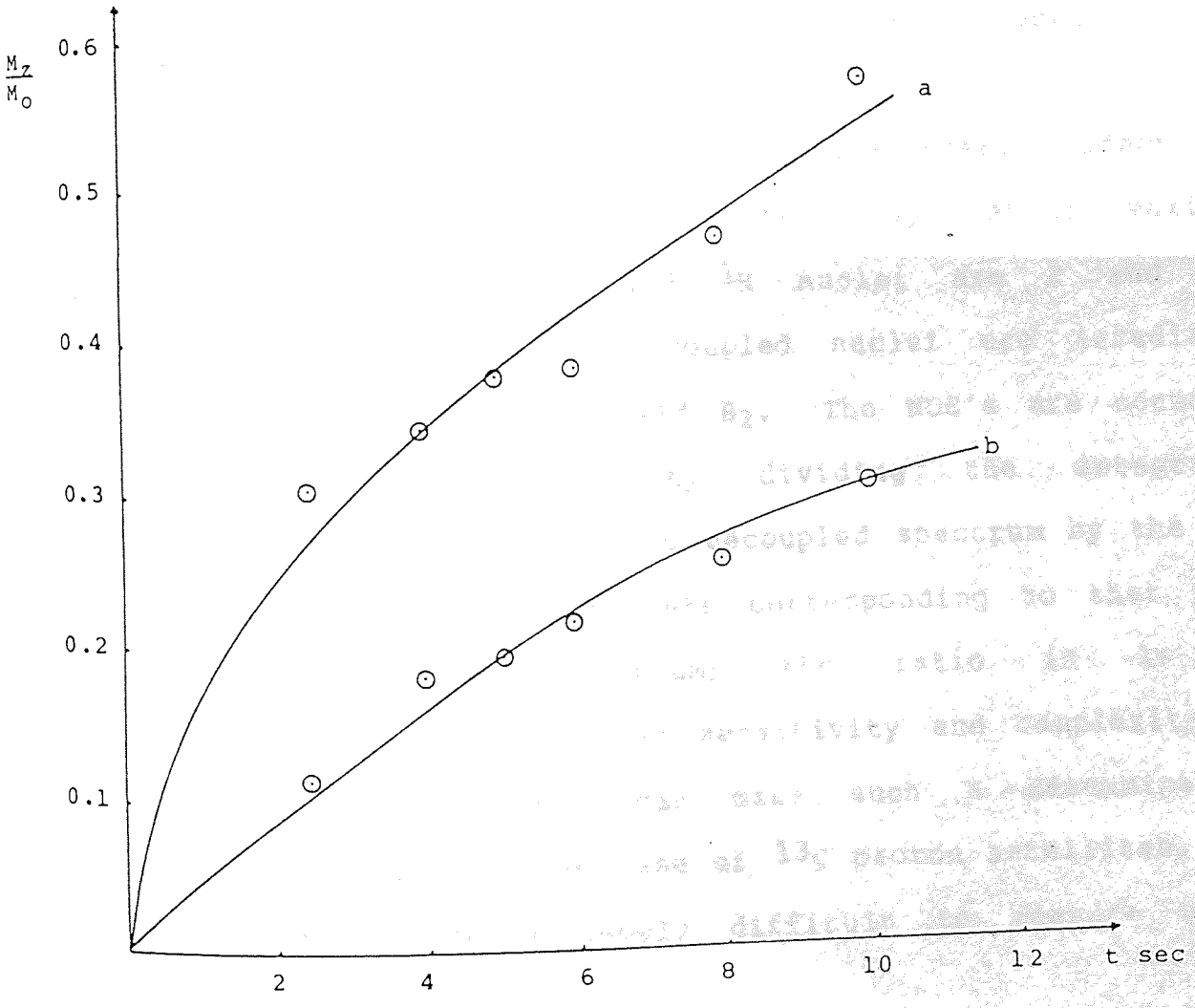

Figure 4.13 Variation of M_z for the aromatic ^{13}C of mesitylene in $Me/C_6H_{12}/TMS$ mixtures $X_{Me}=0.07$, $X_{TMS}=0.62$. Expected T_1 11.3 sec
a) Peak height $T_1=33.8$ sec.
b) Peak areas $T_1=16.2$ sec.

sec. In order to overcome these difficulties due to the broadening process, the relative area of the peaks were estimated by weighing "cut-outs" of the spectra chart. Figure (4.13) shows the change of the normalized intensity M_Z/M_O. The T_1 value obtained by the area weighing method was 16.2 sec and still away from the expected value, but gives an idea of the problems caused by resolution instability. Therefore, the use of the autoshim unit is recommended to avoid this sort of problem as far as possible.

4.4D Measurement of Nuclear Overhauser Effects

In chapter three the nuclear Overhauser effect was discussed and it was shown theoretically that the maximum enhancements for ^{13}C and ^{1}H nuclei are 2 and 0.5 respectively, after the coupled nuclei are irradiated with a saturating rf field B_2. The NOE's are normally calculated practically by dividing the integrated intensity of a peak in the decoupled spectrum by the sum of intensities of multiplets corresponding to that peak in the coupled spectrum; the ratio is $1+\eta$. Unfortunately, the reduced sensitivity and complexity of many coupled spectra can make such a determination difficult, e.g. in the case of ^{13}C proton satellites, the enhancements are extremely difficult to measure using this technique.

In ^{13}C experiments, manipulation of the level of the carbon magnetization is possible using pulse modulated decoupling techniques which allows one to supress the NOE effect in proton decoupled spectra, i.e. decoupled but non-enhanced signals can be detected. This can be done because the saturation of proton resonances has an essentially instantaneous effect on scalar spin-spin coupling, while the ^{13}C polarization resulting from the same irradiation develops with the time constant of the spin-lattice relaxation. The gated decoupler method (194) of measuring the decoupled ^{13}C spectrum without NOE exploits the separate time scales for scalar decoupling and the development of magnetization. The sequence of events in the experiment consists of

a) turning on the proton irradiation simultaneously with a 90° rf pulse at the ^{13}C frequency.

b) collecting the free induction decay immediately after the pulse, with proton decoupling still on, and

c) turning off the decoupler for a relatively long delay period T.

This process is illustrated in Figure (4.14a) and corresponds to the NNE irradiation mode of the Jeol FX90Q instrument when no nuclear Overhauser enhancement is obtained. In Figure (4.14b) the complete decoupling irradiation mode (COM) allows the signal to be obtained with enhancement. From these two measurements, the NOE is given by

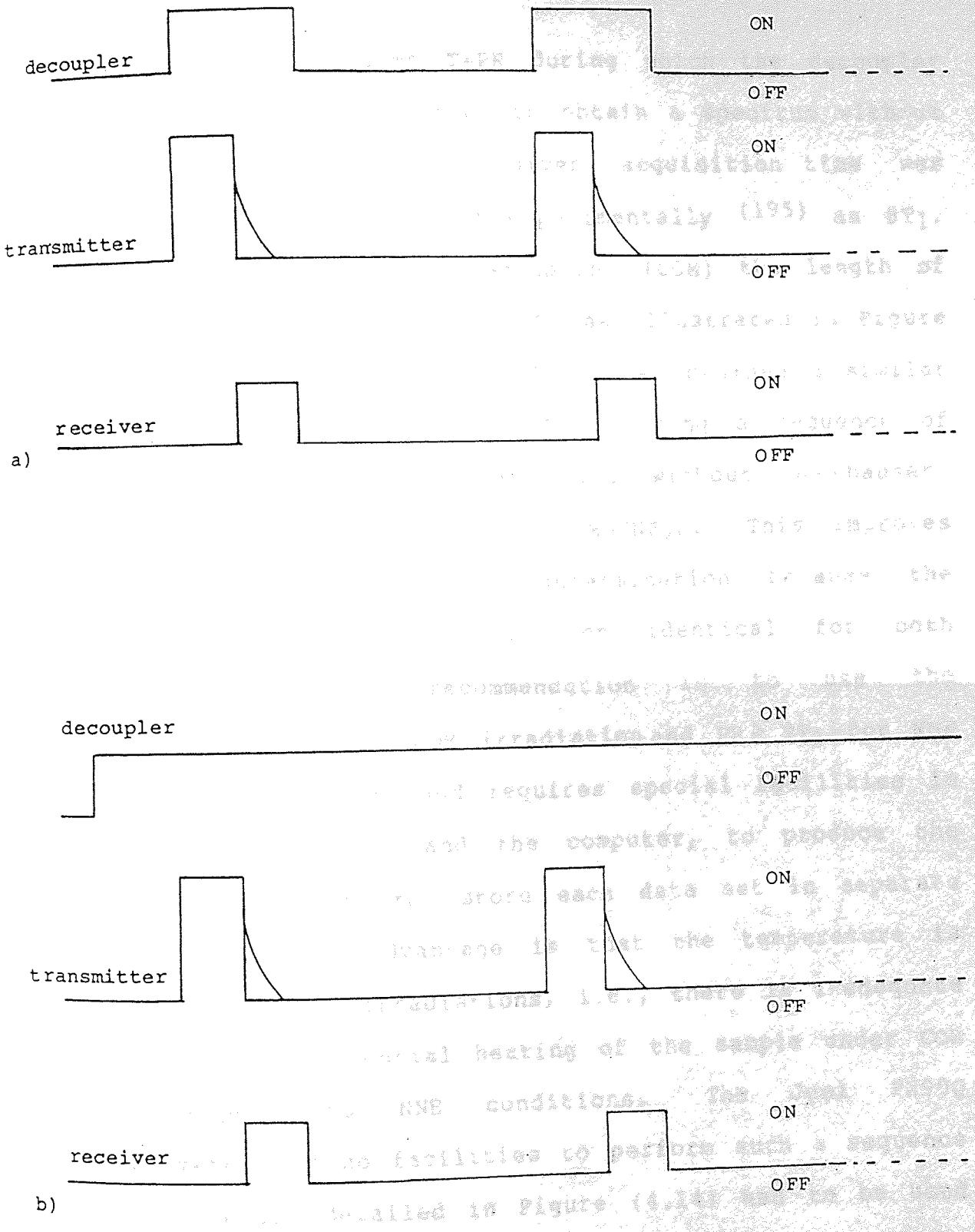

Figure 4.14 Schematic representation of the gated decoupling technique used for the measuring of the NOE
a) the NNE mode
b) the COM mode

$$\eta = \frac{I_{COM}}{I_{NNE}} - 1 \qquad (4.14)$$

The length of time T=PR during which the decoupler must be turned off in order to obtain a spectrum without enhancement (NNE) for a given acquisition time was estimated theoretically and experimentally [195] as $8T_1$. In the case of complete decoupling (COM) the length of time needed was estimated as $5T_1$ as illustrated in Figure (4.15). Harris and Newman [196] have obtained a similar result. They measured the NOE by using a sequence of measurements with Overhauser and without Overhauser enhancement corresponding to $(COM,NNE)_n$. This improves the accuracy of the NOE determination because the spectrometer performance is then identical for both experiments. Their recommendation is to use the condition $PR \geq 6T_1$ for COM irradiation and $PR \geq 9T_1$ for NNE irradiation. This method requires special facilities in the the pulse programmer and the computer, to produce the $(COM,NNE)_n$ sequence and store each data set in separate blocks. Another advantage is that the temperature is the same for both irradiations, i.e., there is inadequate time to get preferential heating of the sample under COM with respect to NNE conditions. The Jeol FX90Q spectrometer has no facilities to perform such a sequence and the method detailed in Figure (4.14) had to be used with allowance being made for temperature differences produced by the COM and NNE irradiation modes.

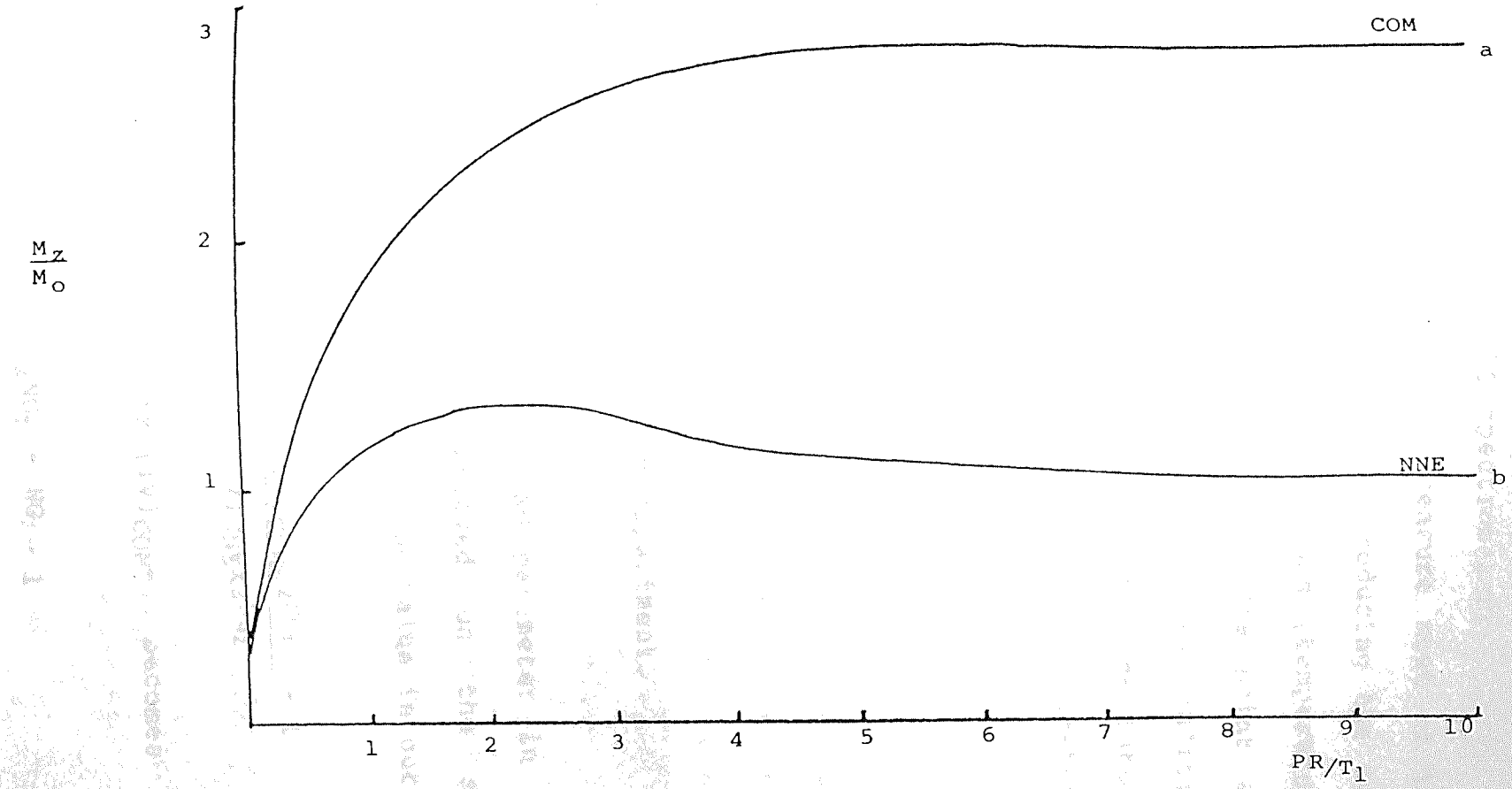

Figure 4.15 Behaviour of the magnetization M_z under two different irradiation modes (195)
a) complete irradiation
b) NON Overhauser enhancement

There are several methods available to measure NOE by using the Jeol FX90Q spectrometer:

a) The method used to measure most of the NOE reported in this work consisted of producing the two spectra (COM, NNE) under the same conditions (temperature, flip angle, acquisition time, number of data point and so on); the peak to be compared under the two conditions was defined by more than four data points. The integration facility was used with the integral parameter fixed to a normalized value of IV=1 for the COM peak. Using the same condition the NNE peak was integrated, without changing the pre-set IV value. A relative value $(IV)_{NNE}$ was thus obtained. If NG_1 was the normalized gain in the COM spectrum and NG_2 the normalized gain in the NNE spectrum; $NG_1 \geq NG_2$ because of the enhancement in the magnetization in the COM experiment.

The meaning of the NG parameter in ACPAR pattern is that the signal displayed on the scope screen is proportional to 2^{NG}. The NOE value in our experiment is

$$\eta = \frac{I_{COM}}{I_{NNE}} - 1 = \frac{(IV)_{COM} \times 2^{NG_1}}{(IV)_{NNE} \times 2^{NG_2}} - 1 \qquad (4.15)$$

which, because we fix $(IV)_{COM}=1$, becomes

$$\eta = (IV)_{NNE}^{-1} \; 2^{NG_1 - NG_2} - 1 \qquad (4.16)$$

b) The same procedure as a) can be followed but the peak heights can be used instead of the integral value of the signals. In general, the two approaches give the same result but if the resolution of the instrument is not stable enough during the experiment, important errors are found.

c) The changes in normalized gain can be avoided when the automatic recorder, IC memory or CMT cassette facilities in the stacking program are used. In these cases, a double pulse sequence 5°-PI-90° has to be used; $PI \geq 6T_1$ or $PI \geq 9T_1$ is the interval between the two pulses according to the mode COM or NNE respectively. The repetition time PR can be selected to be as small as 3 seconds. The double pulse is required because the stacking program does not have initial wait facilities between data. The setting procedure for the stacking program uses the parameters: IRMOD1 for COM and IRMOD4 for NNE or alternatively, those can be changed by using the extension parameter EXTNS 163 for COM and EXTNS 175 for NNE as will be detailed later.

When using the automatic recorder, the signals are plotted on papers after the acquisition of the COM or NNE data and the peak intensities are compared to get the NOE.

The IC memory mode of operation relies on the use of four blocks in the computer memory which requires that the number of data point is set to 4196. In this case

the block distribution is: block 1 for sampling data; block 2 for NNE data; block 3 for COM data and block 4 empty; this approach necessitates NG corrections to be made.

The CMT mode of operation has the advantage that the information is stored on a magnetic cassette data tape. The parameters for COM and NNE are set as above and the analysis program is used to plot the peaks on the paper with the same normalized gain; this information is used to get the NOE value.

These different methods were used to obtain the intermolecular NOE for cyclohexane (80%) in a solution with mesitylene and TMS. The results are presented in table (4.8).

Table 4.8

NOE For Cyclohexane Determined by Several Methods

NOE	METHOD
1.9	a
2.26	b
2.5	c(automatic recorder)
2	c(I.C. memory)
2.2	c(C.M.T. analysis program)
2(i); 1.9(j)	Literature, i(103) j(146) neat C_6H_{12}

According to the results in table (4.7) and in thought of further experience with the technique, it was concluded that method (a) gives the most reliable information.

4.4.E Irradiation Modes in the Jx90Q

The irradiation modes referred to above are set by using the light pen in the constant pattern. In this work, we use COM, NNE, SEL, HOM, EXTSN, where COM and NNE have been described previously.

The COM or noise decoupling mode is normally operated over 1KHz and at 54.5 KHz OFFSET and is centered close to the benzene signal offset 54.68 KHz. However, for each particular sample it is recommended that the irradiation offset parameter is set in the middle of the proton spectra to ensure full saturation. SEL is the heteronuclear selective decoupling which can be used to irradiate a particular proton frequency while ^{13}C is observed. The SEL or selective irradiation allows us to perform coalescence observations on ^{13}C signals when the irradiation offset frequency is changed or the decoupling power reduced. In the first case we can use the Bloch-Siegert equation to evaluate the irradiation power γB_2. HOM is the continuous irradiation mode for the proton spectra but is time shared, which means that the r.f. oscillator generates power for a short time and the receiver is on for short time, so both devices are on and

off in sequence. The extension mode, EXTSN, can be used to combine several irradiation functions. The extension mode of irradiation was used in order to apply irradiation power at the protons equivalent to the NNE when ^{13}C is observed. We defined this mode as HOM(NNE) and this was used to get the enhancement of ^{13}C proton satellites signals, as indicated in table (4.9).

The Jeol instruction manual provides a conversion table between binary codes and decimal numbers and these are related to the following irradiation functions,

a) Homo or hetero irradiation,

b) rf attenuator control

c) hetero-power level,

d) time sharing,

e) gate mode I, II,

f) gated or not,

g) noise modulation on, off,

h) irradiation power.

The status of each function is presented in table (4.9) according to the decimal number conversion. The extension mode is represented by a number, which is the sum of the function numbers. When a function is off the corresponding decimal number is zero, e.g. the irradiation mode COM is used in heteronuclear systems ($^{13}C-\{H\}$) (128); it does not use r.f. attenuation (o), the rf power is high (32), there is no sharing facilities (o), no gate (o). Consequently, the gate mode is (o),

Table (4.9)
Extension Irradiation Modes calculated from the conversion table (73) between binary codes and decimal figures.

EXTNS	hetero/hom	R.f.att.	high-low power hetero	sharing	Gate	Mode	Noise	Irr. Power	Mode
163	128	0	32	0	0	0	2	1	COM
167	128	0	32	0	4	0	2	1	NOE
175	128	0	32	0	4	8	2	1	NNE
81	0	64	0	16	0	0	0	1	HOM
93	0	64	0	16	4	8	0	1	HOM(NNE)
225	128	64	32	0	0	0	0	1	SEL
229	128	64	32	0	4	0	0	1	SEL/NOE
237	128	64	32	0	4	8	0	1	SEL/NNE

the noise modulation is on (2) and the irradiation power is on (1). The sum of these numbers is 163, which means that the extension parameter: EXTNS 163 is equivalent to COM. The extension parameter permits to set new irradiation modes like HOM(NNE). Also, it was noticed that EXTNS 225 is the same irradiation mode as SEL, but with high power (32) which produces a more effective decoupling.

4.4.F Temperature Calibrations

Due to the variation of relaxation times with temperature, it is necessary to measure the temperature within the sample. This is done by observing the chemical shift between the methylene and hydroxyl proton in ethyl glycol.

The 100 MHz instrument VARIAN HA 100D was operated at room temperature and variations throughout the year were compensated by using the magnet coolant control system. Figure (4.16) shows the calibration curve for the chemical shift of ethyl glycol. This was used with a measured chemical shift, e.g. δ =156.3 Hz to reveal the sample temperature (30.5°C). After that the temperature of the magnet coolant was checked and found to be 30.7°C. The temperature measured with a mercury thermometer was 33°C when in contact with the probe and 30°C when not in contact. However, if the magnet was switched off for a long time, variations in temperature

were found, e.g. the water coolant temperature was 27°C but a thermometer inside the probe measured 33°C and the chemical shift between the peaks in ethyl glycol was δ =155.3 Hz which corresponds to 31.5°C. It is evident that adequate time had to be allowed for this magnet system to achieve thermal equilibrium.

The Jeol FX90Q spectrometer uses a variable temperature controller type NM-VTS2 (V.T. controller) the desired temperature can be obtained by transmitting controlled hot or cold air to the sample area. The range of operation varies between -110°C and +180°C. In the high temperature range (30°$\sim$180°C) air from a compressor is heated and the temperature is automatically controlled. The medium range (+33-50°C) proved difficult to operate when set at 30°C because of instabilities in the gas flow.

The use of the different irradiation modes can cause different sample temperature (190)(197) and the temperature calibration is a function of the decoupling power. It was noticed in the medium range that the chemical shift of ethylene glycol in the non-decoupling condition (NON) differs from that in the complete decoupling (COM) mode by about 10 Hz when the set temperature was 10° or 20°C. This means that the approximate difference in temperature between the two irradiation modes was about 10°C. However, this variation seems to be related to the difficulty of

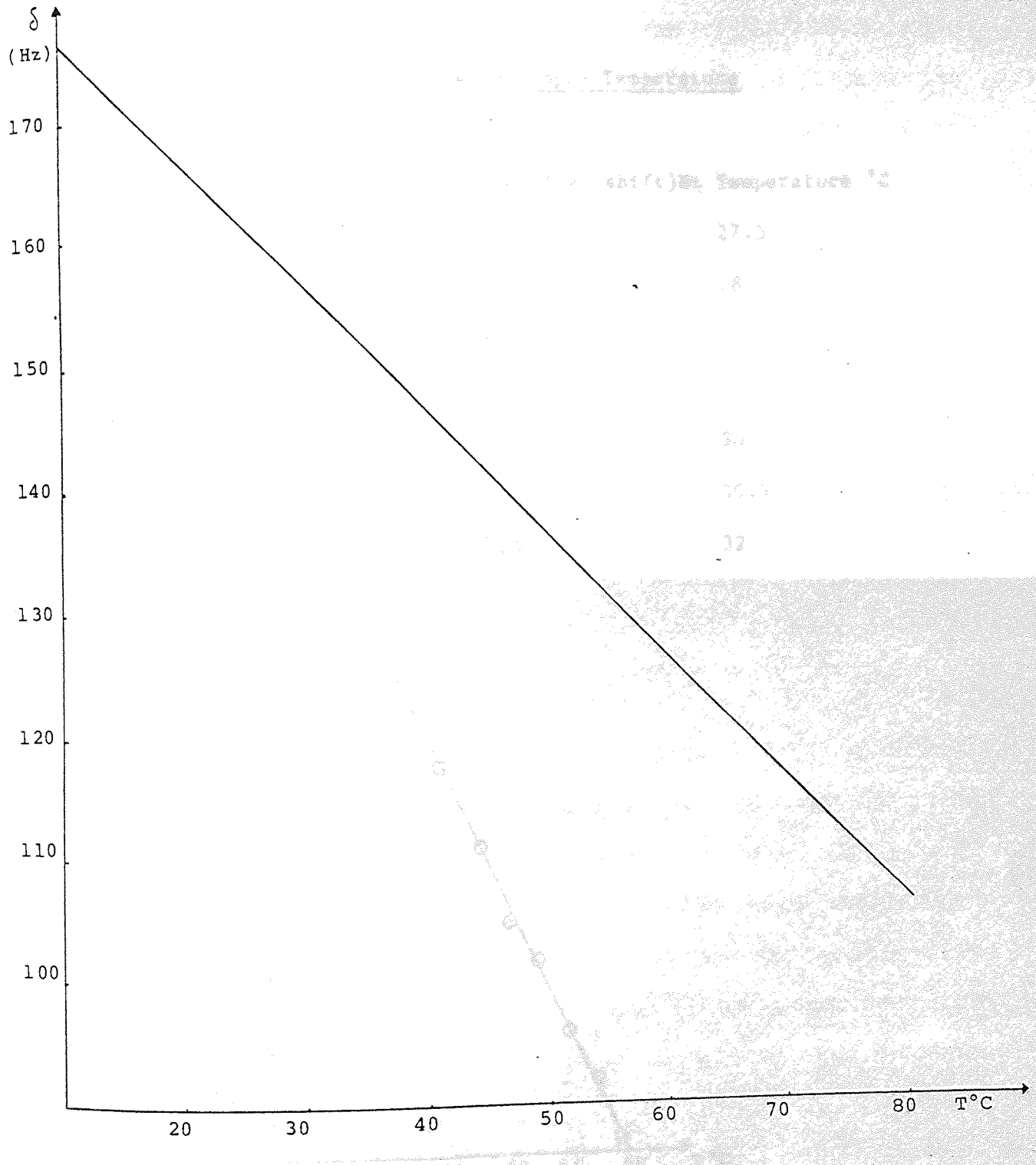

Figure 4.16 Temperature calibration curve for the Varian HA100D using ethylglycol

Table (4.10)

EFFECT of the Irradiation Modes on Sample Temperature

	irradiation mode	(Chemical shift)Hz	Temperature °C
	NON	147.7	27.5
V.T. OFF	SEL	147.4	28
	COM	146.7	29
	NON	145.2	30
V.T. ON	SEL	144.7	30.6
Set at 30°C	COM	143.5	32

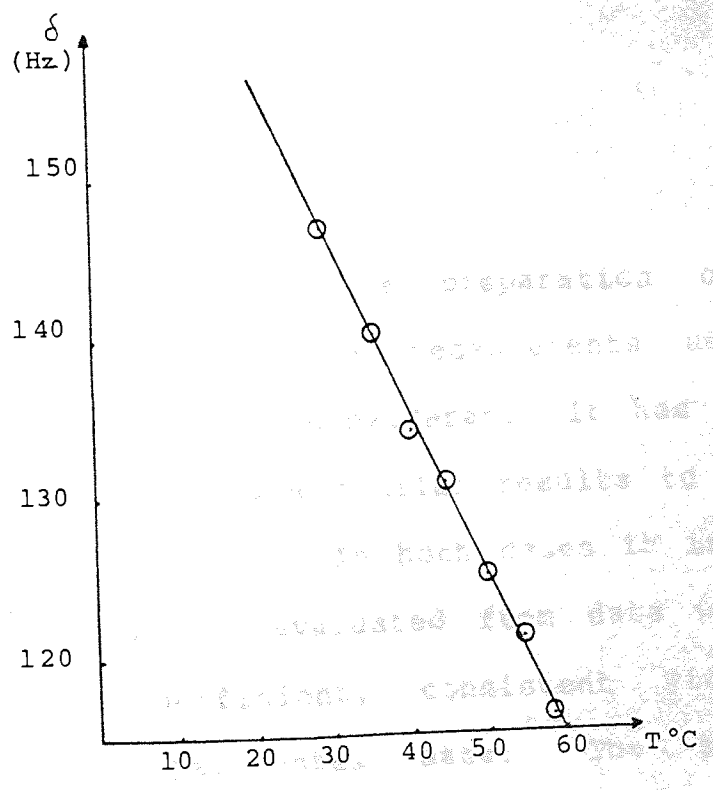

Figure (4.17) Temperature calibration curve for the Jeol FX90Q spectrometer using ethylglycol

operation in this range.

In the high temperature range of operation a better behaviour was found when using the different modes of irradiation. This control range was therefore used to adjust the temperature within the range of values between 28°C and 32°C in accordance with the type of experiment in progress. The calibration curve in the mode NON is shown in Figure (4.17). When the V.T. is off the change in temperature for COM irradiation is approximately 2°C as shown by table (4.10). The variation was about the same with the V.T. on.

The results in table (4.10) indicate that it is possible to set the correct temperature for the sample when operating in the COM mode by setting it 2°C lower than the desired value.

4.5 CONCLUSIONS

In this chapter the preparation of samples and various methods for T_1 measurements using CW or FT techniques have been considered. It has been shown that the ARPS method gives similar results to the progressive saturation technique. In both cases it is shown that the T_1 should only be evaluated from data with the highest correlation coefficient, consistent with an adequate number of experimental data. The settings of the spectrometers used were established by the analysis of T_1 variation with several relevant parameters.

Whilst the ARPS method was employed for CW measurements, the progressive saturation technique was selected for use in the determination of T_1 by F.T. experiments because it proves to be both accurate and the fastest in this case. However, this latter technique is sensitive to sudden change in resolution, which makes it desirable to use an "autoshim" control. The T_1 value of ^{13}C and ^{1}H were shown to depend slightly on the sample size (length) for neat samples but for dilute samples the variations were found to be less important. It was shown that NOE measurements for ^{13}C should be done using peak integration under COM, and NNE irradiation facilities but as the temperature of the sample is higher by about 2°C when using COM, it is important to try to compensate for this increment.

CHAPTER FIVE

Nuclear Spin Relaxation In Solutions

5.1 Introduction

The nuclear spin-lattice relaxation time depends on two kinds of interaction, the intramolecular and the intermolecular interactions. If dilution using deuterated analogues to separate both contribution is not used, it will be necessary to use some theoretical alternative. At first sight, it seems that the intramolecular contribution can be easily evaluated, using the Gutowsky-Woessner (79) equation to get T_1. For this all that is needed essentially, is the molecular geometry and the correlation time. In fact, there are problems with the evaluation of the correlation time.

The obvious model to use is that of Debye but this is incomplete (144)(145) and produces considerable error (81). Also internal motion in the molecule may complicate matters and modify the effective correlation time (90). As the Debye model describes the correlation time as being proportional to the viscosity and the volume of the molecule, it is possible that manipulation of these factors may improve matters.

Perrin (144) introduced the shape of the molecule as an important factor in ellipsoidal molecules finding some improvement in τ_r. Gierrer and Wirtz (198)(199) use the expression

$$\tau_r = \eta \ Vm \ fr \ / \ KT \qquad (5.1)$$

where fr is the microviscosity factor

$$fr^{-1} = 6 \ r_s/r_o + {}^1/(1+r_s/r_o)^3 \qquad (5.2)$$

assuming a spherical solute molecule (radius r_o and volume Vm) surrounded by spherical solvent molecules (radius r_s) in a medium of viscosity η . This model is sufficiently accurate for most purposes.

Steele et al (92)(200)(201) have reported that the magnitude of the rotational correlation time is one order different from the experimental value in some organic compounds. They developed a theory where the frictional constant of a spherical molecule is proportional to the second order angular derivative of the intermolecular potential V. As a result, no torques can act on a rotating molecule if the intermolecular potential function is independent of the angles of orientation of the molecule. In this case, the hydrodynamic boundary condition is called "slip" and the correlation time can be approximated (92) to that of the "free rotor"

$$\tau_{f.r.} = \left(\frac{\pi I}{3KT}\right)^{1/2} \qquad (5.3)$$

where I is the moment of inertia of the molecule. The calculations of T_1 in several non-polar, spheroidal molecules, were in quantitative agreement with the experimental data (92) if the intramolecular contribution was evaluated by using the $\tau_{r.f.}$ correlation time and the translational contribution calculated from the B.P.P. theory.

In the case of polar spherical molecules, the Stokes-Einstein equation still gives a considerable error in the calculation of the correlation time. One important difference of the Steele model from the Debye model is that the latter uses the "stick" boundary condition, following the Stokes-Einstein approach. For the latter the rotating molecule is much larger than the solvent molecules and the solvent molecules, at the surface of the rotating solute molecule, rotate with he solute molecule. The implication of this is that the Debye equation predicts too much friction.

McClung and Kivelson (91) have found that dielectric relaxation and magnetic resonance data indicate that τ_r is proportional to η/T, but that the radius a is almost always smaller than the measured or calculated mean radius r_o of the molecule. Consequently, they introduced a correction factor k, $0 \leq k \leq 1$ as an empirical parameter to compensate for the difference through,

$$a = k^{1/3} r_o \qquad (5.4)$$

A value of k may be deduced from the line width of a signal in E.S.R. (91), but in NMR, k can be determined by dividing the observed τ_r by the Debye expression (202)(203) in the analysis of quadrupole spin-lattice relaxation time for very dilute samples in a deuterated solvent so there are no intermolecular contributions. Kivelson and his collaborators (91)(204) have found that in solutions k is independent of temperature and pressure for a given solute-solvent pair. On the other hand, several high pressure NMR studies (202)(205) have indicated that in neat liquids k increases moderately with temperature and decreases, sometimes very sharply, with density. A theoretical interpretation of k is given by Kivelson et al (206) in terms of anisotropic intermolecular potential energy. The parameter k gives the ratio of the intermolecular torques on the solute molecule to the intermolecular forces on the solvent molecules. The intermolecular potential energy determines both the torque and forces but only its anisotropic part gives rise to the torques. For relatively symmetric molecules, weak intermolecular torques result in small values of k, which seems to be in agreement with the Steele (92) conclusions, i.e. free rotation of the molecules can be associated with small values of k in the Kivelson expression of τ_r

$$\tau_r = 4\pi a^3 \eta\, k/3KT \qquad (5.5)$$

Therefore, the effective viscosity, η_k, is reduced ($k \ll 1$), which can be interpreted as a weak coupling between the molecule and its environment.

Hu and Zwanzig (207) have calculated the rotational friction coefficient for ellipsoids with "slip" boundary conditions and "stick" boundary conditions. Bauer et al (208) (see chapter three) have found a linear relation between the correlation time and the viscosity as shown by equation (5.6)

$$\tau_r = c\eta + \tau_o \qquad (5.6)$$

τ_o is the intercept at zero viscosity and is found to be the "free rotor" reorientation time and C is the viscosity dependence (slope), which represents the degree of translation-rotation coupling. They have found that the slope C is less than that predicted by the Stokes-Einstein equation that is derived from hydrodynamics using "stick" boundary conditions, i.e., $C_{S.E.} = 4/3\pi a^3/KT$ using a factor given by Hu and Zwanzig (207) to predict the coupling for the hydrodynamic slip limits. The results for carbon tetrachloride solutions with solute of similar molecule size, were that the experimental slope C and the predicted C_{slip} were within 50% for nearly all the solutions studied.

Recently, Jonas et al [209] have found for studies of SF_6 using Raman techniques that at low densities the reorientational correlation time deviates strongly from linearity with (η /T). According to them, the extrapolation of τ to zero viscosity as $\tau_{F.R.} = \tau_o$ is no longer valid.

The theory of Hill [95] takes a different approach towards the evaluation of the correlation time. This is based on the same model of a liquid as Andrade's theory of viscosity [210]. For this the molecules of one layer in their vibrations are considered to come into contact with those of an adjacent layer. During this contact they will, in general, enter into a temporary union which lasts long enough for the molecules to acquire a common velocity of translation but because the duration of the union is shorter than a period of vibration there is no possibility of association. The Hill theory [95] has shown that good agreement with dielectric relaxation times could be predicted through the use of the so-called mutual viscosity between the solvent and solute. The mutual viscosity η_{AB} is deduced from the solution viscosity, which is supossed to be given by

$$\eta_m = (f_A^2\ \eta_A\ \sigma_A/\ \sigma_m) + (f_B^2\ \eta_B\ \sigma_B/\ \sigma_m) + 2 f_A f_B\ \sigma_{AB}/\ \sigma_m\ \eta_{AB} \qquad (5.7)$$

for a binary mixture. Here f_A and f_B are the mole fractions of A and B, respectively. σ_A and σ_B are the average distances between molecules in the liquids A and

B, and σ_{AB} is the average distance between molecules in the mixture. Using a model based on mutual viscosity, Hill deduced that the rotational correlation time of molecules of type B in solution with molecules of type A, may be represented by

$$\tau = (1/2KT)\left\{6f_A\,\eta_{AB}\,\sigma_{AB}\,K_{AB}^2+3f_B(3-\sqrt{2})\,\eta_B\,\sigma_B\,K_B^2\right\} \quad (5.8)$$

where

$$K_{AB}^2 = [(I_{AB}\,I_B)/(I_{AB}+I_B)]\,[(m_A+m_B)/m_A\,m_B] \quad (5.9)$$

and I_A and I_B are moments of inertia of A and B about their mass centres; I_{AB} is the moment of inertia of A about the centre of B during collision, and K_B is the radius of gyration of a B-type molecule. The expression for τ_r in nmr terms for dilute solutions is

$$\tau_{rHill} = K_{AB}^2\;\sigma_{AB}\;\eta_{AB}\;/\;KT \quad (5.10)$$

In equation (5.7) the intermolecular distances σ_A, σ_B are calculated (211)(212) using

$$N\;\sigma_A^3 = V_A = M_A/\rho_A \quad (5.11)$$

where V_A is the molar volume, M the molecular weight and ρ the density.

In a different version of the Hill theory, Kivelson et al [213] have used a similar expression for the solution viscosity. They have calculated the correlation time in the limit of low solute concentration for molecules of similar sizes with the result that τ_B (solute) depends linearly on η with a slope that is independent of concentration and with a concentration-dependent intercept at $\eta=0$. This agrees qualitatively with the results of Bauer et al [155] expressed in equation (5.6). Kivelson's equations include the constant k instead of mutual viscosities η_{AB}.

Mitchell and Eisner [81] have calculated the correlation time of several molecules in CCl_4 and CS_2 using three different theories. They found that the Hill theory gave the best agreement with the experimental values. The behaviour of the proton relaxation time T_1 as a function of the concentration was also investigated and interpreted using the Hill diffusion constant

$$D = KT/6 \left(\eta_{AB} \sigma_{AB} f_A + \eta_B \sigma_B f_B \right) \qquad (5.12)$$

in the equation (5.13)

$$1/T_1 = A \tau_r + BV/D \qquad (5.13)$$

where V is the volume fraction of solute and A,B are constants. This approach gave a good explanation of the experimental data.

It can be concluded that the Hill approach has advantages over other models in the evaluation of the rotational correlation time. In particular, it has advantages over the Kivelson method, because the evaluation of this k constant requires the use of different (non-nmr) techniques, and this makes the experimental approach more complex.

In the remainder of this chapter, the applicability of the Hill theory to the calculation of correlation times and the relaxation time T_1 in general, will be examined.

5.2 Evaluation of the Mutual Viscosity Term and the Diffusion Coefficient.

The correlation time and the diffusion coefficient are related to the mutual viscosity term through equations, (5.7), (5.12) and (5.10). The data recorded by Coupland (174) will be used to calculate these parameters for benzene-CCl_4 amd cyclohexane-CCl_4 solutions in order to illustrate the procedure and provide some comparison with Mitchell-Eisner (81) calculations for the same compounds (Table 5.9). From equation (5.11) we obtained σ for the components and σm from the combination of mole contributions of the components σ_A, σ_B, i.e.

$$(N_A + N_B)\,\sigma m = \frac{M_A}{\rho} + \frac{M_B}{\rho} \qquad (5.14)$$

Tables (5.1) and (5.2) show that the mutual viscosity is nearly a constant. Consequently, the average value can be identified as a molecular characteristic of the encounter of the molecule A with B. The average value of $\eta_{AB}\ \sigma_{AB}$ in benzene-CCl_4 is 3.5 C.PÅ which is close to the Mitchell-Eisner value [81] 3.8 C.PÅ. For cyclohexane-CCl_4 we obtain the average 4.1 C.PÅ which is close to 4.4 C.PÅ deduced from Mitchell-Eisner.

The diffusion coefficients can be estimated from tables (5.1) and (5.2). The comparison of the Hill and the Stokes-Einstein diffusion coefficient in tables (5.3) and (5.4) is based for benzene on a being equal to 2.45 Å and for cyclohexane equal to 3.51 Å in equation (5.15)

$$D = KT / 6\pi\eta a \qquad (5.15)$$

It is clear from these results that the Hill values are about twice as large as the Stokes-Einstein values. Obviously, this could have a significant effect on the evaluation of relaxation times.

Mitchell and Eisner [81] have calculated the relaxation times in benzene- CCl_4 and cyclohexane- CCl_4 systems by assuming A and B as constant in equation (5.13) and showed that the Hill theory is adequate. Their data have been used here to check the results from T_1 of C_6H_6 at a volume fraction of 0.2 of benzene in CCl_4. The values of A and B were calculated from equation (5.13) at V=0 and

Table (5.1)

The variation of mutual viscosity with mole fraction for C_6H_6 in CCl_4

ρ (g/cm^3)	X_ϕ	η (c.p.)	σ_m(Å)	$\eta_{AB}\ \sigma_{AB}$(CPÅ)
1.572	0	0.810	5.457	---
1.501	0.1	0.778	5.445	3.483
1.431	0.2	0.749	5.439	3.527
1.360	0.3	0.720	5.429	3.529
1.289	0.4	0.693	5.418	3.541
1.219	0.5	0.660	5.405	3.476
1.148	0.6	0.640	5.391	3.542
1.077	0.7	0.614	5.375	3.532
1.006	0.8	0.589	5.357	3.515
0.936	0.9	0.564	5.335	3.438
0.868	1	0.546	5.304	---

Table (5.2)

The variation of mutual viscosity with mole fraction for C_6H_{12} in CCl_4

ρ g / cm^3	X_{cy}	η(C.P.)	σ_m(Å)	$\eta_{AB}\ \sigma_{AB}$(CPÅ)
1.572	0	0.810	5.457	---
1.461	0.1	0.790	5.506	4.200
1.362	0.2	0.777	5.546	4.066
1.269	0.3	0.765	5.583	4.053
1.181	0.4	0.763	5.617	4.090
1.100	0.5	0.761	5.643	4.123
1.022	0.6	0.761	5.668	4.115
0.951	0.7	0.765	5.683	4.099
0.885	0.8	0.771	5.690	4.079
0.823	0.9	0.779	5.688	3.980
0.768	1	0.790	5.667	---

V=1. It emerged that the calculated value of T_1 is 41.44 sec, which is similar to the experimental value of 38.6 sec. For the same system, but using the Coupland data (174) and tables (5.1) (5.3) we have calculated T_{1Hill}, for V=0.178 as 34.17 sec in agreement with T_{1exp}=35.65 sec. These results indicate that the Hill theory is well founded. Nevertheless, it is considered necessary to evaluate ab initio the intramolecular contribution to T_1 separately, because this is believed to be the key point in the understanding of relaxation processes. In particular, if a good intramolecular value can be predicted, it could be used to separate the intra and intermolecular contributions embodied in the experimental T_1 value.

5.3 Comparison of Hill and B.P.P. Theory on the Calculation of τ_r

Correlation time can be evaluated using several theories. However, two of them have been selected for present purposes, viz the Hill theory and the B.P.P. theory which use the Debye approach in the calculation of τ_r.

Mitchell and Eisner (81) have compared experimental and theoretical values of τ_r for benzene, cyclohexane and chlorobenzene diluted with CCl_4 and CS_2. The data are presented in Table (5.5). The calculation of τ_r from equation (5.10) requires a knowledge of the moment of

Table (5.3)

Comparison of the diffusion constant of C_6H_6 in CCl_4 at several concentrations using the Hill equation (5.12) and the Stokes-Einstein equation (5.15)

X_ϕ	$D_{Hill} \times 10^5 cm^2 sec^{-1}$	$D_{S.E} \times 10^5 cm^2 sec^{-1}$
0.1	2.05	1.175
0.2	2.07	1.22
0.3	2.107	1.27
0.4	2.14	1.32

Table (5.4)

Comparison of the diffusion constant of C_6H_{12} in CCl_4 at several concentrations using the Hill equation (5.12) and the Stokes-Einstein equation (5.15)

X_{cy}	$D_{Hill} \times 10^5 cm^2 sec^{-1}$	$D.S.E \times 10^5 cm^2 sec^{-1}$
0.1	1.66	0.807
0.2	1.69	0.82
0.3	1.68	0.83
0.4	1.66	0.835

inertia of the molecules to evaluate the term K^2_{AB}. We have used atomic models to calculate the components of the moment of inertia about the symmetry axis and other perpendicular axes. The interatomic distances and angles were taken from the Handbook of Chemistry and Physics.[218] The moment of inertia are given in table (5.6) which also contains the average moment of inertia used by Mitchell-Eisner, estimated from their approximate Hill equation (5.16) and the values of τ given in Table (5.5)

$$\tau_{approx} = 2I\eta a/\mu KT \qquad (5.16)$$

where a represents the molecular radii.

The results in table (5.5) show that the Hill theory gives better predictions of the correlation time than the other theories. However, we will test these theories by using them to compare both extremes x-y in figure (5.1) where x,y are the relaxation times for the solute at infinite dilution in solvents that can provide no intermolecular contribution to the relaxation processes.

From equation (5.13) at V=0 and equation (5.10) we obtain for two different solvents A and A'

$$y = x \frac{i_{AB}\ \eta_{AB}\ \sigma_{AB}\ \mu_{A'B}}{i_{A'B}\ \eta_{A'B}\ \sigma_{A'B}\ \mu_{AB}} \qquad (5.17)$$

where $i_{AB} = \frac{IAB\ IB}{I_{AB}+I_B}$ and μ is the reduced mass.

Table 5.5

Comparison of experimental correlation times with theoretical values calculated from different models.

substance/solvent		$\tau_{exp} \times 10^{12}$ (sec)	Hill	Debye	Micro viscosity	Hill approx	$T_{1r} \times 10^3$ sec^{-1}
	CS_2	1.1	1.3	6.8	2.8	1.5	45.4
C_6H_{12}							
	CCl_4	1.5	2.4	17	2.9	2.9	61.7
	CS_2	1.5	1.1	4.1	1.4	1.2	10.98
C_6H_6							
	CCl_4	2.3	1.9	10	0.82	2.3	16.6
	CS_2	2.2	2.6	5	2.1	2.5	12.5
C_6H_5Cl							
	CCl_4	3.8	3.3	13	2.1	4.5	21.2

Table (5.6)

Calculated moments of inertia of the compounds studied.

10^{40} g cm^2	Ix	Iy	Iz	Iav	I M.E.
C_6H_6	147.6	147.6	295.3	196.8	206
CS_2	626.2	626.2	0	417.5	--
CCl_4	487.6	487.6	487.6	487.6	--
C_6H_{12}	198.4	198.4	314	236.9	215
C_6H_5Cl	525	146.8	716	462.6	407

The same comparison can be made using the B.P.P. theory and the Debye expression $\tau_r = 4/3\,\pi\,\eta\,a^3/KT$. From equation (5.13) we obtain at V=0

$$y = x\,\frac{\eta_A}{\eta_{A'}} \qquad (5.18)$$

Table (5.7) gives the calculated values Y_{CAL} from equations (5.17) and (5.18) and the experimental relaxation times at V=0. The values of Y_{exp} are taken from table (5.5).

Analysis of table (5.7) indicates that it is possible to predict the infinite dilution values of T_1 y in Figure (5.1) if we know the corresponding value of x by using the Hill theory. However, it is important to point out that the approach only leads to limited success because of a residual error in the preditions that increases with the mass of the solute. The predictions of the B.P.P. theory are far less satisfactory and are far away from the expected values. This indicates that correlation time calculations are best done using the Hill theory with some as yet unidentified modification to correct for the effect of the mass of the solute. One suggestion to overcome this problem is to use a suitable average for τ_r in such a way that a weighing of the mass distribution in the molecule is achieved. Also, it may be possible to introduce some correction to account for electric forces which constrain the molecule to rotate about certain axes.

Table (5.7)

Comparison of relative intramolecular relaxation times predicted by the Hill theory and the B.P.P. theory, using equations (5.17) and (5.18)

m(g)	system	$Y_{exp} \times 10^3 sec^{-1}$	$Y_{cal} \times 10^3 sec^{-1}$ (Hill)	$Y_{cal} \times 10^3$(BPP)sec^{-1} (B.P.P.)	$\Delta Y/Y_{exp}$% (Hill)	$\Delta Y/ Y_{exp}$% (B.P.P.)
78	C_6H_6	10.98	9.6	6.6	12.5	39.9
84.16	C_6H_{12}	45.4	33.4	18.05	26.4	60.2
112.45	C_6H_5Cl	12.5	16.8	4.97	34.4	60.2

Table (5.8)

Physical characteristics of the compounds studied at 27°C

substance	η(c.p)	σ Å	$\alpha_x \ 10^{23} \ cm^3$	$\alpha_y \ 10^{23} \ cm^3$	$\alpha_z \ 10^{23} \ cm^3$
C_6H_6	0.58	4.9	1.1	1.1	0.73
C_6H_{12}	0.87	5.67	1.1	1.1	0.97
$C6H_5Cl$	0.74	5.54	1.24	1.47	0.82
CCl_4	0.88	--	1.02	1.02	1.02
CS_2	0.35	--	1.51	0.55	0.55

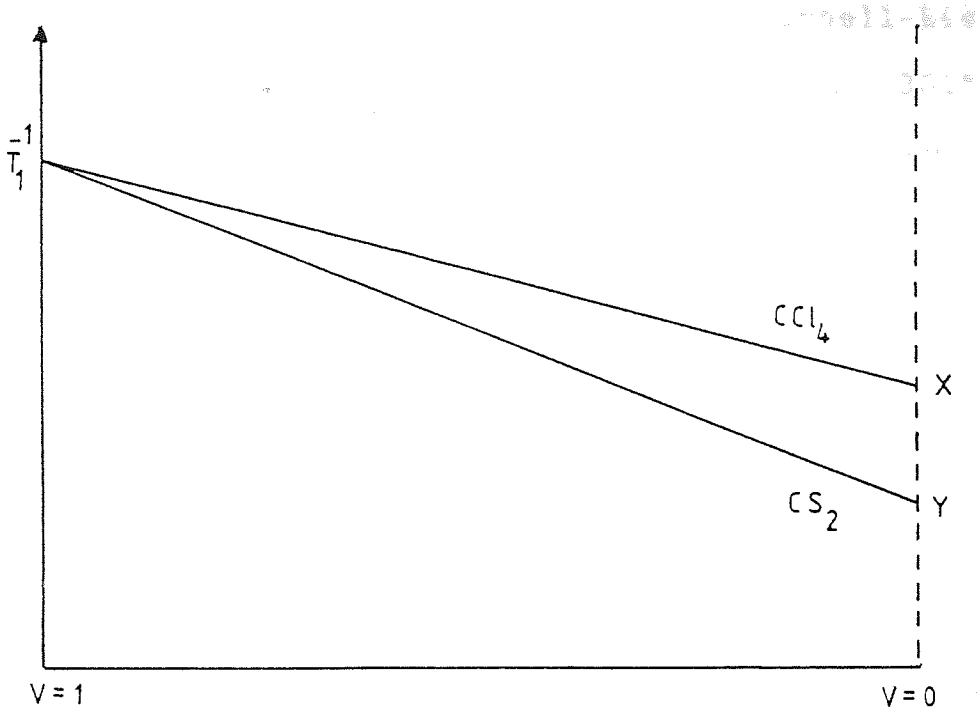

Figure 5.1 Representation of the variation of T_1 with the volume fraction eg. benzene diluted in CCl_4 or CS_2

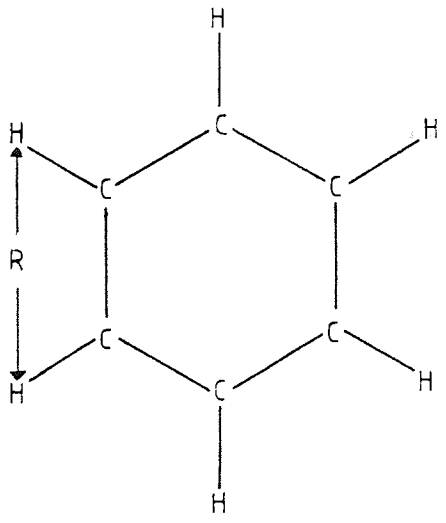

Figure 5.2 Representation of the benzene molecule.

5.4 Use of the Hill Theory in the calculation of T_1.

The data analysed here are from Mitchell-Eisner (81) experiments which were carried out at 301°K. The relaxation times have been calculated using equation (5.13) with A and B assumed to be constant. The basic characteristics of the substances are presented in tables (5.6) and (5.8). The B value can be calculated by using V=1 in equation (5.13). Tables (5.9) and (5.10) give the parameters used to evaluate T_1^{-1} through equation (5.13). There, the sub-index (r) means rotational and (t) translational; (a) refers to Mitchell-Eisner values and (b) to the results in this work. In general, the results of kind (a) are very similar to those of the kind (b) and this indicates that the details of the Mitchell-Eisner approach have been correctly implemented. The differences between the results of type (a) and (b) are due to the different molecular parameters used in the calculation which often happens when there are independent sources of information. It is believed that the procedures used in these calculations will lead to a reasonable representation of the relaxation times in solutions.

Because the molecule motions are unlikely to be isotropic, it was decided to reflect the anisotropic motion in a suitable weight when obtaining the average correlation time. Making the assumption that the intermolecular forces could influence this and that these

Table (5.9)

Parameters used for T_1 calculation at infinite dilution (V=0)

		$\eta_{AB}\sigma_{AB}(a)$ (CPÅ)	T_{1exp}^{-1} ($x10^3 sec^{-1}$)	$\tau_r(a)$ ($x10^{12}$sec)	$\tau_r(b)$ ($x10^{12}$sec)	$D(b)$ ($x10^5$)	$A_{exp(a)}$ ($x10^{-9}$)	$A_{exp(b)}$ (10^{-9})	$A_{exp(\alpha)}$ (10^{-9})	$\tau_r(\alpha)$ 10^{12}sec)
	CS_2	1.8	10.98	1.1	1.27	3.8				1.2
C_6H_6							9.34	8.37	8.9	
	CCl_4	3.8	16.6	1.9	2.05	1.8				1.9
	CS_2	2.0	45.4	1.3	1.64	3.45				1.61
C_6H_{12}							30.32	25.2	25.5	
	CCl_4	4.4	61.1	2.4	2.7	1.57				2.7
	CS_2	2.6	12.5	2.6	3.47	2.6				3.1
C_6H_5Cl							5.6	4.6	4.8	
	CCl_4	4.3	21.2	3.3	4.26	1.6				3.8

A(sec^{-2}); D($cm\ sec^{-1}$)

Table (5.10)

Parameters used for T_1 calculation in neat substances (V=1)

	$T_{1(a)exp}^{-1}$ ($x10^3 sec^{-1}$)	$T_{1r(a)}^{-1}$ ($x10^3 sec^{-1}$)	$T_{1t(a)}^{-1}$ ($x10^3 sec^{-1}$)	$\tau_r(b)$ ($x10^{12}$sec)	$D(b)$ ($x10^5$)	$T_{1r(b)}^{-1}$ ($x10^3 sec^{-1}$)	$T_{1t(b)}^{-1}$ ($x10^3 sec^{-1}$)	$B(a)$ ($x10^8$)	$B(b)$ ($x10^8$)
C_6H_6	49	19	30	2.0	2.4	16.4	32.6	72.6	78.9
C_6H_{12}	139	102	37	3.0	1.4	96.9	42	51.8	58.9
C_6H_5Cl	55	23	32	3.4	1.7	19.5	35.5	54.4	60.3

B($cm^2 sec-2$)

are related to molecular polarizability, the latter was used to weigh on the effective moment of inertia through

$$\bar{I} = \frac{1}{3\,\bar{\alpha}} \sum I_i\,\alpha_i \qquad (5.19)$$

This value $\bar{I}$ was introduced in K^2_{AB} to get the effective correlation time. The influence of this type of correction is very small for benzene and cyclohexane, but it is about 10% for chlorobenzene which seems to indicate a real contribution to the description of molecular motion. The term K^2_{AB} was averaged with respect ot the three moments of inertia by using the expression

$$\bar{K}^2_{AB} = \frac{1}{3\,\mu} \sum_{i=1}^{3} \frac{I_{AB}\, I\, B_i}{I_{AB}+IB_i}$$ but the comparison of this value with K^2_{AB} gives a difference of less than 3%.

5.5 Study of the Theoretical Value of A, its Calculation and the convenience of Averaging τ_r

The value of A can be obtained from Woessner's equation [79] (5.20)

$$T_1^{-1} = \frac{3}{2}\,\hbar^2\,\gamma_i^4 \sum r_{ij}^{-6}\,\tau_r \qquad (5.20)$$

thus, $T_1^{-1} = A\,\tau_r$

where

$$A = \frac{3}{2}\,\gamma_i^4\,\hbar^2 \sum r_{ij}^{-6} \qquad (5.21)$$

A, can therefore be calculated using equation (5.21). This has been done for benzene, cyclohexane and chlorobenzene. In the case of cyclohexane, the distances r_{ij} between its 12 protons used in the calculations were obtained from atomic models, assuming the "chair" configuration. Because is known that the axial protons are equivalent and the equatorial protons are themselves also equivalent this can be used as an useful assumption when estimating r_{ij}.

For benzene and chlorobenzene the calculation is simpler, e.g. in benzene according to figure (5.2) the A value is

$$A=\frac{3}{2}\gamma_i^4\hbar^2\left[2R^{-6}+(2R)^{-6}+2(\sqrt{3}R)^{-6}\right] \qquad (5.22)$$

thus $A=7.57\times10^9$ sec^{-2} when R is taken in Å Table (5.11) shows that the Mitchell-Eisner values A(a) are lower than those calculated by the procedure described above A(b). This is because their value of A represents an approximation because they only took into account the nearest neighbour protons (ortho). Present calculations with the same base almost coincide with M.E. values (see A' in table 5.11).

The experimental correlation time τ_{exp} and the experimental A value A_{exp} in Table (5.12) are calculated from the theoretical A and the calculated τ_r respectively.

Thus,

$$\tau_{rexp} = T_{1r}^{-1} / Acal \qquad (5.23)$$

and

$$A_{exp} = T_{1r}^{-1} / \tau_{rcal} \qquad (5.24)$$

where T_{1r}^{-1} is taken from table (5.9).

It can be seen that our results (b) for benzene in table (5.12) are reasonably consistent. For cyclohexane and chlorobenzene the calculated correlation times $\tau_r(a)$ are in general closer to their experimental values $\tau_{rexp}(a)$ than those values in $\tau_r(b)$, $\tau_{rexp}(b)$. This should be, because of the different values of the moment of inertia and the averaging procedure used in each case.

The value of A_{exp} (b) for benzene indicated in table 5.12 is in good agreement with the theoretical prediction A(b), which gives some confidence in the method used. However, for cyclohexane and chlorobenzene the A_{exp} values are smaller than the calculated A(b). This differences may be due to the calculated correlation time τ_r calc. or the method used to evaluate A(b), which means that some other approach has to be used.

A further analysis for cyclohexane shows that, if we assumed that the molecular motion is restricted to be around the x axis, where Ix=198x10^{-40} g. cm^2 (see table 5.6), the correlation time τ_r decreases from 1.64 to

Table (5.11)

A value in C_6H_6, C_6H_5Cl and C_6H_{12}

$Ax10^{-9}sec^{-2}$	C_6H_6	C_6H_5Cl	C_6H_{12}
A (b)	7.57	6.06	45.68
A (a)	7.22	5.60	41.13
A '	7.23	5.79	43.60

(a) refers to Mitchell-Eisner results

(b) refers to our calculation

A' is an approximate value for closest protons.

Table (5.12)

Comparison of correlation times and A values from Mitchell-Eisner data with those obtained in this work.

	$\tau_{exp(a)}$	$\tau_{exp(b)}$	$\tau_{r(a)}$	$\tau_{r(b)}$	Aexp(a)	Aexp(b)	A(b)
	$x10^{12}sec$		$x10^{12}sec$		$x10^{-9}sec^{-2}$		
C_6H_6 CS2	1.5	1.35	1.1	1.27	9.3	8.37	7.57
C_6H_6 CCl_4	2.3	2.04	1.9	2.05			
C_6H_6 CS_2	1.1	0.99	1.3	1.64	30.3	25.2	45.7
$C_6H_{12}CCl_4$	1.5	1.35	2.4	2.7			
$C_6H_5ClCS_2$	2.2	1.9	2.6	3.47	5.61	4.6	6.06
$C_6H_5ClCCl_4$	3.8	3.3	3.3	4.26			

(a) refer to Mitchell-Eisner results

(b) refer to our calculation

1.37 psec in CS_2 and from 2.7 to 2.25 psec. in CCl_4. Therefore, the average of A_{exp} is 30.25×10^9 sec^{-2} which is closer to the theoretical value A(b). Also, the geometrical distribution of the protons and the internal molecular motion in cyclohexane seems to be important e.g. if we consider only the two closest protons, we obtain from equation (5.21) $A=29.68 \times 10^9$ sec^{-2} which is higher than the average of the reported values A_{exp} (a), A_{exp} (b) in table 5.12 which suggests that the A value is sensitive to the internal movement in the molecule. It is suggested therefore, that the correlation time has to be expressed as a combination of terms similar to those calculated by Woessner (90), who has found reduced values for τ_r due to internal molecular motion. Consequently, it is concluded that the rotational (intramolecular) relaxation time has to be expressed as a combination of terms e.g. $T_{1\ rot}^{-1} = \bar{A}\ \bar{\tau}_r$ or $T_{1\ rot}^{-1} = \sum_{i=1}^{3} A_i\ \tau_i$, where i refers to the symmetry axes of the molecule.

5.6 CONCLUSIONS

The Hill theory adapted by Mitchell and Eisner for the study of relaxation times, has been used to analyze the intramolecular relaxation time of protons in C_6H_6, C_6H_{12} and C_6H_5Cl at infinite dilution in CS_2 and CCl_4. It has been shown that the Hill theory produces a better agreement with the experimental values than the B.P.P. theory. However, there is some indication of a dependence of the calculated correlation time on the mass

of the solute. In the case of the Hill treatment of benzene the accuracy of the prediction is 12% but for cyclohexane and chlorobenzene it is about 30% and so well outside experimental error. In order to improve matters it appears that the correlation time can profitably be based on an average which involves the moment of inertia and the polarizability of the molecule. These factors which anisotropically weigh molecular motion seem to play an important role in the description of molecular rotation.

The use of the equation $T_1^{-1} = A\,\tau_r + B\,V/D$ assuming A and B to be constants seems to be an useful representation of the relaxation times. The constant A and the correlation time τ_r for cyclohexane appear sensitive to the internal motion of the molecule and this suggests the necessity of expressing the intramolecular relaxation time as a combination of average values of A and τr.

CHAPTER SIX

Proton Spin Lattice Relaxation Studies of Mesitylene in Cyclohexane - TMS Mixtures

6.1 Introduction

In a recent study of the gas to solution chemical shift Homer and Percival [51] have indentified a new contribution to the Van der Waals screening constant σ_w, which is called the "Buffeting" interaction. This interaction arises from anisotropic intermolecular collisions between solvent and solute molecules; some of the aspects of the relevant theory, were detailed at the end of chapter one. Essentially these workers have shown that when continuum approaches to the description of σ_w are used, it is necessary to add the buffeting contribution to the classical reaction field component in order to fully characterize σ_w; in some cases these two contributions have the same magnitude [51]. The introduction of the buffeting effect makes it possible to obtain a good representation of certain molecular non-n.m.r. properties, for example the Van der Waals a values and heats of vapourization. It would not appear unreasonable therefore for it to have some influence on T_1 also.

The contribution of the "buffeting" effect to intermolecular forces can be considered to arise through a square electric field E_B^2 just as is the case when only the reaction field is taken into account (214). The magnitude of this field for the interaction between two kinds of molecules (solute-solvent) is governed by two parameters β ,ξ that characterize the anisotropy of molecular collisions enforced by local steric constants. One purpose of the present work is to investigate whether the buffeting interaction mechanism can provide a contribution to spin-lattice relaxation times. It would be imagined that if there is such an effect it would be most marked for the peripheral atoms of a solute at low concentration in some suitable solvent. Consequently, mesitylene with two sterically different proton sites, has been selected for study in cyclohexane/TMS mixtures. Because it cannot be predicted whether buffeting will operate via modulation of the intra- or intermolecular relaxation contribution it will be desirable to analyse the observed relaxation time in terms of these two components.

The relaxation time T_1 is usually described according to the Bloembergen - Purcell - Pound theory (B.P.P.), for which the Debye rotational correlation time (τ_D) and the Stokes - Einstein translational correlation time ($\tau_{S.E.}$) are employed to describe the intramolecular and intermolecular contribution to T_1. The viability of this approach has been questioned in chapter 5.

The fact that so many authors disagree over the most suitable model to explain relaxation times suggests in reality that as yet there is no absolutely satisfactory approach. This may be due to inadequacies in the established approaches or to a general failure, so far, to recognize some effect, such as buffeting, that must be incorporated into whatever basic description of T_1 is employed. From chapter 5 it is evident that even for relatively simple systems the discrepancy between theoretical and practical values of T_1 can be quite large. When more complex than tertiary mixtures are considered, it is likely that the discrepancies could become worse. Consequently, despite preferences for particular basic approaches it would appear reasonable to place initial reliance only on equations (6.1) and (6.2) in which T_1 is expressed as

$$T_1^{-1} = T_1^{-1}\ \text{intra} + T_1^{-1}\ \text{inter} \qquad (6.1)$$

which can be approximated to

$$T_1^{-1} = A\,\tau_r + L\,N\,\tau_t \qquad (6.2)$$

where τ_r, τ_t are the rotational and translational correlations times; A, L are considered constants (81) and N is the proton density.

Consequently when characterizing a binary or tertiary liquid system, it is important to know, the mole fraction of its components, the proton density (N) and the correlation times τ_r, τ_t which as indicated in chapter 5 are related to some sort of mutual viscosity or molecular interaction.

As indicated above, it is necessary to separate the intramolecular term (A τ_r) and the intermolecular term (LN τ_t) from the experimental T_1. This can be done through the use of appropiately deuterated compounds. However practical this method may be, because of the small variation of physical constants (viscosity, density) for deuterated and protonated analogues it is very costly and in the case of some molecules, it would be necessary to work out a method to deuterate them. For the present studies of mesitylene in solution with cyclohexane and TMS, we will use the relaxation time T_1 of mesitylene protons at infinite dilution in CCl_4 as the intramolecular relaxation time, which after adequate correction will represent the intramolecular contribution to T_1 in the mixture.

6.2 Experimental Methods and Results

The spin-lattice relaxation time of the aromatic or aryl (ring) protons and the methyl protons of mesitylene diluted with CCl_4 and cyclohexane - TMS mixtures have been measured. These samples were prepared using the

techniques described in chapter 4, the samples were deoxygenated and then were sealed in n.m.r. tubes under a vacuum of 10^{-3} torr.

The relaxation times T_1 were measured at 303°K with a varian HA100D spectrometer operating at 100MHz. Both adiabatic rapid passage with sampling (ARPS) and progressive saturation (p.s.) techniques were used. These methods were described in chapter 4.

Table (6.1) shows the composition of the mesitylene/CCl_4 samples studied; the mole fraction of mesitylene varies from $X_A \approx 0.05$ to $X_A \approx 0.6$. The same table (6.1) gives the relaxation times measured by the A.R.P.S method together with the correlation coefficient for each set of experimental measurements. These coefficients are all above 0.99 which indicates how good the linearity is in the appropriate semilog. plot of the change of magnetization versus time.

In table (6.2) the values of the relaxation times T_1 measured by the method of progressive saturation are shown. It can be seen that there is a general agreement of these results with the A.R.P.S. results in table (6.1). However, it should be noticed that the progressive saturation values have lower correlation coefficients.

Table 6.1

The spin lattice relaxation times of the ring and methyl protons of mesitylene in CCl_4 using the ARPS technique.

X_A	Correlation Coefficient		T_1 sec	
	ring	methyl	ring	methyl
0.052	0.995	0.997	26.33	6.66
0.057	0.998	0.999	23.7	6.5
0.129	0.998	0.999	22.4	6.3
0.199	0.997	0.999	21.4	6.4
0.246	0.997	0.999	19.3	6.2
0.368	0.997	0.999	16.8	6.1
0.397	0.997	0.999	17.2	5.9
0.451	0.999	0.999	16.5	6.1
0.505	0.999	0.999	15.2	5.6
0.545	0.999	0.999	15.3	5.9
0.608	0.999	0.999	15.0	6.0

Table 6.2

The spin lattice relaxation times of the ring and methyl protons of mesitylene in CCl_4 using the progressive saturation technique.

X_A	Correlation Coefficient		T_1 sec	
	ring	methyl	ring	methyl
0.052	0.997	0.988	27.15	8.07
0.057	0.999	0.985	23.82	6.53
0.129	0.998	0.991	26.3	7.2
0.199	0.999	0.994	20.2	6.0
0.246	0.999	0.999	20.4	6.4
0.397	0.999	0.997	18.1	6.5
0.451	0.992	0.997	14.6	7.5
0.505	0.990	0.998	15.3	6.3
0.545	0.999	0.986	16.4	8.5
0.608	0.999	0.998	16.5	6.2

The dependence of the relaxation times T_1 on the mole fraction X_A is presented in figure (6.1) and figure (6.2) for the A.R.P.S. method and p.s. method repectively. The scattering of the experimental points around the straight line in the p. saturation method is due to the fluctuating values of the correlation coefficients. However, when only the highest correlation coefficients are considered the T_1^{-1} plots define a straight line.

From figure (6.1) it can be seen that the extrapolation of T_1^{-1} to X_A=1 gives the relaxation time in pure mesitylene, which is similar to the literature values reported in table (6.3). This overall agreement validates our experimental results.

Table (6.3)

spin-lattice relaxation times for neat mesitylene.

T_1ring (sec)	$T_1(CH_3)$ sec	reference
10	5	171
13.1	6.1	169
11.36	5.24	this work

The variation of the spin lattice relaxation time of CH_3 with X_A as shown in figure (6.1), indicates that the intramolecular interaction in CH_3 is very efficient because of the proximity of several protons. It dominates the relaxation mechanisms of T_1, making the effect of the intermolecular interaction less obvious.

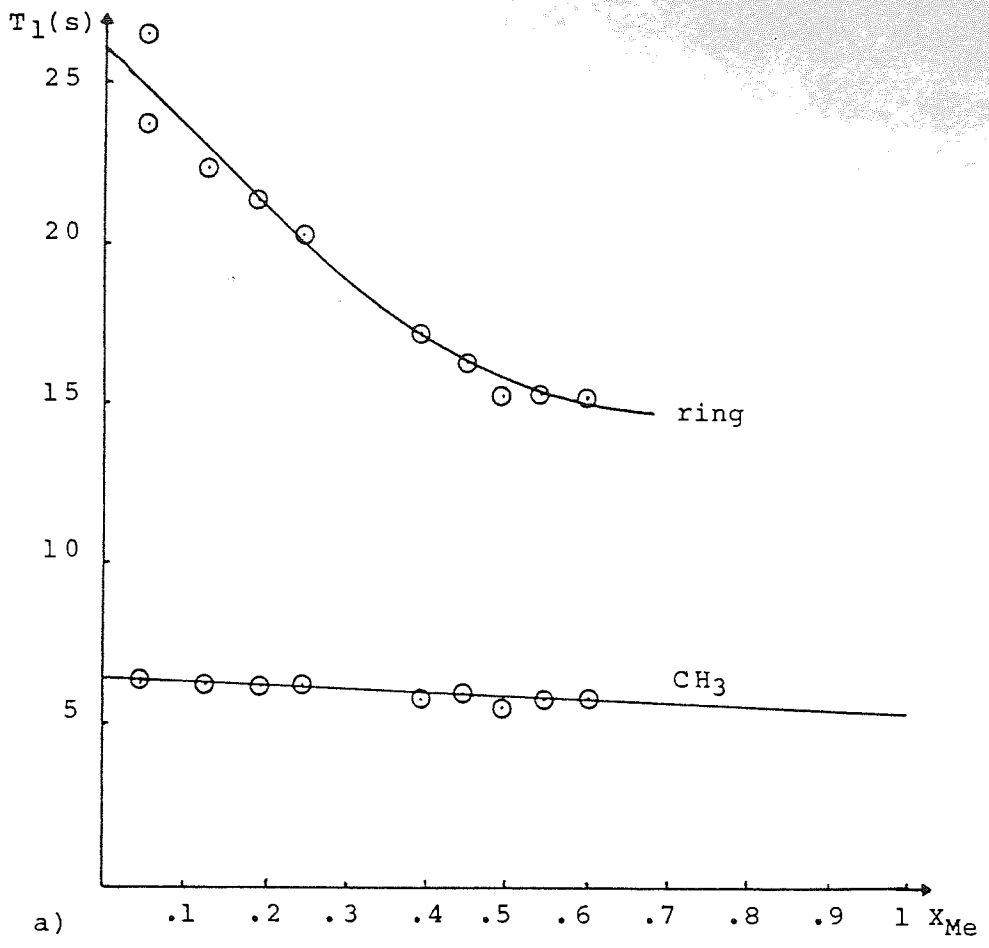

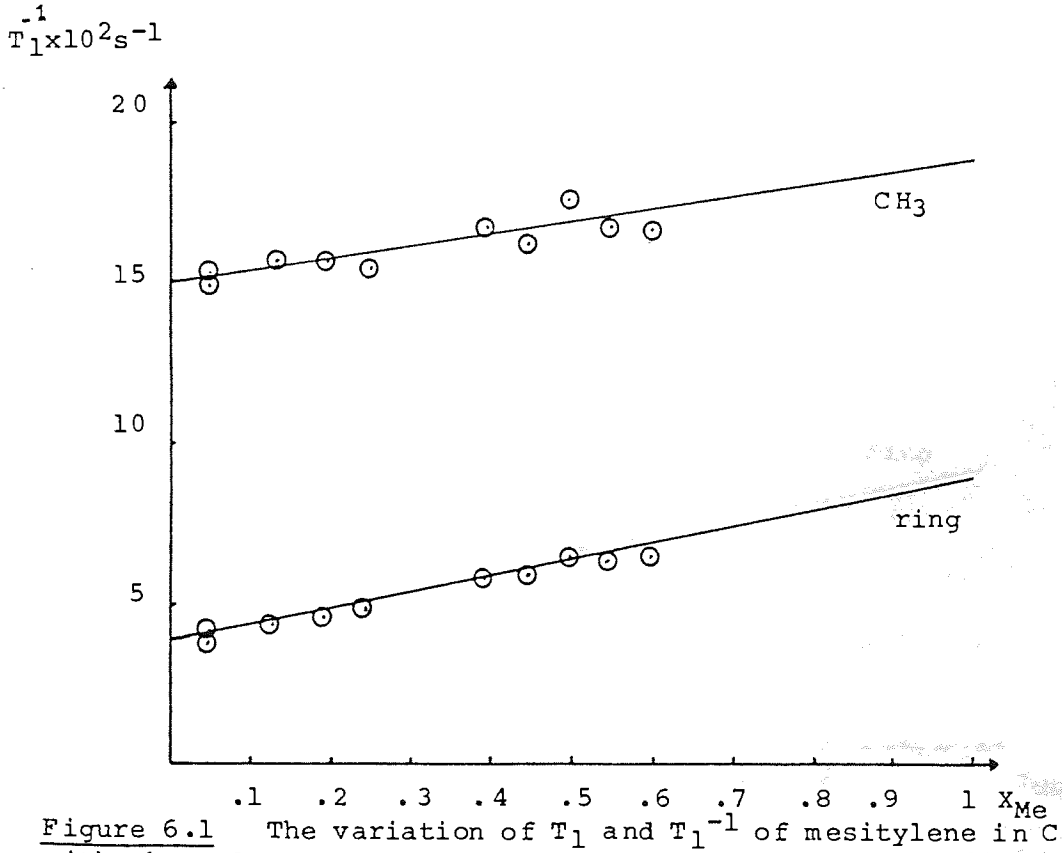

Figure 6.1 The variation of T_1 and T_1^{-1} of mesitylene in CCl_4, with the mole fraction of mesitylene (ARPS method)
a) T_1(s)
b) T_1^{-1} sec^{-1}

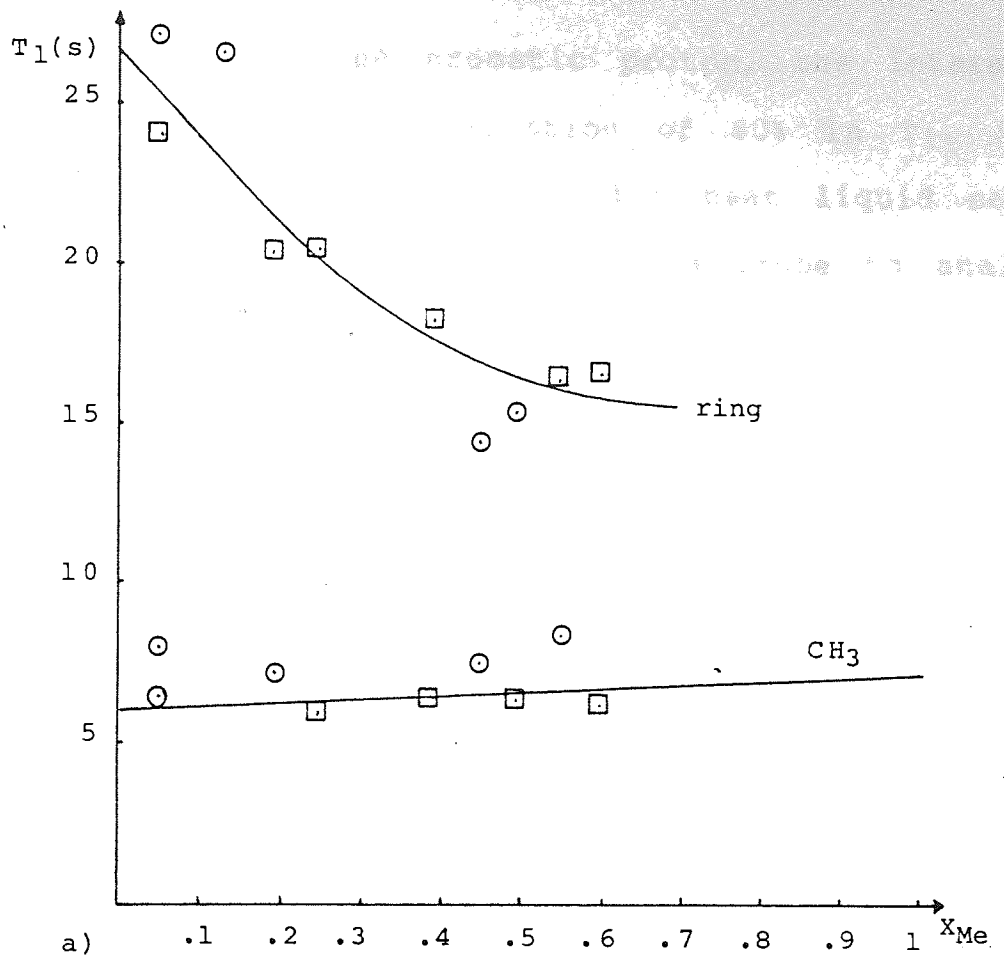

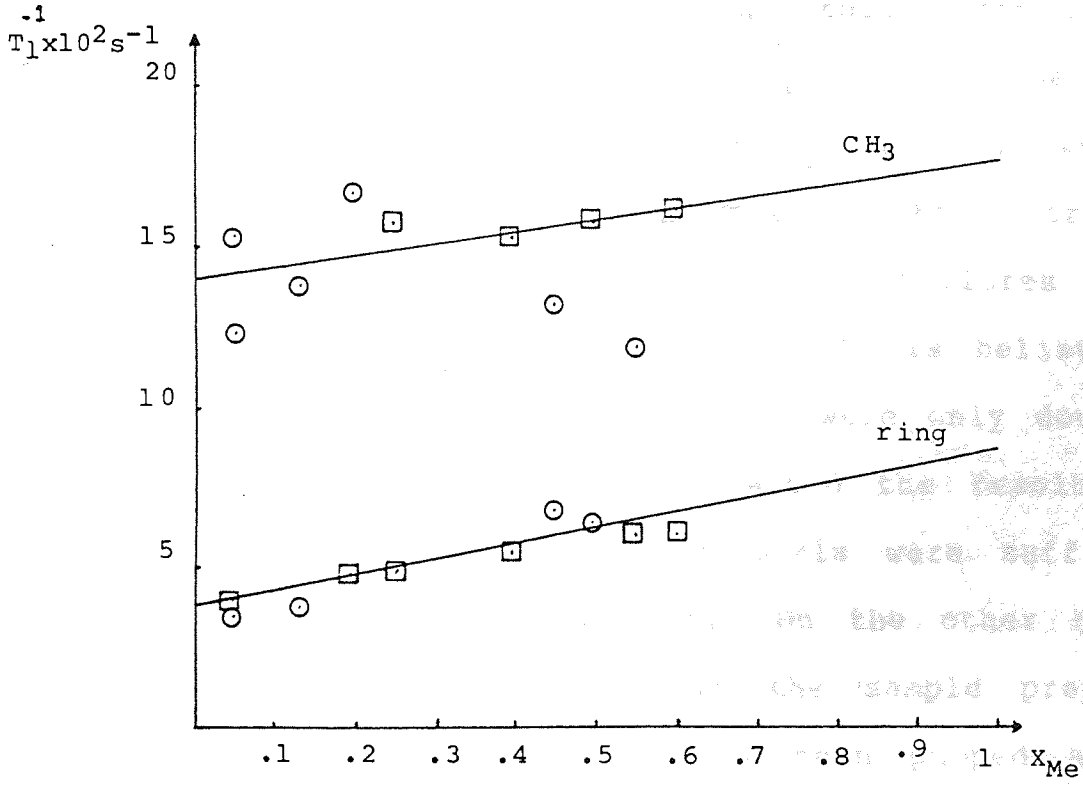

Figure 6.2 The variation of T_1 and T_1^{-1} of mesitylene in CCl_4, with the mole fraction of mesitylene (Progressive saturation method) (□) represent points with higher correlation coefficient.

In the case of the aromatic proton, the intermolecular interaction causes a variation of 60% in T_1, from the infinite dilute condition to the neat liquid condition. This makes the ring proton a good probe to analyse the effect of protonated solvents on T_1.

Because we are interested in the effect of solvents on T_1, a set of samples was prepared where the concentration of mesitylene was kept at a low constant mole fraction X_A=0.07. This has the advantage that the relaxation time will reflect the maximum effect of the solvent, that is particularly important in the case of the aromatic protons. The solvents used in this eXperiment were cyclohexane and TMS because they have the same number of protons, providing similar proton density around the aromatic proton of mesitylene but with different molecular size and shape that might influence β and ξ in a buffeting effect on T_1. After the samples were prepared, the compositions were roughly checked using n.m.r. integration; this showed only slight discrepancies of about $\Delta X \sim \pm$ 0.01 so no major failures in the preparative technique were evident. It is believed that the smallness of some samples, that were only double the length of the receiver coil affected the resolution of the instrument so that the integrals were sufficiently ill-defined to account for ΔX. On the other hand, it has to be acknowledged that in the sample preparation some of the material could have been pumped away and that ΔX is real.

Table 6.4 shows the relaxation times T_1 (A.R.P.S.) of the ring protons and CH_3 protons of mesitylene in solutions of cyclohexane- TMS. In all the samples X_A=0.07. The mole fraction of TMS (X_B) and cyclohexane (X_C) can be expressed as X_C=1-X_B-0.07. The r.f. attenuation used was 18 decibels, in accordance with the optimum conditions described in chapter 4. The correlation coefficients were lower than those in table (6.1), because of the low concentration of mesitylene which reduces the signal to noise ratio and increases the overall T_1's errors. However, figure (6.3) shows that the experimental points with higher correlation coefficients produce a well defined straight line.

The progressive saturation method gives similar results (table 6.5) to those in table (6.4). The relaxation times in table 6.4 with higher correlation coefficients represent the best choice of experimental values. The progressive saturation results in figure 6.4 can be compared to those of the A.R.P.S. in figure 6.3 which coupled with the correlation coefficients recorded in tables 6.4 and 6.5 suggests that the A.R.P.S. data are more reliable than those obtained from progressive saturation, because of the smaller scatter of the data.

In spite of having the same number of protons, the effects of cyclohexane and TMS on the relaxation times of the aromatic protons of mesitylene can be seen to be quite different from figure 6.3. Some of the factors

Table 6.4

The variation of T_1 for mesitylene with X_{TMS} in the mixture mesitylene - C_6H_{12}-TMS, where X_A=0.07 (ARPS method).

X_{TMS}	Xc	correlation coefficient		T_1 (sec)	
		ring	methyl	ring	methyl
0.091	0.839	0.987	0.998	14.97	5.37
0.106	0.824	0.993	0.999	15.6	5.93
0.180	0.750	0.982	0.940	14.7	5.48
0.205	0.725	0.986	0.998	16.27	6.6
0.207	0.723	0.996	0.997	15.6	6.7
0.329	0.601	0.985	0.987	16.67	6.2
0.448	0.482	0.988	0.991	18.4	6.6
0.493	0.437	0.991	0.999	17.99	6.5
0.621	0.309	0.997	0.999	19.7	7.2
0.798	0.132	0.996	0.988	20.7	7.8

Table 6.5

The variation of T_1 for mesitylene with X_{TMS} in the mixture mesitylene-C_6H_{12}-TMS, where X_A=0.07, (Progressive saturation method).

X_{TMS}	Xc	correlation coefficient		T_1 (sec)	
		ring	methyl	ring	methyl
0.091	0.839	0.989	0.983	15.4	6.2
0.106	0.824	0.994	0.998	18.3	6.7
0.180	0.750	0.994	0.992	15.7	6.5
0.205	0.725	0.998	0.990	16.96	5.9
0.207	0.723	0.997	0.995	18.7	6.2
0.329	0.601	0.993	0.986	20.2	6.5
0.448	0.482	0.993	0.997	22.4	6.1
0.493	0.437	0.996	0.994	20.8	6.5
0.621	0.309	0.990	0.978	22.3	6.4
0.798	0.132	0.999	0.998	25.5	6.7

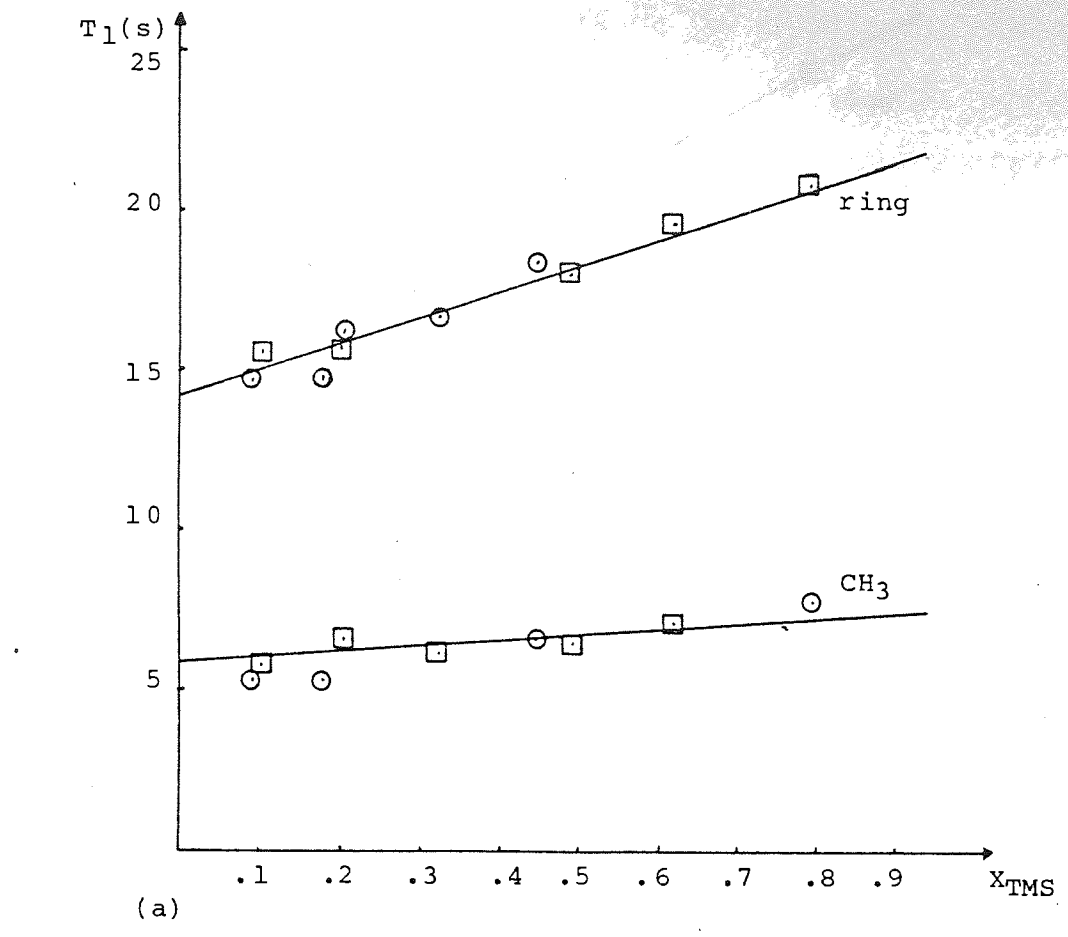

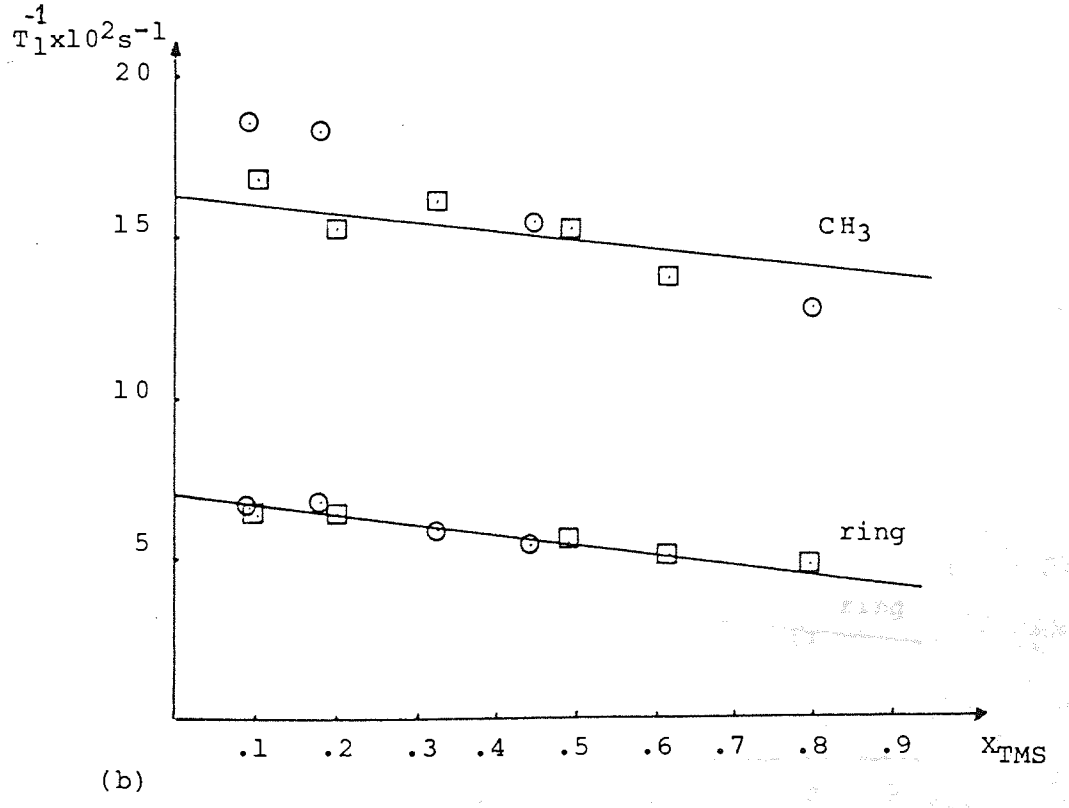

Figure 6.3 The variation of T_1 and T_1^{-1} of mesitylene in TMS and cyclohexane, with the mole fraction of TMS where X_A=0.07 (ARPS method) (□) refer to higher correlation coefficient.

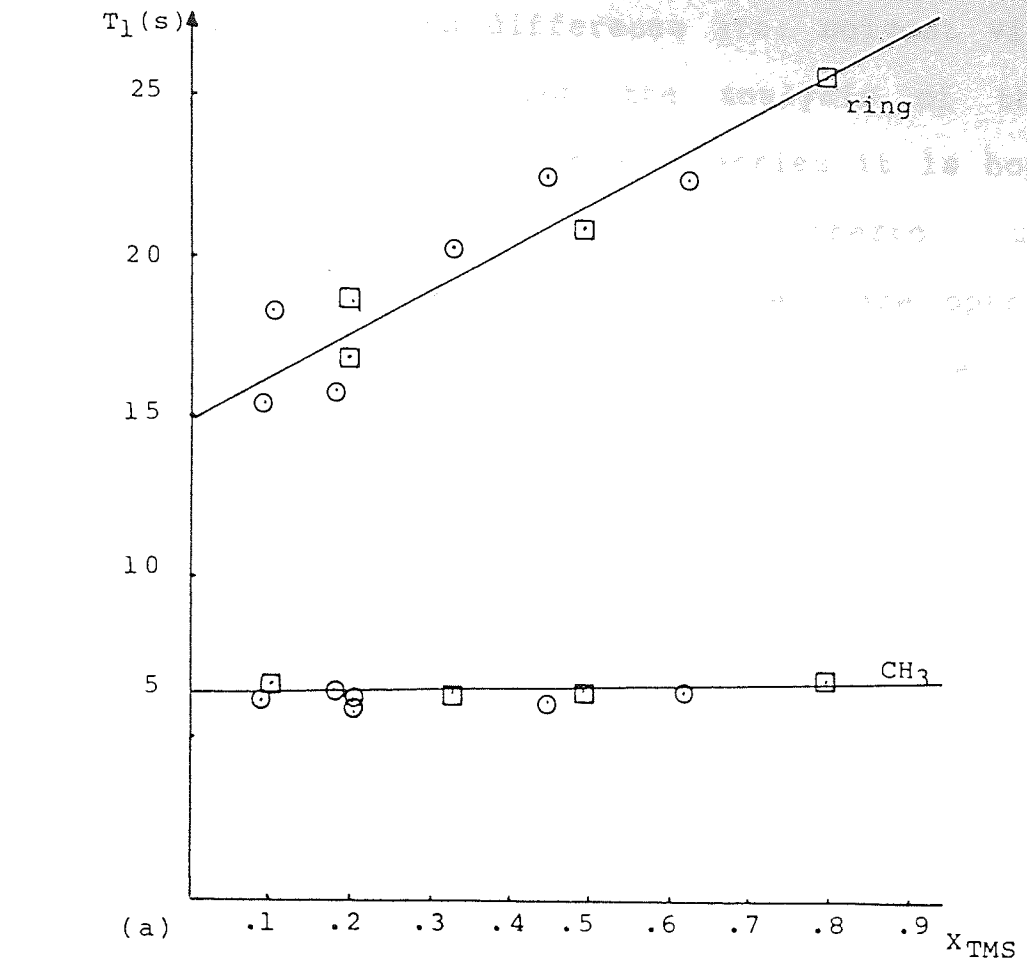

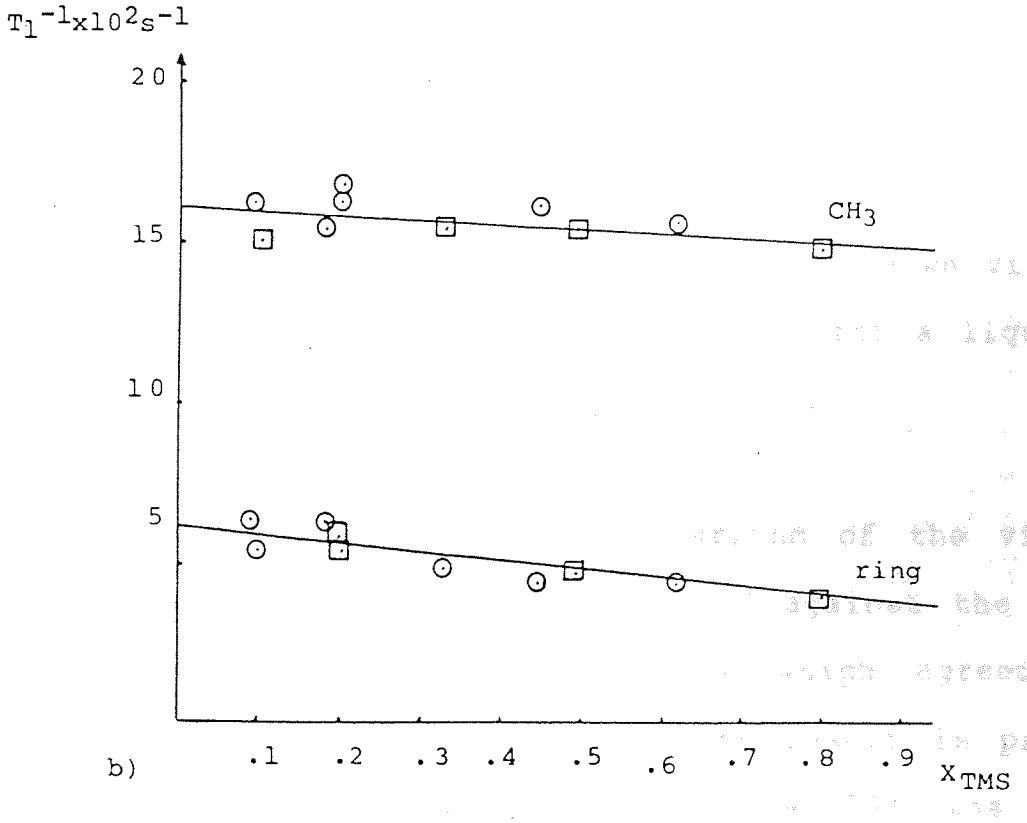

Figure (6.4) The variation of T_1 and T_1^{-1} of mesitylene in TMS and cyclohexane, with the mole fraction of TMS (X_A=0.07) progressive saturation method. (□) refer to points with higher correlation coefficient.

that may cause this difference are: solvent viscosity and proton density and from the analysis of these results within the frame of existing theories it is hoped to find out whether some other hitherto unrecognized contributions to T_1 in these systems are operative. For this to be possible the viscosities of the mixtures had to be measured.

6.3 Determination of the Viscosities of Mesitylene Cyclohexane- TMS Mixtures.

The viscosity measurements reported in table (6.6) were obtained with an Ostwald viscosimeter contained in a constant temperature bath. The viscosimeter was calibrated with water and checked against the viscosities of the substances which were used in the solution. The viscosity was calculated [215] from equation (6.3)

$$\eta_x = \frac{\rho_x}{\rho_{H_2O}} \quad \frac{tx}{tH_2O} \quad \eta_{H_2O} \qquad (6.3)$$

where x refers to the substances of unknown viscosity, ρ is the density and t is the time needed for a liquid to pass through the marks on the viscosimeter.

It was found that the logarithm of the viscosity of TMS reported in table 6.6 plotted against the inverse of temperature was a straight line which agreed with the equation [216] $\eta = a \exp {}^{b}/_{T}$. This result is presented in figure (6.5). The viscosity of TMS at 30°C was obtained

Table 6.6

Some physical parameters of water , mesitylene (A), cyclohexane (C), TMS (B) and their mixtures $\eta' = \eta_{A+C}$, $\eta'' = \eta_{A+B}$. Where $X_A = 0.07$

(a)	T(°C)	ρ_B(gcm^{-3})	ρ_{H_2O}(gcm^{-3})	η_{H_2O}(C.P.)	t_B(sec)	t_{H_2O}(sec)	η_B(C.P.)
	10	0.64298	0.99970	1.307	113,1	367,6	0.258
	15	0.63277	0.99913	1.139	108,4	319,1	0.245
	20	0.62256	0.99823	1.022	103,5	285,3	0.231
	25	0.61235	0.99707	0.890	99,0	254,6	0.215
	30	0.60214	0.99507	0.797	-	229,8	0.204

(b)	T(°C)	ρ_A(gcm^{-3})	ρ_{A+B}(gcm^{-3})	η_A(C.P)	tA+B(sec)	η''_{exp}(C.P.)	η''cal(C.P.)
	20	0.8651	0.6468	0.693	115.2	0.267	0.277
	30	0.8570	0.6271	0.598	-	-	0.242

where $X_A = 0.07$, $X_B = 0.93$

(c)	T(°C)	ρ_c(gcm^{-3})	ρ_{C+A}(gcm^{-3})	η_C(C.P)	tc(sec)	t_{C+A}(sec.)	η'(C.P.)
	30	0.7693	0.777	0.793	295.8	264.2	0.715

where $X_A = 0.07$, $X_C = 0.93$

(a) Parameters of TMS and water.

(b) Parameters of mesitylene and TMS. η''_{exp} is a measured value but η'' calc, is calculated

(c) Refers to data of mesitylene and cyclohexane.

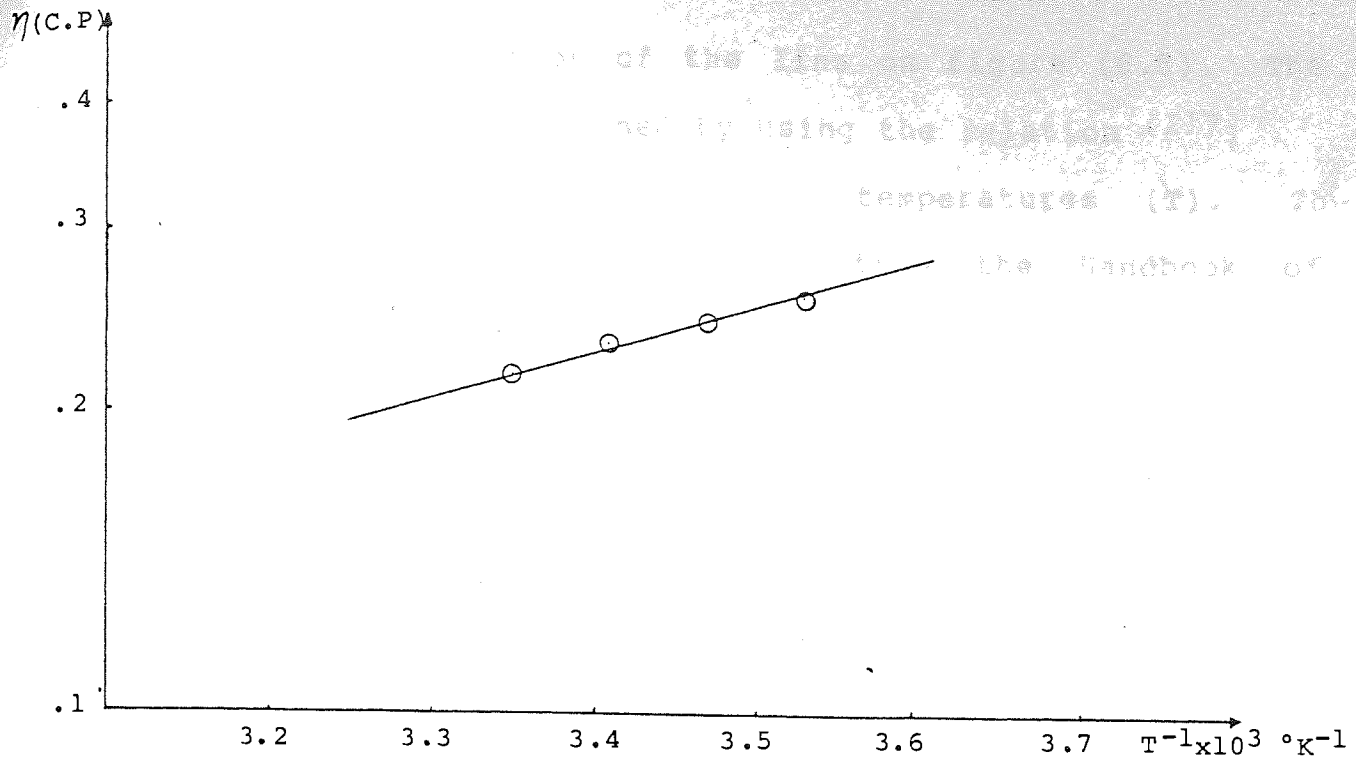

Figure 6.5 The variation of viscosity for TMS with temperature.

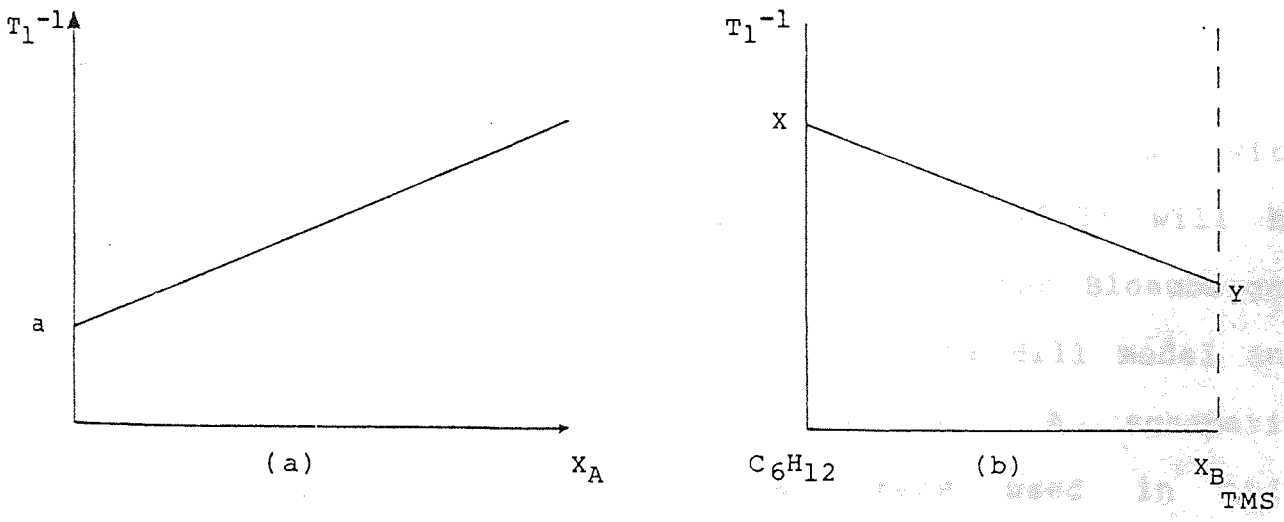

Figure 6.6 Representation of the parameters a,X,Y used in the test of relaxation models
a) T_1^{-1} of mesitylene in CCl_4
b) T_1^{-1} of mesitylene in TMS and C_6H_{12} with X_A=0.07
T_1 is measured by the ARPS method.

from the extrapolation of the line on figure (6.5). The density of TMS was obtained by using the relation (217) $\rho = 0.6634 - 0.002042T$ at several temperatures (T). The densities of water were taken from the Handbook of Chemistry and Physics (218)

The viscosity of mesitylene (A) in TMS (B) where $X_A=0.07$ and $X_B=0.93$ is represented in table 6.6 as η''. The viscosity of mesitylene (A) in cyclohexane (C) where $X_A=0.07$ and $X_C=0.93$ is represented as η'. The viscosity of mesitylene in TMS at 30°C was calculated from $\eta''=X_A\,\eta_A+X_B\,\eta_B$. In table (6.6b) the result of $\eta''_{exp.}$ at 20°C differs from the calculated value η'' by 37%. The densities of the mixtures were calculated by $\rho''=V_A\rho_A+V_B\rho_B$, where V is the volume fraction and $\rho'=V_A\rho_A+V_C\,\rho_C$.

6.4 Test of Relaxation Models.

The variation of the relaxation times with composition of mixtures shown in figure (6.3) will be used to test three relaxation models: I) the Bloembergen - Purcell - Pound (B.P.P.) model, II) the Hill model and III) a combination of I with II. A schematic presentation of the basic parameters used in this analysis is shown in figure (6.6) where a represents the intramolecular contribution $T_1^{-1}=a=3.9\times10^{-2}$ sec^{-1} for mesitylene at infinite dilution in CCl_4. X and Y are intercepts for $X_B=0$ and $X_C=0$ respectively in the plots for the mixture of mesitylene in cyclohexane and TMS,

at constant concentration of mesitylene (X_A=0.07), where $1=0.07+X_B+X_C$. Other important parameters used in the test are the viscosity of CCl_4, $\eta_o = \eta CCl_4 = 0.843$(C.P.) (218) and the proton density in the mixture of mesitylene with cyclohexane or TMS i.e. N' or N" respectively with $N' = 0.6474 \times 10^{23}$ protons cm^{-3} and $N" = 0.4951 \times 10^{23}$ protons cm^{-3}

I The B.P.P. Model.

The B.P.P. model uses the Debye rotational correlation time τ_r and the Stokes-Einstein translational correlation time τ_t both of which are proportional to viscosity. Therefore, we can rewrite the equation (6.2) for the mixtures of mesitylene – TMS (extreme Y) and mesitylene – cyclohexane (extreme X) on figure (6.6.b) as

$$Y = T_1^{-1} = P\,\eta" + QN"\,\eta" \qquad (6.4)$$

and

$$X = T_1^{-1} = P\,\eta' + QN'\,\eta' \qquad (6.5)$$

where P, Q are assumed to be constants (81), as A and B were in chapter 5. These equations should be valid for both the ring and CH_3 protons of mesitylene. Undoubtely, equations (5.13), (6.2) and (6.4) represent the same basic phenomenon but the constants are accomodated to suit a particular model.

The procedure to test model I consists of taking the value of P obtained from studies using CCl_4 as solvent i.e. $P=a/\eta_o$ where $\eta_o = \eta_{CCl_4}$ and substituting P in equation 6.5 to get Q from the mixture of mesitylene - cyclohexane. Consequently, the extreme Y on figure (6.6.b) can be obtained from the intramolecular contribution to T_1 of mesitylene in CCl_4 after viscosity correction i.e. $P \cdot \eta'' = a\eta''/\eta_o$. Therefore, the intermolecular contributions to Y and X

$$Y_{inter} = (Y - a\,\eta''/\eta_o) = QN''\,\eta'' \qquad (6.6)$$

and

$$X_{inter} = (X - a\,\eta'/\eta_o) = QN'\,\eta' \qquad (6.7)$$

If the equations (6.6) and (6.7) are a representation of the relaxation mechanism, we can predict the observed T_1 value in the extreme Y by using the intermolecular contribution in X. i.e. from equation (6.7) and the intramolecular part of Y; it gives

$$Y = Y_{intra} + X_{inter}\,\frac{N''\,\eta''}{N'\,\eta'} \qquad (6.8)$$

or

$$Y = a\,\eta''/\eta_o + (X - a\,\eta'/\eta_o)\,\frac{N''\,\eta''}{N'\,\eta'} \qquad (6.9)$$

similarly

$$X = a\,\eta'/\eta_o + (Y - a\,\eta''/\eta_o)\,\frac{N'\,\eta'}{N''\,\eta''} \qquad (6.10)$$

The analysis of these equations is made using the A.R.P.S. data in figure (6.3), since the progressive saturation data appear to be slightly less reliable. In table (6.8) the results for the extreme Y and X are shown. The magnitude of the difference between the calculated values of X or Y and the corresponding experimental values is more than 45%. This is similar to the results of the analysis discussed in chapter 5 and again indicates the inadequacy of the B.P.P. model.

II. The Hill Model

This model can be tested using a similar procedure to that for the B.P.P. model. Instead of using equation (5.13) we have to change the constant B in that to C, in order to express the intermolecular term as a fraction of the proton density. Thus

$$T_1^{-1} = A\,\tau_r + C\,\frac{N}{D} \qquad (6.11)$$

From the analysis of the Hill theory in chapter 5, we can use the equations (5.10) and (5.12):

$$\tau = K_A^2\ \sigma_{AB}\ \eta_{AB}\ /KT \qquad (5.10)$$

$$D = KT/6\ (\ \eta_{AB}\ \sigma_{AB}\ f_A + \eta_B\ \sigma_B\ f_B) \qquad (5.12)$$

to get the extremes X and Y as we did for the model I.

The equivalent equation to (6.9) in the Hill model, with K_A^2 approximated to $I_{A/\mu}$ is

$$Y = T_1^{-1} = a \frac{\mu_{AO}}{\eta_{AO}\ \sigma_{AO}} \frac{\eta_{AB}\ \sigma_{AB}}{\mu_{AB}} + \frac{N''D'}{D''N'} (X-A') \quad (6.12)$$

where A' is the intramolecular part of X i.e.

$$A' = a \frac{\mu_{AO}}{\eta_{AO}\ \sigma_{AO}} \frac{\eta_{AC}\ \sigma_{AC}}{\mu_{AC}} \quad (6.13)$$

D' and D" are obtained from equation (5.12), μ_{AO} is the reduced mass of mesitylene - CCl_4; $\eta_{AO}\ \sigma_{AO}$ and $\eta_{AB}\ \sigma_{AB}$ are the mutual viscosities in the systems mesitylene - CCl_4 and mesitylene - TMS.

In order to check the extreme X in the same way implicit in equation (6.10) we can write an equivalent Hill expression:

$$X = a \frac{\mu_{AO}}{\eta_{AO}\ \sigma_{AO}} \frac{\eta_{AC}\ \sigma_{AC}}{\mu_{AC}} + \frac{N'\ D''}{D'\ N''} (Y-A'') \quad (6.14)$$

where A" is the intramolecular part of Y i.e.

$$A'' = a \frac{\mu_{AO}}{\eta_{AO}\ \sigma_{AO}} \frac{\eta_{AB}\ \sigma_{AB}}{\mu_{AB}} \quad (6.15)$$

The evaluation of equations (6.12) and (6.14) is possible only after all the parameters in equation (5.7) have been calculated, by using equations (5.11) and (5.14). Some of the relevant parameters are included in table (6.7). Also the average distances between molecules in neat liquids are needed and estimated from equation (5.11).

It was deduced that σ_A=6.153 Å, σ_B=6.24Å , σ_C=5.67Å and σ_O=5.45 Å , respectively for mesitylene TMS, cyclohexane and CCl_4. The diffusion ratio was obtained from equation (5.12) as D'/D"=0.659.

Table (6.7).

Basic parameters used in the test of the Hill theory.

System	$\mu_{1,2}$(g)	$\eta_{1,2}\sigma_{1,2}$(C.P.Å)	σ_m(Å)	D($cm^2sec^{-1}x10^5$)
Mesitylene-CCl_4	68.26	4.265	5.52	--
Mesitylene-C_6H_{12}	49.5	4.171	5.70	1.696
Mesitylene-TMS	50.88	2.493	6.23	2.572

where 1,2 refer to the mixture and σ_m refer to eq. (5.7)

The results of using the Hill model for the correlation of the extremes X and Y in equations (6.12) and (6.14) are included in table (6.8). It shows a difference of about 20-50% between the experimental and calculated values of X or Y. Despite the improvements in accuracy over the B.P.P. model, it seems necessary to search for a better model.

III Combined Hill and B.P.P. model.

In view of the failure of the previous models in correlating the extremes X and Y of the figure (6.6b), we will use a similar approach to that of Steele (92).

This combines the intramolecular interaction, expressed in our case by the Hill equation, which has proved to be reasonably accurate; with the B.P.P. intermolecular term, which has been found [92] to offer a good representation of this term.

The correlation between X and Y can be expressed now as a combination of equation (6.9) and (6.12) for Y and equations (6.10) and (6.14) for X. Thus,

$$Y = a \frac{\mu_{AO}}{\eta_{AO}\,\sigma_{AO}} \frac{\eta_{AB}\,\sigma_{AB}}{\mu_{AB}} + (X - A') \frac{\eta''N''}{\eta'N'} \qquad (6.16)$$

where A' is given by equation (6.13)
and

$$X = a \frac{\mu_{AO}}{\eta_{AO}\,\sigma_{AO}} \frac{\eta_{AC}\,\sigma_{AC}}{\mu_{AC}} + (Y - A'') \frac{\eta'N'}{\eta''\,N''} \qquad (6.17)$$

where A" is given by equation (6.15)

Table (6.8) shows the results of using equations (6.16) and (6.17). Without doubt, model III is the most accurate, although, it is observed that there are still important differences between the calculated and experimental data for the aromatic protons of mesitylene. In particular, the first term of the model equations called ρintra in table (6.8) is always bigger than the corresponding ρinter in the case of the extreme Y in TMS. For the extreme X in cyclohexane the opposite effect is evident. Perhaps this is related to expected errors when the intra-molecular contribution to T_1 is calculated, as we showed in table (5.7) chapter five.

Table 6.8

Extreme values X and Y of figure 6.6 calculated from three different relaxation models. ρ_{intra} and ρ_{inter} represent the first and second term in each model's equations.

Model	BPP (I)		HILL (II)		HILL-BPP(III)	
$(X,Y)x10^2 sec^{-1}$	ring	methyl	ring	methyl	ring	methyl
Yexp	4	13.7	4	13.7	4	13.7
ρ_{intra}	1.12	4.31	3.05	11.74	3.05	11.74
ρ_{inter}	0.98	1.05	2.7	4.75	1.39	2.44
Ycalc	2.1	5.36	5.75	16.5	4.44	14.2
$\Delta Y/Y_{exp}$ %	47.5	60.8	43.7	20.4	11	3.6
Xexp	7.1	16.1	7.1	16.1	7.1	16.1
ρ_{intra}	3.3	12.73	1.7	6.7	1.7	6.7
ρ_{inter}	11.2	34.3	1.9	2.9	3.7	5.6
Xcalc	14.4	47.0	3.6	9.6	5.4	12.3
$\Delta X/X_{exp}$ %	100	194	49	40.5	24	23.5

Our interest now is to see whether it is possible to improve the Hill-B.P.P. model III by introducing a term due to the buffeting interaction.

6.5 Buffeting Correction

In the analysis of relaxation times, especial attention has been dedicated to the distance of closest approach between molecules (87)(88). Hubbard (86) has considered that in liquids containing polyatomic molecules, the distance of closest approach of nuclei in different molecules is actually less than the diameter of one molecule, which means that if proper account is taken of this a greater contribution to the relaxation time will be predicted than if a molecular diameter is used. Hertz (87) has pointed out that the effective distance of closest approach of two molecules, will lie somewhere between the real distance and the molecular diameter. Inlow et al (88) have adjusted the effective distance in accordance with the type of interacting molecules.

Table (3.1) in chapter 3 presents the values of the intramolecular and intermolecular contributions to the relaxations times of aromatic and methyl protons of several compounds. We can see that even a few protons close to the nucleus of interest can make an important contribution to T_1 from intramolecular effects. In the case of methyl protons, the intramolecular contribution is bigger than the intermolecular one. Therefore,

the effect of N(proton density) in the intermolecular expression for T_1 equation 6.2, basically weighs the efficiency with which protons from neighbour molecules can approach the protons that are being studied. Consequently, it would be imagined that the main contribution to T_{1inter} comes from the first shell around the molecule under study and in particular those at the closest distance of approach.

The time dependence of the relative position of two nuclei in different molecules depends on the translational and rotational motion of the molecules. Whilst this affects the effectiveness of the dipolar-dipolar interaction, this is affected in real molecules by the ability of other molecules to actually come into contact with the protons studied. In the case of mesitylene in solution with the protonated solvents cyclohexane and TMS, the aromatic proton is somewhat hidden within the molecule. This leads us to consider a contact surface as shown in figure (6.7) where the lines L and L' pass through the points p and p' for two symmetrical collisions in the plane of the ring. Evidently, steric restrictions can be placed on the collisions between the solvent and ring proton. Therefore, it is possible to define for the proton a contact surface for possible collisions.

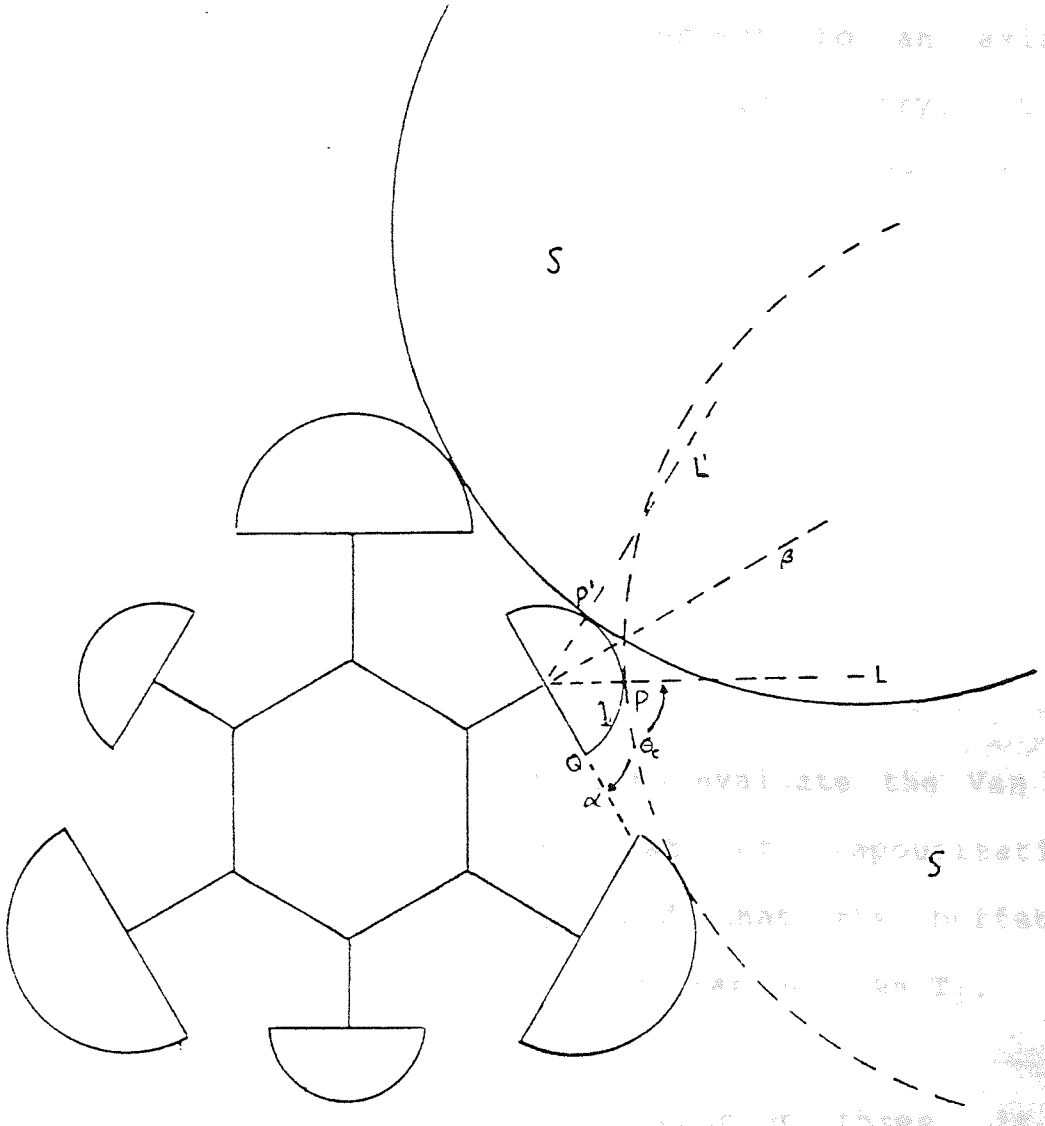

Figure 6.7 Schematic representation of the collision of mesitylene with solvent molecules.

The buffeting interaction described at the end of chapter one, provides a way to consider this contact surface. There, the anisotropy of the collisions is represented by two empirical constants β, ξ; related to a contact angle θ_c made with respect to an axially symmetric bond. As a result of this theory, it is predicted that a resultant electric field generates a buffeting contribution to the Van Der Waals screening term indicated by equation (1.75)

$$\sigma_w = -B \langle Eb \rangle^2 \qquad (1.75)$$

where $\langle Eb \rangle = K(2\beta - \xi)^2 / r^{-6}$

These statements have been confirmed (51) and also, that the buffeting effect can be used to evaluate the Van Der Waals a constant and the heat of vapourization. Therefore, it might be anticipated that the buffeting effect can contribute also to the relaxation time T_1.

From the equation (3.11) in chapter three, it is possible to establish that the inverse of the relaxation time is proportional to the square of the magnetic local field i.e. $T_1^{-1} \propto \langle B_{LOC} \rangle^2$. By analogy with equation (1.75), it seems that the relaxation mechanism between solute protons and solvent protons can be modulated as well by $(2\beta - \xi)^2$. In order to assess this, we will calculate β and ξ for mesitylene in cyclohexane and TMS, and apply the buffeting correction in a new test to models II and III for T_1.

The parameters β and ζ have been defined at the end of chapter one. With this basis, we will consider the ring hydrogen of mesitylene in figure (6.7), where θ_c represents the contact angle. The hydrogen atom is divided in four octants in a laboratory model of the molecule. In addition a disc represents the solvent molecule (S). For each octant the contact angle can be different and is measured from the arc length (l) between the point P and Q on figure (6.7), therefore $\theta_c = {}^{l}/_{r}$ (radian), where r is the hydrogen radius in the model. It gives $\theta c° = 360 \times \theta_c rad/2\pi$. The scale used in the model is 1Å=1.666cm. When the angle of contact is smaller than 45°, i.e. $\theta_c < 45°$, the contact is type α as indicated by equation (1.81), otherwise it is type β according to equation (1.82).

Table (6.9) shows the parameters which allow the calculation of β and ζ , that is, arc length (l) contact angle θ_c, and the distance d, in which the modulation of the effect type α or β is lost. Then, after the use of equation (1.81) and (1.82) we obtain ζ_c and β_c. The value of R_{AV}^{-6} is obtained from equation (1.83), where d is the integration limit r'. Finally β_T and ζ_T are calculated from equation (1.84).

The same procedure was followed to calculate β and ζ for the ring and methyl hydrogens of mesitylene in cyclohexane and TMS. The results are shown in table (6.10).

Table (6.9)

Parameters used in the determination of β and ξ for the aromatic hydrogen of mesitylene with cyclohexane as solvent.

Quadrant	S(cm)	θc	βc	ξc	d(cm)	$R_{AV} x 10^4 cm^{-6}$	R_{AV}/r_{III}	β_T	ξ_T
I	2.7	77.3	0.281	0	2.6	0.685	0.281	0.483	0
II	1	38.6	1	0.727	1.3	1.124	0.461	1	1.314
III	2.3	65.8	0.536	0	2.8	0.644	0.264	0.658	0
IV	1	28.6	1	0.727	1.3	1.124	0.461	1	1.314

Table (6.10)

Values of β and ξ of mesitylene hydrogen groups with TMS and cyclohexane as solvents.

solvent	ring		methyl		ring	methyl
	β	ξ	β	ξ	$(2\beta - \xi)^2$	$(2\beta - \xi)^2$
TMS	0.694	0.706	0.916	0.837	0.4651	0.990
C_6H_{12}	0.785	0.657	0.913	0.858	0.83357	0.937

We will use the Gutowsky-Woessner expression for T_{1inter} [79] to identify the constant Q in equation (6.4). Thus,

$$T_{1inter}^{-1} = 3\pi^2 \hbar^2 \gamma^4 \eta N \frac{a}{KT} \frac{1}{r^\circ} \qquad (6.18)$$

where r° is the closest distance between nuclei in different molecules, normally taken as 2a, where a is the molecular radii.

The buffeting correction can be assumed to reduce equation (6.18) to

$$T_{1inter}^{-1} = 3\pi^2 \hbar^2 \gamma^4 \eta N \frac{a}{KT} \frac{(2\beta - \xi)^2}{r^\circ} \qquad (6.19)$$

The results on table (6.11) for mesitylene in TMS give some confidence in equation (6.19) as a representation of the intermolecular interaction. However, when the solvent is cyclohexane, the results are very different from those expected from table (6.8) which indicates that not only is the buffeting correction necessary, but in addition some correction to the closest approach distance r° and perhaps to the local proton density at the observed nucleus. In addition to that, it has to be remembered that the viscosity η can be a good parameter to represent the diffusion of the molecules, but not their rotational motion. This implies that the intermolecular interaction as described by equation (6.19) does not take into account the real modulation effect due to internal or rotational motion of the solvent molecules.

Table (6.11)

The values of T_1^{-1}inter for Mesitylene calculated from equations (6.18) and (6.19) at 30°C.

	T_1^{-1}inter x 10^2(sec^{-1})					
	(a)		(b)		(c)	
solvent	ring	methyl	ring	methyl	ring	methyl
TMS	1.39	2.44	2.41	2.41	1.12	2.38
C_6H_{12}	3.7	5.6	9.3	9.3	7.75	8.7

(a) refers to experimental data in table (6.8) model III

(b) correspond to equation (6.18)

(c) correspond to equation (6.19)

The implication of the foregoing analysis, is that a simple model of the intermolecular interaction is difficult to obtain and the best way to describe it, is through information about the intramolecular contribution to T_1, obtained from theoretical models or experimental data.

The buffeting correction applied to the relaxation model III, only modifies the intermolecular contributions to Y and X in equations (6.16) and (6.17). Thus,

$$Y = \frac{a\ \mu_{AO}}{\eta_{AO}\ \sigma_{AO}} \frac{\eta_{AB}\ \sigma_{AB}}{\mu_{AB}} + (X - A') \frac{\eta''\ N''}{\eta'\ N'} \frac{(2\beta - \xi)''^2}{(2\beta - \xi)'^2} \qquad (6.20)$$

$$X = \frac{a\ \mu_{AO}}{\eta_{AO}\sigma_{AO}} \frac{\eta_{AC}\ \sigma_{AC}}{\mu_{AC}} + (Y - A'') \frac{\eta'\ N'}{\eta''\ N''} \frac{(2\beta - \xi)'^2}{(2\beta - \xi)''^2} \qquad (6.21)$$

where $(2\beta - \xi)''^2$ and $(2\beta - \xi)'^2$ refer to the mixture of mesitylene with TMS and cyclohexane respectively. Table (6.12) shows the values of Y and X obtained from the model III after buffeting correction. The same correction is applied to the relaxation model II on the intermolecular term $N''D'/D''N'$ in equations (6.12) and (6.14). The results are shown in table 6.12. According to this, model III gives the best values after buffeting correction.

Despite the accurate results obtained from model III in table (6.12), it is important to point out that the buffeting contributions to the Van Der Waals screening

Table (6.12)

Buffeting correction $(2\beta - \zeta)^2$ applied to the relaxation models II and III in table 6.8.

	Hill (II)		Hill-B.P.P. (III)	
X, Y x 10^2 sec^{-1}	ring	methyl	ring	methyl
Y_{exp}	4	13.7	4	13.7
ρintra	3.05	11.74	3.05	11.74
ρinter	1.5	5.02	0.78	2.58
Y_{cal}	4.55	16.76	3.83	13.22
$\Delta Y/Y_{exp}$	13.7%	22.3%	4.2%	3.5%
X_{exp}	7.1	16.1	7.1	16.1
ρintra	1.7	6.7	1.7	6.7
ρinter	3.40	2.74	6.63	5.3
X_{cal}	5.1	9.44	8.33	12
$\Delta X/X_{exp}$	28.17%	41.3%	17.3%	25.6%

Table (6.13)

Buffeting correction $(2\beta - \zeta)^{-2}$ applied to the relaxation models II and III in table 6.8

	Hill (II)		Hill-B.P.P. (III)	
X, Y x 10^2 sec^{-1}	ring	methyl	ring	methyl
Y_{exp}	4	13.7	4	13.7
ρintra	3.05	11.74	3.05	11.74
ρinter	4.84	4.49	2.49	2.31
Y_{cal}	7.89	16.23	5.54	14.05
$\Delta Y/Y_{exp}$	97.2%	18.46%	38.5%	2.5%
X_{exp}	7.1	16.1	7.1	16.1
intra	1.7	6.7	1.7	6.7
inter	1.06	3.06	2.06	5.9
X_{cal}	2.76	9.76	3.76	12.6
$\Delta X/X_{exp}$	61%	39.4%	47%	21.7%

factor σ_w in equation (1.80) represents deviation from isotropic effect i.e. this contribution should be zero in isotropic interactions.

For T_1^{-1} the isotropic effect represents the maximum interaction. Under these circumstances it might be necessary to postulate that the buffeting correction applies only to anisotropic situations. On the other hand, it is possible to use different empirical factors like $(2\beta - \xi)^{-2}$, $1-(2\beta - \xi)^2$, or $(2(1-\beta)-(1-\xi))^2$, etc. From the evaluation of these factors, it was concluded that only $(2\beta - \xi)^{-2}$ gives adequate results as table (6.13) shows for the case of ring protons. The use of factors different from $(2\beta - \xi)^2$ may be related to the effective distance of closest approach r° in equation (6.18), which has been reported to be between 1.2a and 4a, where a is the molecular radius (88).

6.6 CONCLUSIONS.

The ARPS and progressive saturation techniques, have been used to study the relaxation times of mesitylene protons in cyclohexane- TMS mixtures at a mole fraction of mesitylene X_A=0.07. Despite the low concentration of the solute, we were able to obtain reliable information on T_1 at several concentrations of TMS and cyclohexane. Both techniques gave similar information which was selected according to the correlation coefficient of the relaxation time measured. The ARPS technique was used to

analyze the relaxation times of mesitylene, because the data were more accurate.

It has been shown that the B.P.P. model of relaxation can not be used to explain the values of the relaxation times of mesitylene in the mixture used. This provides further support to the conclusion of chapter five. The Hill model gives better results, in particular for the methyl proton where the intramolecular interaction is higher. A combination of the two models has shown to be quite accurate in the calculation of T_1. But it can be due to compensation of errors from the intramolecular contribution, which suggests that a more accurate estimation of the intramolecular contribution to T_1 should be attempted.

The buffeting correction has been used to improve the Gutowsky-Woessner expression for T_1inter. Also this correction was applied to the relaxation model III with better results.

CHAPTER SEVEN

^{13}C NMR Relaxation studies of mesitylene in solutions and their use in the calculation of the intramolecular contribution to T_1 of ring protons.

7.1 Introduction

The implications of the work described in chapter 6 are that a combined BPP-Hill approach may be used to satisfactorily rationalize proton spin-lattice relaxation times. It should however, be noticed that it is only the overall self-consistency of the investigative approach that is apparently satisfactory. It could of course be that the approach is in fact invalid but that this is camouflaged by opposing and self-cancelling inadequacies in the treatment of the intra and intermolecular components of T_1. The intention now is to attempt to separate the intra and intermolecular contributions to the T_1 of mesitylene and separately test the adequacy of the theoretical descriptions of both terms.

The separation of the intramolecular and intermolecular contributions from ^1H relaxation times is often facilitated by dilution studies involving the perdeuterated analogue $A(^2H)$ of the molecule $A(^1H)$ under study (109)(219). Another method which has been used is to dilute the compound $A(^1H)$ in suitable compounds such as CCl_4 or CS_2 (81) that produce ineffective dipolar

contributions to the T_1. Both methods have disadvantages. The former is expensive and the latter gives the intramolecular relaxation time of the compound in CCl_4 or CS_2 and this can not be used to represent the intramolecular relaxation time when the solvent is changed even if the viscosity correction described earlier (chapter 5) is employed. The failure of the viscosity correction is accepted to derive from inadequacies in the Debye expression for the rotational correlation time (81)(92)(91) and although some other models have been used to calculate the rotational correlation time, these are still imprecise.

The ^{13}C NMR spin-lattice relaxation time T_1, can be related to the reorientational correlation time τ_{NMR} which depends on the rotational diffusion coefficients $\theta_{\|}$, $\theta_{\perp}$, parallel and perpendicular to the symmetry axis of the molecule (149) (156). Pecora et al (156) have found a different behaviour of the corresponding correlation coefficients $\tau_{\|}$, $\tau_{\perp}$ with changes in the solution viscosity as indicated in Figure 3.5 (these parameters have to be determined by light scattering and N.M.R. techniques). The use of viscosity as an appropriate parameter for characterizing the averaged rotational correlation time of a molecule has therefore to be reconsidered.

A further approach to the separation of intra and intermolecular contribution to T_1 of selected systems is

possible using the approach of Vold et al (189). They have found that the intramolecular proton correlation time determined from relaxation studies of mixtures of benzene and perdeuterobenzene has the same value as the one calculated from the ^{13}C spin lattice relaxation time of neat benzene. This is to be expected because the benzene molecule is a planar symmetric rotor, and τ_{C-H} and τ_{HH} are necessarily equal (189). The extension of this approach to other aromatic molecules like mesitylene seems well founded, in particular, for the ring proton. The approach will be to use the measured intramolecular relaxation time from ^{13}C experiments to evaluate the corresponding intramolecular ^{1}H term and then separate the intermolecular contribution from the observed relaxation times. The results can then be examined by a similar test to that used for the relaxation model III in chapter 6. In this way, it might be possible to asses how best to correlate the intermolecular relaxation contributions in two different solvents.

The intramolecular or rotational contribution to T_{1DD} has been demonstrated by Mitchell and Eisner (81) to be adequately represented by the Gutowsky and Woessner equation (79) (7.1).

$$\frac{1}{T_{1(rot)i}} = \hbar^2 \gamma_i^2 \left(\frac{3}{2} \gamma_i^2 \sum_j r_{ij}^{-6} + \frac{4}{3} \gamma_f^2 (I_f+1) I_f \sum_f^* r_{if}^{-6} \right) \tau_{rot} \qquad (7.1)$$

where γ , I and r refer respectively to the gyromagnetic ratios, nuclear spins and separations between the different dipoles; Σ is over nuclei of the same type as the ith and Σ^* is over all others in the same molecule.

For all practical purposes equation (7.1) may be rewritten as

$$T_1^{-1}{}_{intra} = A \ \tau_{eff} \qquad (7.2)$$

If two nuclei, such as ^{13}C and ^{1}H, in a particular molecule, have precisely the same motional characteristics it is evident that

$$T_1^{-1}{}_{intra}^{H} = \frac{AH}{A_C} \ T_1^{-1}{}_{intra}^{C} \qquad (7.3)$$

consequently, if the intramolecular dipolar contribution to the ^{13}C relaxation can be isolated and the ratio A_H/A_C determined, the intramolecular contribution to the ^{1}H T_1 can be determined from the ^{13}C value even if the ^{1}H T_1 is influenced by an intermolecular mechanism.

It is frequently found that the ^{13}C relaxation times are not influenced by intermolecular effects because the operative interdipole distances are large. This being the case the intramolecular dipole-dipole contribution to the ^{13}C T_1 can be deduced from nuclear Overhauser studies. ^{1}H double irradiation yields the n.o.e. (η) for ^{13}C which can be inserted in equation (7.4) to obtain $T_1^{-1}{}_{intra}^{C}$

$$T_{1intra}^{-1\ C} = T_{1obs}^{-1\ C} \frac{\eta}{1.988} \qquad (7.4)$$

By conducting ^1H and ^{13}C measurements on a molecule at infinite dilution in a solvent such as CCl_4 the molecular constant A_H/A_C can be determined using equation (7.3) and then used to evaluate $T_{1intra}^{-1\ H}$ from ^1H and ^{13}C T_1's measured in any other solvent system whether or not this is dipolar in nature.

7.2 Experimental

The samples of mesitylene-CCl_4 and mesitylene-cyclohexane-TMS were prepared using the method described in chapter 4. All the experiments were carried out on a Jeol FX90Q spectrometer. The ^{13}C T_1 relaxation times were measured using the progressive saturation technique in order to get the most results in the shortest possible time. It was found that these results agreed reasonably with those obtained by the inversion recovery method. The 90° pulse for ^{13}C was 24 μ sec. and 30-40 scans were normally required to measure T_1's for the CH_3 carbons; for the ring carbons (CH) 20-25 scans were required. The sample temperature was 30°C±1°C. And this was set using the Jeol temperature control which was checked with a calibration curve (chapter 4) for a probe sample of (ethylglycol) and monitored for a period of time similar to the duration of the T_1's experiments. The NOE factor was obtained from the integral (I) of the peaks, using the Harris-Newman technique [196], waiting $5T_1$ between

pulses with the noise decoupler on (COM), and $10T_1$ between pulses with the decoupler gated (NNE). The NOE was calculated using equation (7.5)

$$\eta = \frac{I_{COM}}{I_{NNE}} - 1 \qquad (7.5)$$

7.3 Results and Discussion

The ^{13}C spin-lattice relaxation times for several concentrations of mesitylene in CCl_4 are given in table (7.1). Both the ring (CH) and CH_3 carbons relaxation times are presented in table (7.1) and illustrated graphically in Figure (7.1). Comparing the values of T_1 in table (7.1) or Figure (7.1) with those in table (7.3), it can be seen that for neat mesitylene there is a good agreement between the values of the relaxation times found experimentally and those from the literature. It can also be seen from figure (7.1) that the ^{13}C T_1 is higher for CH_3 than for the ring (CH) ^{13}C T_1 despite the presence of three protons. The reason for this is the averaging due to the internal rotation of the CH_3 group (137). In figure (7.2) the ^{13}C T_1 of the ring (CH) and CH_3 carbons of mesitylene in the mixture Me-C_6H_{12}-TMS are represented. There, the concentration of mesitylene is kept constant at X_{Me}=0.07. Table (7.2) contains the T_1's values for each case. When the mole fraction of TMS is increased, T_1 for the ring ^{13}C, (CH) grows steadily. This means that the molecular motion of mesitylene has undergone some sort of change. This effect is also seen

Table (7.1)

Relaxation times and NOE for ^{13}C and ^{1}H nuclei of mesitylene in mixtures with CCl_4

X_{Me}	T_{1C}/sec ^{13}CH	T_{1CH3}/sec $^{13}CH_3$	T_{1H}/sec ring (a)	$\eta(^{13}C-\{^{1}H\})$ ^{13}CH
0.05	7.3	11.8	23.7	1.89
0.129	7.1	11.7	22.45	
0.199	7.2	12.2	21.4	1.99
0.368	6.8	11.9	16.8	
0.451	6.9	11.4	16.46	1.8
0.545	6.7	12	15.33	
0.608	7.13	11.4	15.04	1.96

(a) hydrogen data taken from table 6.1 and Figure 6.1b

Table (7.2)

Relaxation times and NOE for ^{13}C and ^{1}H nuclei of mesitylene (X_{Me}=0.07) in mixtures of C_6H_{12}/TMS

X_{TMS}	T_{1C}/sec ^{13}CH	T_{1CH3}/sec $^{13}CH_3$	T_{1H}/sec ring (a)	$\eta(^{13}C-\{^{1}H\})$ ^{13}CH
0.09	10.65	12.8	14.97	1.88
0.18	10.3	12.6	14.7	
0.207	11.0	13.2	15.63	1.94
0.345	10.9	12.7	16.67	
0.44	10.9	13.3	17.99	2.1
0.62	11.3	13.2	19.7	
0.79	11.35	12.9	20.7	1.8

(a) hydrogen data taken from table 6.3 and Figure 6.3b

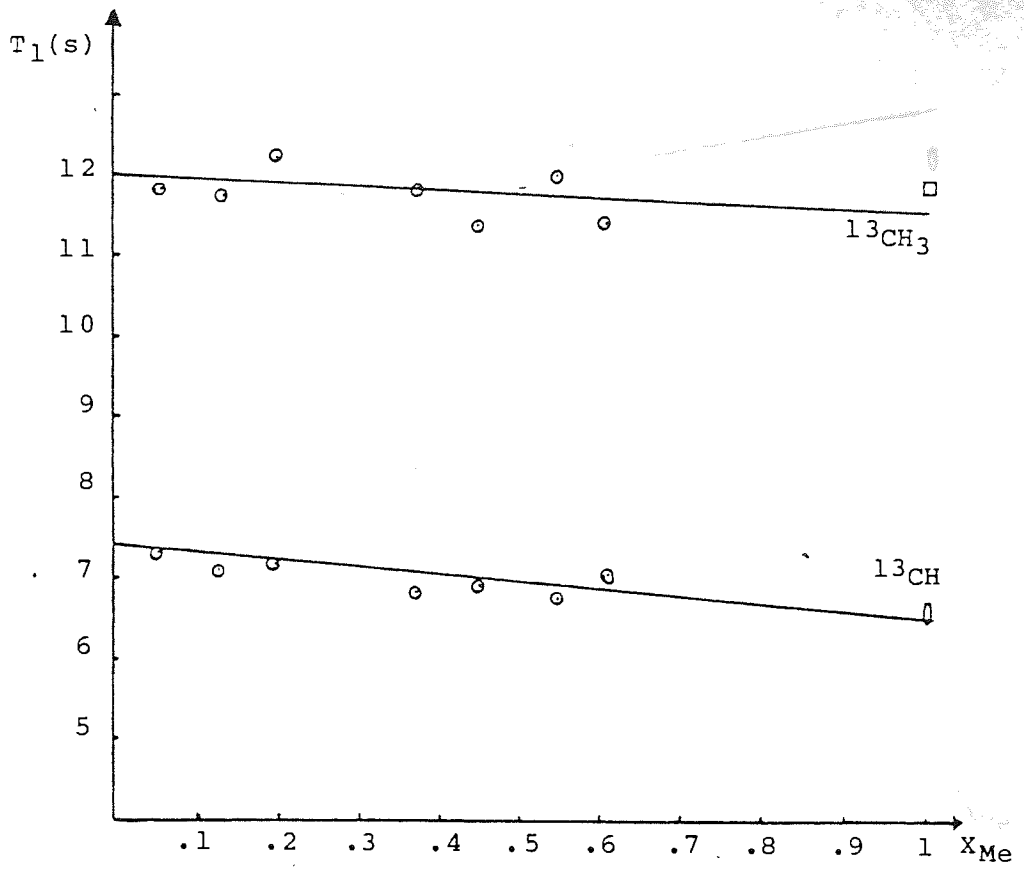

Figure 7.1 The variation of ^{13}C T_1's of mesitylene in CCl_4 with the mole fraction of mesitylene. (□, 0) literature values.

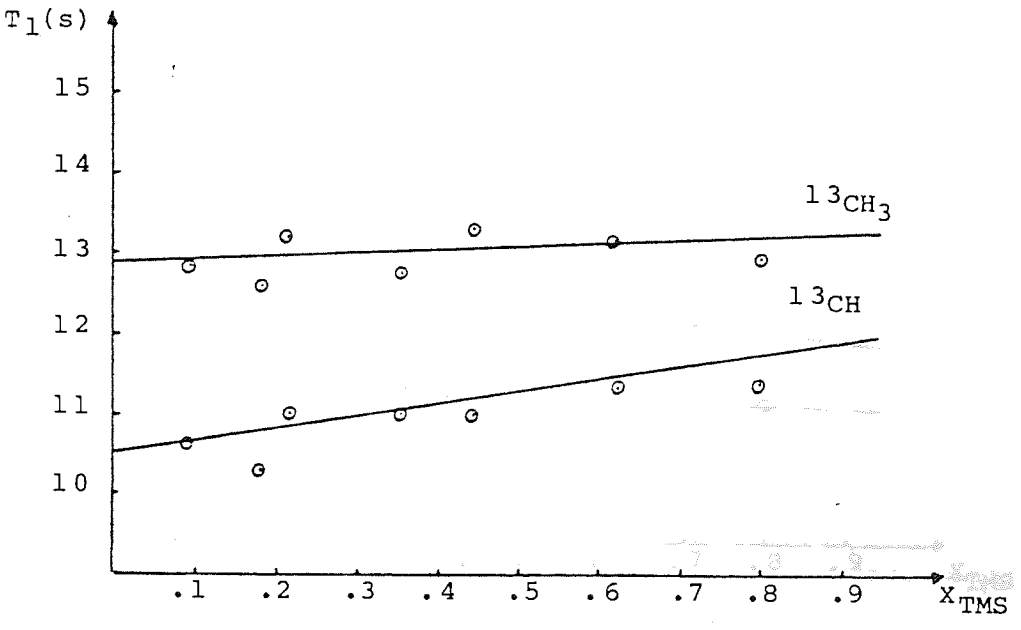

Figure 7.2 The variation of ^{13}C T_1's of mesitylene in TMS cyclohexane mixtures, with the mole fraction of TMS

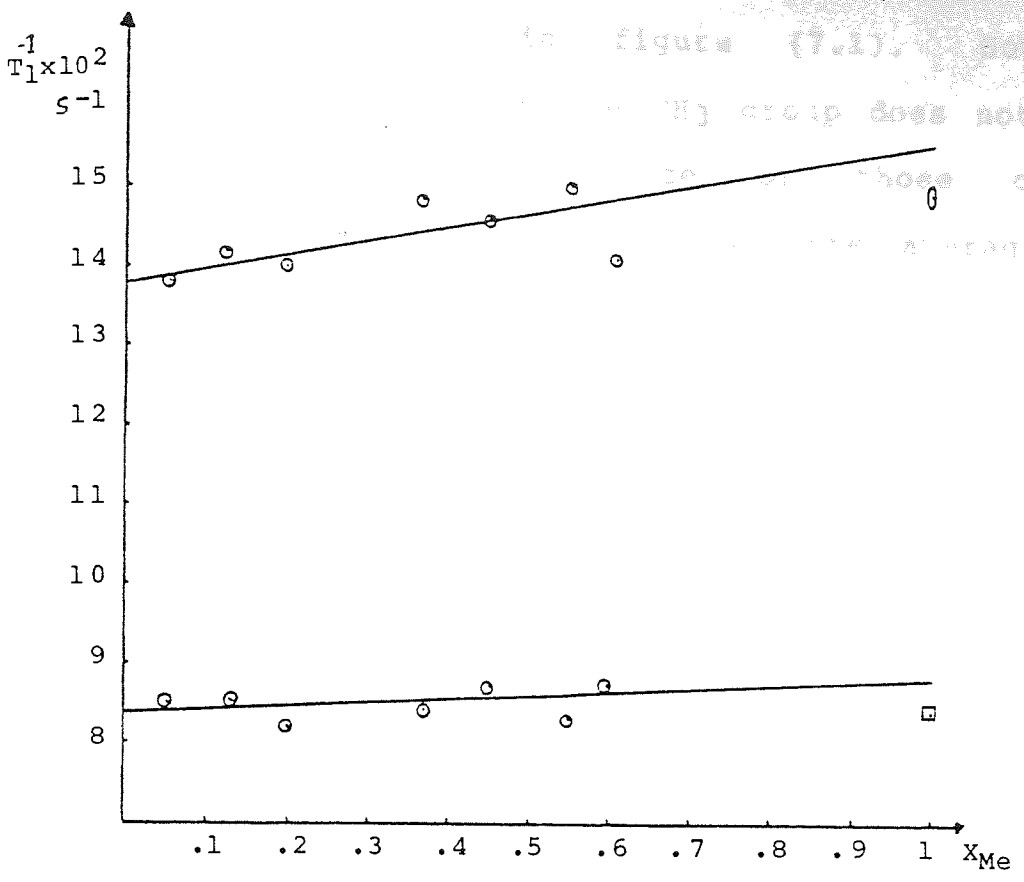

Figure 7.3 The variation of ^{13}C T_1^{-1} of mesitylene in CCl_4 with the mole fraction of mesitylene

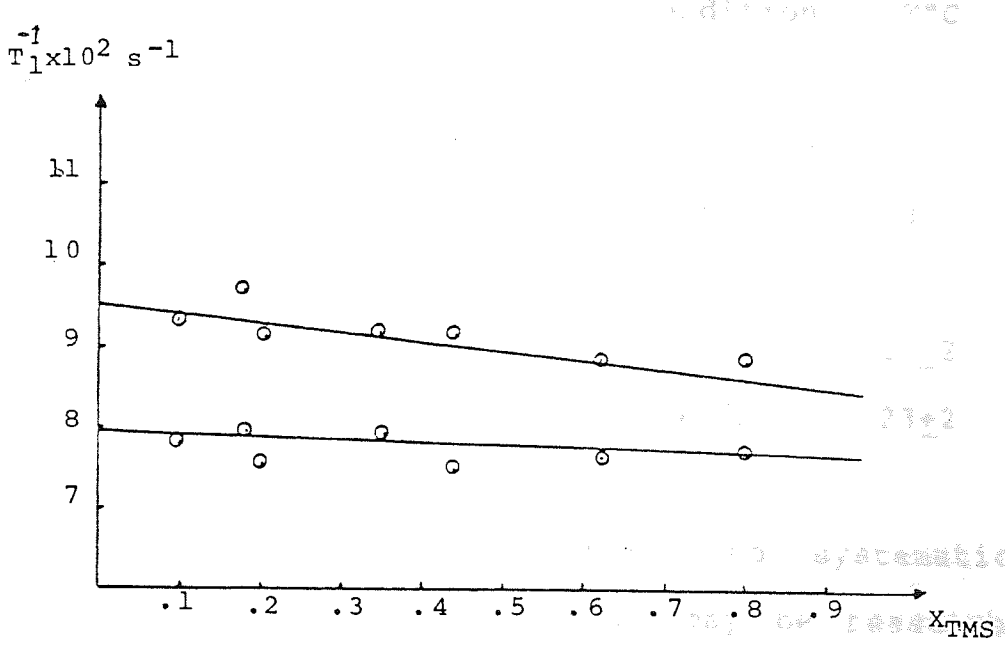

Figure 7.4 The variation of ^{13}C T_1^{-1} of mesitylene in TMS cyclohexane mixtures, with the mole fraction of TMS

when mesitylene is at low concentrations in Me-CCl_4 mixtures as shown in figure (7.1). However, the behaviour of ^{13}C T_1 of the CH_3 group does not seem very sensitive to the influence of those changes in concentration, perhaps because of the averaging due to internal motion which dominate the T_1.

The NOE factor for the ring carbons (CH) in mesitylene-CCl_4 and Me-C_6H_{12}-TMS mixtures are reported in tables (7.1),(7.2) which are illustrated graphically in Figure (7.5) (7.6). These values of η agreed with those reported from the Literature in table (7.3).

Table (7.3)

Literature values of ^{13}C T_1's and NOE for mesitylene

T_1 sec		**NOE(η)**		**condition**	**T°C**	**reference**
CH(ring)	CH_3	CH(ring)	CH_3			
				undegassed		
7.8	11.9	2	1	neat	40	(137)
				degassed		
5.7		2		neat	23±2	(156)
9.3		2		50% $^{V}/_{V}$ in i-C_5H_{12}	23±2	(156)

It can be seen that there is no systematic variation in η in either series and it may be reasonably assumed that T_{1c}, contains little or no intermolecular contributions. However, the averaged values of 1.91 and 1.93 for the NOE in Me-CCl_4 and Me-Cy-TMS respectively are marginally less than the theoretical maximum of 1.988.

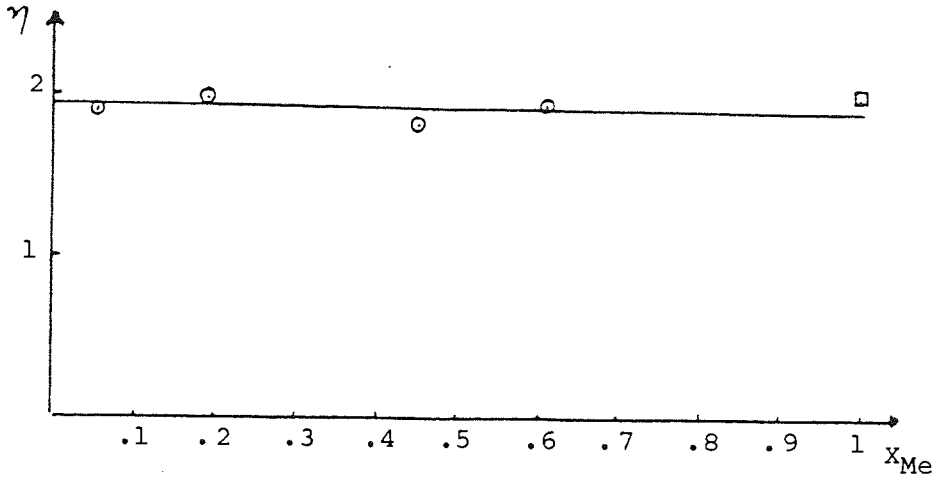

Figure 7.5 The variation of η(NOE) for ^{13}C-H nuclei of mesitylene in CCl_4 with the mole fraction of mesitylene.

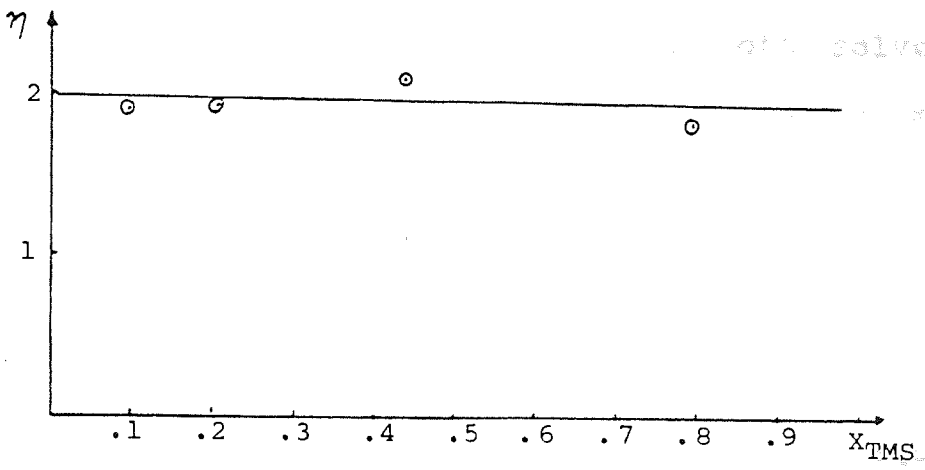

Figure 7.6 The variation of η(NOE) for ^{13}CH nuclei of mesitylene in TMS-cyclohexane mixtures, with the mole fraction of TMS

Therefore, it is probable that the T_{1c} contains a small contribution from spin-rotation or chemical shift anisotropy. The C.S.A contribution was found to be negligible for the ^{13}C-H nuclei of mesitylene in CCl_4 (X_{Me}=0.545), where it was obtained T_1=6.6 sec. at 270 MHz and T_1=6.7 sec. at 90 MHz. The dipolar-dipolar contribution to T_1 will be calculated using η average in equation 7.4.

Tables (7.4) and (7.5) contains the dipolar components of the ^{13}C relaxation rates $T_{1intra}^{-1\ C}$ deduced from the observed rates T_{1obs} and $\langle\eta\rangle$ using equation (7.4). The observed proton relaxation rates given in tables (7.4)(7.5) have been devolved into the intra, and intermolecular contributions using equation (7.3) with the value of A_H/A_C=39.0/131.6 for both solvent systems. This has been possible without recourse to the theoretical estimation of any terms such as A or τ_{eff}. With the information of the intramolecular and intermolecular proton relaxation rates it is now possible to use these together with the corresponding ^{13}C rates to obtain reliable correlation times, τ_{eff}. Equation (7.1) contains a definition of the molecular constant A and this was used to calculate the aryl hydrogen and methyl hydrogen contributions to A_C and A_H given in Table (7.6). Because the methyl group is a free rotator the effect of this group was deduced by considering it to be represented by 3 hydrogen atoms located at the centre of the base of the cone defined by the motion of the C-H bonds. Using the values of A_C and A_H given in table

(7.6) with $T_{1intra}^{-1\ C}$ and $T_{1intra}^{-1\ H}$ (Tables 7.4 and 7.5) values for τ_{eff} were calculated via equation (7.2). These are given in tables (7.7) and (7.8). Whilst it can be seen that the two values of τ_{eff} deduced for any one sample are similar, they are not identical. The reason for this is probably due to the crudity of the representation of the methyl group. By increasing the separation of the H_3 centre from the molecular centre, along the CH_3 three-fold axis, by 0.1258 Å (from 3.299 Å) almost identical values for τ_{eff} are obtained from the ^{13}C and ^{1}H data in any one sample. The corrected values for τ_{eff} are given in tables (7.7) and (7.8).

Knowing τ_{eff} it is now possible to deduce the individual contributions to $T_{1intra}^{-1\ H}$. This is composed of terms ρ_{HH} and ρ_{HCH_3} that are caused respectively by the dipolar interactions of the aryl and methyl hydrogens according to equation (7.6)

$$T_{1intra}^{-1\ H} = \rho_{HH} + \rho_{HCH_3} \qquad (7.6)$$

Using the values of A_{HH} and AH_{CH_3} given in table (7.6) with the appropriate values of τ_{eff} permits the calculation of ρ_{HH} and ρ_{HCH_3}. Values for these are given in tables (7.9) and (7.10). As is to be expected, the relaxation rate caused by the methyl groups is far higher than that caused by the aryl hydrogens because the former contain more dipoles that are closer to the resonant nuclei than the other aryl hydrogen.

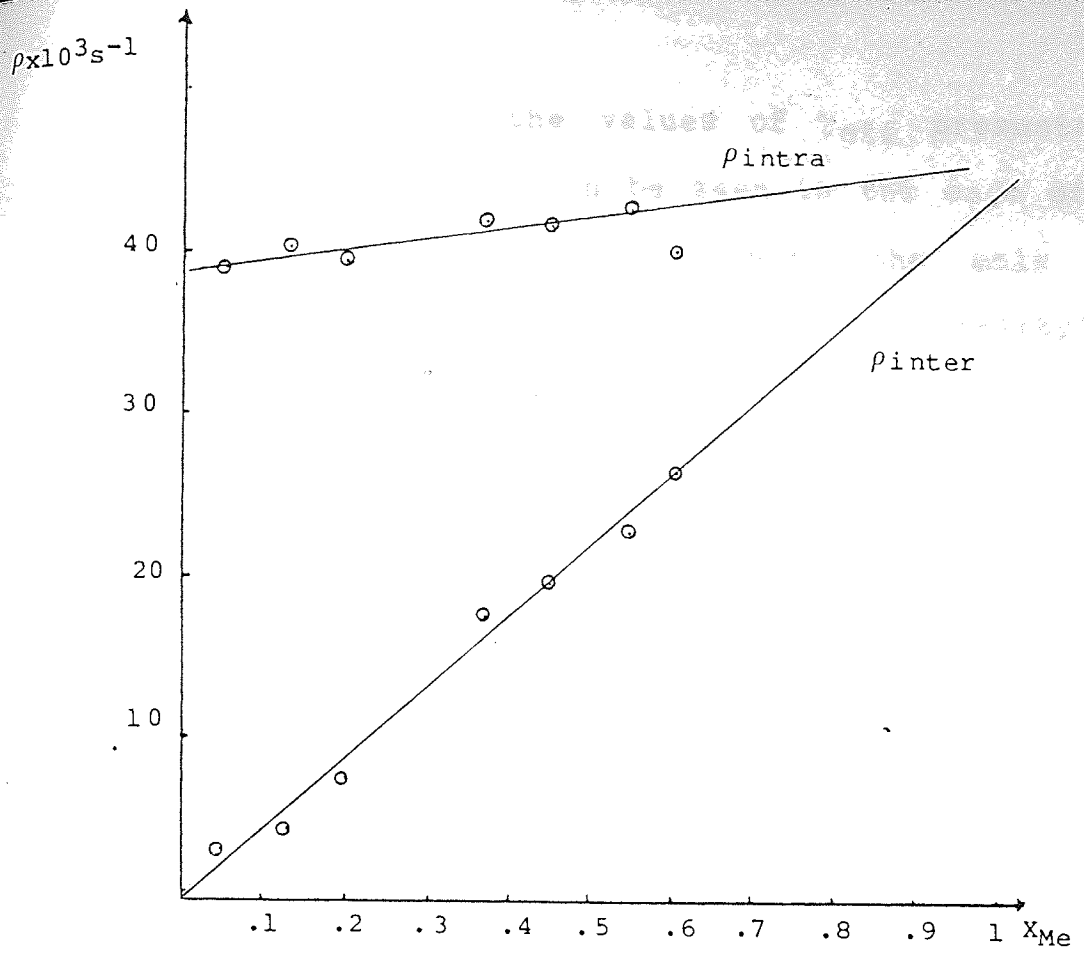

Figure 7.7 The variation of ρintra, ρinter for ^1H ring protons of mesitylene in CCl_4 with X_{Me}.

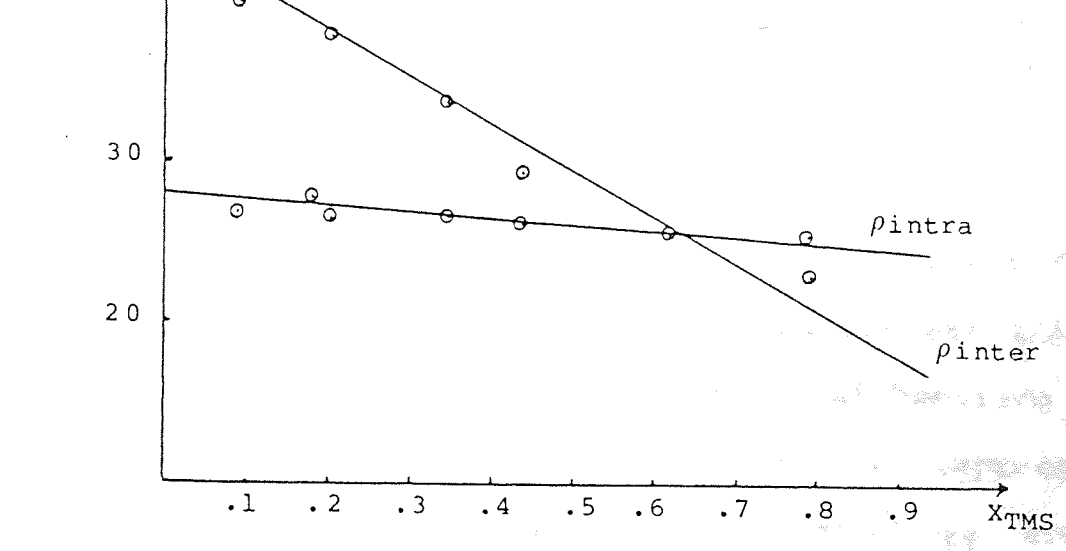

Figure 7.8 The variation of ρintra, ρinter for ^1H ring protons of mesitylene in TMS-cyclohexane mixtures, with X_{TMS}

Returning to the values of τ_{eff} presented in tables (7.7) and (7.8) it can be seen in the case of mesitylene/CCl_4 that τ_{eff} increases with the mole fraction of mesitylene. Because the viscosity of mesitylene is less than that of CCl_4 the above observation is contrary to the prediction of the Debye equation $\tau_r = 4\pi\eta a^3/3KT$. This could be due to the existence of "slip boundary" conditions at high concentration of CCl_4 which would have the effect of reducing the effective viscosity and hence τ_{eff}. In the case of the C_6H_{12}/TMS system τ_{eff} decreases with increasing mole fraction of TMS. This variation is consistent with viscosity considerations but might also be enhanced by the existence of "slip boundary" conditions at high concentrations of TMS.

According to Gutowsky and Woessner the intermolecular proton relaxation rates given in tables (7.4) and (7.5) should be capable of explanation through equation (7.7)

$$\frac{1}{T_{1(inter)i}} = \frac{\pi\hbar^2 \gamma_i^2 N}{a^2}\left[6\gamma_i^2 \Sigma {}^1/_{r_{ij}^{\circ}} + \frac{16}{3}\gamma_f^2 (I_f+1) I_f \Sigma^* {}^1/_{r_{if}^{\circ}}\right]\tau_{trans}. \qquad (7.7)$$

where ${}^1/_{r_{ij}^{\circ}}$ is the mean value of ${}^1/_{r_{ij}}$ for two molecules in contact, N is the number of nuclei per unit volume and the summations are over nuclei of neighbouring molecules τ_{trans} in equation (7.7) may be represented by the Stokes-Einstein relation $\tau_{trans} = \pi\eta a^3/2KT$ from which it can be seen that the values of $T_{1inter}^{-1}{}^H$ given in tables (7.4) and (7.5) should, like their intramolecular

Table (7.4)

Relaxation rates x $10^3 sec^{-1}$ for the aromatic carbons and hydrogen of mesitylene in mixtures with CCl_4

X_{Me} (a)	T_{1obs}^{-1} C	T_{1intra}^{-1} C	T_{1obs}^{-1} H	T_{1intra}^{-1} H	T_{1inter}^{-1} H
0	137.0	131.6	39.0	38.99	0.01
0.05	137.0	121.6	42.2	38.99	3.21
0.129	141	135.5	44.54	40.16	4.38
0.199	138.8	133.4	46.73	39.53	7.2
0.368	147	141.2	59.52	41.84	17.68
0.451	144.9	139.2	60.75	41.25	19.5
0.545	149	143.2	65.23	42.44	22.79
0.608	140.2	134.7	66.49	39.92	26.57
1.0(a)	154	148.0	88.03	43.86	44.17

(a) Extrapolated data

Table (7.5)

Relaxation rates x 10^3 sec^{-1} for the aromatic carbons and hydrogens of mesitylene in mixtures with C_6H_{12} and TMS

X_{TMS}	T_{1obs}^{-1} C	T_{1intra}^{-1} C	T_{1obs}^{-1} H	T_{1intra}^{-1} H	T_{1inter}^{-1} H
0(a)	95	92.2	71.0	27.32	43.68
0.09	93.8	91.1	66.8	27.0	39.80
0.18	97	94.2	68.03	27.92	40.11
0.207	90.9	88.2	64.00	26.14	37.86
0.345	91.6	88.9	59.98	26.35	33.63
0.44	91.4	88.7	55.58	26.29	29.29
0.62	88.5	85.9	50.76	25.46	25.30
0.79	88.1	85.5	48.31	25.34	22.97
0.93(a)	84.0	81.6	40.0	24.18	15.82

(a) Extrapolated data

Table (7.6)

Data relevant to the calculation of A_C and A_H

r_C P3-H	1.09Å
r_{CS} P2-H	1.09Å
$r_{CSP^2-CSP^2}$	1.395Å
$r_{CSP^2-CSP^3}$	1.54 Å
γ^1_H	2.6753×10^4 rad S^{-1}gauss^{-1}
γ^{13}_C	0.6728×10^4 rad S^{-1} gauss^{-1}
A x 10^{-10} sec^{-2}	
A^{13}_{CH}	2.15228
$A_{13_{CCH_3}}$	0.03980
A_C	2.19208
A^1_{HH}	0.02700
$A^1_{HCH_3}$	0.74459
A_H	0.77159

Table 7.7

Rotational correlation times ($\tau_{eff} \times 10^{12}$ sec) for mesitylene in mixtures with CCl_4

X_{Me}	$\tau_{eff} \times 10^{12}$ S		Rationalized $\tau_{eff} \times 10^{12}$S	
	^{13}C	^{1}H	^{13}	^{1}H
0	6.003	5.053	6.026	5.984
0.05	6.003	5.053	6.026	5.984
0.129	6.181	5.205	6.204	6.164
0.199	6.086	5.123	6.108	6.067
0.368	6.441	5.422	6.465	6.422
0.451	6.350	5.346	6.374	6.331
0.545	6.533	5.500	6.557	6.514
0.608	6.145	5.174	6.168	6.127
1.0	6.752	5.684	6.777	6.732

Table (7.8)

Rotational correlation times τ_{eff}, for mesitylene in mixtures with C_6H_{12} and TMS (X_{Me}=0.07)

X_{TMS}	$\tau_{eff} \times 10^{12}$ S		Rationalized $\tau_{eff} \times 10^{12}$S	
	^{13}C	^{1}H	^{13}C	^{1}H
0	4.206	3.541	4.222	4.193
0.09	4.156	3.499	4.171	4.144
0.18	4.297	3.618	4.313	4.285
0.207	4.024	3.388	4.039	4.012
0.345	4.056	3.415	4.071	4.044
0.44	4.046	3.407	4.061	4.034
0.62	3.919	3.300	3.933	3.908
0.79	3.900	3.284	3.915	3.889
0.93	3.723	3.134	3.736	3.711

Table 7.9

Contribution to the intramolecular aryl proton relaxation rate of mesitylene in mixtures with CCl_4

X_{Me}	$\rho_{HH} \times 10^3 s^{-1}$	$\rho_{HCH_3} \times 10^3 s^{-1}$
0	1.616	37.374
0.05	1.616	37.374
0.129	1.664	38.499
0.199	1.638	37.892
0.368	1.734	40.109
0.451	1.710	39.541
0.545	1.759	40.684
0.608	1.654	38.267
1.0	1.818	42.045

Table 7.10

Contribution to the intramolecular aryl proton relaxation rate of mesitylene in mixtures with C_6H_{12} and TMS

XTMS	$\rho_{HH} \times 10^3 s^{-1}$	$\rho_{HCH_3} \times 10^3 s^{-1}$
0	1.132	26.188
0.09	1.119	25.882
0.18	1.157	26.762
0.207	1.083	25.057
0.345	1.092	25.257
0.44	1.089	25.195
0.62	1.055	24.408
0.79	1.050	24.289
0.93	1.002	23.177

counterpart, vary linearly with viscosity. However, it is evident from equation (7.7) that $T_{1inter}^{-1\ H}$ can depend on small changes in internuclear distances and more importantly on dipolar nuclear density. The data in table (7.4) suggest that N plays the dominant role in governing the variation $T_{1inter}^{-1\ H}$. In the other system covered by table (7.5) both solvents have the same number of protons per molecule (the basis of their choice). However, because the macroscopic density of TMS is less than that of C_6H_{12} (0.6021 g cm^{-3}), and (0.7693 g cm^{-3}) respectively it is evident once again that N dominates the variation of $T_{1inter}^{-1\ H}$ with the composition of the mixture studied.

It can be pointed out here that the variations of τ_{eff} in tables (7.7) and (7.8) with η yield values of $4\pi\eta a^3/3KT$ from the Debye equation that are a factor of ~40 larger than the theoretical estimate.

The ^{13}C method used in the calculation of the intramolecular contributions to T_1 of the ring protons in mesitylene seems to be quite reliable. With this basis, the intra and intermolecular contribution to T_1 will be calculated by several theories to assess their validity.

7.3.A Analysis of the intramolecular contribution to T_1

a) Prediction of T_{1intra} using the Gutowsky-Woessner equation (7.1) with the BPP and Hill theories.

The G.W. equation (7.1) for the ring proton of mesitylene is

$$T_{1intra}^{-1} = A_H \tau_r \qquad (7.8)$$

where A_H is given in table (7.6). It emerges that

$$T_{1intra}^{-1} = 0.0077159 \times 10^{12} \tau_r \ sec^{-1} \qquad (7.9)$$

In order to predict T_{1intra}^{-1}, it is necessary to use a suitable model for τ_r eg. B.P.P. or the Hill theories as indicated in equations (7.10) and (7.11)

$$\tau_{BPP} = \frac{4}{3} \pi a^3 \frac{\eta}{KT} \qquad (7.10)$$

$$\tau_{Hill} = K_A^2 \frac{\eta_{AB} \sigma_{AB}}{KT} \qquad (7.11)$$

where $K_A^2 = i_{AB}/\mu$, with $i_{AB} = \frac{I_{AB} I_A}{I_{AB}+IA}$

The values of a were estimated using the closest packing equation $4/3 \pi Noa^3 = 0.74$ Vm. These parameters are presented in table (7.11). The values of T_1^{-1} deduced using equation (7.8) are presented in table (7.12). These results show that the Hill based correlation time is the more accurate. Its value for mesitylene in TMS is very close to the one determined by the ^{13}C method. The most probable reason for the discrepancy in C_6H_{12} is that the Hill equation is still too imprecise.

b) Variations in T_{1intra} based on the BPP and Hill models.

The experimental results shown in table (7.5) can serve as true values of ρ_{intra} to test the ability of the Hill and BPP theory to correct them from TMS to C_6H_{12} and viceversa. Thus, as indicated in chapter 5, the value of $\rho_{intra\ y}$ and $\rho_{intra\ x}$ for the extremes x,y, in table (7.5) are:

$$\rho_{intra\ y\ calc} = \rho_{intra\ x\ exp}\ f_{1\ BPP} \qquad (7.12)$$

with

$$f_{1\ BPP} = \eta''/\eta' = 0.3384$$

where η', η'' are the viscosities of mixtures of mesitylene in C_6H_{12}, TMS indicated on table (7.11) and

$$\rho_{intra\ y\ calc} = \rho_{intra\ x\ exp}\ f_{1\ Hill} \qquad (7.13)$$

where

$$f_{1\ Hill} = \frac{\mu_{AC}}{\mu_{AB}}\ \frac{\eta_{AB}}{\eta_{AC}}\ \frac{\sigma_{AB}}{\sigma_{AC}} = 0.5817$$

The f_1Hill factor is calculated from table (7.11). When the values of $\rho_{intra\ x\ calc}$ are required, the correction factor must be inverted. Table (7.13) shows the results of this test, which again indicate that the Hill theory

Table 7.11

Parameters used in the evaluation of T_{1intra} through equation (7.8)

compound	μ	K_A	η_{AB} σ_{AB}	η	I	a	Vm
	g	$x10^{17}$ g cm^2	C.P.Å.	C.P.	$x10^{40}$ g cm^2	Å	cm^3
TMS	50.88	60.2	2.493	0.242	143	3.5	146.5
C_6H_{12}	49.5	61.34	4.171	0.715	236.9	3.17	109.4
Me	--	--	--	--	548	3.45	140

where μ, K_A, $\eta_{AB}\sigma_{AB}$, η, refer to mesitylene (X_{Me}=0.07) in TMS and C_6H_{12}(CY)

Table (7.12)

Intramolecular contribution to T_1 of the ring proton of mesitylene calculated for several model with equation (7.8)

	BPP		Hill		^{13}C method (b)	
solvent	CY	TMS	CY	TMS	CY	TMS
τ_r(psec)	29.4	9.95	6.12	3.59	4.22	3.74
T_1^{-1}intra $x10^3$ sec^{-1}	226.8	76.8	47.2	27.7	27.3	24.2
T_{1intra} sec	4.4	13.0	21.2	36.1	36.6	41.3
$\frac{\Delta T_1}{T_1}$ % (a)	88	69	42	12.6	--	--

(a) this % is evaluated respect data in (b), which are taken from table (7.8) and (7.5)

Table 7.13

Intramolecular relaxation times calculated using the Hill and BPP theories on extremes x,y in table (7.5)

(X,Y) x 10^2	BPP	Hill
ρintra y exp	2.42	2.42
ρintra y calc	0.91	1.57
%	62	36
ρintra x exp	2.73	2.73
ρintra x calc	7.15	4.16
%	165	54

gives good approximation to the true values of T_{1intra}. However, neither the BPP nor the Hill theories are satisfactory

7.3.B Analysis of the intermolecular contribution to T_1

The intermolecular contribution to T_1 for the ring proton of mesitylene can be estimated from the values of ρ_{intra} indicated in table (7.5) and are considered to be the true values of ρ_{inter}. Using these results, the Gutowsky-Woessner equation (7.7), the Hill and BPP models can be tested.

a) The Gutowsky-Woessner equation

The G.W. equation (7.7) can be tested using the Stokes-Einstein relation $\tau_{trans} = \pi\eta a^3/2KT$ resulting in

$$T^{-1}_{1inter} = 3\pi^2\hbar^2\gamma^4\eta N \frac{a}{KT}\frac{1}{r_o} \qquad (7.14)$$

From this equation for $r_o=2a$ the values of ρ_{inter} for the ring proton of mesitylene ($X_{Me}=0.07$) in mixtures of C_6H_{12} and TMS as solvent can be calculated. The results are shown in table (7.14) which includes also the results of using the buffeting correction factors $(2\beta-\xi)^2$ and $(2\beta-\xi)^{-2}$. It can be seen in this table that for TMS the G.W. value is close to the "true" value. But there is no indication of improvement after using the empirical buffeting factors from table (6.10)

b) Test on the BPP and Hill models.

A test similar to the one applied to the intramolecular model II (Hill) and III (BPP), can be used on the values of ρinter reported in table (7.5). Thus in equation (7.15) the extreme of the table (7.5) ρinter $_x$ is used to calculate the other extreme ρinter $_y$ by using a correction factor f_2 i.e.

$$\rho \text{inter}_{\,y\ \text{calc.}} = \rho \text{inter}_{\,x}\ f_2\ \text{BPP} \qquad (7.15)$$

with

$$f_2\ \text{BPP} = \frac{N''\,\eta''}{N'\,\eta'} = 0.259$$

where N", N', η', η" are data reported in chapter 6. similarly

$$\rho \text{inter}_{\,y\text{calc}} = \rho \text{inter}_{\,x}\ f_2\ \text{Hill} \qquad (7.16)$$

with

$$f_2\ \text{Hill} = \frac{N''}{D''}\ \frac{D'}{N'} = 0.50428$$

where D', D" are the diffusion coefficients reported in table (6.7).

Table (7.15) shows the results of equations (7.15) and (7.16) applied to the extremes x,y of table (7.5). It is difficult to decide which model is better because both have the same degree of inaccuracy. The combination of

Table 7.14

Intermolecular contribution to T_1 of the ring protons of mesitylene calculated from the Gutowsky-Woessner equation (7.14)

solvent	ρ_{inter} (a) x 10^2 sec^{-1}	ρ_{inter} (b) x 10^2 sec^{-1}	(b) $\rho_{inter}(2\beta-\xi)^2$ x 10^2 sec^{-1}	(b) $\rho_{inter}(2\beta-\xi)^{-2}$ x 10^2 sec^{-1}
TMS	1.58	2.41	1.12	5.18
C_6H_{12}	4.37	9.3	7.75	11.15

a) refer to the ρinter values on the extremes x,y of table (7.5)

b) refer to the values calculated from equation (7.14)

Table (7.15)

Intermolecular contribution to T_1 of the ring protons of mesitylene calculated using the Hill and BPP models on the extremes x,y of table (7.5)

(X,Y)x10^2sec^{-1} buffeting factor(a)	BPP	Hill	BPP $(2\beta-\xi)^2$	Hill $(2\beta-\xi)^2$	BPP $(2\beta-\xi)^{-2}$	Hill $(2\beta-\xi)^{-2}$
ρinter y exp 1.58						
ρinter y calc	1.13	2.2	0.64	1.24	2.04	3.97
%	28%	40%	60%	22%	29%	151%
ρinter x exp 4.37						
ρinter x calc	6.1	3.1	11	5.6	3.4	1.7
%	39%	29%	148%	27%	22%	60%

(a) the buffeting correction is applied as in equation (6.20)

ρintra exp + ρinter calc. for both models give similar accuracy when compared with T_1^{-1} observed. Also, it is noticed that ρintra calc Hill + ρinter calc Hill agrees better with T_1^{-1} observed than the combined ρintra calc Hill + ρinter calc. BPP value. From this point of view, the Hill model gives a good result, but as suspected, this appears to be due to opposing errors in the intra and intermolecular terms. In conclusion the evidence presented in table (7.15) does not yet permit the decision about whether the intermolecular contribution can be represented by the BPP or the Hill model

7.3.C Buffeting correction $1-\frac{2}{3}(2\beta-\xi)^2$

The G.W. equation depends on the closest distance of approach of molecules and if this varies so may T_{1inter}. Normally the evaluation of such distances would not take into account constraints of collisional processes. However, such constraints are implicit in the buffeting approach to σw. It would appear desirable therefore, to investigate whether terms of the type $(2\beta-\xi)^2$ can be used to improve the characterization of intermolecular relaxation rates. In consequence we will review some of the basic principles to obtain a better approach.

The buffeting contribution to the Van der Waals screening term σw, is calculated from equation (7.17)

$$\sigma w = -B \langle E^2 \rangle \qquad (7.17)$$

using

$$\vec{E} = 3\,(\vec{m}.\vec{r})\,\frac{\vec{r}}{r^5} - \frac{\vec{m}}{r^3} \qquad (7.18)$$

it was shown by Percival (51) that

$$\langle E^2 = (2\beta-\zeta)^2\,\frac{\text{constant}}{r^6} \qquad (7.19)$$

so equation (7.17) becomes

$$\sigma_{BI} = -\frac{B.K}{r^6}\,(2\beta-\zeta)^2 \qquad (7.20)$$

In this approach, the buffeting contribution to the screening should be zero for isotropic systems i.e. (β=1 and ζ=2).

The magnetic field generated by a magnetic dipole $\vec{\mu}$ at a distance $\vec{r}$ is given by (55)

$$\vec{B} = 3\,(\vec{\mu}.\vec{r})\,\frac{\vec{r}}{r^5} - \frac{\vec{\mu}}{r^3} \qquad (7.21)$$

which is similar to equation (7.18). The expression of T_1^{-1} in terms of the local magnetic field is (16).

$$T_1^{-1} = \gamma^2\,[\,\bar{B}x^2 + \bar{B}y^2\,]\,\tau_c \qquad (7.22)$$

From this equation, we can establish an analogy with the case of σ_w in equation (7.17). For T_1^{-1} the magnetic field interaction only includes Bx, By because the field Bz does not affect T_1, so the overall contribution from

the local magnetic field assuming isotropic systems is $^2/_3\ B^2_{LOC}$

The buffeting contribution to T_1^{-1} would be expected to depend on $(2\beta-\xi)^2$ but notice has to be taken of the fact that for isotropic collisions σ_w is a minimum whereas the analogous contribution to T_1^{-1} must be a maximum. Consequently, one possible expression for the buffeting contribution to T_1^{-1} could depend on $1-(2\beta-\xi)^2$. However, we have to consider that the overall contribution from the magnetic field is $\frac{2}{3}\ B^2_{LOC}$ so that the buffeting factor would then be $1-\frac{2}{3}\ (2\beta-\xi)^2$.

This proposed buffeting correction will now be applied to the Gutowsky-Woessner equation (7.14), the BPP and the Hill models for intermolecular contribution to T_1.

The values of $1-\frac{2}{3}\ (2\beta-\xi)^2=f_B$ for mesitylene in TMS and C_6H_{12} are:

in C_6H_{12} $\quad fB = 0.4443$

in TMS $\quad f_B = 0.6899$

Table (7.16) shows the values of ρ_{inter} calculated using the Hill and BPP models that were presented in table (7.15) and the Gutowsky-Woessner (G.W.) values in table (7.14). But with these values multiplied by the buffeting factor f_B or h_B; h_B for TMS is $f_B(TMS)/f_B(C_6H_{12})$ and the inverse of h_B is used for C_6H_{12}. The results obtained for the BPP model and the (G.W.) equation are quite good. In addition to that, table (7.17) shows the

Table 7.16

Comparative results of ρinter calculated in tables (7.14) and (7.15) after buffeting correction by $1-\frac{2}{3}(2\beta-\xi)^2$

ρ x 10^2 sec^{-1} solvent	TMS	C_6H_{12}	% TMS(c)	$\%C_6H_{12}$ (c)
ρinter (a)	1.58	4.37	---	---
ρinter calc (Hill)	2.2	3.13	40%	29%
ρinter calc (BPP)	1.13	6.1	28	39
ρinter (G.W.)	2.41	9.3	53	112
ρinter calc (Hill)xh_B(b)	3.42	2.0	117	54
ρinter calc (BPP)xh_B(b)	1.75	3.9	12	10.5
ρinter (G.W.) f_B	1.66	4.13	5	6

a) refer to the intermolecular values of the extremes x,y in table (7.5)

b) h_B is the ratio f_B (TMS)/f_B C_6H_{12} when applied in TMS solvent and the inverse when applied to C_6H_{12} solvent.

c) refer to the relation $\Delta\rho/\rho$ (a)

Table 7.17

Comparison of ρintra + ρinter evaluated from two methods with the observed T_1^{-1}(x10^2 sec^{-1})

solvent	T_1^{-1}observed	ρintra+ ρinter(a)	%	ρintra+ρinter(b)	%
TMS	4	4.1	2.5	4.2	5
C_6H_{12}	7.1	6.8	4	6.6	7

a) ρintra is taken from table (7.5), ρinter(a) refers to the (G.W.) values on table (7.14)

b) ρinter(b) refers to the BPP value in table (7.15)

calculation of the complete T_1^{-1} i.e ρintra + ρinter with ρintra taken from the values in table (7.5) for the extremes x,y and ρinter (a) refers to the (G.W.) equation after buffeting correction, ρinter (b) refers to ρinter calc.(BPP) after buffeting correction. Both methods produce very good values for T_1^{-1} which indicates that the buffeting correction factor $1-\frac{2}{3}(2\beta-\xi)^2$ can also be used in other systems.

7.4 Conclusions

Studies of the relaxation times and the nuclear Overhauser effect for the ring ^{13}C of mesitylene in solutions of CCl_4 and C_6H_{12}-TMS have been used in the evaluation of the intramolecular relaxation times for the ring protons of mesitylene. From these results the effective molecular correlation times for the rotation of mesitylene have been evaluated.

This approach to separate intra and intermolecular relaxation contributions has the advantage of its lack of dependence on any theoretical calculation.

The correlation times τ_r calculated from the Hill and BPP models were used with the Gutowsky-Woessner equation to evaluate the intramolecular contribution. It was found that the Hill theory gives better agreement with the true value.

The intermolecular contribution to T_1 was analysed using the G.W. equation and the BPP and Hill models but it was not possible to determine which model provides the best description of ρinter.

A buffeting contribution to T_1 was invoked by analogy with the work done on buffeting contribution to the Van der Waals screening term. An equation was proposed which takes into consideration the characteristics of molecular encounters and the properties of the relaxation times. The application of a buffeting correction to the G.W. equation for ρinter gave good agreement with that evaluated by the ^{13}C method. Also good results were achieved by using the BPP model that incorporated a buffeting correction. The overall result of calculating ρintra + ρinter based on the experimental value of ρintra deduced from ^{13}C methods and ρinter evaluated from G.W. equations or B.P.P. equations is to give close agreement with the observed T_1^{-1} value within 7 and 2.5% for the BPP or G.W. bases respectively. The unfortunate consequence of this is that the value of the widely favoured Hill theory is thrown into doubt.

CHAPTER EIGHT

Novel Methods for separating intra and intermolecular contributions to proton spin-lattice relaxation times

8.1 Introduction

In chapter seven the value of being able to unambiguously separate the intra and intermolecular contributions to proton spin-lattice relaxation times was illustrated. Because the procedure described therein depends on dilution studies it was considered desirable to search for alternative procedures that avoid dilution studies and facilitate the analysis of the T_1 in single samples. In the present chapter two procedures are described that fulfil the required objectives. The first method makes use of relaxation studies of ^{13}C proton satellite spectra and the second depends on intermolecular nuclear Overhauser studies.

8.2 Proton (^{13}C) Satellite Studies

The low natural abundance of ^{13}C (1.1%) assures that the resonances of hydrogen attached to ^{13}C correspond to those obtained from ^{12}C bound hydrogen in molecules at very low concentration in an appropriate solvent. Moreover, the satellite spectra uniquely identify hydrogen nuclei that may in ^{12}C molecules be part of a

set of equivalent spins. Evidently, studies of ^{13}C and ^{12}C bond hydrogen can provide different relaxation information. The present intention is to investigate whether the two sets of relaxation data can be used to yield intra and intermolecular contributions to proton spin-lattice relaxation times.

Because of the high concentration of hydrogen the proton satellite T_1 must contain both intra and intermolecular contributions. Nevertheless, in certain circumstances the unique identity afforded by hydrogen attached to ^{13}C can result in it having a different relaxation rate from that of the corresponding hydrogen bond to ^{12}C. This difference can be used to identify T_{1intra} and T_{1inter}.

In order to simplify matters the relaxation rates for hydrogen in a pure compound will be considered. Considering one magnetically unique hydrogen, i, an extension of the Solomon approach yields the rate equation

$$\frac{dI_i}{dt} = -R_i\,(I_{zi}-I_{oi}) - \sum_{i\neq j}\sigma_{ij}(I_{zj}-I_{oj}) - \sum_{x}\sigma_{ix}(I_{zx}-I_{ox}) \qquad (8.1)$$

where I is proportional to the integrated intensities of the resonance of the appropriate spin, R_i the total direct relaxation rate of spin i is given by

$$R_i = \sum_{j\neq i}\rho_{ij} + \rho_i^{*} \qquad (8.2)$$

where ρ_{ij} is the direct dipolar relaxation between spins i and j, and ρ_i^* is the direct relaxation of i due to other mechanisms not included in $\sum_{j \neq i} \rho_{ij}$ and for present purposes will be considered to arise from intermolecular dipolar interactions. The cross-relaxation terms, σ, are assumed to arise only from dipole-dipole interactions so that

$$\rho_{ij} = 2\,\sigma_{ij} \qquad (8.3)$$

If i in equation (8.1) refers to one magnetically unique proton in a ^{12}C molecule the change in its magnetic identity when attached to ^{13}C cannot alter the form of equation (8.1), although R_i contains an additional contribution, $\rho_i{}^{13}C$, due to the interaction with the ^{13}C dipole.

In order for ^{12}C and ^{13}C bond protons to have substantially different relaxation rates it is necessary for the hydrogen considered to be one of a set of N equivalent spins.

In the first instance one nucleus, S, out of N_S equivalent spins will be considered the subject of the measurements so that N_S-1 nuclei, labelled D, will be detected simultaneously but not the subject.

The other molecules in the bulk sample will be considered to contain solvent nuclei, X. The rate equation for the subject ^{12}C bound nucleus is

$$\frac{dI_S}{dt} = -R_S(Iz_S-Io_S) - \sum_{N_S-1} \sigma_{SD}(Iz_D-Io_D) - \sum_{X} \sigma_{SX}(Iz_X-Io_X) \qquad (8.4)$$

Because $Iz_D=Iz_S$ and $Io_D=Io_S$ equation (8.4) reduces to

$$\frac{dI_S}{dt} = -(R_S + \sum_{N_S-1} \sigma_{SD})(Iz_S-Io_S) - \sum_{X} \sigma_{SX}(Iz_X-Io_X) \qquad (8.5)$$

There are, of course, N_S equations of the type (8.5) but because each acts independently at the nuclear level only one need be considered. Nevertheless, because the individuals values of I are proportional to the total integrated signal intensities, the latter may be used with equation (8.5).

For inversion recovery, or progressive saturation experiments for systems having bi-exponential recovery rates it has been shown that semi-logarithm plots of (I_Z-I_O)vs t for the initial recovery data yield accurate values of the relaxation rate (220). The experimental relaxation rate R_{SS} may thus be determined and evaluated through equation (8.6)

$$R_{SS} = R_S + \sum_{N_S-1} \sigma_{SD} = \frac{3}{2} \rho_{intra} + \rho_{inter} \qquad (8.6)$$

If the same nucleus S is considered attached to ^{13}C this is now located in a system with (N_S-1) non equivalent spins (N). Consequently, the analogue of equation (8.4) is

$$\frac{dI_S}{dt} = -R_S'(I_{zS}-I_{oS}) - \sum_{N_S-1} \sigma_{SN}(I_{zN}-I_{oN}) - \sum_{X} \sigma_{SX}(I_{zX}-I_{oX}) \qquad (8.7)$$

By applying a saturating rf field at the position of the ^{12}C bound proton resonance not only are the satellite spectra reduced to single resonances but $Iz_N=Iz_X=0$. Consequently, equation (8.7) reduces to

$$\frac{dI_S}{dt} = -R_S'(I_{zS}-I_{oS}) + \sum_{N_S-1} \sigma_{SN}.I_{oN} + \sum_{X} \sigma_{SX}\, I_{oX} \qquad (8.8)$$

and R_S' can be obtained precisely from a conventional semi-logarithm plot of the appropriate data. However R_S' is now given by

$$R_S' = \rho_{intra}' + \rho_{inter} \qquad (8.9)$$

where

$$\rho_{intra}' = \rho_{intra} + \rho_{HC} \qquad (8.10)$$

Provided ρ_{HC} can be determined, equations (8.6) and (8.9) can be used to obtain ρ_{intra} and ρ_{inter}.

It is possible to estimate ρ_{HC} from $^{13}C-\{^1H\}$ nOe studies, because the observed ^{13}C relaxation time T_{1obs}^C is related to its dipole-dipole component and the nOe, η, by equation (8.11).

$$\sum_{N_S} \rho_{CH}^{-1} = T_{1DD}^C = T_{1obs}^C \quad \frac{1.988}{\eta} \qquad (8.11)$$

Implicit in this is the usual assumption that solvent contribution to ^{13}C relaxation times and nOe's are negligible. It should be noted that equation (8.11) yields $\sum_{N_S} \rho_{CH}^{-1}$ and not the required ρ_{CH}. However, the percentage of $\sum_{N_S} \rho_{CH}^{-1}$ attributable to ρ_{CH} can be estimated using the classical equation (8.12)

$$T_{1DD}^{-1\,C} = \hbar^2 \gamma_{13_C}^2 \gamma_{1_H}^2 \sum_{N_S} r_{CH}^{-6} \tau_C \qquad (8.12)$$

for which, in the present context, only values for the hydrogen-carbon distances r_{CH} are required.

Although the above approach appears attractive because of its simplicity it does have limitations that limit its applicability. In order to illustrate this the subject nucleus will again be considered one of a set of N_S equivalent spins in the ^{12}C molecule so that equations (8.5) and (8.6) again apply. If, however, the presence of ^{13}C results in S being one of a set of N_E equivalent spins, E, the appropriate rate equation is

$$\frac{dI_S}{dt} = -R_S''(I_{ZS} - I_{OS}) - \sum_{E \neq S} \sigma_{SE} (I_{ZE} - I_{OE})$$

$$- \sum_{N_S - N_E} \sigma_{SN} (I_{ZN} - I_{ON}) - \sum_{X} \sigma_{SX} (I_{ZX} - I_{OX}) \qquad (8.13)$$

which when the ^{12}C bound proton resonance is saturated reduces to

$$\frac{dI_S}{dt} = -(R_S'' + \sum_{N_E-1} \sigma_{SE})(I_{ZS}-I_{oS}) + \sum_{N_S-N_E} \sigma_{SN} I_{oN}$$

$$+ \sum_{X} \sigma_{SX} I_{oX} \qquad (8.14)$$

for which the measured rate constant R''_{SS} is

$$R''_{SS} = R_S'' + \sum_{N_E-1} \sigma_{SE} = \rho_{HC} + \rho intra + \frac{1}{2} \sum_{E \neq S} \rho_{HH} + \rho inter \qquad (8.15)$$

where $\sum_{E \neq S} \rho_{HH}$ is the total of the direct dipole-dipole effects on S of the remainder of the set of spins E. It follows that the intra and intermolecular effects can only be separated if $\sum_{E \neq S} \rho_{HH}$ as well as ρ_{HC} can be estimated.

In order to test the above proposals benzene 1,4 dioxane and mesitylene have been studied.

8.2.A The ^1H spectra of benzene, 1,4 dioxane and general considerations of satellite spectra

The proton magnetic resonance spectra of benzene and 1,4 dioxane are characterized by a central line and the appearance of small multiplet satellites signals on both sides of the main signal. Studies of the ^{13}C proton satellites lines are difficult due to the low 1.1% abundance of the ^{13}C isotope and thus the attached hydrogen. However, such studies can provide important information about the structure of the molecule. In particular, the "inner ^{13}C satellites", located within a

few Hertz of the resonance of protons bound to ^{12}C atoms (221) can be detected by using a second rf field B_2 to modulate the ^{13}C signal; changes caused by this will be transmitted to the coupled protons, whose signals are detected after substracting the modified spectrum from the normal proton signal by using a computer. In this way the "satellite spectra" are obtained free of interference from the main ^{12}C proton signal.

The external or outer satellite signals have been detected by using a special pulse technique (222) that has been demonstrated to give good S/N after 64 transients using non ^{13}C enriched acetaldehyde.

Some work on the relaxation of ^{13}C satellites in proton spectra has previously been reported. For instance Briguet et al (223)(224) have measured the proton relaxation time of $^{13}C^{1}HCl_3$ in natural abundance. Fujiwara and coworkers (225) have analysed the T_1 of the satellites in a sample of 40% ^{13}C enriched formic acid. London et al (226) have measured the proton relaxation times in 90% ^{13}C enriched aminosugars.

In the present work it is shown that the value of the ^{13}C proton satellite relaxation time can be used to obtain the values of the intramolecular and intermolecular contribution to the proton relaxation times of the molecules studied.

8.2.B Analysis of T_1 for ^{13}C proton satellites

In a system with two spins I, S the relaxation time of the spin I, can be measured after saturation of the spin S. The rate of recovery of the magnetization of I after a 180° pulse is:

$$R_I(\tilde{I},\bar{S}) = \frac{1}{T_{XI}} + \frac{1}{T_{1D}} \qquad (8.16)$$

where $\tilde{I}$ represents a 180° pulse, $\bar{S}$ represents the saturated spin and T_{XI} is a non dipolar interaction.

Freeman et al (221)(227) have shown that the initial recovery will have the same value as equation (8.16) $R_i^{\circ}(\tilde{I}) \cong R_I(\tilde{I},\bar{S})$ even without irradiation of the spins S, if the interval of time (t) considered in the measurement is small i.e. $t \ll 2T_{1D}$; in reality the recovery is governed by a double exponential equation. When the interval of time considered is longer, the situation will differ, eg. if $t = R_i^{\circ -1}$ with $T_{XS} \gg T_{1D}$ and $T_{1D} \simeq 2T_{XI}$, the value of R_I° will differ by 5% from R_I due to the effect of "cross relaxation" (220). If we use short values of t i.e. only the initial points in the semilog. plot of Mz vs t, we can be sure of making only small errors in the determination of T_1.

In the case of ^{13}C proton satellites, it is possible to reduce the multiplet satellite spectra to the type AB (^{13}C-^{1}H) by irradiation of the central signal with a

second rf field B_2, and use the above arguments to calculate T_1 from the experimental data.

8.2.C Experimental procedures

The experiments were carried out on benzene, 1,4 dioxane and mesitylene which were deoxygenated using the method described in chapter 4.

The relaxation times of the ^{13}C proton satellites were measured using inversion recovery and progressive saturation techniques; the 90° pulse was 45 μ sec. The double irradiation field B_2 was placed at the main signal ^{12}C-H with a power just enough to decouple the proton (S) attached to the ^{13}C isotope from the other intramolecular protons. As a result, a single line was detected for each satellite.

The ^{13}C relaxation times were measured by using the progressive saturation technique. In this case the 90° pulse was 24 μ sec. The ^{13}C N.O.E. factors η for samples studied were measured by using the Gated irradiation technique (196) waiting $5T_1$ between pulses when using continuous irradiation and 10 T_1 between gated pulses.

8.2.C1 Methods of detection

The ^{13}C proton satellite signals are very small. For example in the case of neat chloroform each satellite is

about 0.55% of the size of the main signal and therefore smaller than the spinning sideband signals that should be about 1-2% of the main peak. When the satellites signals are multiplets as in the case of benzene or 1,4 dioxane the signals are spread over a significant spectral width. In benzene the multiplet covers around 20Hz and is composed of 45 lines (228). As a result, the signal level is cut to 0.012% of the main peak.

The theoretical spectrum of 1,3,5-Trichlorobenzene (221) plotted in terms of increasing frequency in figure (8.1) gives a general idea of the location of the satellites with respect to the central signal.

Because of the difficulty of observing satellite spectra the experiments were done first using the R12 Perkin Elmer n.m.r. instrument. And the results were compared with those obtained from the ^{13}C spectra obtained using the FX90Q spectrometer. Table (8.1) shows that the coupling constant $J(^{13}C-H)$ for benzene, mesitylene and 1,4 dioxane can be measured from the proton spectra or the ^{13}C spectra; the ^{13}C spectra were obtained in the irradiation mode NON(no r.f. irradiation).

The ^{13}C proton satellites of benzene, because of the spectral multiplicity and the dynamic range of the FX90Q are very difficult to observe. However, the detection is greatly improved by using an r.f. irradiation field B_2

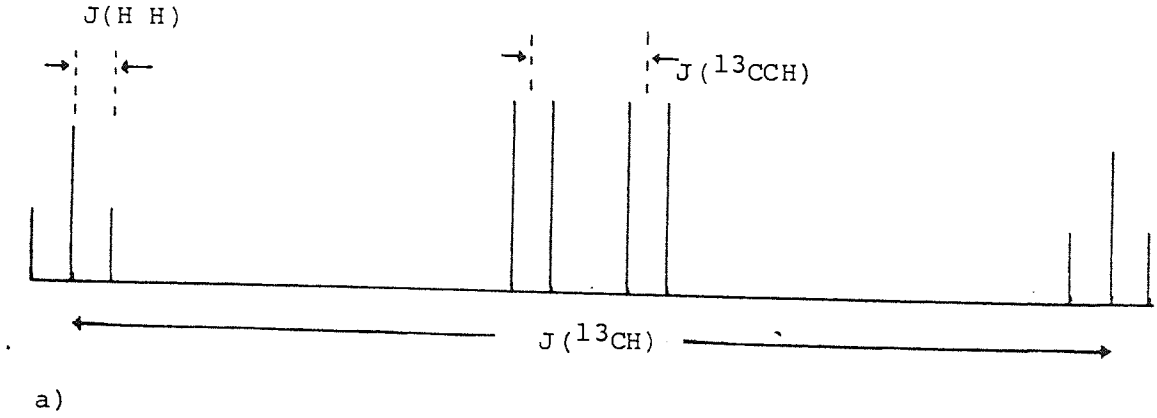

a)

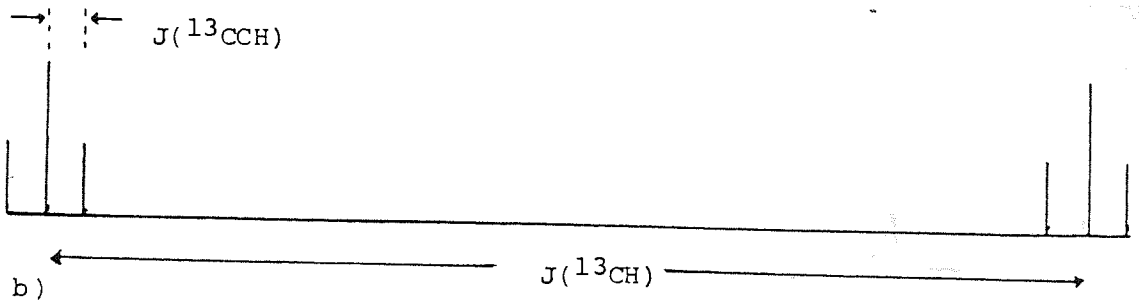

b)

Figure 8.1 Theoretical spectra of 1,3,5 trichlorobenzene
a) Proton spectrum
b) ^{13}C spectrum

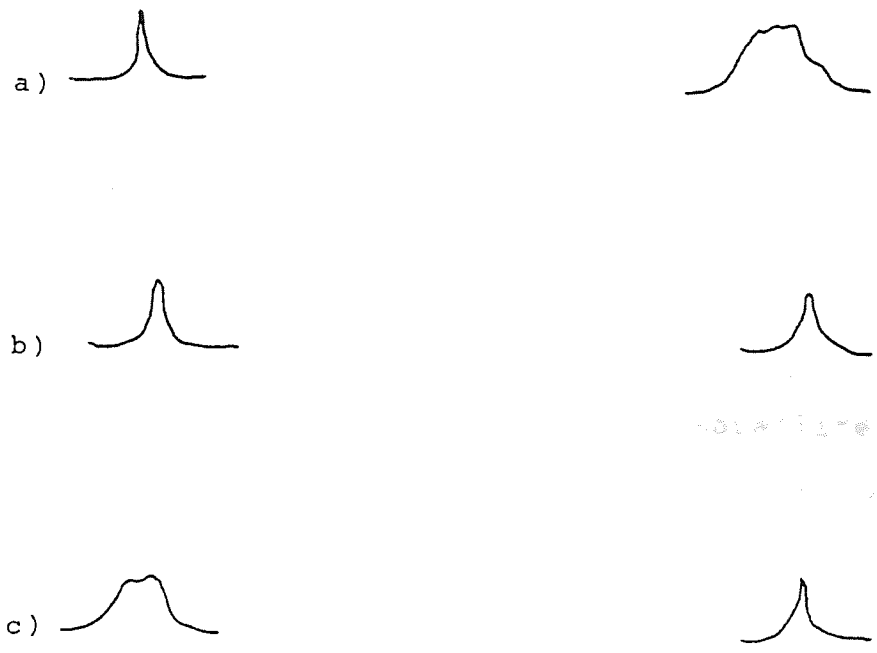

Figure 8.2 ^{1}H benzene spectra showing only the ^{13}C proton satellites at three different irradiation settings.
a) offset 54.680 KHz
b) offset 54.675 KHz
c) offset 54.670 KHz

applied at the main signal as shown in figure (8.2b). The effect of this is to produce single line spectra of improved S/N

8.2.C2 Effect of B_2

When a second r.f. field B_2 is applied at the position of the normal central proton peak of benzene, the satellites become sharp singlets if the irradiation frequency is at the right place and of the appropriate power. From a ^{13}C spectrum of benzene it was observed that the secondary proton (o,m,p) coupling results in multiplets covering 20Hz. If we compare this with figure (8.1), the conclusion is that the "inner spectra" at the main signal of benzene may be spread over 20Hz; this is more or less consistent with the satellite spectra of figure (8.2) where the irradiation field is applied at 54.675 $\pm$ 0.005 KHz of irradiation offset. However, because the B_2 r.f. power does have a finite bandwidth, it can be expected that some irradiation still occurs outside this frequency range.

The working conditions for B_2 in the studies of benzene were irradiation level highx5.5 and at 54.675 KHz of irradiation offset. For 1,4 dioxane the corresponding conditions were high 5.5 and 54.390 KHz (high 5.5 refers to an irradiation level of 55 decibels according to figure (8.3) from the Jeol instruction manual). Figure (84b) shows how the line width of the satellite envelopes

changes with the irradiation level. The optimum value of the line width in this experiment is $\Delta\omega \approx 2$Hz and this was obtained with B_2 set at high 5.5 and irradiation offset frequency 54.675 KHz. For slight changes in the frequency setting ($\pm$ 1Hz) changes could be detected in the appearance of the residual satellite lines which sometimes split into two signals. This occurs because of the differing extents to which the irradiation field saturates the different lines in the inner satellite spectra. When the r.f. field B_2 is increased from high 5, as indicated in figure (8.4a) the separation between the satellites changes, i.e. the coupling constant $J(^{13}C\text{-}H)$ has become a residual coupling Jr, as happens with standard ^{13}C spectra (229). From this variation it is possible to calculate the homodecoupling r.f. power.

One advantageous effect of the irradiation field B_2 is to saturate the main signal and allow the detection of the satellites signal with more dynamic range. The signals detected by the receiver are: signal= $\varphi^{12C\text{-}H}$signal + B_2signal + side band + satellites + noise when the detection is performed with homodecoupling irradiation mode which uses time sharing between the acquisition of the data and irradiation; the amount of perturbation arising from B_2 is at about the noise level. As has been shown in figure (8.2), the identification of the satellites signals is then possible and their variation with pulse sequence can be used to obtain the appropriate relaxation time.

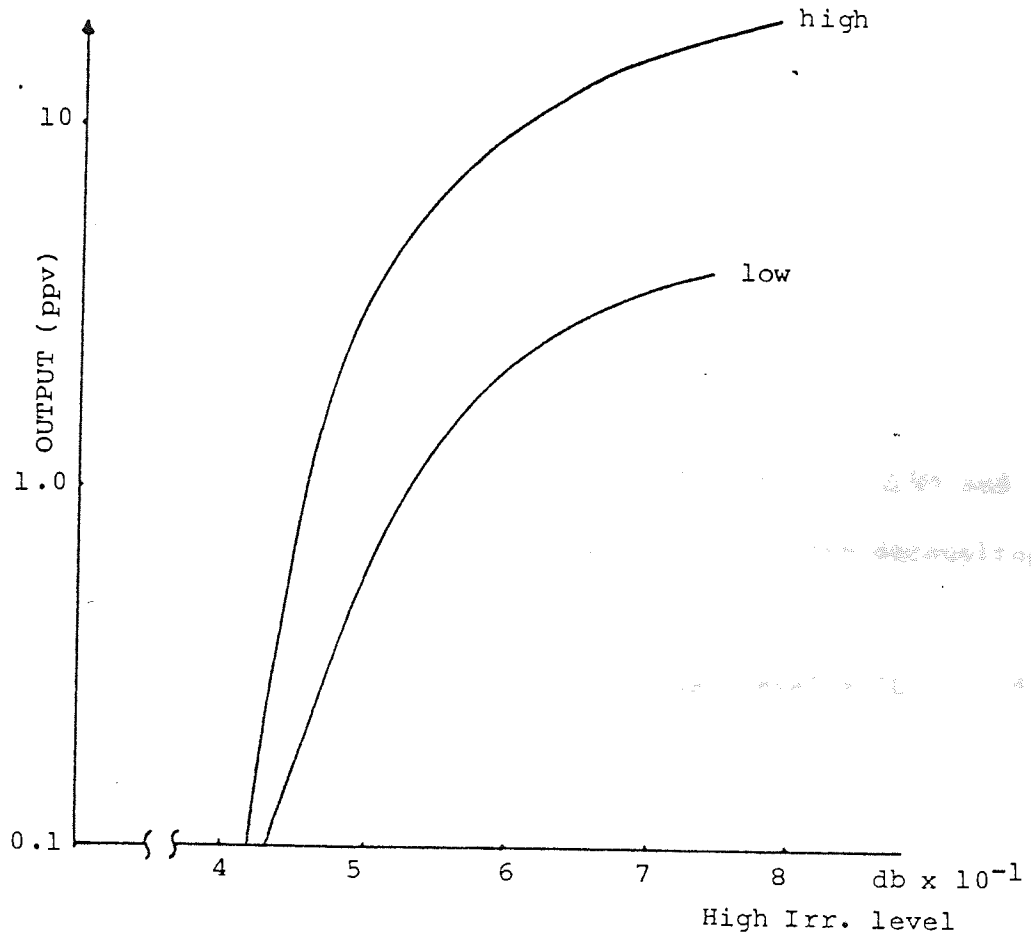

Figure 8.3 Typical R.F. OUTPUT (Homo decoupling AMP).

Table 8.1

Measurements of J(^{13}C-H) coupling constant in benzene, mesitylene and 1,4 dioxane from ^{1}H spectra and ^{13}C spectra

Compound	J(^{13}C-H) H_z	Spectra	Spectrometer
benzene	155.7	^{1}H	R12
benzene	156	^{13}C	FX90Q
mesitylene (ring)	153.3	^{1}H	R12
mesitylene (ring)	154.3	^{13}C	FX90Q
mesitylene (CH_3)	126.6	^{1}H	R12
mesitylene (CH_3)	125.9	^{13}C	FX90Q
1,4 dioxane	141.6	^{1}H	R12
1,4 dioxane	142	^{13}C	FX90Q

Table 8.2

Variation of the ^{13}C proton satellite line width (ΔW) and residual coupling constant Jr of benzene with the decoupling power

ΔW (H_z)	Jr(H_z)	IRR. Level x 10^{-1} db(a)
15	156	0
15	160	3
15	161	4
5	161.1	5
2	161.8	5.5
5	167	6
5	172	6.5
7	187	7
10	203.8	7.5

a) the switch is in the High position, according to figure (8.3)

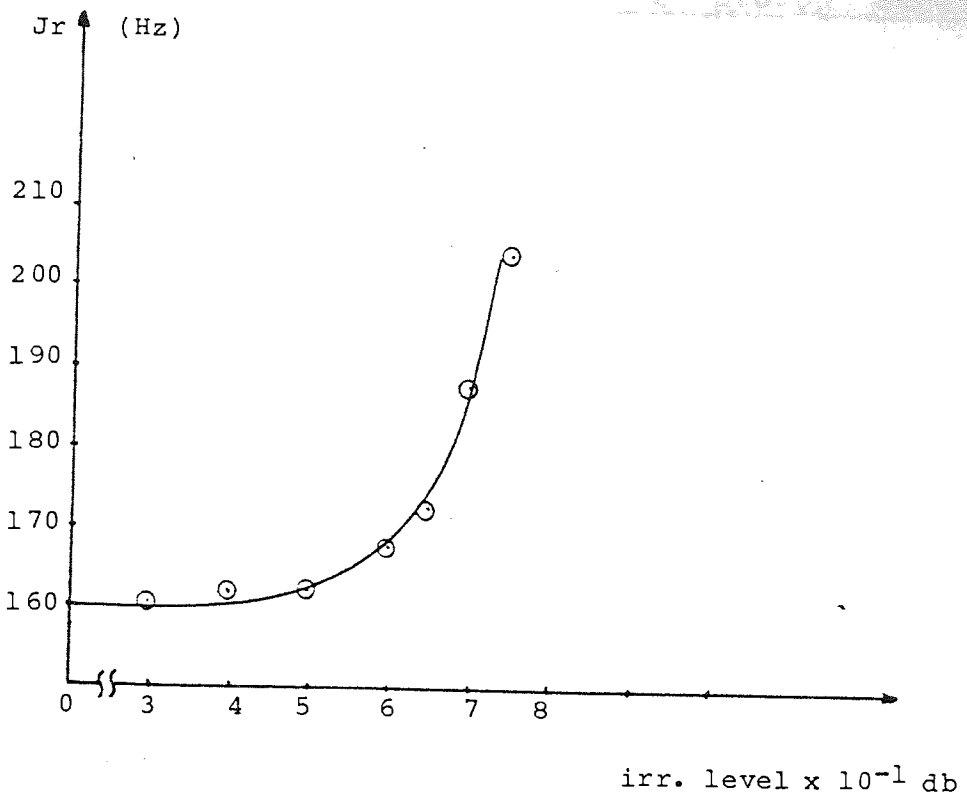

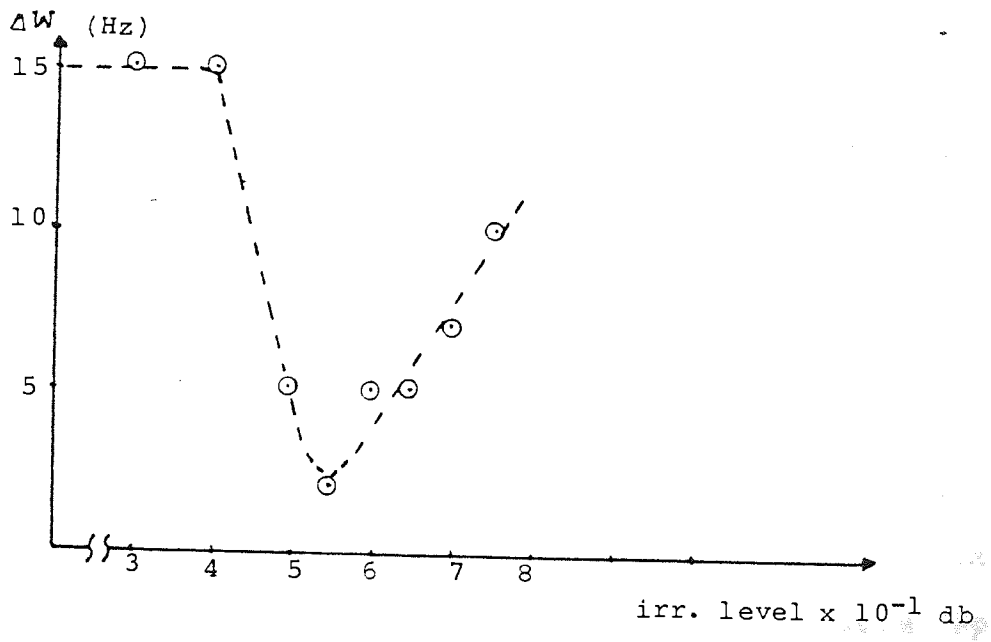

Figure 8.4 Variation of the satellite line width ΔW and residual coupling constant Jr with the decoupling power.

8.2.C3 Measurement of ^{13}C proton satellite relaxation times

After using the irradiation procedure described above, we are able to see singlet satellite signals. In practice it proved easiest to select only one of the satellite signals for investigation. This was the left or low field satellite because the right satellite signal was close to a side band of the water peak from the D_2O Lock signal.

In order to apply the Freeman approximation (220) the inversion recovery method should really be used to measure T_1. However, the progressive saturation method gives similar results.

The setting of the conditions for the measurements of satellite relaxation times was optimized during experience gained over quite a period of time. From the earliest measurements, the average relaxation time for benzene was 14.97 sec $\pm$ 1.2 sec. From later experiments summarized in figures (8.5) to (8.10) an average for T_1 of 14.8 $\pm$ 0.24 sec was obtained which is taken to be the true value. In order to get reliable spectra, the B_2 power was found to have a required setting of between high 5.5 and high 6 and an irradiation frequency offset of about 54.680KHz. The temperature of the sample was 28°C. To get the required spectra it was necessary to use at least 20 scans. The 90° pulse was 45 μsec.

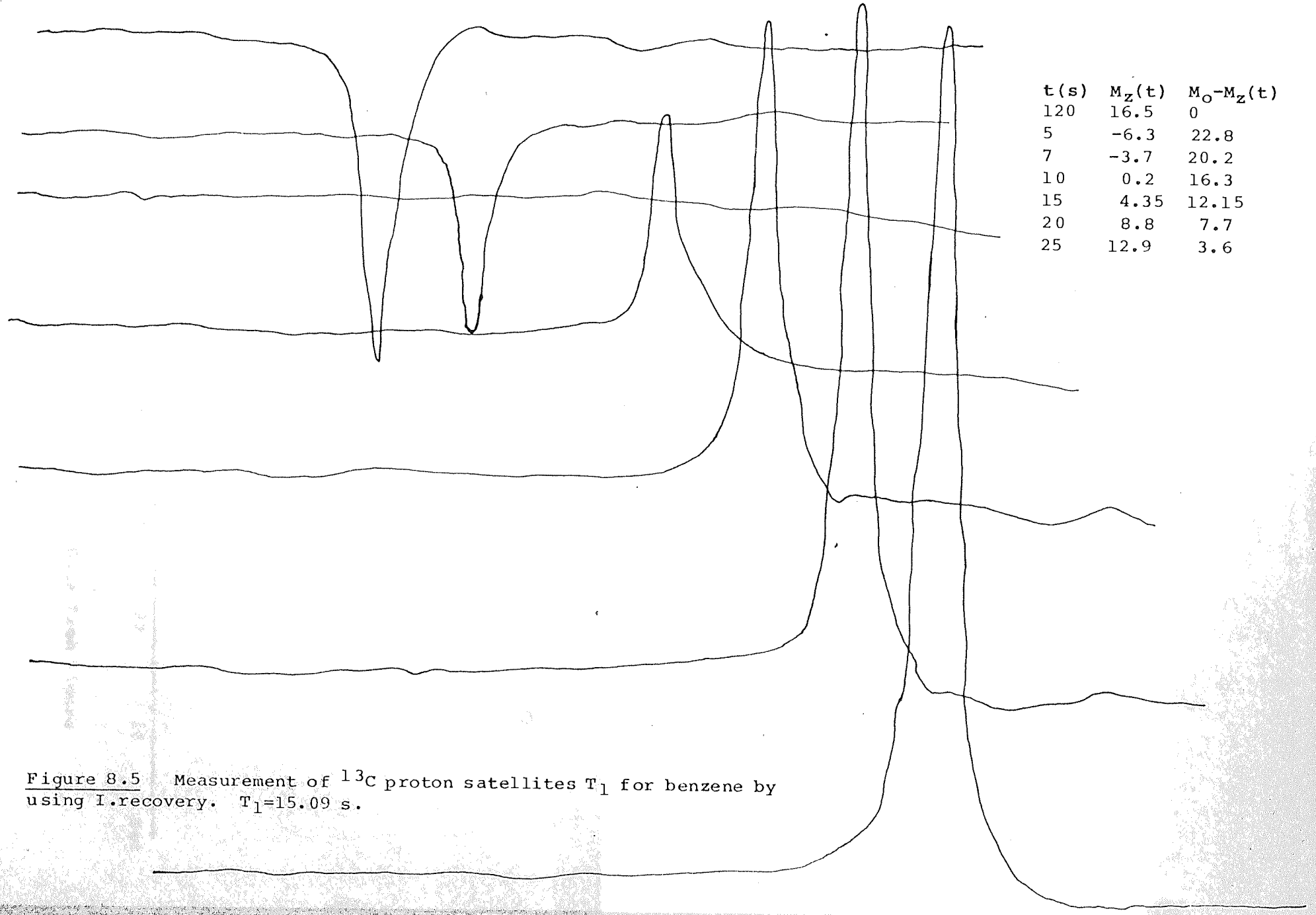

t(s)	$M_z(t)$	$M_o-M_z(t)$
120	16.5	0
5	-6.3	22.8
7	-3.7	20.2
10	0.2	16.3
15	4.35	12.15
20	8.8	7.7
25	12.9	3.6

Figure 8.5 Measurement of ^{13}C proton satellites T_1 for benzene by using I.recovery. T_1=15.09 s.

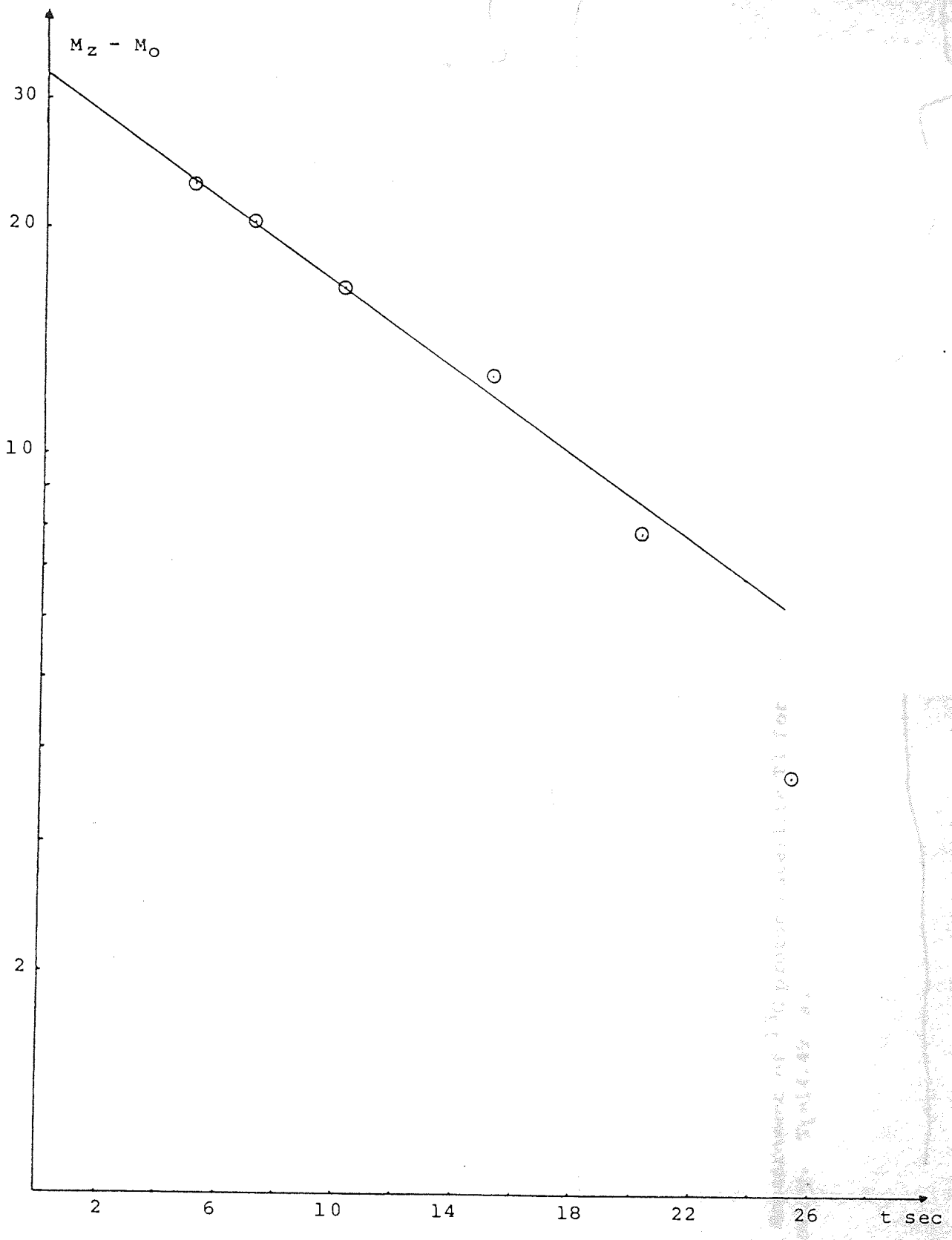

Figure 8.6 The variation of $M_z - M_o$ with t. Data from figure (8.5). T_1=15.09 sec.

t(s)	$M_z(t)$	$M_o-M_z(t)$
120	13.6	0
5	-5.3	18.9
8	-1.9	15.5
10	-0.2	13.8
15	3.6	10
20	6.6	7
25	9.4	4.2

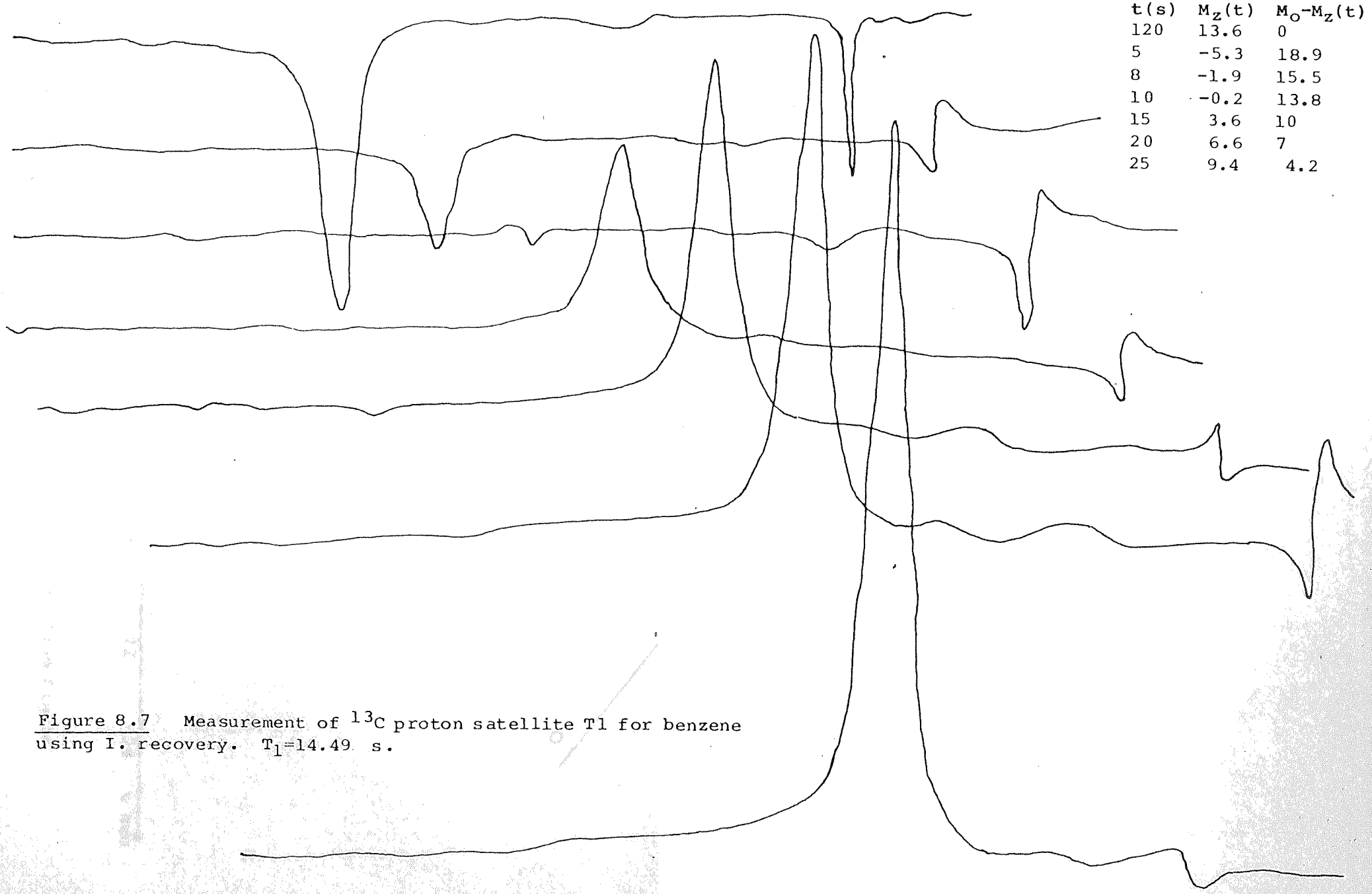

Figure 8.7 Measurement of ^{13}C proton satellite T1 for benzene using I. recovery. T_1=14.49 s.

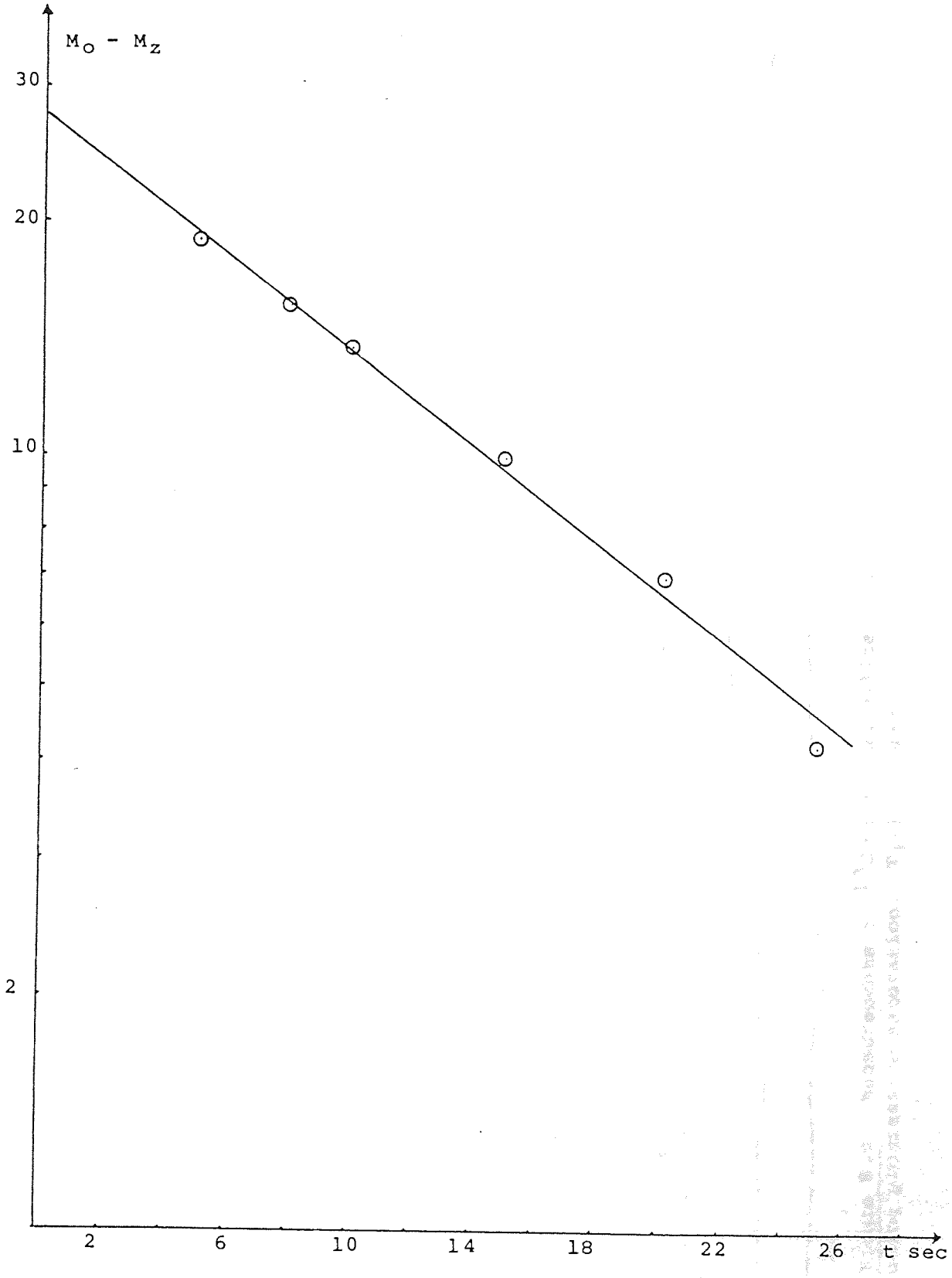

Figure 8.8 The variation of $M_o - M_z$ with t. Data from figure (8.7). T_1=14.49 sec.

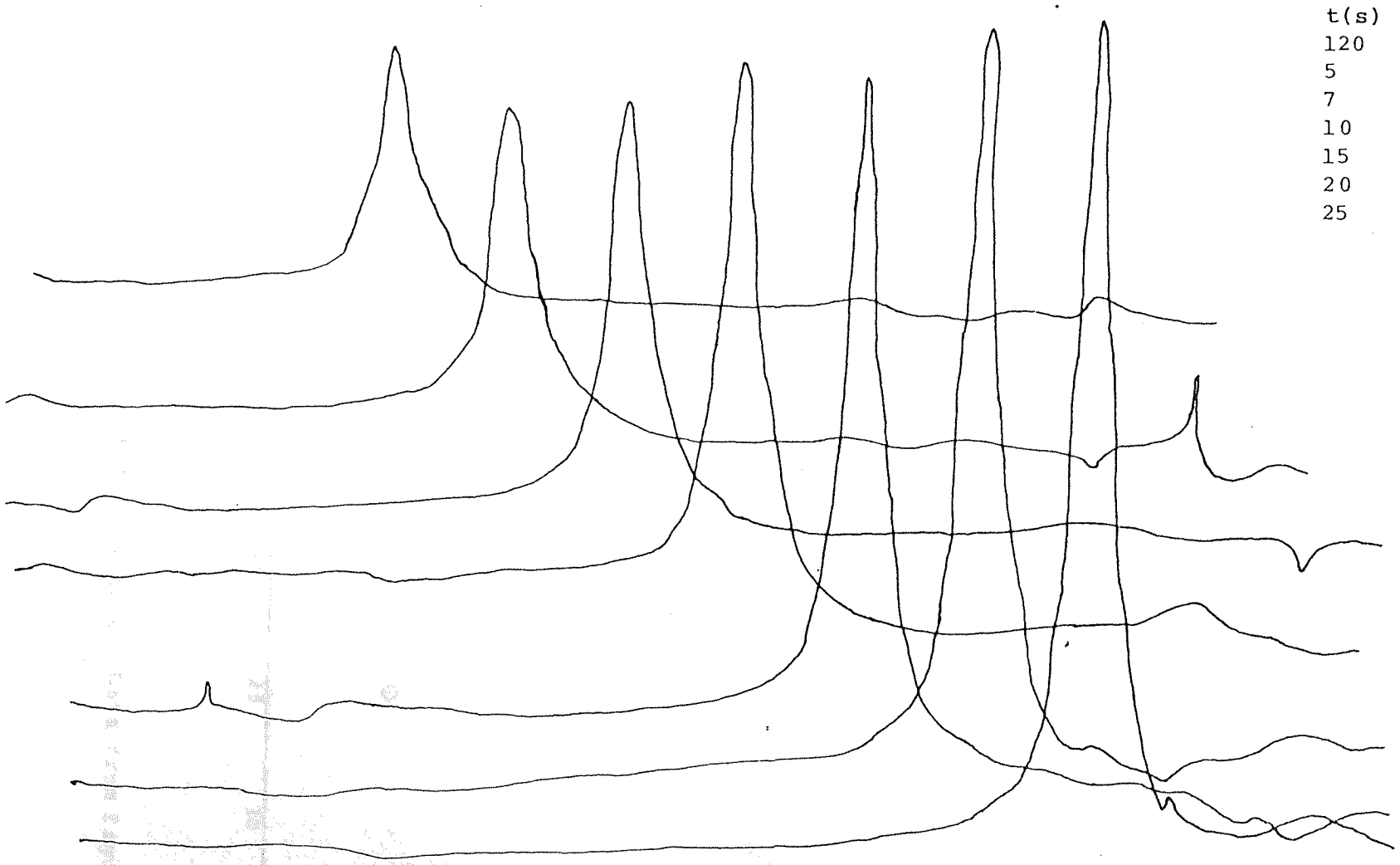

t(s)	$M_z(t)$	$M_o-M_z(t)$
120	12.8	0
5	3.6	9.2
7	47	8.1
10	6.25	6.55
15	7.85	4.95
20	9.65	3.15
25	11.4	1.4

Figure 8.9 Measurements of ^{13}C proton satellite T_1 for benzene using progressive saturation. T_1=14.92 sec

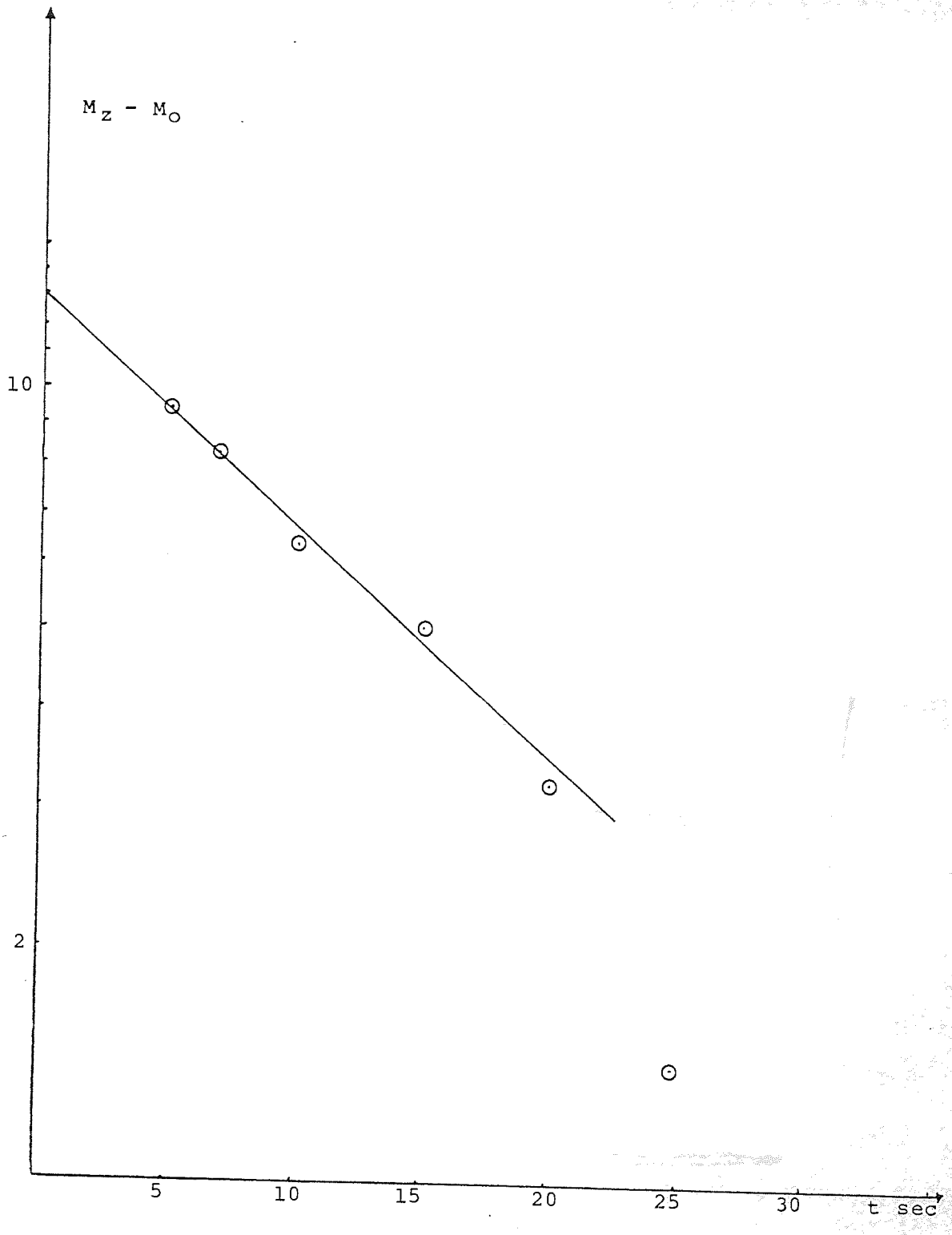

Figure 8.10 The variation of $M_o - M_z$ with t. Data from figure (8.9). T_1=14.92 sec

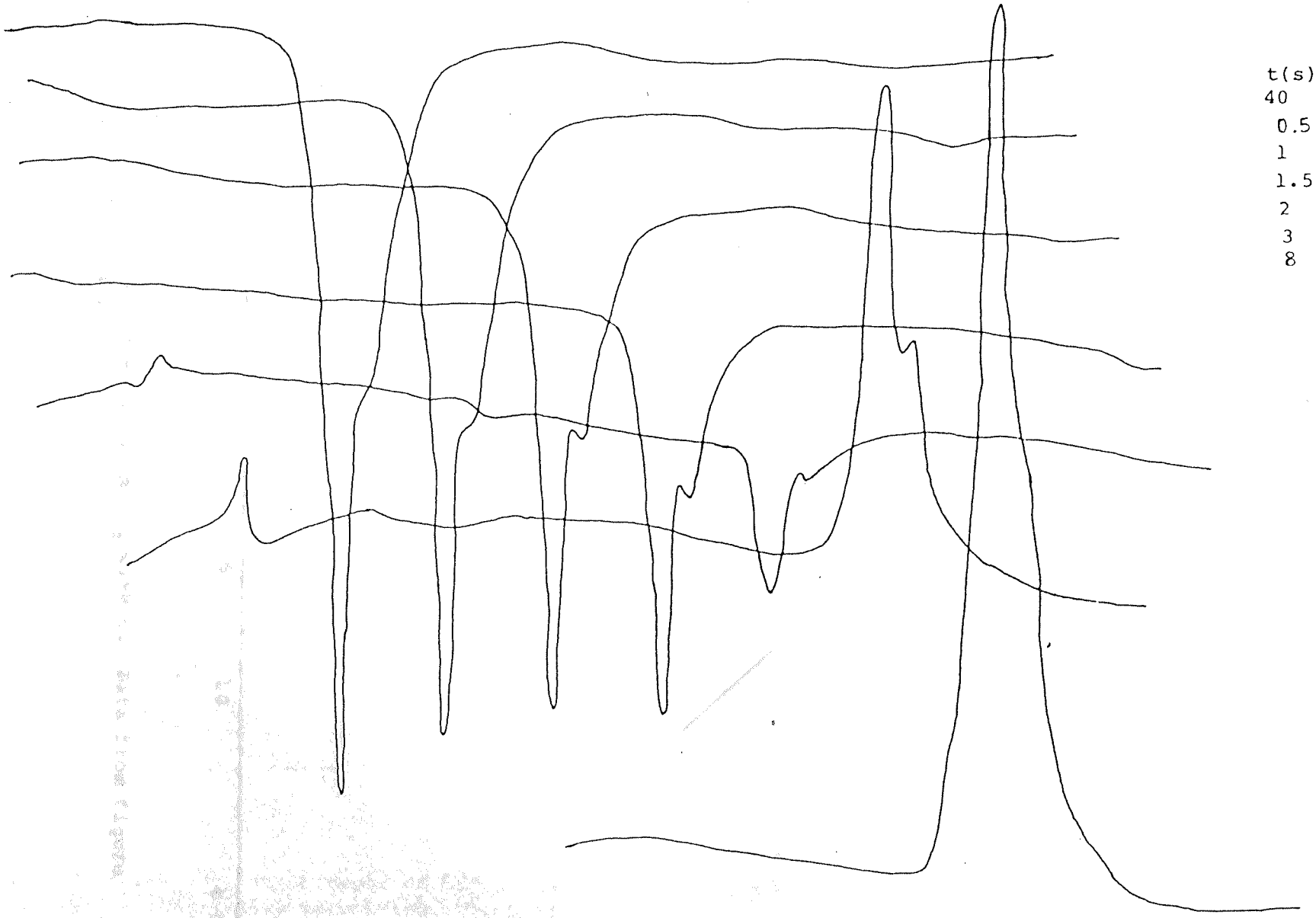

t(s)	$M_z(t)$	$M_o-M_z(t)$
40	14.3	0
0.5	-12.7	27
1	-10.4	24.7
1.5	-8.65	22.95
2	-6.9	21.2
3	-2.9	17.2
8	8.2	6.1

Figure 8.11 Measurement of ^{13}C Proton Satellite T_1 for dioxane using I. recovery. T_1=5.04 s.

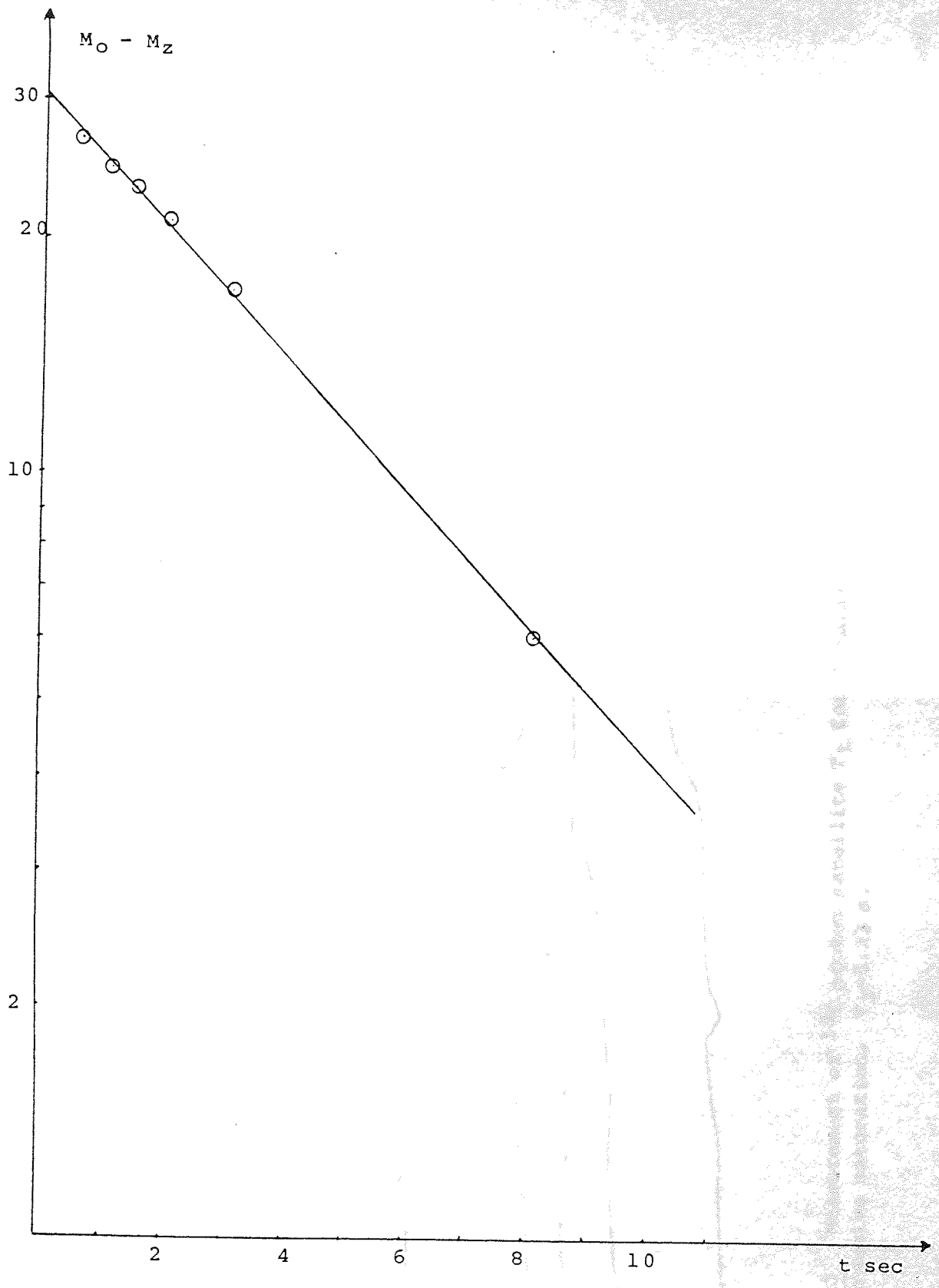

Figure 8.12 The variation of $M_o - M_z$ with t. Data from figure (8.11). T_1=5.04 sec.

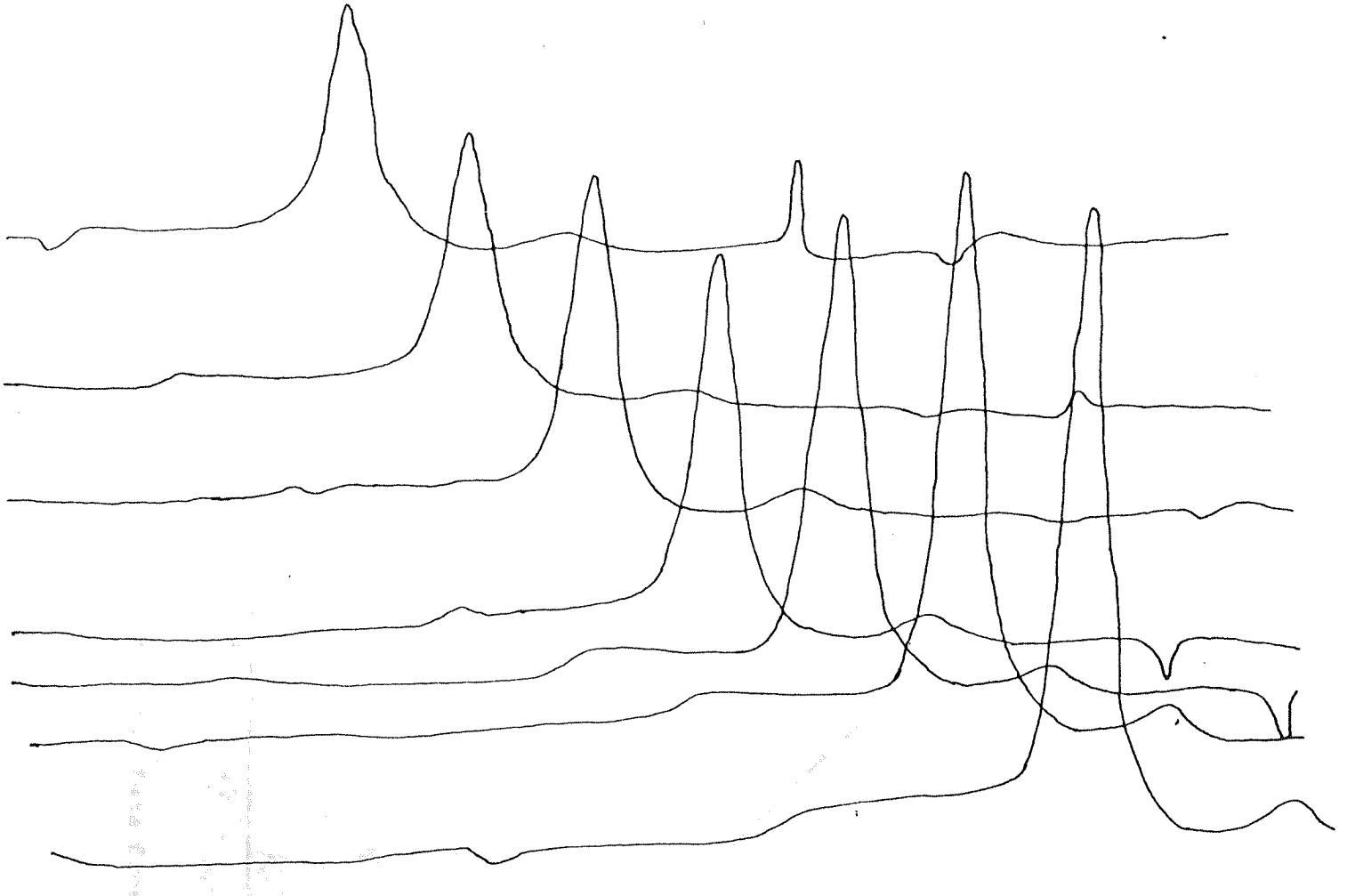

t(s)	M_z	M_o-M_z
50	8.8	0
2.5	3.35	5.45
3	3.75	5.05
4	4.7	4.1
5	5.4	3.4
7	6.6	2.2
12	7.9	0.9

Figure 8.13 Measurement of ^{13}C proton satellite T_1 for dioxane using Progressive saturation. T_1=5.23 s.

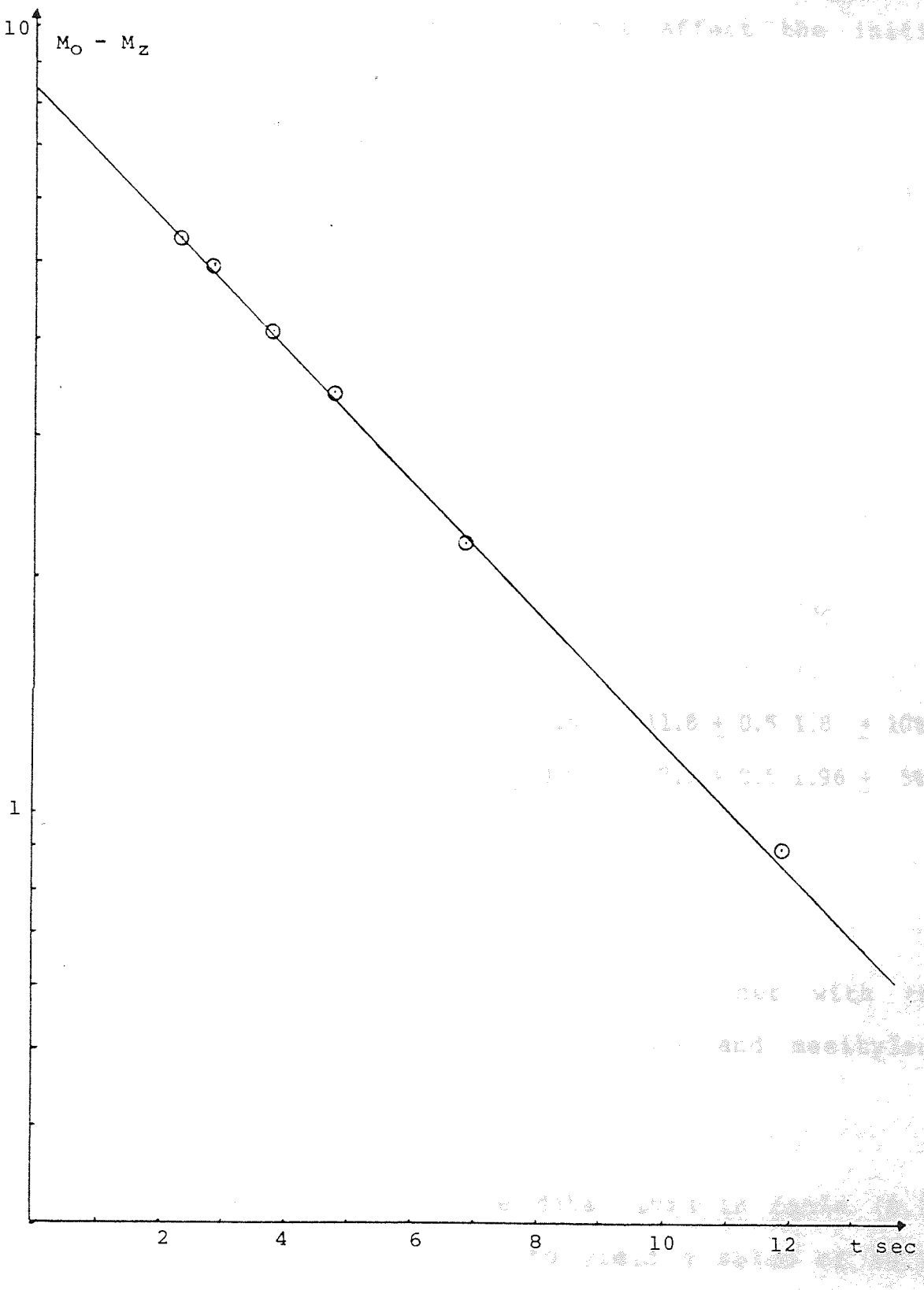

Figure 8.14 The variation of $M_o - M_z$ with t. Data from figure (8.13). T_1=5.23 sec.

The semilogarithm plot of $M_Z - M_O$ vs time in figures (8.6), (8.10) shows the last point away from the best linear correlation but this does not affect the initial rate of recovery of the magnetization.

In obtaining the ^{13}C T_1 values, the progressive saturation technique was used with a value of 24 μsec for the 90° pulse. The results of the relaxation studies are presented in table (8.3).

Table 8.3

Relaxation times and NOE's for benzene, 1,4 dioxane and mesitylene.

Sample	^1H sat. T_1(s)	^1H main T_1(s)	^{13}C T_1(s)	^{13}C η
benzene	14.8 ± 0.5	21 ± 0.5	32.9 ± 1	1.6 ± 10%
1,4 dioxane	5.4 ± 0.5	6.6 ± 0.5	11.8 ± 0.5	1.8 ± 10%
mesitylene(ring)	5.1 ± 0.5	15.0 ± 0.5	7.1 ± 0.5	1.96 ± 5%

8.2.D Results and discusion

The ^1H and ^{13}C relaxation times together with the $^{13}C-\{^1H\}$ nOe's for benzene, 1,4 dioxane and mesitylene are recorded in table (8.3)

In the case of benzene the data given in table (8.3) were used with equation (8.11) to yield a value of 40.75 sec. for T_{1DD}^c. If the distances from the ^{13}C proton satellite to the ortho, meta and para protons is a,b,c respectively and a',b',c' the distances from the ^{13}C to

the same protons, then from the standard benzene geometry indicated in figure (5.2) values a= 2.48 Å , b=4.3 Å and c=4.9 Å were obtained. This implies that a'=2.126Å, b'=3.34Å and c'=3.81Å. Therefore the ^{13}C dipolar-dipolar relaxation time is

$$T_1^{-1}{}_{DD}^{C} = \hbar^2 \gamma_{^{13}C}^2 \gamma_H^2 [2a'^{-6}+2b'^{-6}+c'^{-6}]\tau_c + T_1^{-1}{}_{^{13}CH\ sat} \tag{8.17}$$

as the distance ^{13}C-Hsat is 1.09Å, the equation (8.17) becomes

$$T_1^{-1}{}_{DD}^{C} = \hbar^2 \gamma_{^{13}C}^2 \gamma_H^2 [0.023426 + 0.596]\tau_c sec^{-1} \tag{8.18}$$

thus, it implies that $\rho_{CH} = 0.96\ T_{1DD}^{-1\,C}$. This, together with the other parameters in table (8.3) was used with equations (8.6), (8.9) and (8.10) to obtain T_{1intra}=92.6s and T_{1inter}=27.2s. Zeidler (105) and also Powles (109) have deduced from studies of C_6H_6 in C_6D_6 that T_{1intra}=111s and T_{1inter}=23s; T_{1intra}=87s and T_{1inter}=25s respectively. It can be seen that these values are consistent with those reported herein.

In the case of 1,4 dioxane $\rho_{CH}=2T_{1DD}^{-1\,C}$ so that the apropriate data in table (8.3) yield via equation (8.11) ρ_{HC}^{-1}=26.06s. Although the value of $\sum_{E\neq S} \rho_{HH}$ required for equation (8.15) is not available experimentally, it was estimated using the appropriate form of the Gutowsky-Woessner equation (8.19)

$$\sum_{E\neq S}\rho_{HH} = \frac{3}{2}\ \gamma_H^4\ \hbar^2\ r_{HH}^{-6}\ \tau_c \qquad (8.19)$$

for adjacent protons; a value of τ_c being deduced according to the Mitchell-Eisner approximation

$$\tau_c = \frac{\bar{I}}{\mu}\ \frac{2\eta\ a}{KT} \qquad (8.20)$$

where $\bar{I}$ (200.7×10^{-40}g cm^2) is the average moment of inertia of 1,4 dioxane, μ (44.06g) its reduced mass, a(2.67Å) its average radius and η (1.087 c.poisse) its viscosity. In this way $\sum_{E\neq S}\rho_{HH}^{-1}$ was estimated to be 9.49s. Using the values of $\sum_{E\neq S}\rho_{HH}$ and ρ_{HC} referred to above, together with the other relevant data in table (8.3) with equation (8.6) and (8.15) enabled the values of 8.33 s. and 31.64s to be deduced for T_{1intra} and T_{1inter} respectively.

In the case of mesitylene, it was measured the ring ^{13}C proton satellite T_1 in a mixture of mesitylene in CCl_4. The data obtained is presented in table (8.3). The experimental method used to get T_1 was inversion recovery.

The intramolecular contribution to T_1 arise from the ρ_{H-H} interaction and ρ_{HCH_3}. From equations (8.6) and (8.15) it is possible to obtain ρ_{HH}. In order to do that, it was used T_{1C-H}^{-1} from table (7.4) with a small correction due to the A values on table (7.6) which let us estimate the contribution to T_1 from the ring proton

in 98.2%. Therefore the value 0.1347 sec^{-1} for T_{1DD}^{-1C} change to 0.1323. Consequently $^3/_2\rho$ for the ring proton is 7.5×10^{-3}, which is higher than the value 1.65×10^{-3} reported for this interaction in table (7.9). This is due to the reduced S/N and the fact that changes in T_1 smaller than 0.5 sec produce significant variation in the calculated ρ_{HH}.

8.2.E CONCLUSIONS

It would appear that, for selected molecules, relaxation studies of ^{13}C and ^{12}C bounded hydrogen, coupled with $^{13}C-\{^1H\}$ *NOE* measurements can be used to isolate the intra and intermolecular contributions to the proton spin-lattice relaxation time. In order to minimize the dependence of the approach on the theoretical estimation of necessary parameters it is necessary to confine the approach to situations where the presence of ^{13}C differentiates one proton from an otherwise equivalent set of spins. It is likely, therefore, that the approach will only prove of significant value in the analysis of the relaxation times for protons such as those of the aryl hydrogens in symmetrically substituted aromatic compounds.

8.3 The use of intermolecular NOE's in the analysis of proton relaxation times in binary liquid mixtures

8.3.A Introduction

One of the mechanisms causing magnetic relaxation of hydrogen nuclei in liquids is the dipole-dipole interaction between protons in different molecules. When a molecule A is surrounded by other molecules of different kind B, the saturation of the proton signals of B, will enhance the resonance signals of the molecule A(125). This can be explained by invoking a collision complex model (126)(230) in which there is a coupling between protons in A and B.

In order to find the intermolecular contribution to the relaxation time of the protons in the molecule A, it is possible to employ dilution studies involving the deuterated B molecule (109)(219), this is normally costly. Another possibility, is to extend and adapt the Solomon equations (231) to describe the spin-lattice relaxation of systems of this nature in order to obtain equations that can be used with the *NOE* enhancement of the signal of the A molecule after saturation of the B signal to provide quantitative information about the interaction between molecules (127)(128)(189). Some such general equations will now be discussed.

In order to illustrate the present proposals a molecule, the solute, containing solute nucleus, s, out of Ns such nuclei is considered to be the subject of the investigations. When setting up the rate equation of this nucleus the effects of the remaining (N_{s-1}) equivalent nuclei, D, that are detected simultaneously but are not the subject have to be considered, as do the effect of the other set of N_E nuclei of type E in the solute and also those of the solvent nuclei. Such a general situation would be applicable to mesitylene in C_6H_{12} or TMS as has been the subject of earlier discussions in this thesis.

Following Solomon's approach the relevant rate equation is given by equation (8.21)

$$\frac{dI_{zs}}{dt} = - R_s (I_{zs} - I_{os}) - \sum_D \sigma_{SD} (I_{ZD} - I_{OD})$$

$$- \sum_E \sigma_{SE} (I_{ZE} - I_{OE}) - \sum_X \sigma_{SX} (I_{ZX} - I_{OX}) \qquad (8.21)$$

Where Ii is proportional to the integrated intensity of the resonance of i, I_{zi} and I_{oi} are respectively the values of Ii at some time t and at equilibrium. Rs is the total direct relaxation rate of S, given by equation (8.22)

$$R_s = \sum_{s \neq j} \rho_{sj} + \rho_s^* \qquad (8.22)$$

due to the effect of j(D and E). If ρ_s^* is the sum of ρ_{inter} (the intermolecular dipole-dipole rate, $\sum_X \rho_{SX}$) and ρ°, the rate contribution due to mechanisms other than dipole-dipole equations (8.22) may be written as

$$Rs = \sum_D \rho_{SD} + \sum_E \rho_{SE} + \sum_X \rho_{SX} + \rho^\circ \qquad (8.23a)$$

$$Rs = \rho_{intra} + \rho_{inter} + \rho^\circ \qquad (8.23b)$$

In equation (8.21), the terms σ_{sj}(j=D,E and X), represent cross-relaxation between j and s.

Although equation (8.21) describes the relaxation of the single spin S it has to be remembered that Is cannot in fact be measured. Only the total integrated intensity corresponding to that for S and N_{S-1} nuclei of the same type that have been artificially labelled D. The immediate reaction is to sum N_S equations of the type (8.21) in order to obtain an equation containing measurable intensities i.e. $N_S I_Z$. However, the result of so doing would be to multiply the last two terms by N_S. This would be quite incorrect because equations such as (8.21) refer to the nuclear and not the macroscopic level. In other words the relaxation of one subject nucleus, whether it be labelled S or D can, for example only be influenced by $\sum_E \sigma_{SE}(I_{ZE}-I_{OE})$ and not N_S times this. Consequently, observed bond intensities must be considered equivalent to single spin intensities.

If experiments are conducted in which the solvent resonance is saturated and slow passage conditions prevail $dI_{zs}/dt=I_{zx}=0$. By use of the general equations (8.24a)(8.24b)

$$\frac{\sigma_{sj}}{\rho_{sj}} = \frac{I_s\,(I_{s+1})}{2I_j\,(I_{j+1})} \qquad (8.24a)$$

$$I_{oj} \propto I_j(I_j + 1)\ \nu_j \qquad (8.24b)$$

and defining the *NOE* factors, f, by equation (8.25)

$$\frac{I_{zs} - I_{os}}{I_{os}} = f_{sx} = f_s(X) \qquad (8.25)$$

$$\frac{I_{zD} - I_{oD}}{I_{oD}} = f_{Dx} = f_D(X) \qquad (8.26)$$

Equation (8.21) can be rearranged to give equation (8.27)

$$2\,R_s\,f_{sx} = -\sum_D \rho_{SD}\,f_{DX}\,\frac{\nu_D}{\nu_S} - \sum \rho_{SE}\,f_{EX}\,\frac{\nu_E}{\nu_S} + \sum \rho_{sx}\,\frac{\nu_X}{\nu_s} \qquad (8.27)$$

However $f_{sx}=f_{Dx}$ and equation (8.27) becomes equation (8.28)

$$f_{sx}\,(2R_s + \sum_D \rho_{SD}\,\frac{\nu_D}{\nu_S}) = -\sum_E \rho_{SE}\,f_{EX}\,\frac{\nu_E}{\nu_S} + \Sigma \rho_{SX}\frac{\nu_X}{\nu_S} \qquad (8.28)$$

Although equation (8.21) corresponds to a triexponential rate equation it has been shown (220) that initial relaxation rates for a system that is correctly described by such an equation can be evaluated as though they obey a single exponential recovery without significant error being introduced into the relaxation rate so deduced. Under these conditions it is evident

that a value may be obtained for R_{SS} that is defined in equation (8.29)

$$R_{SS} = R_S + \sum_D \rho_{SD}/2 \qquad (8.29)$$

This permits equation (8.28) to be rewritten as equation (8.30) considering $\gamma_D = \gamma_S$

$$\sum_X \rho_{SX} \frac{\gamma_X}{\gamma_S} = 2R_{SS}\, f_{SX} + \sum_E \rho_{SE}\, f_{EX} \frac{\gamma_E}{\gamma_S} \qquad (8.30)$$

Information is now required for ρ_{SE} and this can be obtained from NOE experiments conducted by saturating the signal of E. By following the approach leading to equations (8.30), but additionally assuming that $f_{XE} \approx 0$ because of the low concentration of E in X it emerges that equation (8.31) now applies

$$\rho_{SE} \frac{\gamma_E}{\gamma_S} = 2R_{SS}\, f_{SE} \qquad (8.31)$$

substituting equation (8.31) into (8.30) gives equation (8.32)

$$\rho_{SX} = \rho_{inter} = 2 \frac{\gamma_S}{\gamma_X} R_{SS} (f_{SX} + f_{SE}\, f_{EX}) \qquad (8.32)$$

combining equation (8.23) and (8.29) permits R_{SS} to be expressed as in equation (8.33)

$$R_{SS} = \frac{3}{2} \rho_{intra} + \rho_{inter} - \frac{1}{2} \sum_E \rho_{SE} + \rho_o \qquad (8.33)$$

which combined with equations (8.31) and (8.30) gives equation (8.34)

$$\rho_{intra} = \frac{2}{3}\left[R_{SS}\left(1-2\frac{\gamma_S}{\gamma_X}\left(f_{SX}+f_{SE}f_{EX}\right)+\frac{\gamma_S}{\gamma_E}f_{SE}\right)-\rho_o\right] \qquad (8.34)$$

For practical purposes equations (8.32) and (8.34) can often be simplified. For example, when only homonuclear interactions contribute to the relaxation mechanisms $\gamma_S=\gamma_E=\gamma_X$ and equations (8.35) and (8.36) are obtained

$$\rho_{inter} = 2R_{SS}\left(f_{SX} + f_{SE}\,f_{EX}\right) \qquad (8.35)$$

$$\rho_{intra} = \frac{2}{3}\left[R_{SS}\left(1-2f_{SX} - 2f_{SE}f_{EX}+fSE\right)-\rho_o\right] \qquad (8.36)$$

It must be stressed, however, that when making simplifications of this type, confusion may arise if reference is not made to the full rate equation such as (8.27). For example, if the general system described above is simplified only in that S now becomes a unique nucleus, i.e. not one of an equivalent set of nuclei, the equations for ρ'inter and ρ'intra are (8.37) and (8.38)

$$\rho'_{inter} = 2\frac{\gamma_S}{\gamma_X}R_{SS}\left(f_{SX} + f_{EX}\,f_{SE}\right) \qquad (8.37)$$

$$\rho'_{intra} = R_{SS}\left(1-\frac{2\gamma_S}{\gamma_X}\left(f_{SX}+f_{EX}\,f_{SE}\right)\right)-\rho^\circ \qquad (8.38)$$

If the molecule is further simplified by making $N_E=0$ with the molecule containing only one unique spin S the relevant equations are

$$\rho''_{inter} = 2\frac{\gamma_S}{\gamma_X} R_{SS} f_{SX} \qquad (8.39)$$

$$\rho''_{intra} = 0 \qquad (8.40)$$

which means that there are no dipolar-dipolar intramolecular contributions.

There are several molecules that are used for fundamental studies of relaxation times which contain only one set of equivalent spins. The relevant equations in this case are

$$\rho'''_{inter} = \frac{\gamma_S}{\gamma_X} 2R_{SS} f_{SX} \qquad (8.41)$$

$$\rho'''_{intra} = \frac{2}{3}\left[R_{SS}\left(1-2\frac{\gamma_S}{\gamma_X} f_{SX}\right) - \rho^\circ\right] \qquad (8.42)$$

The equations (8.32), (8.34) and (8.42) can only be used to isolate both intra and intermolecular relaxation rates if ρ° is known. In the majority of systems having S, E and X as protons only, it is often safe to assume that $\rho^\circ = 0$. However, for heteronuclear studies the situation is not so simple. For example, ^{13}C relaxation mechanisms may involve finite contributions to ρ°. Natural abundance ^{13}C studies actually correspond to the circumstances surrounding equations (8.37) and (8.38). Selective $\{^1H\}-^{13}C$ irradiation experiments yield data appropriate to these equations but ρ° is unknown. However, whilst considerations of noise decoupling ($\{^1H\}-^{13}C$) experiments of X and E do not result in separate equations for the intra and intermolecular rates, they do provide the useful equation (8.43)

$$(2f_S(EX)-\frac{\gamma_X}{\gamma_S})(\rho'intra+\rho'inter)=-2f_S(EX)\rho^\circ \qquad (8.43)$$

Because the measured relaxation rate is given by equation (8.44)

$$R_S = R_{SS} = \rho'intra + \rho'inter + \rho^\circ \qquad (8.44)$$

and $\gamma_X/2\gamma_S$ may be equated to the maximum NOE, f_o, the familiar equation (8.45) holds

$$\rho'intra + \rho'inter = R_S \frac{f_S(EX)}{f_o} \qquad (8.45)$$

More importantly, for present purposes, equation (8.46) applies

$$\rho^\circ = R_S (1 - \frac{f_S(EX)}{f_o}) \qquad (8.46)$$

and so all contributions (equation (8.44)) to the measured relaxation rate can be isolated without the need to establish whether or not T_{1SR} and T_{1CSA} are finite by relaxation studies at various temperatures and resonant frequencies respectively.

The approach underlying the various equations presented above can be tested initially by reference to literature data available for systems that correspond to equations (8.41) and (8.42) with $\gamma_S = \gamma_X$. The data for these, together with one set corresponding to equations (8.39) and (8.40), are given in table (8.4). For comparison purposes values of T_{1intra} and T_{1inter}

obtained for the various solutes from dilution studies are presented in table (8.5).

Dilution studies of molecules such as benzene, cyclohexane and acetone necessarily yield $\frac{3}{2}\rho$intra ($\frac{2}{3}T_{1}$intra) and ρinter assuming ρ° is zero. Even having allowed for the factor of $^{2}/_{3}$ a direct equivalence of the values of T_{1}intra obtained from dilution studies and from nOe measurements is not expected because the two approaches employed involve different solvents that cause τ_{rot} to differ because of their viscosities. Similarly T_{1}inter obtained by the two approaches would be expected to be different because of the two different viscosities necessary for an equation such as

$$\tau_{trans} = \pi \eta a^{3}/2KT \qquad (8.47)$$

Additionally, in the case of T_{1}inter different solvents will involve different values for N and the intermolecular distances specified in equation (7.7). Nevertheless, the values for T_{1}intra and T_{1}inter deduced here are similar to those deduced from dilution studies.

It should be noted that in the case of chloroform referred to in table (8.4) the value associated with T_{1}intra must be attributed to T_{1SR} and not T_{1DD}. Similarly, in the case of acetone some part of the value of 39.77S attributed to T_{1}intra may be due to a spin-rotation contribution

Table 8.4

T_{1intra} and T_{1inter} evaluated from observed relaxation times, $T_{1obs}(R_{SS}^{-1})$, and intermolecular nOe's, f_{SX}, for various solutes at infinite dilution in protic solvents; the equations used are given in parentheses.

Solute	Solvent	ref.	T_{1obs}/s	f_{SX}	T_{1intra}/s	T_{1inter}/s
benzene	cyclohexane	174	17.0	0.37	98.1 (42)	23.0(41)
benzene	acetone	127	32.5	0.26	101.6 (42)	62.5(41)
cyclohexane	Benzene	174	13.76	0.2	34.4 (42)	34.4(41)
chloroform	cyclohexane	127	19.5	0.34	61.7 (40)	28.7(39)
acetone	benzene	127	17.5	0.17	39.77(42)	51.5(41)

Table 8.5

Values of T_{1intra} and T_{1inter} deduced for various compounds from dilution studies

Solute	Solvent	T_{1intra}/s	T_{1inter}/s	Ref.	$\frac{1}{3}T_{1intra}$/s	T_{1inter}/s
benzene	benzene-d6	111	23[a]	105		
	benzene-d6	87	25[a]	106		
	CS_2	91	33[b]	81		
	CCl_4	60		81		
	cyclohexane			c	65.4	23.0
	acetone			c	67.7	62.5
cyclohexane	CS_2	22	27[b]	81		
	CCl_4	16.2		81		
	benzene			c	22.9	34.4
acetone	acetone-d6	29	34[a]	105		
	benzene			c	26.5	51.5

a) deduced for pure material

b) calculated

c) from table 8.4

8.3.B Experimental methods, results and discussion

A general description of the method for measuring NOE is given in chapter four. In this section we will refer to specific applications of some techniques illustrated in table 4.9.

In the measurement of ^{13}C NOE's the irradiation modes COM, NNE were used. For selective irradiation the extension mode EXT 237 described in table 4.9 as SEL(NNE) was used, therefore the combinations SEL, EXT 237 or EXT 225, EXT 237 can be used to obtain the NOE value. In irradiation modes, complete or selective, the equations (8.48) and (8.49) are used

$$\eta = \frac{I_{COM}}{I_{NNE}} - 1 \qquad (8.48)$$

$$\eta = \frac{I_{SEL}}{I_{EXT\ 237}} - 1 \qquad (8.49)$$

where I refers to the integrated area of the signal under study.

Because of the normalization facility on the JX90Q spectrometer, the integral value has to be corrected according to the NG value indicated in the ACPAR pattern as shown in equation (4.15).

The evaluation of the proton NOE's requires special irradiation techniques, because of the proximity between the irradiated signal and the observed signal. This problem is overcome by the irradiation mode HOM, which is time shared, i.e., it has short alternate periods of irradiation and detection. The NOE can be calculated from equations (8.50) and (8.51)

$$\eta = \frac{I_{HOM}}{I_{EXT\ 93}} - 1 \qquad (8.50)$$

$$\eta = \frac{I_{EXT\ 81}}{I_{EXT\ 93}} - 1 \qquad (8.51)$$

where EXT 93 is described in table 4.9 and is a gated irradiation mode similar to the NNE mode. The extension irradiation mode EXT 81 is similar to HOM but they seem to have slightly different r.f. power distributions. The method indicated by equations (8.50) (8.51) is very convenient in the case of multiplet signals, where the applied rf field B_2 reduces the signal to a single peak with higher S/N. This is the best method available to determine the NOE for ^{13}C proton satellites in section 8.4.

The homogated irradiation mode HMG can be used in combination with the NON irradiation mode to obtain the NOE. For HMG the irradiation occurs after the sampling has been finished, so that there is enhancement without decoupling of the spectra. The resultant NOE is

$$\eta = \frac{I_{HMG}}{I_{NON}} - 1 \qquad (8.52)$$

This method has shown good performance but care has to be exercised with the r.f. power level which is quite high. As an example, in table (8.6) the NOE values for several rf power settings of the HMG mode for a sample of mesitylene in CCl_4 where $X_{Me}=0.05$ are presented. In this experiment the ring proton is observed and the group CH_3 is irradiated. As T_1 for the ring protons is 26sec, they are easily saturated. It was observed that the optimum rf power setting for HMG is low x 5.

The NOE in binary mixtures described in section 8.3.B can be illustrated with the results presented in table 8.9. For that purpose, the NOE values were calculated using the methods described above, which are indicated with the equation number in parentheses in tables (8.7) and (8.8).

In table (8.9) it can be observed that the calculated contribution ρ_{inter} for ^{13}C T_1 in benzene is 11% of the total dipolar dipolar interaction. This should be related to the high proton density of the sample. The results of ρ_{inter} and ρ_{intra} for benzene in cyclohexane confirm the results calculated from the literature in tables (8.4) and (8.5). In the case of mesitylene in TMS-C_6H_{12} the calculated values for ρ_{intra} and ρ_{inter} are similar to those shown in table 7.5 for the same mixture.

Table 8.6

The variation of the NOE for ring protons of mesitylene (X_{Me}=0.05) in CCl_4 with the r.f. power using the equation (8.52)

η(NOE)	Irradiation level x10^{-1} db
0.27	Low x 1
0.345	Low x 3
0.508	Low x 5
0.309	High x 1
0.20	High x 2
0.124	High x 3
0.135	High x 4
-0.075	High x 5
-0.11	High x 6

Table 8.7

Relaxation time T_1 and NOE for benzene ($X_\phi \approx 0.1$) diluted in cyclohexane. The equations used to evaluate the NOE are given in parentheses.

Irradiation	^1H T_1 (sec)	$^{13}CT_1$ (sec)	$\eta^{13}C$	η^1H
{COM}	17	33	1.5 (48)	
{ϕ}			1.4 (49)	
{Cy}			-0.15(49)	
{Cy}				0.37 (51)
{Cy}				0.37 (52)

Table 8.8

Relaxation time T_1 and NOE for mesitylene in the mixture Me-TMS-Cy with $X_{Me}=0.07$ $X_{TMS}=0.8$. The equations used to evaluate the NOE are given in parentheses

irradiation	^1H T_1(sec)	η^1H_{ring}	$\eta^1H_{CH_3}$
	20.7		
{TMS}		0.162 (52)	0.1 (52)
$\{CH_3\}$		0.27 (52)	
{Cy}		0 (52)	

Table 8.9

Values for ρ_{intra}, ρ_{inter} and ρ_o for various compounds evaluated from T_{1obs} and NOE's. The equations used are given in parentheses.

Nuclei	ρ_{intra}^{-1}(sec)	ρ_{inter}^{-1}(sec)	$\frac{2}{3}$ T_{intra}(sec)	ρ_o^{-1}(sec)
^{13}C benzene in C_6H_{12}	57.1 (44)	178.3 (37)		134.7 (46)
^1H benzene in C_6H_{12}	98.1 (42)	23 (41)	65.3 (42)	
^1H ring mesitylene in TMS-Cy	34.7 (36)	55.6 (35)		

In conclusion the method described in this section to calculate the intra and intermolecular contribution to T_1 seems to produce good results.

8.4 Studies of the NOE for the ^{13}C proton satellites in benzene and 1,4 dioxane.

Earlier in this chapter it was demonstrated that relaxation studies of the ^{13}C proton at the corresponding ^{12}C-proton spectra of benzene and dioxane could help separate the intra and intermolecular contribution to T_1 for the pure samples. However, the method proposed depended on the theoretical estimation of C-H dipolar relaxation rates. In view of the initial success of the use of NOE's to achieve the same end that has just been described, it is proposed to adapt this for the analysis of ^{13}C proton satellite relaxation times.

The intention is to establish if it is possible to get the intramolecular relaxation component of the ^{13}C proton satellite by selective irradiation of the ortho-meta-para protons in the same molecule. As was shown earlier in this chapter the ^{13}C proton satellite in the proton spectrum can be detected as a single line after appropriate double irradiation. In order to evaluate the NOE of the satellite proton it will be assumed that the ortho, meta and para proton signals, denoted by E, can be saturated with a weak irradiation power.

If it is assumed that irradiation at the ^{12}C bound hydrogen resonance saturates a fraction of the spins, it is reasonable to subdivide the intermolecular contribution as shown below,

$$- \sigma_{SX} \alpha (I_{ZX}-I_{OX}) - \sigma_{SX} (1-\alpha) (I_{ZX}-I_{OX}) \qquad (8.53)$$

so that the intermolecular components may be defined as

$$\sigma_{SX}\alpha = \rho_{SX}\alpha/2 = \rho''_{inter/2} = \alpha \rho_{inter/2} \qquad (8.54)$$

and

$$\sigma_{SX}(1-\alpha) = \rho_{SX}(1-\alpha)/2 = \rho'inter/2 = (1-\alpha)\rho_{inter/2} \qquad (8.55)$$

Consequently, from equation (8.27) it is obtained

$$2Rs\, f_S(E,X) = \rho_{SE} + \rho''_{inter} - \rho'_{inter}\, f_X(E) - \frac{\gamma_{^{13}C}}{\gamma_{^1H}} \rho_{^{13}CS}\, f_{^{13}C}(E) \qquad (8.56)$$

where S refers to the ^{13}C proton satellite, E to the ortho, meta and para hydrogen atoms in the benzene molecule and X to the hydrogen atoms in benzene molecules without a ^{13}C isotope. The value of the equation (8.56) will now be assessed.

8.4.A Experimental methods, results and discussion

The experiments were carried out in degassed samples of benzene and 1,4 dioxane. The method employed to

determine the NOE of the ^{13}C proton satellite consisted in the application of the r.f. irradiation field B_2 on the main signal, using the irradiation modes EXT 81, HOM, EXT 93 and equations (8.50) and (8.51). As usual a $5T_1$ period of time was allowed between pulses for EXT 81 and HOM, and a $10T_1$ when using EXT 93.

The integrated areas of the resultant decoupled signal were cut out and weighed to determine the NOE's. Some of the NOE's results calculated for benzene and 1,4 dioxane are presented in table (8.11), where the equation used is indicated in parentheses.

From measurements of the integrated area of the TMS signal in the sample of Me-TMS-Cy used in section 8.3 it was noticed that the irradiation mode EXT 81 has about 50% more power than HOM. This explains why in several experiments the NOE calculated from equation (8.51) was negative, i.e, EXT 81 produced partial saturation of the observed signal. For a similar reason, the NOE calculated from equation (8.50) gives, in some cases, values higher than 0.5; this is due to partial saturation of the signal detected in EXT 93 mode during the acquisition time.

These observations were used in the analysis of ^{13}C proton satellites. For example, in benzene, the inner satellite spectrum should spread for about 20 Hz, so in order to decouple the spins it is needed HOM power of the

order irradiation level high x 5. In these conditions, as indicated in table (8.10) and figure (8.15), the saturation coefficient α, which is defined by equation (8.57) from the ratio of the integrated area of the saturated signal divided by the integrated area of the non saturated signal has an approximate value of 0.95.

$$\alpha = 1 - \frac{Iv}{Iv^{\circ}} \qquad (8.57)$$

The expected value of the ^{13}C proton satellite NOE can be calculated from equation (8.56). For benzene the contribution of the first term is

$$\frac{\rho_{SE}}{2\,R_S} \approx \frac{2}{3}\;\frac{111^{-1}}{2.15^{-1}} = 0.0045 \qquad (8.58)$$

where 111 sec is the intramolecular value of T_1(105). The $^2/_3$ factor is introduced to eliminate the $^3/_2$ factor for identical spins which is irrelevant now and 15^{-1} is the approximate value of R_S.

The negative contribution in equation (8.56) due to the ^{13}C isotope is

$$-\frac{\gamma_{^{13}C}}{\gamma_{^1H}}\;\frac{\rho_{^{13}CS}}{2}\;f_{^{13}C}(E) \qquad (8.59)$$

where

$$\frac{\gamma_{^{13}C}}{\gamma_H} = 0.2514 \quad \text{and} \quad r_{H_S\,H^{\circ}} = 2.485\ \text{Å}$$

$$r_{^{13}C\text{-}H_S} = 1.09\text{Å} \quad \text{and} \quad r_{^{13}C\text{-}H^{\circ}} = 2.126\ \text{Å}$$

Then, if we approximate $\rho_{H_S H_E} \approx 2\rho_{H_S-H^\circ}$ where H° refers to the ortho hydrogen, it results in

$$\frac{\rho_{^{13}CH_S}}{\rho_{H_S H_E}} = \frac{\hbar^2 \gamma_H^2 \gamma_{^{13}C}^2 r_{C-H_S}^{-6}}{2\hbar^2 \gamma_H^2 \gamma_H^2 r_{H_S-H^\circ}^{-6}} \frac{\tau}{\tau} = \frac{1}{2}\left(\frac{\gamma_{^{13}C}}{\gamma_H}\right)^2 \left(\frac{r_{CH_S}}{r_{H_S H^\circ}}\right)^{-6} \tag{8.60}$$

Equation (8.60) can be written as

$$\rho^{^{13}C-H_S} \approx 4.4 \ \rho_{H_S H_E} \tag{8.61}$$

The enhancement $f_{^{13}C}(E)$ must be small. From chapter three we have

$$f_{^{13}C}(E) \approx f_{^{13}C}(2H^\circ) \approx f_{^{13}C}(H^\circ) + f_{^{13}C}(H^\circ) \tag{8.62}$$

where

$$f_{^{13}C}(H^\circ) = \frac{\rho_{^{13}C-H^\circ}}{2R_{^{13}C}} \frac{\gamma_H}{\gamma_{^{13}C}} \approx 0.009 \tag{8.63}$$

Then using equations (8.61) and (8.62) we obtain the negative contributions of the ^{13}C term in equation (8.56) that is $-0.005\ \rho_{H_S H_E}$. It is negligible respect to $\rho_{H_S H_E}$. Therefore, equation (8.56) becomes

$$f_S(E,X) = 0.045 + \frac{\rho_{inter}}{2R_S}[\alpha-(1-\alpha)f_X(E)] \tag{8.64}$$

The effect of saturating the main signal was estimated by integration of the remainder of the signal. The results are presented in table (8.10) and figure (8.15). In these experimental conditions the values of $1-\alpha$ are very small, i.e, $1-\alpha \approx 0.05$, which means that negative contributions arising from non-saturated protons

in the benzene molecule can be neglected. With this in mind, the expected result of the enhancement for the satellite is

$$f_S(E,X) \approx 0.045 + \frac{\rho_{inter}}{2R_S} \alpha \qquad (8.65)$$

If it is assumed that at the irradiation level high x5 is $\alpha \approx 0.95$ and with $\rho_{inter} = 23^{-1} sec^{-1}(105)$ and $R_S = 15^{-1}$ sec^{-1} equation (8.65) gives

$$f_S(E,X) \approx 0.356 \qquad (8.66)$$

In the case of 1,4 dioxane a similar analysis of equation (8.56) gives equation (8.67)

$$f_S(E,X) = 0.05 + \frac{\rho_{inter}}{2R_S} \alpha \qquad (8.67)$$

where α is taken to be 0.95, ρ_{inter} 31.6^{-1} sec^{-1} (section 8.3) and $R_S = 5.4^{-1}$ sec^{-1} (table 8.3). Then $f_S(E,X)$ becomes

$$f_S(E,X) \approx 0.131 \qquad (8.68)$$

In table (8.11) the expected values for the NOE are compared with the experimental values obtained from equations (8.50) and (8.51). When the irradiation method related to equation (8.51) is used the rf power has to be adjusted carefully as well as the irradiation site around the main signal to obtain a reliable NOE; otherwise, negative values can be obtained, which means that some

Table 8.10

Variation of the integrated signal of benzene with the r.f. irradiation power.

irradiation level	irradiation frequency (KHz)	Iv°/Iv	α
5	54.673	28	0.964
5.5	54.673	20	0.950
6	54.673	17	0.941
6.5	54.673	57	0.982
7	54.673	164	0.994
5.5	54.683	18.5	0.946
5.5	54.680	37.5	0.973
5.5	54.680	42.7	0.976
5.5	54.677	61.5	0.984

Table 8.11

NOE values and T_{linter} for the ^{13}C proton satellites of benzene and 1,4 dioxane. The equation used to evaluate the NOE and T_{linter} are given in parentheses.

		benzene	1,4 dioxane
Expected NOE		0.355 (65)	0.131 (67)
Measured NOE's	a	0.215 (51)	0.157 (51)
	b	0.46 (50)	0.155 (51)
	c	0.068 (51)	-0.15 (51)
	d	-0.016 (51)	0.256 (50)
	e	0.09 (51)	0.30 (50)
Expected T_{linter}		25 i	31.6 i
calculated T_{linter}		24 (65) j	24.2 (67) j

(i) determined in section 8.3

(j) calculated with the average values of the NOE a,b in this table.

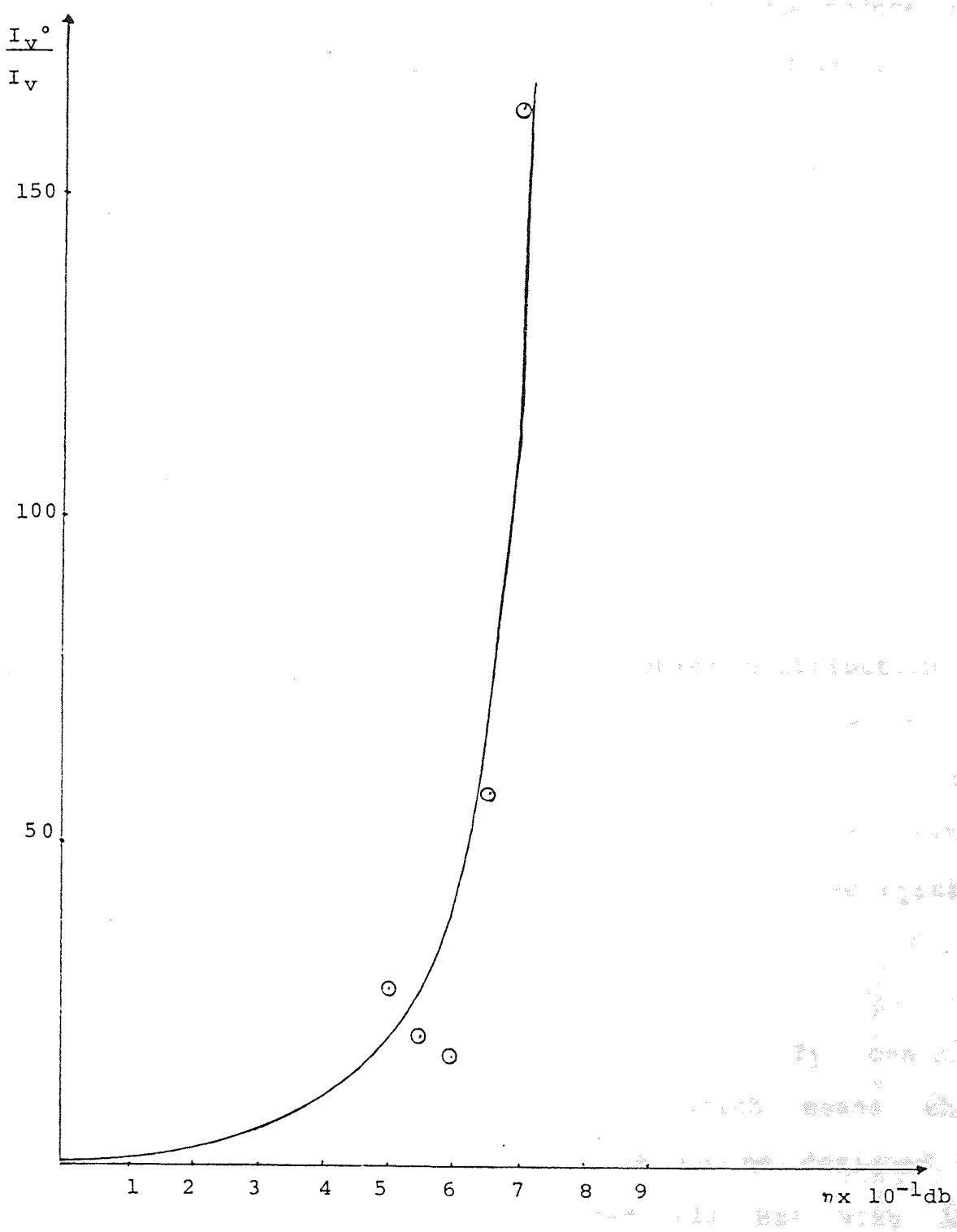

Figure 8.15 Relation between the integrated area I_v° of the signal of neat benzene and the integrated area of the saturated signal I_v at several irradiation setting (HOM. high level)

saturation is present. When using equation (8.50) the obtained NOE values can be higher than expected due to saturation with the irradiation mode EXT 93 during the acquisition time. Then, it is convenient to reduce the r.f. level for EXT 93 in order to obtain better results.

In table (8.11) the average value of the NOE results a,b for benzene is 0.34 which is very close to the expected result. For 1,4 dioxane the NOE results a,b and d are close to the expected value, the average a,b is 0.156. This indicates that despite the difficulty in reaching the appropriate experimental condition it is possible to obtain a reliable value for the NOE at the irradiation level high x5.

Table (8.11) shows the intermolecular contribution to T_1 for benzene and 1,4 dioxane calculated by the use of equations (8.65) and (8.67) and the average of the experimental NOE values a,b and α=0.95. The calculated values T_1inter are in agreement with the expected T_1inter values.

The intramolecular contribution to T_1 can be calculated experimentally for α=0, which means that adequate irradiation facilities have to be designed to modulate a large frequency spread (20 Hz) with low irradiation power in order to ensure saturation of the inner satellite spectrum but weak saturation of the main

signal. Otherwise, the saturation of the main signal will contribute considerably to the enhancement of the satellite signal.

8.5 Conclusions

The relaxation times of the ^{13}C proton satellite signal in benzene, 1,4 dioxane and mesitylene have been measured. These values were used to obtain the intramolecular and intermolecular contributions to T_1 which agree with results in the literature.

The Solomon equation for several multispin systems have been derived and used to analyse the NOE's produced by solvents. The expressions obtained were applied to several solute-solvent systems in order to separate the intra and intermolecular contribution to T_1. Satisfactory results were obtained.

Finally, the NOE for ^{13}C proton satellites were also evaluated. The best results were used to calculate the intermolecular contribution to T_1, which agrees with the expected results.

Chapter Nine

General Conclusions

9.1 General Conclusions

Detailed analyses of experimentally determined spin-lattice relaxation times indicate that they are inadequately explained by existing theories. The principal reason for this is attributed to gross errors in the classical equations for the intermolecular contributions, T_{1inter}, to the relaxation time. It is demonstrated that this situation can be rectified by the inclusion of a factor arising from the constraints imposed on the relative orientations of molecules during collisions; a similar effect, known as "buffeting" has been shown by Homer and Percival to contribute to the Van der Waals contribution to nuclear screening.

The ^{13}C method for the evaluation of T_{1intra} and the Gutowsky-Woessner equation modified by a buffeting factor for T_{1inter} appears, for the system studied here, to account precisely ($\pm$ 4%) for the magnitude of observed spin-lattice relaxation times.

Because of the necessity of improving the contemporary level of understanding of the individual intra and intermolecular contributions to T_1, methods have been devised for their isolation from the total observed values. These new methods have been shown to work satisfactorily.

APPENDIX

Some examples of T_1 calculations

The study of the relaxation times, normally involves the calculation of T_1 in neat compounds or mixtures. In this appendix the ^1H and ^{13}C relaxation times for the benzene molecule are calculated using standard methods referred to in this thesis.

a) The intramolecular contribution to T_1 in benzene can be written from the Gutowsky Woessner equation (3.17) as

$$T_1^{-1}\ \text{intra} = \frac{3}{2}\ \gamma^4 \hbar^2 \sum_{i \neq j} r_{ij}^{-6}\ \tau_r \qquad (A.1)$$

which according to figure (5.2) can be rewritten as

$$T_1^{-1}\text{intra} = \frac{3}{2}\ \hbar^2\ \gamma^4\ [2R^{-6} + (2R)^{-6} + 2(\sqrt{3}R)^{-6}]\tau_r \qquad (A.2)$$

where $\hbar = 1.05443 \times 10^{-27}$ erg sec. $\gamma = 2.6753 \times 10^4$ rad/sec gauss

and $R = 2.485\ \text{Å} = 2.485\ 10^{-8}$ cm

equation (A.2) reduces to

$$T_1^{-1}\text{intra} = 85.36 \times 8.8738 \times 10^{-3} \times 10^{-54} \times 10^{16} \times 10^{48}\ \tau_r \qquad (A.3)$$

or

$$T_1^{-1} \text{ intra} = 7.57 \times 10^9 \tau_r \text{ sec}^{-1} \qquad (A.4)$$

where the rotational correlation time τ_r can be calculated from the models described in chapter five or measured using the method given in chapter seven.

In the case of a mixture of benzene at infinite dilution in CCl_4, the Hill equation (A5) can be used to evaluate τ_r,

$$\tau_r = K_{AB}^2 \ \eta_{AB} \ \sigma_{AB}/KT \qquad (A5)$$

where

$$K_{AB}^2 = \frac{1}{\mu} \ \frac{I_{AB} \ I_B}{I_{AB}+I_B} \qquad (A.6)$$

and

$$I_{AB} = I_B + Md^2 \qquad (A.7)$$

In equation (A.7) I_B is the moment of inertia of benzene (table 5.6) M the mass of CCl_4 and d the distance between the centers of the molecules of benzene and CCl_4. The radii of these molecules are 2.45Å and 3.37Å respectively. Then, equation (A.6) becomes

$$K_{AB}^2 = \frac{192.66}{51.75} \times 6.02 \times 10^{23} \times 10^{-40} \text{ cm}^2 \qquad (A.8)$$

where 51.75g is the reduced mass μ.

Therefore the value of K_{AB}^2 is $22.4.10^{-17}\text{cm}^2$. From table (5.9) $\eta_{AB} \ \sigma_{AB}$ is 3.8Å c.p. Substituting these values in equation (A5) at 27°C, gives

$$\tau_r = \frac{22.4 \times 10^{-17} \times 3.8 \times 10^{-8} \times 10^{-2}}{1.38 \times 10^{-16} \times 300} = 2.05 \times 10^{-12}\text{sec} \quad (A.9)$$

The use of this value in equation (A4) produces an intramolecular contribution to T_1 of 64.4 sec.

b) For neat benzene, the intramolecular contribution to T_1 can be calculated in a similar form. The values of σ_B=5.304Å, η_B=0.546 c.p. reported in table 5.1 and I_B=196.84 x 10^{-40}g cm^2 (table 5.6) can be used in equation (A5) and (A6) to give

$$K_{BB}^2 = \frac{185.78}{39} \times 6.02 \times 10^{23} \times 10^{-40} = 28.67 \times 10^{-17}\text{cm}^2 \quad (A.10)$$

and

$$\tau_r = \frac{28.67 \times 10^{-17} \times 5.304 \times 10^{-8} \times 0.546 \times 10^{-2}}{1.38 \times 10^{-16} \times 306} = 1.96 \times 10^{-12}\text{sec} \quad (A.11)$$

substituting the value of τ_r in equation (A4) gives an intramolecular contribution to T_1, T_1intra = 67.4 sec. at 33°C

c) The intermolecular contribution to T_1 in neat benzene, can be calculated from the Gutowsky-Woessner equation 3.17, which can be written as

$$T_1^{-1}{}_{inter} = 3\pi^2 \hbar^2 \gamma^4 \eta N \frac{a}{KT} \frac{1}{r_o} \quad (A.12)$$

The distance of closest approach is taken to be 2a; η=0.546 c.p., ρ=0.868 g/c.c and N=4.0155 x 10^{22} protons/c.c at 33°C (174). Therefore the value of $T_1^{-1}{}_{inter}$ is

$$T_1^{-1}inter = \frac{3\pi^2\ 1.11x10^{-54}x\ 51.22\ x\ 10^{16}\ x\ 0.546\ x\ 10^{-2}\ x\ 0.4015x10^{23}}{2\ x\ 1.38\ x\ 10^{-16}\ x\ 306}$$

which gives T_{1inter}=22.88 sec.

d) For ^{13}C nuclei in neat benzene, the Gutowsky Woessner equation 3.17 is

$$T_1^{-1}_{DD} = \gamma_C^2\ \gamma_H^2\ \hbar^2\ \tau_c/r^{-6} \qquad (A.13)$$

where only the interaction of ^{13}C with the closest hydrogen at a distance r is considered. In this case we obtain

$$T_1^{-1}_{DD} = \frac{7.157\ x\ 0.4526\ x\ 10^{-16}\ x\ 1.11\ x\ 10^{-54}\ x\ \tau_c}{(1.09)^6\ (10^{-8})^6} \qquad (A.14)$$

which becomes

$$T_1^{-1}_{DD} = 2.1438\ x\ 10^{10}\ \tau_c \qquad (A.15)$$

For neat benzene, if we use the value of τ_c 1.96 p.sec obtained in b) it gives T_{1DD}=23.8 sec. this result is not adequate because we have measured for ^{13}C, T_1=32.9 sec (table 8.3). Therefore T_{1DD} must have a higher value.

The use of Zeidler's result (105) for benzene in C_6D_6 that is T_{1intra}=111sec, in equation (A.4) gives $\tau_r = \tau_c$=1.19 ps. Using this value in (A15), it gives T_{1DD}=39.2 sec., which agrees with the values reported in table (8.3) and the one obtained from equation A.16 (T_{1DD}=40.9sec)

$$T_{1DD} = T_{1obs}\ \frac{1.988}{\eta} \qquad (A.16)$$

where η = 1.6

REFERENCES

1 W. Pauli, Naturwiss, 12, 741, 1924

2 W. Gerlach and D. Stern, Ann Physik. 74, 673, 1924

3 I.I. Rabi, J.R. Zachrias, S.Millman and P. Kusch, Phys-Rev 53, 318, 1938

4 C.J. Gorter, Physica. 3, 995, (1936)

5 C.J. Gorter and L.F.J. Broer, Physica, 9, 591(1942)

6 C.M. Purcell, H.C. Torrey and R.V. Pound, Phys. Rev. 69, 37 (1946)

7 F. Bloch, W.W. Hansen and M. Packard. Phys. Rev. 69, 127 (1946)

8 Emsley J.W., J. Feeney & L.H. Sutcliffe in "High resolution nuclear magnetic resonance spectroscopy"
Pergamon Press. Oxford (1965)

9 Charles Poole, H.Farach. Relaxation in magnetic Resonance. Academic Press. New York. 1971

10 L. Pauling and E. Wilson in "Introduction to Quantum mechanics" Mcgrawhill Book Co. New York 1935

11 J. Schwinger, Phys. Rev. 51, 648 (1937)

12 I.Rabi, Phys. Rev. 51, 652 (1937)

13 C.P. Slichter, in "Principles of magnetic resonance" 2nd ed. Springer-Verlag-Berlin 1978

14 A. Einstein, Phys. Rev. Z 18,121 (1917)

15 E.M.Purcell, Phys. Rev. 69, 681 (1946)

16 Alan Carrington & A. Mclachlan, "Introduction to magnetic resonance" Harper Ed. New York 1969.

17 F.Bloch, Phys. Rev. 70, 460, (1946)

18 F.Bloch, Phys. Rev. 70, 104, (1946)

19 G.V.D. Tiers. J.Phys. Chem. 65, 1916 (1961)

20 E.Hann, Phys. Rev 80, 580, (1950)

21 G.E. Pake, J. Chem. Phys. 16, 327, (1948)

22 J. Van Vleck, Phys. Rev. 74, 1168 (1948)

23 E.RAndrew, R.GEades Proc. Roy. Soc.-A. 218, 537 (1953)

24 A. Buckingham, J. Pople, Discuss. Faraday Soc. 22, 17, (1956)

25 W.E. Lamb, Phys. Rev. 60, 817, (1941)

26 A.Saika, C.P. Slichter, J.Chem. Phys. 22, 26, (1954)

27 H.M. McConnell, J.Chem. Phys. 27, 226(1957)

28 W.C. Dickinson, Phys. Rev. 81, 717 (1951)

29 J.A. Pople, W. Schneider and H.J. Bernstein in "High resolution nuclear magnetic resonance" McGrawhill New York 1959 chap. 16

30 A.A. Bothner By and R.E. Glick, J.Chem. Phys. 26, 1651 (1957)

31 J.R. Zimmermann and M.R. Foster, J. Phys. Chem 61, 282 (1957)

32 J.Homer and D.L. Redhead, J.Chem soc. Faraday Trans. I. 68, 1049, (1972)

33 A.D. Buckingham, Can. J. Chem. 38, 300, (1960)

34 T.H. Scholte, Physica. 15, 15, 437 (1949)

35 A.J. Dekker, Physica 12, 209 (1946)

36 P.Diehl and R. Freeman, Mol. Phys. 4, 39 (1961)

37 G.C. Pimental and A.L. McClellan. The Hydrogen bond, Freeman, San Francisco, 1960.

38 E.A. Moelwyn, Hughes. Physical Chemistry. Pergamon, London. 1957 chap 7

39 J. Homer, App. Spect. Rev. 9.1, 1975

40 P.H. Weiner, E.R. Malinowski, A.R. Levinstone. J.Phys. Chem 74, 4537 (1970)

41 W.T. Raynes, M.A. Raza, Mol. Phys. 17, 157 (1969)

42 A. Buckingham, T. Shaefer. and W. Schneider. J.Chem. Phys 32. 1227 (1960)

43 M.J. Stephen, Mol. Phys. 1,223 (1958)

44 T.W. Marshall and J.A. Pople, Mol. Phys. 1, 199 (1958)

45 B.B. Howard, B.Linder, and M.T. Emerson. J. Chem. Phys. 36, 485 (1962)

46 F.H.A. Rummens, 1975, NMR, 10, Principle and Progress Ed. P.Diehl, E.Fluch and R. Kosfield. (Springer-Verlay)

47 De Montgolfier P, J.Chem Phys. 64, 639 (1967)

48 DE Montgolfier P, J.Chem Phys. 66, 685 (1969)

49 F.H.A. Rummens, J.Chem Phys. 72, 448, (1975)

50 F.H.A. Rummens, Can J. Chem. 54, 254, (1976)

51 C. Percival. PhD. Thesis University of Aston in Birmingham 1981.

52 L. Onsager, J. Amer. Chem. Soc, 58, 1486 (1936)

53 W.G. Proctor and F.C. YU, Phys. Rev 81, 20 (1951)

54 H.S. Gutowsky and D.W. McCall, Phys. Rev. 82, 748 (1951)

55 P.W. Atkins in Molecular Quantum Mechanics Claredon Press. Oxford. 1970 chapter (11)

56 W.E. Quinn and R.M. Brown, J.Chem. Phys. 21 (1605) (1953)

57 J.A. Pople and D.P. Santry, Mol. Phys. 8, 1, (1964)

58 N.F. Ramsey and E.M. Purcell, Phys. Rev. 85, 143 (1952)

59 F.London Trans. Farad. Soc. 33, 8, (1937)

60 T. Yonemoto, Can J. Chem 44, 223 (1966)

61 R.B. Williams, Annals N.Y. Acad. Sci. 70, 890 (1958)

62 A. Abragam. "The Principles of nuclear magnetism" Clarendon Press, Oxford 1961.

63 F.Bloch, W.W. Hansen and M.E. Purcell, Phys. Rev. 70, 474 (1946)

64 VARIAN HA100D NMR spectrometer, system manual Varian, Associates, PaloAlto.

65 H.Y. Carr and E.M. Purcell, Phys. Rev. 94, 630 (1954)

66 W.G. Clark. Rev. Sci. Instr. 35, 316 (1964)

67 A.G. Redfield and R.K. Gupta in Advances in Magnetic Resonance. Vol-5, Ed. J.S. Waugh. Academic Press, New York 1971.

68 J.D. Ellet, M.G. Gibby, U. Haeverlen, L.M. Huber, M.Mehring, A.Pines and J.S. Waugh in "Advances in Magnetic Resonance". Vol 5, Ed. J.S. Waugh. Academic Press. New York 1971 p.117

69 K.Jefrey and R. Armstrong. Rev. Sci-instr. 38, 639 (1967)

70 G.C. Levy and I.R. Peat, J. mag. Res. 18, 500 (1975)

71 J.W. Cooper, Comput. Chem. 1, 55 (1976)

72 J.W. Cooper, The Computer in F.T. NMR, in TOPICS in carbon-13 NMR. Vol-2, Ed. G.Levy, Wiley, New York 1975

73 JEOL F.T. NMR. Spectrometer, JNM. FX90Q Instruction Manual.

74 N.Bloembergen, E.M.Purcell, and R.V.Pound, Phys. Rev. 73, 679, (1948)

75 F.Reif, "Pundamentals of statistical and thermal physics" McGrawhill Co. (1965)

76 R. Kubo, K. Tomita, J. Phys. soc. Japan, 9, 888 (1954)

77 I. Solomon, Phys. Rev. 99, 559, (1955)

78 Debye "Polar molecules", Dover publications N.York (1945)

79 H.S. Gutowsky & D.E. Woessner, Phys. Rev. 104, 843 (1956)

80 P.S. Hubbard, Phys. Rev. 109, 1153 (1958)

81 R.W. Mitchell & M. Eisner, J.Chem. Phys. 33, 86 (1960); 34, 651 (1961)

82 G.W. Kattawar & M. Eisner, Phys. Rev, 126, 1054 (1961)

83 J.Powles, Proc. Phys. Soc, 78, 377, (1961)

84 H.C. Torrey, Phys. Rev, 107, 962 (1953)

85 M.D. Zeidler, Mol. Phys. 30, 1441. (1975)

86 P.S. Hubbard, Phys. Rev. 131, 275, 1963

87 H.G. Hertz. Progress NMR. Spectros. 3, 159 (1967)

88 R.O. Inlow, M.Juesten, J.R. Vanwazer, J.Phys. Chem. 79, 21, (1975)

89 D.E. Woessner, J.Chem. Phys. 37, 647 (1962)

90 D.E. Woessner, J.Chem. Phys. 42, 1855,(1965)

91 R.Mclung, D. Kivelson, J.Chem Phys. 49, 3380 (1968)

92 W.B. Moniz, W.A. Steele and J.D. Dixon J.Chem, Phys. 38, 2418 (1963)

93 L. Giulotto, G. Lanzi, L. Tosca, J.Chem, Phys. 24, 632 (1956)

94 J. Homer, A. Coupland. J.Chem Soc Faraday Trans. II, 74, 1330 (1978)

95 N.E. Hill, Proc. Phys. Soc. (London) 67B, 149, (1954); 68B, 209, (1955)

96 J.G. Powles, and D.J. Neale, Proc. Phys. Soc. (London) 78, 377 (1961)

97 J.G. Powles, Ber Bunsenges Physik. Chem 67, 328, (1963)

98 P.S. Hubbard, Phys. Rev. 131, 1155, (1963)

99 R.V. Pound. Phys. Rev. 79, 675 (1950)

100 T.Tsang and T.C. Farrar, J.Chem, Phys. 50, 3498 (1969)

101 U. Haeberlen, Advances in Magnetic Resonance Ed. J.S.Waugh, Academic Press, N.York (1976)

102 G.C. Levy, J.D. Cargioli and F.A. Anet, J. Amer. Chem Soc. 95, 1527 (1973)

103 T. Alger, D. Grant, J.Phys. Chem, 75, 2538, (1971)

104 J.R. Lyerla, D.M. Grant, J.Phys. Chem. 75, 3967 (1971)

105 M.D. Zeiddler, Ber. Bunsenges. Phys. Chem. 69, 659 (1965)

106 D.K. Green and J.G. Powles, Proc. Phys. Soc. London, 85, 87, (1965)

107 C.A. Reilly and R.L. Strombothe, J.Chem. Phys. 26, 1338, (1957)

108 A.M. Pritchard and R.E. Richards, Trans Faraday Soc. 62, 2014, (1966)

109 J.G. Powles and R.Figgins, Mol. Phys. 10, 155, (1966)

110 R.G. Parker and J.Jonas, Jour. Mag. Res. 6, 106, (1972)

111 J.H. Noggle and R.E. Schirmer, "The Nuclear Overhauser Effect," Academic Press, London (1971)

112 A.W. Overhauser, Phys. Review, 92, 411 (1953)

113 I. Solomon and N. Bloembergen, J.Chem. Phys. 25, 261 (1956)

114 R. Kaiser, J.Chem. Phys. 39, 2435, (1963)

115 S. Forsen and R. Hoffman, J.Chem. Phys. 39, 2892 (1963)

116 J.H. Noggle, J.Chem. Phys. 43, 3304, (1965)

117 P.C. Lauterbur in "Determination of Organic Structures by Physical Methods", Academic Press, N.York, 1962, Chapter 7.

118 F.A. L.Anet and A.J. Bourn, J.Amer. Chem. Soc, 87, 5250 (1965)

119 R.A. Bell and J.K. Saunders, Can. J.Chem, 48, 1114, (1970)

120 R.E. Schirmer, J.H. Noggle, J.P. Davis and P.A. Hart, J.Amer. Chem. Soc, 92, 3266, (1970)

121 P.D. Kennewell, J.Chem. Ed, 47, 278 (1970)

122 G. Bachers and T. Schaeffer, Chem. Rev, 71, 617, (1971)

123 R.A. Bell and J.K. Saunders, Can. J.Chem, 46, 3421, (1968)

124 R.A. Bell and J.K. Saunders, Can J. Chem, 48, 512, (1970)

125 R. Kaiser, J.Chem. Phys, 42, 1838, (1965)

126 E.L. Mackor and C.Maclean, J.Chem. Phys. 42, 4254 (1965)

127 M. Alla Eesti, NSV. Tead. Akad. Toim, Fuus. Mat. 19, 4 (441) (1970)

128 J. Homer and A. Coupland, J.C.S. Faraday II, 74, 2187, (1978)

129 K.Kuhlmann, D.M. Grant, R. Harris, J.Chem. Phys. 52, 3439 (1970)

130 J.R. Lyerla and D.M. Grant, in International Review of Science, Physical Chemistry Series, C.A. McDowell ed; (1972); Vol. 4.

131 J.R. Lyerla and G.C. Levy in "Topics in Carbon-13 Spectroscopy", Ed. G.C. Levy, Vol. 1, Chap 3, Wiley, N. York, (1974)

132 J. Kempf, H.W. Spiess, U. Haeberlen and H.Zimmermann, Chem. Phys. Lett, 17, 39, (1972)

133 J. Kempf, H.W. Spiess, U. Haeberlen and H.Zimmermann, Chem. Phys, 4, 269, (1974)

134 H.W. Spiess, D. Schweitzer, U. Haeberlen and K. Hausser, J. Mag. Res. 5, 101, (1971)

135 H.W. Spiess in "Organic Liquids: Structure, Dynamics and Chemical Properties", Chap. 9, Ed. A.Buckingham, Wiley, N.Y. (1978)

136 T.D. Alger, S.W. Collins and D.M. Grant, J.Chem. Phys. 54, 2820, 1971

137 K.Kuhlmann and D.M. Grant, J.Chem. Phys. 55, 2998, (1971)

138 B. Ancian, B.Tiffon, J.E. Dubois, J. Mag. Res. 34, 647, (1979)

139 I.D. Campbell and R.Freeman, J.Chem. Phys, 58, 2666 (1973)

140 D. Duddrell, A. Allerhand, J. Amer. Chem. Soc., 93, 1558 (1971)

141 S. Berger, F. Kreissl, D.M. Grant and J. Roberts, J.Amer. Chem. Soc., 97, 1805 (1975)

142 I.M. Armitage, H. Huber, D. Live, H. Pearson and J. Roberts, J. Mag. Res 15, 142, (1974)

143 S. Collins, T. Alger, D.M. Grant, K. Kuhlmann and J.J. Smith, J. Phys, Chem, 79, 2031, (1975)

144 F. Perrin, J. Phys. Radium, 5, 497 (1934)

145 F. Perrin, J. Phys. Radium, 7, 1 (1936)

146 S. Berger, F.R. Kreissl, J.D. Roberts, J.Amer. Chem. Soc., 96, 4348, (1974)